SEISMIC STUDY OF THE MAT AND SYLHET FAULTS IN THE SURMA VALLEY, NORTH EAST INDIA

By

SAITLUANGA

Ph.D. Regd. No. MZU/Ph.D/59/16.12.2004

Thesis Submitted in fulfillment for the award of the Degree of Doctor of Philosophy in Geology

MIZORAM UNIVERSITY

AIZAWL

2010

ACKNOWLEDGEMENTS

At the beginning I express my deep sense of gratitude to my supervisor Prof. R.P. Tiwari, Department Geology, Mizoram University, Aizawl, Mizoram for his invaluable guidance, help and encouragement which has been the source of inspiration throughout the course of my research work.

I am heartily thankful to my joint supervisor, Dr. Saurabh Baruah, Scientist and Head, Geoscience Division, North-East Institute of Science and Technology (NEIST), Jorhat, Assam, whose encouragement, advice, guidance and support from the initial to the final level enabled me to develop an understanding of the subject. His truly scientist intuition has made him as a constant oasis of ideas and passions in science, which exceptionally inspire and enrich my growth as a student and as a researcher. I am indebted to him more than he knows.

It is an honor for me to thank the Principal, Pachhunga University College, Aizawl, Mizoram for his kind permission and necessary assistance during my research work. I must acknowledge the direct encouragement, help and support that I received from him during my research.

I express my sincere thanks and gratitude to Dr. P.G. Rao, Director, North-East Institute of Science and Technology, Jorhat, Assam, for his kind permission to let me used a CSIR laboratory to carry out my research. Also my sincere thanks go to the Vice Chancellor, Mizoram University for his support.

I would like to thank the Head, teachers, research scholars and staffs of Department of Geology, Mizoram University for their invaluable advice and assistance.

I am indebted to my colleagues and staffs at Geology Department, Pachhunga University College for their unflinching encouragement and support in various ways.

I would like to show my gratitude to Dr. Pabon Kumar Bora, Scientist, Geoscience Division, NEIST-Jorhat for his interest and his crucial contributions.

It is a pleasure to pay tribute to Mr. Santanu Baruah, Mr. Aditya Kalita, Mr. Dipok Kumar Bora and Mrs. Sumana Goswami, Research Scholars, Geoscience Division, NEIST, Jorhat. Throughout my constant visits at NEIST, they are always there to support me, been overly generous with their time and I will always admire their enthusiasm, keen interest in the subject, friendship and the cordial reception which I received from them.

My parents deserve special mention for their inseparable support and prayers. I was fortunate to have all supports from my father, Mr. Lalmalsawma Sailo and my mother Mrs. Vanlalchhuani, who sincerely raised me with their caring and gently love and showing me the joy of intellectual pursuit ever since I was a child.

I express my deepest appreciation to my wife Rita and my daughters Amawitei and Zualtei whose dedication, love and persistent confidence in me, has taken the load off my shoulder. I thank them for all the support that they gave me during the years I have been working on this thesis, especially during my long and constant visits at NEIST, Jorhat.

Lastly, I expressed my gratitude to the Almighty God for the reason that this thesis would not have been materialized without His presence.

Aizawl (SAITLUANGA)

Date

CONTENTS

LIST OF TABLES

LIST OF FIGURES

	versus Ts denote interval between the arrival time of P- and S-waves and arrival time of P- and S-waves at a seismic station respectively. Linear relations for the determination of P- and S-wave at a specific depth, involving Ts-Tp/Tp, Ts-Tp/Ts and origin time (O.T) are also shown.	
5.7	Wadati diagrams (A, B, C, D, E and F) for the earthquakes associated with events in the northern part of Surma valley at depths (h) ranging between 41-60 km. Ts-Tp versus Tp and Ts-Tp versus Ts denote interval between the arrival time of P- and S-waves and arrival time of P- and S-waves at a seismic station respectively. Linear relations for the determination of P- and S-wave at a specific depth, involving Ts-Tp/Tp, Ts-Tp/Ts and origin time (O.T) are also shown.	56-57
5.8	Riznichenko diagrams (A, B, C and D) of earthquakes associated with events in the northern part of Surma valley as recorded in different selected seismic stations in the northeast. Linear relation between Tp-To and epicentral distance (**+**) are also shown for the events at different depth ranges.	56-57
6.1	Vp/Vs variation at different depth ranges in Surma valley. The color scale indicate the Vp/Vs ratio. The area covers 22-25^{0}N and 90^0-94.5^{0}E.	66-67
6.2(a)	Depth Variation at 0-20 km range in Mat fault region (eastern Surma valley). The velocity Vp/Vs ratios varies between 1.75 to 1.83.	66-67
6.2(b)	Depth Variation at 21-40 km range in Mat fault region (eastern Surma valley). The velocity Vp/Vs ratios increases from 1.69 to a maximum of 1.79.	66-67
6.2(c)	Depth Variation at 41-60 km range in Mat fault region (eastern Surma valley). Vp/Vs ratios vary from 1.7 to 1.75.	66-67
6.3(a)	Depth Variation at 21-40 km range in Sylhet fault region (northern Surma valley). Sudden changes in velocities Vp/Vs ratios are observed at depths of 23 and 33 km.	66-67
6.3(b)	Depth Variation at 41-60 km range in Sylhet fault region (northern Surma valley). Velocity (Vp/Vs) ratio is more or less uniform through the range.	66-67
7.1	Fault Geometry used in earthquake studies. A: area affected on the fault plane (After Kanamori and Cipar, 1974).	73-74

CHAPTER-I

INTRODUCTION

1.1 PROLOGUE

Northeastern region of India lies at the junction of the Himalayan arc to the north and the Burmese arc to the east. It is seismically one of the six most active regions of the world, the other five being Mexico, Taiwan, California, Japan and Turkey. It is placed in zone V, the highest zone, of the seismic zonation map of India. The region has experienced 18 large earthquakes (M=7) during the last hundred years including the great earthquakes of Shillong (1987, M=8.7) and Assam Tibet border (1950, M=8.7) (Fig. 1.1). Besides, several hundred small and micro earthquakes have also been recorded in the region. The high seismicity in the region is attributed to the collision tectonics between the Indian plate and the Eurasian plate in the north and subduction tectonics along the Indo-Burma region (IBR) in the east (Dewey and Bird, 1970; Kayal, 1996, 1998; Molnar and Tapponnier, 1975,1977 and Sarmah, 1999). Verma et al., (1976, 1977) stated that the lithospheric subduction at the Himalayan belt ceased during Pliocene time and shallow seismic activity is the effect of continental-continental collision. Subduction, on the other hand, is still continuing in the IBR, which is evidenced by the intermediate to deep focus earthquakes in this range. Incidentally, maximum seismic activity has also been recorded in this range. Earthquakes of historic importance experienced by Northeast India are listed below:

Place	Year	Magnitude	Remarks
Cachar	March 21, 1869	7.8	Numerous earth fissures and sand craters
Shillong plateau	June 12, 1897	8.7	About 1542 people died
Sibsagar	August 31, 1906	7.0	Property damage
Myanmar	December 12, 1908	7.5	Property damage
Srimangal	July 8, 1918	7.6	4500 km^2 area suffered damage
SW Assam	September 9, 1923	7.1	Property damage
Dhubri	July 2, 1930	7.1	Railway lines, culverts and bridges cracked

Assam	January 27, 1931	7.6	Destruction of property
Nagaland	1932	7.0	Destruction of property
N-E Assam	October 23, 1943	7.2	Destruction of property
Arunachal	July 7, 1947	7.5	Destruction of property
Upper Assam	July 29, 1949	7.6	Severe damage
Upper Assam	August 15, 1950	8.7	About 1520 people died. One of the largest known quake in the history
Patkai Range, Arunachal	1950	7.0	Property damage
Manipur-Burma border	1954	7.4	Property damage
Darjeeling	1959	7.5	Property damage
Indo-Myanmar border	August 6, 1988	7.5	No casualty reported

It is evident from the above table that the region has experienced two great earthquakes of magnitude >8 during the last hundred years. The June 12, 1897 earthquake of the Shillong Plateau is one of the greatest event of the world. Casualty was only 1,542 in spite of the magnitude of the event being 8.7. This is so because the event occurred at 5.15 p.m when most of the people were outdoor. Damage to the property was, however, severe. All concrete structures within an area of 30,000 square miles were practically destroyed. There was evidence of two surface faults, namely, Chedrang and Dudhnoi. It is the first instrumentally recorded event in the country. Another event of matching magnitude occurred on August 15, 1950 in the Syntaxis Zone. It caused 1520 death but was more damaging than the 1897 event. Railway line and roads were considerably damaged, landslide triggered in many places and fissures and sand vents occurred. The last major event (M=7.5) in the region occurred on August 6, 1988 with its epicenter in the Myanmar side of the IBR. This rocked the whole northeastern region. The tremor lasted for about two minutes killing four human and damaged buildings, railway tracts and roads (Tiwari, 2000).

Earthquakes cannot be prevented from occurring and they cannot be diverted to other places. Much-talked about earthquake prediction has so far not been realized in seismology even after spending billions of dollars during the last three decades. Of course, there are isolated instances of successful prediction, namely, Haicheng earthquake of 1975 in China (Magnitude 7.3). It was predicted on the basis of micro-seismic activity, ground tilting and unusual animal behaviour. This technique, however, cannot be applied everywhere. Moreover, prediction will not be helpful in avoiding or reducing damages caused by earthquake because building and other structure cannot be evacuated (Tiwari, 2002). Lack of reliable quake prediction technology forces us to learn to live with the earthquake by reducing their disastrous impact on human life and property. Earthquake hazards of Northeast India cannot be changed; however, earthquake disaster can be mitigated. High seismic risk in the region calls for an urgent and sustained mitigation efforts. Yokohama Declaration, 1994 (at the mid-term review conference of IDNDR) reads: " Disaster prevention, mitigation and preparedness are better than disaster response in achieving the goals and objectives of the decade. Disaster response alone is not sufficient as it yields only temporary results at a very high cost. Prevention contributes to lasting improvement in safety and is essential to integrate disaster management".

The importance of seismological studies lies in the fact that information generated can be used to mitigate the earthquake hazards. Preparation of seismotectonic/seismic zonation maps is the first step in this direction. The basic data required for the preparation of these maps are (i) A carefully compiled earthquake catalogue incorporating details about magnitude, location of epicenter, depth of focus etc., (ii) Delineation of seismic source zones from all possible sources like recurrence relation, tectono-geological consideration, palaeoseismicity etc., (iii) Estimation of upper bound magnitude through statistical procedure, cumulative seismic energy release, active fault length etc. and (iv) Attenuation of ground shaking for better results (Das Gupta, 1999). Seismic microzonation is recommended for better result. These maps give an idea about the possibility of occurrence of earthquakes in the region and are very useful for evaluating the risk involved before designing and constructing heavy engineering structures like dam, bridges, flyovers and large towers, etc. These are also useful for planning human settlements that would remain

safe during the occurrence of an earthquake. Seismic risk evaluation is also possible from these maps.

In the present study earthquake epicenters have been recomputed from the data collected from different networks existing in the region. Travel time for P- and S-waves have been calculated. The use of microearthquakes to determine the orientation of active faults, focal mechanism solution and details of local crustal structure strongly depends on the velocity model used in the earthquake location process (Nicholson and Simpson, 1985). Moreover, it is well known that the accuracy of local earthquake location depends not only on the crustal velocity structure between the source and the station, but also on the distribution of recording stations. While employing the principal techniques that involve the construction and analysis of Wadati and Riznichenko diagrams, the travel time of P- and S-waves and subsequently the velocities and their rational upper crustal depths and origin times, that is independent of crustal velocity model and based on which the P-wave travel times as a function of epicentral distance are derived so as to obtain the P-wave velocities in the upper crust. From the Wadati diagram, origin times (To) have been obtained and used to determine P-wave travels times in order to obtain the Riznichenko diagram that depicts (Tp-To) as a function of epicentral distance (✚). The Riznichenko diagrams clearly show the change in shape of the travel time versus distance curve with increasing focal depth indicative of both a geometrical effect and an increasing P-wave velocity. The velocity ratio Vp/Vs is computed directly from a diagram P-S interval against travel time (T) of P, a linear relation between the two being presumed by many authors. Apart from variation of Vp/Vs ratio with depth, source characterization of the earthquake hypocenter are made through waveform modeling by generating synthetic seismogram with estimation of Green's function constrained by the matching of observed and synthetic seismogram.

Practically, the estimate is greatly affected by the assumed values of Vp/Vs, the velocity ratio of P- and S-waves, in the calculation. So far, structures of the earth's crust were studied and classified in relation to the velocity of seismic waves, chiefly of P-waves.

1.2 DESCRIPTION OF THE STUDY AREA

The area under investigation is the northeastern prolongation of the Indian Shield comprising Surma valley and Indo-Burmese Range bounded by Post-Barail unconformity. It lies between 90^{o}E and 95^{o}E longitudes and 22^{o}N and 26^{o}N latitudes. Two prominent faults- the NE-SW trending Sylhet fault in the northern part of Surma valley (Nandy et el., 1983) and NW-SE trending Mat fault in the eastern part of Surma valley are conspicuously present in the study area (Fig. 1.2). The seismotectonics of the region is the matter of interest for several researchers. Four major earthquakes have occurred in the study area during the past hundred years. These are: Cachar Earthquake of 1869 (M=7), Srimangal Earthquake of 1918 (M=7.6), Cachar Earthquake of 1984 (M=5.8) and Indo-Burma Earthquake of 1988 (M=7.5). Other main tectonic domains in the study area are E-W trending Dauki fault (which demarcates the boundary between the Meghalaya plateau and Bengal basin), NE-SW Hail-Hakula lineament, N-S Jamuna fault, N-W Padma lineament, N-W Tista fault, and Tuipui fault. The area is mostly covered by thick marginal marine to shallow marine sedimentary succession of Oligocene to Pliocene age and belongs to Barail Group, Surma Group and Tipam Group. Surma Group of Lower –Middle Miocene is the main lithostratigraphic unit in the study area. Bhuban and Bokabil Formations constitute Surma Group. This group consists of alternating succession of arenaceous and argillaceous sedimentary rocks. The main rock types are sandstone, siltstone, shale and mudstone and their admixture in various proportions. Mizoram has been considered as the depocentre of Surma succession having exposed thickness of ~6500m. Another 5000m of the succession is concealed.

1.3 REVIEW OF LITERATURE

Although significant progress has been made in monitoring of the earthquakes in northeastern India by establishing a number of seismic network stations over the past few years, many of the questions concerning the location and nature of the potential seismic source zone/ seismogenic faults still remain unsolved. However, in this study attempt has been made to identify the suspect potential faults through tectonic and seismotectonic analysis. The practical earthquake hazard assessment involves 1) identification of seismogenic structures forming the source and, 2) evaluation of maximum possible earthquake related to the seismogenic structure and frequency – magnitude relation for individual source zone/tectonic blocks traversed by different tectonic elements.

So far, only statistical analysis of historical earthquake data has been resorted for predicting future earthquakes without due consideration to the distinct source zones in northeastern India (Gupta, et al.,1982, 1986; Gupta, 1985; Guha, et al., 1984; Das Gupta, et al., 1998; Khattri, 1987). Precursor signals like clustering of fore-shocks, change in resistivity and gravity values were considered for predicting earthquakes in the region (Gupta, et al., 1989; Kayal, 1991).

Gupta (1985) considered the 1984 Cachar earthquake which lies in the region of Tripura-Mizo fold belt as a precursory event for large earthquakes. Kayal (1991) attempted to correlate the observed change in resistivity, Vp/Vs ratio and microgravity values in the western part of the Meghalaya Plateau as precursors for the 1984 Cachar earthquake (Mb=5.5) and also for the 1988 North Myanmar earthquake (Mb=7.5) which occurred at a distance of more than 200 km from the site of measurement of precursor signals. This observation and correlation seems to be too much of inferences for such far field events. Guha, et al. (1984) have reported significant precursory decrease in b-value in the northeastern region of India, and indicated probability of occurrence of great earthquakes (M>8) in the near future. Gupta and Singh (1989) studied the earthquake sequence which occurred before the 1984 Cachar earthquake and 1988 North Myanmar earthquakes. Studying the seismicity pattern in different time-intervals within a 5^{o}-6^{o} space window, they suggested that precursory swarm hypothesis of Evison (1977) could be made predictive in the northeastern region of India.

Temporal occurrence of earthquakes having magnitudes >5.5 and 6.0 was statistically analyzed for the seismically active northeastern region of India. Non-stationary Poisson distribution provide a good fit to analyze the earthquake sequence for the entire area for which there has been 90% probability for the occurrence of at least one earthquake of magnitude Mb>6 in any time window of 5 years, while the probability has been 98% for an event of Mb>5.5 in any two years time slot. Similarly, for the eastern Himalayan tectonic domain, probability was found to be 70% and for the Myanmar arc it was 90% for at least one earthquake of Mb>6.0 within the recurrence period of 10 years. Seismic hazards maps with percent probabilities for the occurrence of at least one earthquake of Mb>6.0 with return periods of 20 and 50 years have been prepared based on such analyses (Das Gupta, et al., 1998)

Many previous workers have studied seismicity in relation to overall tectonics of the region and their studies gave valuable information on seismotectonics, subduction process and plate kinematic setting of the Burmese arc, Bengal Basin and adjacent regions (Santo, 1969; Fitch, 1970, 1972; Chandra, 1975, 1978; Verma et al., 1976; LeDain et al., 1984; Kayal, 1987, 1996; Mukhopadhyay and Dasgupta, 1988; Chen and Molnar, 1990; Nandy and Dasgupta, 1991; Holt et al., 1991; Ravikumar and Rao, 1995; Satyabala, 1998). Detailed investigations on regional geology, morphotectonics and their relation to gravity anomalies in this region have been made by Verma et al. (1976), Nandy (1986) and Mukhopadhyay and Dasgupta (1988). Based on the morphotectonic trends and the seismicity pattern, Mukhopadhyay and Dasgupta (1988) divided the Burmese arc region into four sectors. Sector I corresponding to the Naga hills area in the north to Sector IV covering Arakan-Yoma region of Coastal Burma in the south. Based on detailed seismotectonic evaluation of Northeast India, Kayal (1996) identified five broad tectonic zones viz., the Himalayan collision zone, Indo-Burman subduction zone, the Syntaxis zone (Mishmi hills), Shillong Plateau and Assam valley area, and the Bengal Basin-Tripura fold belt area. Studies by Nandy and Dasgupta (1991) and Kayal et al. (1993) reveal that the Kopili-Bomdila fault zone is seismically the most active region in the eastern Himalayas with many of the events displaying strike-slip motion along the NW nodal plane oblique to the Himalayan trend. East of the Indo-Burman ranges, the Sagaing fault in the back arc region is seismically very active. LeDain et al. (1984) and Ni et al. (1989) suggested that most of the right-lateral slip of India is accommodated along the Sagaing fault. Further east, the Shan Plateau belonging to the Asian plate is also seismically active and intraplate deformation in this region is distributed over several left-lateral faults (Haines and Holt, 1993).

Fault-plane solutions of about 50 events were published by different authors (e.g. Fitch, 1970; Rastogi, 1973; Tandon and Srivastava, 1975; Verma et al., 1976 a and b; Mukhopadhyay, 1984, Dube et al., 1986; Mukhopadhayay and Dasgupta, 1988) using the polarities of P-waves reported in published bulletins. These solutions were compiled by Kayal (1996). These solutions are annotated in the depth sections as N (Normal faulting), T (Thrust faulting) and as S (Strike slip faulting), which fairly explain the Benioff zone earthquakes and the overriding plate earthquakes. Although some of these solutions are fairly consistent with the CMT solutions, it is difficult to

assess the quality of these solutions because of inconsistent readings and often unreliable bulletin data (Chen and Molnar, 1990). Chen and Molnar (1990) presented 17 reliable fault-plane solutions for the region after re-analyzing the source parameters using the original seismograms and taking care of necessary corrections.

The Indo-Burma earthquake of August 6, 1988 (7.5) is the largest earthquake that occurred beneath the Indo-Burman ranges in recent years. The fault-plane solutions obtained by Chen and Molnar (1990) is almost similar to the CMT solutions. The solution is a mixture of reverse and strike-slip faulting showing a NNE-SSW compressional stress. The earthquake events of May 31, 1973 and May 6, 1984 occurred close together, both having similar magnitude ~ 5.7 and depth 57 $\pm$ 5 km, and show almost similar solutions with large strike-slip components. Similar fault-plane solutions are also obtained for the events of May 29, 1970, December 29, 1991 and May 21, 1975 having magnitudes ~ 5.1 – 5.6, focal depths 40-60 km in the Indo-Burman ranges. The solution for the earthquake of February 18, 1965 (M 5.4), which shows a large component of normal faulting, is the only solution that differs from the oblique thrust faulting observed for the other events beneath the Indo-Burman ranges.

Two events of December 27, 1968 (M 5.1) and February 02, 1971 (M 5.4), that occurred beneath the Bengal Basin show large component of thrust faulting with NNE-SSW compressional stresses (Chen and Molnar, 1990). These two events occurred at a depth of 30-40 km, below the folded sedimentary rocks, possibly in the lower crust. None of the nodal planes of the solutions are parallel to the trend of the local NNE thrust/folds in the area. The Cachar earthquake of December 30, 1984 (M 5.8) occurred at shallower depth, is a damaging earthquake that occurred in the Tripura-Mizo fold belt in recent years, which shows a near thrust faulting on either of the two moderately dipping nodal planes that strike northwesterly. Again the strikes of the nodal planes are oblique to the local NNE trend of the Indo-Burman ranges. Ni et al. (1989) reported 15 reliable fault-plane solutions in the Indo-Burman ranges. Their solutions of five earthquakes that occurred within the Indian slab below the central and northern Burma ranges, show strike slip faulting with P-axes that plunge towards north-northeast, parallel to the oblique convergence.

Rao and Kalpna (2005) studied CMT solutions of 60 earthquakes (M 4.5- 6.5) within the subducted Indian plate in the Indo-Burma region for stress inversion. It

may be noted that the solutions show three types of faulting. There is a clear segregation of normal, strike-slip and thrust type solutions along the dipping slab; the thrust/reverse solutions are observed in the lower portion of the down going slab below 90 km and above that depth, normal and strike-slip solutions are observed. The stress inversion indicates distinct stress fields above and below 90 km along the subducted Indian lithosphere. In the upper part of the slab, the P and T axes trend NNE and ESE respectively, in conjunction with the ambient stress field of the Indian plate. These observations suggest that the upper part of the slab is governed by the NNE oriented horizontal plate tectonic forces, whereas the lower part is governed entirely by tensile forces due to gravitational loading on the subducted slab.

Whatever be the assessment of future earthquakes from such statistical analysis or analysis of past earthquake events it is unlikely to yield any tangible and useful result until in-depth knowledge of tectonic evolution, characteristics of individual and distinct tectonic domain is obtained through rigorous field geological and geophysical investigations. Therefore, an attempt has been made in this study to synthesize all available updated information on geology, tectonics, seismicity including those derived from the remote sensing techniques, source characterization of the faults in Surma valley and adjoining regions to bring out the tectonic activity of the region and to identify the seismogenic structures or earthquake source zones so that future research in these fields can be rightly oriented with identified thrust areas having the objective of mitigation of earthquake hazards in this highly vulnerable part of our country.

In spite of the facts already stated, Bengal Basin and Indo-Burma region in northeastern India remains to be highly vulnerable to earthquake hazards as revealed by the damages and destructions inflicted by the past earthquakes. It is also noted with alarm that people living in this region have almost forgotten their past experiences; thus they have built and are also building multi-storied brick masonry and RCC houses in many towns, especially in Shillong and Guwahati which were almost razed to the ground during the 1897 great earthquake, in place of conventional Assam type houses which are ‘earthquake proof’ to a great extent.

1.4 OBJECTIVES

The eastern extension of the Himalaya, a part of the great orogeny, covers sizable part of the northeastern region of India (NER). The complexity in geotectonic setup puts NER India to one of the most seismically active zone in the World. The seismic activity of NER India is well reflected by the occurrences of the two Great earthquakes of June 12, 1897 and August 15, 1950; and 20 large earthquakes occurred during the last 100 years. The NER India is being over thrust on two sides; in the North-Northeast along the eastern Himalayas and in the East-Southeast along the Naga Hills and the Arakan Yoma ranges.

The Surma Valley is subducting beneath the Indo-Myanmar collision. Because of plate subduction, earthquakes occur actively along the plate boundary, within the subducted plate and the shallow portion of the overriding continental plate. Besides, in Surma valley we find an area of folded sediments which is characterized by westerly convex, sinuous structural ridges and valleys. This basin is wider to the north and narrower to the south. Extraction of tectonic information from this particular region needs accurate hypocentral locations. Seismically active features such as faults and lineaments can be delineated from hypocenter distribution maps and better determination of seismogenic faults are dictated by precise earthquake locations of events. Prime and preliminary approach in earthquake seismology is the accurate phase picking of P- and S-wave arrivals for precise determination of earthquake locations. Application of various earthquake location techniques in the seismically active region of Surma valley of northeastern India provides useful constraints to select suitable algorithm of earthquake relocation on the basis of relative errors in travel time residuals, epicenter location and depth. Magnitude of the hypocentral region of an earthquake is greatly affected by the assumed values of Vp/Vs, the velocity ratio of the P- and S-waves in the calculation. Therefore, and also from the point of view that the existence of local complexity of the structure that makes a measure of distinct classification, the velocity ratio of P- and S-waves impart significant knowledge to best tackle the regional tectonics, since the region consist of

heterogeneous structures on a vast range of spatial scales including complications such as varying geology and tectonics. Sylhet (a NE-SW trending oblique lineament bordering Surma basin towards NW) and MAT (a NW-SE trending lineament within the Surma basin) are the two important faults that maybe responsible for seismicity in this basin. Therefore, true footprints of these complications may be arising from the study of these two faults that are recorded on broadband seismograms, facilitating the precise estimation of these heterogeneities subjected to lateral and vertical variations. The prime objectives of the present investigations are:

1. Precise location of hypocentral parameters to understand the seismicity pattern.
2. Precise estimation of travel time of P- and S-waves of local earthquakes in order to obtain preliminary estimates of crustal structure in the region. The region is devoid of a precise velocity model in spite of being seismically, geologically and geotectonically complex.
3. Source characterization study of some of the local events originated in the region to understand the characteristics of the source.

The first objective of this study is the precise earthquake locations. For this, initially the earthquakes have been located by the HYPOCENTER (Lienert et. al., 1986) using 1D velocity model. These events are relocated after number of trials and revisits to accurate phase picking from seismic waveform so that least error estimates are achieved, for e.g. least RMS value.

In order to achieve the second objective, an attempt has been made to determine P- and S-wave travel times to obtain the Riznichenko diagrams that depicts travel time of P as a function of epicentral distance (**+**). Simultaneously, in particular, variations of Vp/Vs versus depth are observed.

The third objective of the study is the determination of focal mechanism solutions to characterize the source of the earthquake events utilized in the study. These solutions also characterize the associated faults from which these earthquakes are originated. Besides determination of first motion P-wave solutions, a state-of- the-art waveform inversion technique is utilized.

1.5 OVERVIEW OF THE THESIS

The outcome of the entire study is organized into various chapters that deal with individual method applied for the data analysis in the study area. A brief account of the chapters is as follows.

Chapter-II contains the details on the tectonics and seismotectonics of Surma Valley and Indo-Burma Region. GIS based tectonics map of Mizoram and its vicinity has been delineated and discussed in this chapter alongwith the geology and structures of Mizoram.

Chapter-III briefly describes about the instrumentation part pertaining to seismic stations in the study area. A brief description of recorders, seismometers, digitization procedure is outlined here.

In general, the digital seismic stations are equipped with GPS time synchronized data acquisition system. The RETEK-72A series data acquisition system (M/S REFTEK, USA) and the GURALP Data Communication Module (M/S Guralp, UK) are coupled with 3-component broadband seismometers (e.g. CMG-40T).

Chapter-IV deals with the methodology for determination of precise hypocentral parameters and relocations in some cases. A total number of 2758 events recorded during 1982 to 2009 by the local seismic networks (RRL-Jorhat and NGRI-Hyderabad) are used in this study. Uncertainties involved in estimates in origin time are of the order of 0.03-0.1 for about 75% of the total events.

In Chapter-V, an attempt has been made to determine the travel time of P- and S-waves of the earthquakes originated in the study region. The principal technique involves the use of Wadati (1933) and Riznichenko (1958) diagrams. Both methods have had a long history of use as primary tools in earthquake location process. Both the techniques may be used for determining origin times, focal depths and velocities in the subduction zones, provides terms to account for the sphericity of the earth which is based on a linear relationship between the arrival times of P (Tp) and the time difference between P and S (Ts-Tp).

Chapter-VI deals with the crustal properties towards estimation of upper crustal velocity that is the variation of Vp/Vs along the crustal depth. This technique incorporates travel times of P- and S-waves as a prime input constrained by Snell's law subjected to crustal inhomogeneity. Data required for this velocity analysis using Wadati Riznichenko diagram are restricted to respective individual station.

Chapter-VII deals with the source characterization of the events associated with Sylhet and Mat faults and its vicinity. This characterizes the

respective faults which are seismically active in the region. Besides these, the direction of compressional and extensional axes are evolved both in horizontal and vertical domain. The map view of the focal mechanism solution could be obtained in several sections along Sylhet and Mat fault. From theoretical considerations it could be established that various parameters like seismic moment, moment magnitude, Green's functions and source time function can be estimated accordingly.

CHAPTER-II

GEOTECTONIC SETTINGS OF SURMA VALLEY

2.1. INTRODUCTION

Northeastern Region (NER) of India and its adjoining area is one of the most complex tectonic provinces in the world. The geographical boundary with latitude 22^{o}-30^{o}N and longitude 89^{o}-98^{o}E covers a considerable portion of NER, India. Plate boundary zone and the intraplate area are the main components of NER, India (Nandy, 2001). Among plate boundary zones, the broad tectonic domains are; (a) the Eastern Himalayan collision belt to the north, which includes the Trans-Himalayan Tethyan zone, the Andean type grano-diorite margin comprising the Main Boundary Thrust (MBT) and Main Central Thrust (MCT), (b) the Assam syntaxis zone where the Himalayan and Burmese arc meet the Mishmi Block. This zone is folded and trusted by the Lohit and Mishmi Thrust and, (c) the Indo-Burma subduction zone to the east where Indian lithosphere is believed to be subducting below Indo-Burman Ranges. The intraplate part of the region comprises the Shillong Plateau, the Mikir Hills and the Assam valley jawed between the Himalayan and Burmese arc, Tripura folded belt, Brahmaputra Valley and the intermontain depression of upper Assam (Curray et al., 1982). Besides these, Surma valley is also a complex tectonic feature comprising two active faults namely Mat and Sylhet faults. All these features with its complicated geotectonic setup as shown in Figure 2.1 (a and b) influence the NER, India to be seismically very active which can be revealed from smaller magnitude earthquakes that release sizable energy daily. During the last 100+ years the region experienced 20 large ($M \geq 7.0$) and two great earthquakes of June 12, 1897 ($M \geq 8.5$; Oldham, 1899) and August 15, 1950 (M=8.7 ; Poddar, 1950 ; Tillottson, 1953). These two great earthquakes have caused extensive destruction in the region.

Geological, tectonic, geophysical, seismotectonic and G.I.S. studies of the region are briefly reviewed in order to provide a context for the subsequent analysis and bring out the complexities of the nature of subduction which are also reflected by the seismicity and kinematics of plate motion of the Surma valley and its surrounding.

2.2 TECTONIC SETTINGS

2.2.1 Surma Basin

The Surma Basin on the western boundary of the Burma plate has undergone a complex history of tectonics. The Sylhet trough, a sub-basin of the Surma Basin, records transition from a passive rifted continental margin to a foreland basin on the margins of two mobile belts, the Indo-Burman ranges and the Himalayas (Johnson and Alam, 1991). Subsidence rate of the Sylhet trough accelerated in the Miocene epoch and increased 3-8 times from Miocene to Pliocene-Pleistocene time, mainly in response to continued encroachment of the Indo-Burman Ranges and south-directed overthrusting of the Shillong Plateau on the Dauki Fault. The time of uplift of the Shillong Plateau has been inferred from a coarsening of sediment lithology that starts in the Pliocene (Johnson and Alam, 1991) and the rate of vertical uplift has been estimated to be 2.5 ± 1 mm/yr by Bilham and England (2001). To the south of the Indo- Burma region is the Andaman spreading ridge where spreading is understood to have been initiated about 13 Ma during Mid-Miocene (Curray et al., 1979).

The Basin is bounded on the north by the Shillong-Plateau, east and southeast by the Chittagong-Tripura folded belt of the Indo-Burman ranges and to the west by the Indian Shield platform. To the South and Southwest it is open to the main part of the Bengal Basin. The topography is predominantly flat with some north-south trending ridges of twenty to several hundred meters elevation present in the northeastern border. The published bouguer anomaly map show gradual higher values (negative) towards the center of the basin. Mizoram lies in the Neogene Surma basin which is bounded by the post-Barail unconformity, subsequently faulted to the east; the E-W Dauki fault and NE-SW Disang thrust to the north and northeast; the NE-SW Sylhet fault and Barisal-Chandrapur high concealed below the alluvium of Bangladesh to the west and north-west (Nandy, 2001). To the south, the basin is extended up to the Arakan coastal area of Myanmar. Within this vast terrain of Surma valley lies Mizoram along with the states of Tripura, Cachar and Karimganj districts of Assam and western part of Manipur, Sylhet and Chittagong districts of Bangladesh and Arakan coastal zone of Myanmar. There are many NE lineaments/faults in Surma basin which show strike-slip displacement of the fold axes along them. Mizoram is

flanked by many oblique faults like Mat, Tuipui, Saitual and Sateek faults which run across the breadth of the state in NW directions and which are in turn traversed by smaller lineaments/faults at many places. Extensive work have been carried out on the seismicity of the Northeast but studies on the seismic status of Mizoram in particular is lacking.

2.2.2 Indo-Burman (Arakan-Yoma) Ranges

Indo-Burman orogen is an important geotectonic element in Assam-Arakan region. The presence of the subducted slab of the Indian plate, dipping east along the Burmese arc is well established (Das and Filson, 1975; Ravikumar, 1996, Satyabala, 1998). According to Mitchell and Mckerrow (1975), the evolution of the arc to a process of eastward subduction of Indian plate lies to the west of Myanmar folded belt.

Indo-Burmese ranges are believed to have been formed during Oligocene as a result of eastward subduction (Brunnschweiler, 1966). The bulk of these ranges are composed of thick turbiditic sequences of Cretaceous to Upper Eocene shales and sandstones, deposited on the oceanic crust to the west. The structural trends in these ranges change from NE-SW direction in the Naga hills to NW-SE direction along the Arakan Yoma and Chin hills. To the east of Eastern Boundary Thrust (EBT), there is a 200 km wide and 1400 km long Palaeogene and Neogene Central Myanmar sedimentary basin. This basin is bounded by north-south San-Sagaing fault to the east and the Sino-Myanmar highland. The study by various workers based on seismicity data suggests that the Indian plate is actively subducting below the Burmese plate as indicated by well defined Benioff zone (Das and Filson, 1975; Mukhopadhyay and Das Gupta, 1988; Rai et al., 1996 and Satyabala, 1998 etc.).

2.3 SEISMOTECTONICS IN AND AROUND SURMA VALLEY

Based on the distribution of epicenters, fault plane solutions and geotectonic features, northeastern region can be divided into five seismotectonic zones. There are Eastern Himalayan collision zone, Indo-Myanmar subduction zone, Syntaxis zone of Himalayan arc and Burmese arc (Mishmi Hills), Plate boundary zone of the Shillong Plateau and Assam Valley and Bengal Basin and Plate Boundary Zone of Tripura

Mizoram fold belt (Kayal, 1996; Nandy, 2001). Tectonic setting of Surma valley is shown in Figure 2.2. Following is the brief description of these zones.

2.3.1 Bengal Basin and Tripura-Mizoram Fold Belt

Situated in the western foreland part of the Indo-Burman orogenic belt is the Tertiary Surma Basin. The Shillong Plateau and the Sylhet Trough bound the Surma Basin in the north and, at its eastern limits, are the nearly north-south fold belts of Tripura and Chittagong Hills. The Shillong Plateau has a maximum elevation of about 2 km and is bounded to the south by the Dauki Fault. The Dauki Fault forms the contact between the Shillong Plateau and the Sylhet trough. The eastern and northern parts of the Bengal Basin have been subjected to more structural modification than the western and southern parts and a similar distribution applies to recorded seismicity (Morgan and McIntire, 1959). A number of high angle thrust faults have been recognized across the Chittagong-Tripura hills (Khan, 1991). Folds and thrusts in the Bengal Basin are also seen on the Landsat imagery (Le Dain et al., 1984; Nandy, 1980) and field investigations reveal that not only Early Tertiary rock but Pliocene and Pleistocene sediments have also been involved in the folding and underthrusting. North-South trending folds that are uplifted in the Chittagong-Tripura fold belt plunge northward into the Sylhet trough subsurface (Johnson et al., 1991) and the folds decrease in amplitude westward and are not present west of about 91^0, where the Sylhet fault trough merges with the main part of the Bengal Basin. Within about 40 km south of the Dauki fault, the north-trending folds in the subsurface of the Sylhet trough are deflected to a northeast trend. Marine seismic surveys show that the beds close to the seafloor are deformed over anticlinal structures without any thinning or wedging of beds over the structures (Khan, 1991). The maximum thickness of the sedimentary section in the basin is more than 10 km and it thickens further to the east to 20 km or more (Ganguly, 1997).

The main tectonic domains in this zone are E-W trending Dauki fault (which demarcates the boundary between the Meghalaya plateau and Bengal basin), NE-SW trending Sylhet fault, Gumti fault, NE-SW Hail-Hakula lineament, N-S Jamuna fault, NW-SE Padma lineament, NNW Tista fault and NW-SE Mat and Tuipui faults.

2.3.2 Indo-Myanmar Subduction Zone

The Indo-Burma subduction boundary is highly oblique to the direction of relative velocity of the Indian tectonic plate with respect to the Eurasian plate. Burma (Myanmar) is situated in a complex tectonic zone with a hyper-oblique subduction at its western boundary, a dextral transform fault on the eastern boundary, the Mishmi thrust in the north acting as a buttress and the spreading Andaman ridge in the south. The area has features of active subduction zones such as a Wadati-Benioff zone (WBZ) of earthquakes, a magmatic arc, thrust and fold belts. Although this region is seismically active, fault plane solutions of this region do not show underthrusting at the subduction interface and the P axes are oriented nearly parallel and not perpendicular to the trend of the thrust and fold belts of the region (Le Dain et al., 1984; Chen and Molnar, 1990). On this basis, even though there is no other independent evidence of a recent change in the stress regime of the Indo-Burma region, there is almost a consensus that the subduction in this region is no longer active (e.g., Guzman-Speziale and Ni, 1996). However, the region has seismicity features comparable to other active subduction zones. For example, an examination of the relationship between the Wadati-Benioff zone geometry and the principal axes of the CMT solutions showed that the degree of clustering of the T axes in the down-dip direction is comparable to that in active subduction zones around the world (Satyabala, 1998).

Seismotectonics of the region has been the focus of several studies. Early work (e.g., Fitch, 1970; Rastogi et al., 1973; Molnar et al., 1973; Chandra, 1975; Saikia, 1986) recognized an eastward dipping zone of seismicity consistent with subduction along the Burma Arc. Le Dain et al., (1984) studied active faulting and tectonics of the region by integrating information derived from Landsat imagery, historical seismicity and fault plane solutions of earthquakes from 1964 to 1977, and information available on Cenozoic and Quaternary tectonics of the region. Landsat images reveal roughly parallel, north-south trending folds often vergent to the west and with a wavelength of a few kilometers between 20-22^{0}N near 94^{0}E implying east-west shortening (Le Dain et al., 1984). Chen and Molnar (1990) found that the earthquakes beneath the northern Indo-Burman ranges define a gently dipping ESE zone with a depth of 30-45 km beneath the Bengal basin and of 40-90 km beneath the ranges. They inferred that these earthquakes may have occurred within the subducting Indian lithosphere and not at the interface between the subducting and overriding plates because the P axes of these earthquakes are parallel to the north-south trending

seismic zone and the north-south trending folds of the Indo-Burman ranges. On this basis Chen and Molnar (1990) concluded that either recently or in geologic time (since 1 Ma) the orientation of maximum compression may have changed dramatically, or, more likely, the deformation in the Indo-Burman ranges is decoupled from that in the underlying Indian plate while the northward movement of the ranges must be accommodated along the Sagaing and other faults farther east. The great Assam earthquake of 1950, which occurred in the eastern Syntaxis bounding the Burma plate in the north, is understood to have occurred on a gently NNE dipping thrust fault (Molnar and Pandey, 1989).

This is a highly seismic zone in which about 10 large earthquakes ($M \geq 7.0$) have occurred during the last 100 years. The depth of focus of this zone goes upto 200 km south of 26^{o}N latitude, and north of this, the depth becomes lesser. This may be due to the subduction process, south of this latitude and collision process north of it (Mitchell and Mc Kerrow, 1975; Kayal, 1987, 1996). The structural trend in this zone swings from NE-SW in the Naga Hills to N-S along the Arakan-Yoma and Chin Hills and the main discontinuities in this zone are Naga thrust and Disang thrust.

2.4 GIS BASED TECTONIC MAP OF MIZORAM AND ITS VICINITY, SURMA VALLEY

In order to have a comprehensive idea of geologic and tectonic settings, it is essential to prepare a tectonic map based on geological field observations. Some parts of Surma valley, NER, India are inaccessible and it is difficult to conduct geological field surveys in these places. Geological Survey of India (GSI) made an attempt for the first time to produce the regional geology of the entire Northeast India and the adjoining regions with the help of remotely sensed data available as satellite imagery studied in conjunction with available geologic maps of the area (Nandy, 2001). The satellite imageries were generated by NASA, USA and are obtainable through EROS data center, USGS. All morphotectonic lineaments were drawn and their significance was evaluated later by comparing the available information on ground truth.

With the advancement of technology and information available in the internet, high quality imageries are available under certain terms and conditions for personal use and research purposes. Many of the data available online are developed by reputed private and government organizations like NASA, Google Inc., etc. The high resolution satellite imageries are generated using sophisticated instruments and

advanced techniques which make them very reliable and précise and can endure extreme close-up. The GIS maps used in this chapter are constructed using imageries taken from NASA World Wind and Google maps available free of cost for research purposes.

The GIS maps and satellite imageries depicted in this chapter are obtained from Google map (Figs. 2.1b, 2.3, 2.4) and World Wind (Fig. 2.5). Google Maps (formerly Google Local) is a web mapping service application and technology provided by Google, free (for non-commercial use), that powers many map-based services, including the Google Maps website, Google Ride Finder, Google Transit, and maps embedded on third-party websites via the Google Maps API. It offers street maps, a route planner for traveling by foot, car, or public transport and an urban business locator for numerous countries around the world. Google Maps satellite images are not in real time due to security reasons.

Google Maps uses a close variant of the Mercator projection, so it cannot show areas around the poles. Google Maps provides high-resolution satellite images for most urban areas in the United States (including Hawaii, Alaska, Puerto Rico, and the U.S. Virgin Islands), Canada, and the United Kingdom, as well as parts of Australia and many other countries. The high-resolution imagery has been used by Google Maps to cover all of Egypt's Nile Valley, Sahara desert and Sinai. Google Maps also covers many cities in the English speaking areas. Not all areas on satellite images are covered in the same resolution; less populated areas usually get less detail. Some areas may be obscured by patches of clouds.

With the introduction of an easily pannable and searchable mapping and satellite imagery tool, Google's mapping engine prompted a surge of interest in satellite imagery. Sites were established which feature satellite images of interesting natural and man-made landmarks, including such novelties as "large type" writing visible in the imagery, as well as famous stadia and unique geological formations. With the addition of contour lines to the terrain view on April 2, 2008, the application of Google map has increased manifold, especially to the community of researchers. The coordinates are reliable enough and the quality of the map is of high resolution. The GIS maps used in this chapter (Figs. 2.1b, 2.3 and 2.4) are developed using Google terrain map after careful merging.

World Wind is an open source (released under the NOSA license) virtual globe developed by NASA and the open source community for use on personal purposes. Old versions need Microsoft Windows but the more recent Java version, World Wind Java, is a cross platform and provides a suite of demo applications. The World Wind Java version was awarded NASA Software of the Year in November 2009 for 2010. The program overlays NASA and USGS satellite imagery, aerial photography, topographic maps and publicly available GIS data on 3D models of the Earth and other planets.

World Wind was released for the first time in 2004 by NASA. The latest version (1.4), developed mainly by open source community members from World Wind Central/Free Earth Foundation, had its premiere on February 14, 2007.

Apart from the Earth there are several worlds in World Wind: Moon, Mars, Venus, Jupiter (with the four Galilean moons of Io, Ganymede, Europa and Callisto) and SDSS (imagery of stars and galactics). All these worlds are available in the File menu.

Users can interact with the selected planet by rotating it, tilting the view, and zooming in and out. Five million place names, political boundaries, latitude/longitude lines, and other data can be displayed. World Wind provides the ability to browse maps and geospatial data on the internet using the OGC's WMS servers (version 1.4 also uses WFS for downloading place names), import ESRI shapefiles and kml/kmz files. This is an example of how World Wind allows anyone to deliver their data. The resolution inside the US is high enough to clearly discern individual buildings, houses, cars (USGS Digital Ortho layer) and even the shadows of people (metropolitan areas in USGS Urban Ortho layer). The resolution outside the US is at least 15 meters per pixel.

Microsoft has allowed World Wind to incorporate Virtual Earth high resolution data for non-commercial use. World Wind uses digital elevation model (DEM) data collected by NASA's Shuttle Radar Topography Mission. This means one can view topographic features such as the Grand Canyon or Mount Everest in three dimensions. In addition, World Wind has bathymetry data which allows users to see ocean features, such as trenches and ridges, in 3D. Many people using the applications

are adding their own data and making them available through various sources, such as the World Wind Central or blogs mentioned in the link section below. All images and movies created with World Wind using Blue Marble, Landsat, or USGS public domain data can be freely modified, re-distributed, and used on web sites, even for commercial purposes.

Figure 2.5 is prepared using NASA World Wind version 1.3, the program overlays NASA and USGS satellite imagery, aerial photography, topographic maps and GIS data on 3D models of the Earth. In this digital elevation model (DEM) map, both Sylhet fault in Bengal Basin and Mat fault in the Tripura Mizo fold belt are visible which are demarcated by red lines.

The faults and lineaments present in Figure 2.3 are digitized separately using a software package, MAPINFO version 5.5. For digitization it is essential to define the position of geographical objects relative to a standard reference grid, which is called Geo-coding. Since the tectonic map is well demarcated by geographical coordinates (Latitudes and Longitudes), it is easier to Geo-code the map. After Geo-coding minimum 4 reference points, accurate information regarding geographical coordinates of all the ungeocoded parts of the maps can be obtained. After the process of Geo-coding any desired fault and lineaments can be extracted into a file having ASCII format. All the digitized faults and lineaments are combined into a single layer in MAPINFO and superimposed onto the base map as shown in Figure 2.3a, thereby obtaining the modified tectonic map (Fig. 2.3b) of the region. The faults and lineaments in Figure 2.3b, present in the Tripura-Mizo fold belt, which are observed from the high resolution GIS map are marked as A, B, C, D, E, F, G, H, I and J. It appears that these labeled faults and lineaments are not identified nor describe earlier.

The folded structure of the Arakan Yoma and the Tripura ranges are found at the junction of two moving continental plates (i.e. Indian and Burmese Plates). It is an actively deforming transgressional plate margin and associated with fold-thrust belt and is generally referred to as the Indo-Burmese fold-thrust belt or the Arakan-Yoma Orogen. This structure comprises of early Miocene and late Paleocene clastic sediment of Surma Group. The northern and eastern parts of the basin are far more complicated than the southern and western portions. The relief and complexity increases towards the east. The anticlines are commonly faulted. The folds decrease in

amplitude westward, and are not present west of about 91°, where the Sylhet trough merges with the main part of the Bengal Basin. The folded belt of Mizoram is a part of Tripura-Mizo folded belt which can be divided into a frontal sub-belt consisting of narrow box like anticlines separated by wide flat synclines of Tripura and South Assam and inner mobile belt consisting of tight linear folds of Mizoram and West Manipur**.** It comprises a series of sub parallel arcuate elongated doubly plunging folds arranged en-echelon with asymmetric and tight anticline and broad syncline and trending in an average North–South direction with a slight convexity towards the west. An accretionary prism best characterizes the tectonic setting of the region. The major outcrop of stratigraphic succession in Mizoram comprises of Upper and Middle Bhuban Formations.

The area is dominated by north-south trending structural systems, the prominent features is the NW- SE trending Mat fault, which cut across the entire area and divides into two distinct sections (Figs. 2.3 and 2.5). It can be easily identified when observed in satellite imageries from GIS maps obtained from NASA World Wind and Google Terrain maps. A conspicuous valley exists where the fault cuts through (Figs. 2.6 and 2.7). It is rather easy to identify this feature in the field as the fault strike in NW-SE direction, which is against the regular trend of the ridges i.e., in N-S direction. A river called 'Mat' flows along the fault scarp in the valley between the towns of Serchhip and Thenzawl (Fig. 2.8) from which the name, Mat fault is adopted. Almost all of the anticline in the northern part of the section has slightly west-vergent structural geometries with steeper western limbs than eastern limbs indicating an overall top-to-the-west direction of shear and tectonic transport during development of the structures. From Mat fault to the southern side, the west-vergent asymmetry of folds is less pronounced. Most of the folds within the southern part of the section appear to be symmetric, upright, sub-vertical folds. A number of the anticlines are doubly-plunging structural uplifts. Mizoram, as being a part of Bhuban formation of Surma Group and Tipam Group belonging to Miocene - Pliocene age of Tertiary Period, comprises of about 99% of sedimentary rocks. The structures are very complex and are traversed by repetitions of anticlines and synclines.

CHAPTER-III
SEISMIC INSTRUMENTATION

3.1 INTRODUCTION

Quantitative analysis of seismic waves generated by a source during an earthquake requires the time domain instrumental record of the earth's vibration. The instrumentation is designed in such a way that it must be able to detect the transient vibrations within a moving reference frame (since the instrument moves with the earth as it shakes) and operate continuously with a very sensitive detection capability with absolute timing so as to get the ground motion as a function of time. In order to get actual ground motion, it must have known linear response to ground motion (i.e. instrument calibration). This type of instrumentation used in earthquake seismology is known as seismograph while the time history of the ground vibration recorded by it is known as seismogram. The fundamental components of a seismograph are the sensor, recorder, timing system and power supply. In digital seismograph, a digitizer is an essential component for converting the analogue signal to digital format. Seismic sensors are the mechanical or electromechanical assemblies that convert earth motion into electrical signals which can be digitized with the help of a digitizer and stored in a separate storage device. An assembly of digitizer and storage device together is known as seismic recorder.

Many successful seismic recorders and sensors have been developed over the last century. Almost all the sensors are designed based on the concept of an inertial pendulum (Richter, 1958). The early seismic instrument such as seismoscope existed in China as early as 132 AD, which can only indicate the occurrence and direction of an earth vibration. Out of different types of seismic instruments, the Wood-Anderson seismometer is used to define local Richter scale magnitude of an earthquake (Richter, 1958). Developments of instruments to record earthquake have been remarkable in view of timing accuracy, frequency of ground motion, and detection thresholds of seismic station networks. During the last ten years, recording devices based on digital technology have completely replaced the old analogue systems. This chapter deals with the brief description of the analogue and digital instrumentation of the seismic stations used for the present study.

Considering the high seismic activity in NER of India and the past history of destructive earthquakes, North East Institute of Science & Technology, Jorhat (RRL-J) collaboration with National Geophysical Research Institute, Hyderabad (NGRI) established progressively 14 vertical component and 2 three component seismic stations equipped with short period instrumentation in the year 1982. In the beginning, the seismic stations were equipped with analogue recording system. In the year 1991 two Digital Telemetered seismic station network were established in the region with central recording units located at Jorhat and Tezpur in Assam. Finally most of the seismic stations are upgraded to GPS time synchronized digital broadband seismic station since 2001. In the recent past, Gauhati University (GAU), Manipur University (MAN) and Mizoram University (AZL) have established digital broadband seismic stations for continuous monitoring of the seismic activities in the region. The locations of the seismic stations (Table 3.1) are shown in Figure 3.1. The data from these stations has been used for the present study.

This chapter deals with a brief description of instrumentations involved in earthquake monitoring in NER, India. Development of response curve to existing digital recording system is a part of this study.

3.2 SEISMOGRAPH

A seismograph consists of a sensor or seismometer installed vertically over an RCC pier constructed on a solid hard rock in order to respond to the ground motion. The pier is usually separated by about 6-inch gap all around it and filled with heat insulating material like dry sand, saw dust etc, which enables the propagation of minimum level of noise. The sensor consists of a mass with the attachment of coil suspended in a magnetic field. Due to an earthquake there will be a relative movement between the mass and frame of the seismometer that is induced as an electro motive force (e.m.f.) in the coil. The e.m.f. generated in this way is fed to the recording system after undergoing attenuation or amplification with the help of attenuation /amplifier circuitry system. In vertical component seismograph, mass of the sensor moves up or down relative to the recorder. The mass continues to move up and down for some time, like a free pendulum, even after the ground ceases to move. To avoid this, a damping arrangement is made, so that it responds only to the ground movement. Using the same principle, the horizontal component of the ground motion

can also be recorded with a suitable arrangement by making the pendulum to move like a two-way swing door. In order to get a three-dimensional representation of the ground motion, it is necessary to record it in three orthogonal (perpendicular) directions, generally, in vertical (Z), north-south (N) and east-west (E) directions. Depending on the type of recorder, there are mainly two types of seismographs: analogue and digital seismograph.

3.2.1 Analogue Seismograph

In case of analogue seismograph the seismometer senses the ground vibrations and the analogue signals are recorded continuously on a paper. All analog paper recorders are based on the principle of recording on a rotating drum and a pen which moves along an axis parallel to the rotating axis to provide a continuous trace for the whole recording period, usually 24 hour. The time marks are typically generated at each minute, hour and 24 hour and have different length. The time mark generator can usually be synchronized with an external time reference (e.g. time signal relayed by National Physical Laboratory (NPL), New Delhi). Analogue seismic station comprises various components e.g. recorder and seismometer etc.

3.2.1.1 Recorders

There are various types of analogue recording systems depending on recording media e.g. the ink recording, recording on a smoke paper, heat sensitive paper and photographic paper etc. Previously in some seismic stations the conventional photographic recording was used which now a days is getting obsolete because of high recurring costs involved in photographic charts. Portacorders and Helicorders are most commonly used in the analogue seismic stations in NER India.

3.2.1.1.1 Portacorder

The Portacorder is a visible recording system. It is a complete self contained, battery-powered unit containing an amplifier, a smoked drum recorder, an accurate chronometer and internal batteries. Four high-cut and three low-cut filter positions are selectable by switch. Portacorder of model RV-320 operates on two batteries each having 12 volt and 3 amp hours, whereas only one battery is required for the model RV-320B to ensure less power consumption. The signals are recorded on smoked paper that is changed 24 hourly basis. The drum speed is generally 60 or 120 mm/min

and second marks are superimposed on the trace to provide precise timing. Standard radio time code is directly recorded on the seismograms twice a day, i.e., at the beginning and the end of each record, to provide absolute time. The length of a second on the traces is 2 mm. P- and S-wave arrivals on the traces are timed to one hundredth of a second by use of a microscope. Therefore, the P- and S-wave readings have an accuracy of 0.01 sec.

3.2.1.1.2 Helicorder (RV-301B)

In some seismic stations the rectilinear writing model RV-301B of Helicorder (M/S Teledyne Geotech make) is used which provides a versatile system that produces a distortion free seismogram. It is a drum recorder for producing traces of analogue data on a set of heat sensitive paper. The trace is a helix that translates with each turn of the drum. A variety of chart speeds can be chosen, permitting as much as 72 hours of continuous data to be recorded on a single sheet of paper. The Helicorder, Model RV-301B may be supplied with 1, 2 and 3 recording channels. Helicorder is powered from precision 115 V (AC), 50 Hz power coming from the TG-120 timing system so that drum speed is very stable. The time marks are placed on records via TG-120 timing system and the Helicorder amplifiers. The recording speed and the translation rate are generally 60 mm/min and 1mm/revolution respectively.

3.2.1.1.3 MEQ-800

One of the most commonly used analog field recorders is the Sprengnether MEQ-800 which can record on either ink or smoked paper. It is a self-contained unit with amplifier, helicorder and internal clock. This recorder gives instant display of recording in the field without the use of computers and it has a very low power consumption of 0.4 Watt.

3.2.1.2 Seismometer

Most of the analogue seismic stations are equipped with three component seismometers. The seismometers used in analogue seismic stations are as discussed below.

3.2.1.2.1 S-13 Seismometer

The Teledyne Geotech model S-13 seismometer is a portable short period seismometer which provides high sensitivity, stable and reliable output. The seismometer may be operated in either the horizontal and vertical positions and the period is adjustable from 1.33 to 0.91 second (0.75 to 1.1 Hz). The cover and electrical connections are watertight so that the instrument may be submerged in up to 100 feet of water without leakage. All operational adjustments for the period, mass position and instrument leveling are external to the instrument. The seismometer is equipped with an electromagnetic calibrator, which consists of a calibration coil fixed to the instrument frame and a permanent magnet attached to the mass. The seismometer can give stable output within the temperature range -51^{o} to 60^{o}C.

3.2.1.2.2 Benioff Seismometer

Benioff seismometers are of reluctance type. The reluctance seismometer constructed by Benioff uses a transducer, which consists of permanent magnet, pole pieces of soft iron, armature of soft iron and coils. The magnet is attached to the seismometer pendulum, while the armature and the coils are fixed to the frame or vice-versa. Upon motion of the magnet in relation to the armature, the air gaps between the armature and the pole pieces of soft iron are varied and thus the magnetic reluctance. The reluctance changes with a corresponding variation of the magnetic flux through the magnetic circuit. Consequently an electromotive force is induced in the coils and this is then recorded via a galvanometer. When an earth vibration reaches the instrument site, the frame or the body of the seismometer resting on the ground vibrates with it, but the mass of the seismometer, hanging loosely from the support due to the property of inertia, tries to remain stationary. Thus, relative movements are created between the frame of the seismometer and its mass. Electromotive force is induced in the transducer due to the relative motion.

3.2.1.3 Timing System

Timing system TG-120 is used to provide accurate date/time stamps for the analogue data received from the field stations. Precision timing marks for the Helicorders are generated by the TG-120 timing system. This instrument features a temperature compensated crystal controlled clock and a built-in comparator that provides a LED read out of the exact difference in time between a radio time signal

and the clock time. If the drift does not occur, it is quickly adjusted by pressing a panel-mounted button until the read out difference is cancelled. The TG-120 also has a button in power amplifier that generates precision 115-VAC, 50Hz power for the Helicorder drum motors. The power amplifier has an output of 50VA and therefore auxiliary power amplifiers are sometimes supplied to supply the power for additional recorders.

The time maintained in most of the analogue stations is Coordinate Universal Time (UTC); the time signals relayed by National Physical Laboratory (NPL), New Delhi are taken as the reference of time standard and the accuracy is 0.1 sec.

3.3 DIGITAL SEISMOGRAPH

In analogue seismograph station there are some difficulties concerning the recording and storage of analogue records. These difficulties have been removed by replacing the analogue systems with recent digital equipments. The technological progress in digital signal processing, data storage techniques and highly integrated digital circuits leads nowadays to several instruments available, that all fulfill the basic requirements of a seismic recording instrument and offer several more advanced features as well.

In general, the digital seismic stations in NER, India are equipped with GPS time synchronized data acquisition system. REFTEK-72A series data acquisition system (M/S REFTEK make, USA) is used in these stations coupled with 3-component seismometers (e.g. CMG-40T, CMG-3ESP and CMG-3T etc.). The digital stations are operated both in continuous and event – trigger mode and recorded at a rate of 100 samples per second. In order to avoid the contamination of frequencies higher than Nyquist frequency of a spectra (aliasing effect) a sharp (higher order) low pass filter with corner frequency 50 Hz is applied. The data acquisition systems and different types of seismometers used in these stations are discussed below:

3.3.1 Data Acquisition System (DAS)

Almost all the digital seismic stations of NER, India operated by RRL-J and NGRI-H are equipped with REFTEK 72A series Data Acquisition System (usually 72A-07 and 08 type). REFTEK 72A series data acquisition system is a versatile, portable, microprocessor based high-resolution instrument for unattended field use.

The power is generally supplied by 12-volt batteries, which are charged either by electricity or by solar panel. The 72A series DAS can operate unattended for more than a month when power is supplied continuously by a 12-volt battery. REFTEK 24-bit analogue-to-digital (A/D) converters are used in both the 72A-07 and –08 types. The REFTEK data acquisition system configured for 3 channels with A/D conversion resolution 24 bits can record through as many as eight different data streams simultaneously within the frequency band 0-250Hz at the rate 1-1000 samples per second (SPS). A 24-bit digitizer can count from –8388608 (-2^{23}) to 8388608 (2^{23}) and gives a dynamic range of 138 db (Bhattacharya et al., 2000). Higher dynamic range of the digitizer gives the advantage to record the ground motion from very small magnitude earthquake as well as large magnitude earthquakes without saturation.

3.3.1.1 REFTEK 72A-07 DAS

Refraction Technology (Dallas, USA) produces three main variants of the baseline 72A-07 DAS. The first model of 72A-07 has a disk but no GPS board is available. The other modified systems are 72A-07/ND (No disk), 72A-07/G/ND (with a GPS board and no disk) and 72A-07/G/1000 (or 2000) for those units with both a GPS board and a disk drive. The minimal functional DAS consists of an input signal analogue to digital (A/D) converter board (RT373), a central processor unit (usually RT319), communication board (RT371) and a DC power converter board (RT344). The data input accommodates upto three channels and the analogue input data is digitized at 24-bit resolution. There are ten options for selecting different sampling rates. The gain setting is programmable at either unity or 30 dB on each active channel. The central processing unit (CPU) board has 1MB RAM; half is used by the system and half is available to store data. A 12-volt DC power supply is required for proper functioning of the DAS and the peripheral device like the disk. A crystal oscillator in the CPU provide time to an accuracy of better than 0.5 □□Sec / Sec. This clock is synchronized with an external GPS clock.

3.3.1.2 REFTEK 72A-08 DAS

This is a high resolution data acquisition system configured for three channels of 24-bit recording. The 72A-08 (model-3) has only three channels of 24-bit whereas 72A-08 (model-6) has six 24-bit channels and uses two A/D converter board (RT-373). Maximum internal data storage of 12 MB is available. External data recorder

can be used in 72A-08 DAS. Data is collected based on user defined parameters using DOS based control interface like Field Setup Controller (FSC) software. In this data acquisition system user can set up maximum of eight data streams for simultaneous recording with different sampling rates. This is possible because it has digital signal processor (DSP). The A/D converter operates at 1000 SPS and the digital signal processing continuously samples at 1000 SPS then filters and decimate its output at sampling rate below 1000 SPS. Input parameters are set through data acquisition software so that an automatic data transfer to the external storage device take place when RAM is approximately 70% filled. Data is transferred over the SCSI bus to an external disk recorder. An internal crystal oscillator provides real time to 5 x 10^{-7} seconds accurately, which is synchronized with REFTEK-111A Global Positioning System clock.

In most of the seismic stations, two data streams are used; one records in continuous mode and the other stream records in trigger mode at the rate of 100 samples per second. In the trigger mode recording is based on the ratio of short – term average (STA) to long-term average (LTA) of the recorded signal. Timing at which this ratio exceeds a predefined threshold value is called trigger time. Recording starts a few second (set by pre-event time) before the trigger time which continues till the signal amplitude restores to the background value, after the STA/LTA ratio falls below the threshold value (Refraction Technology, 1996).

3.3.2 Storage Device

A 3-component digital seismograph, recording continuously at a sampling rate of 100 SPS per channel with ADC resolution of 24 bits (3 bytes) would require a storage capacity of -

3(*comp*) x 100 (*SPS*) x 3 (*byte*) x 24 (*hour*) x 3600 (*sec*) = 77.76 MB per day.

The REFTEK series data acquisition system records the data in REFTEK recording format (Refraction Technology, 1996). DAS units format data blocks into 1,024-byte packets and store them in random access memory (RAM). Without altering the format, DAS units move the packets to external disk e.g. REFTEK 72A-05 Disk recording subsystem (SCSI hard disk) over a SCSI port. This type of SCSI hard disc used for storing data has storage capacity of 4GB. Data in Reftek format is converted into the required format of data analysis software packages like PC-SUDS (Seismic

Unified Data System ported to 16-bit DOS platform created at the U.S. Geological Survey), SEISAN (Seismic Analysis Software; Havskov and Ottermoller, 2001) and SAC (Lawrence Livermore National Laboratory's Seismic Analysis Code).

3.3.3 Seismometers

Different seismometers used in the digital seismic stations are briefly described.

3.3.3.1 CMG-40T

The CMG-40T (M/S Güralp Systems) is a lightweight broadband seismometer consisting of three sensors in a sealed case to measure north-south, east-west and vertical ground motion simultaneously. Sensor elements are designed so that no mechanical clamping is required. The sensor does not have to be leveled or centered as long as the base is within 3^o of horizontal. The response of the seismometer is flat to velocity for the frequency band 0.033-50Hz (30 sec). The seismometer draws a nominal current of 48 mA from a 12-volt power supply, when in use. The seismometer can operate over a wide temperature range (-10^oC to $+75^oC$). However the sensor mass is sensitive to fluctuation in local temperature.

3.3.3.2 CMG-3ESP

The CMG-3ESP is a 3-component seismometer of class Broadband having three sensors in a sealed case to measure north-south, east-west and vertical component of ground motion. This seismometer is suitable for local, regional and teleseismic recording. Each sensor is sensitive to ground vibrations in the frequency range 0.003-50 Hz. These instruments do not require precise leveling of the sensor package to obtain long period mechanical response and can be used without leveling the sensor case up to □□2.5 degrees of tilt. A microprocessor controlled remote centering is provided. There is a sensor feedback electronics housed within the sensor package for creating the damping mechanism necessary for the seismometer. The seismometer unit is self-contained apart from its 12 V power supply. It consumes low power (0.75 Watts) and can operate over 10 to 30 Volt power input range. The damping of the seismometer is, h = 0.707. The velocity sensitivity of the seismometer is 1400 v/m/s.

3.3.3.3 CMG-3T

CMG-3T is a tri-axial seismometer consisting of three sensors in a sealed case which can measure the north-south, east-west and vertical components of ground motion simultaneously. It has been designed to provide seismic information over the complete seismic spectrum from very low frequencies (0.001 Hz) up to 50 Hz. Various frequency response options are provided for the user and optionally the high frequency corner of the sensor response can be increased beyond 50 Hz. The broadband frequency response is made possible by advanced force balance feedback electronics. Because of this wide response range, CMG-3T replaces many of the instruments conventionally used in a seismic observatory. The response of CMG-3T is the same as that of a pendulum seismometer with a free period of 120 sec, electrodynamic constant 1400 mv/(mm/sec) and damping of $h = 0.707$.

3.3.4 Global Positioning System (GPS) as Timing System

The GPS is an essential element of digital seismograph which is capable of providing both time and position information accurately. It comprises 24 satellites, each of which has an atomic clock synchronized to GPS Time (offset by a constant from International Atomic Time) and transmitting time codes. A GPS receiver receiving transmissions from several satellites can determine its position (latitude, longitude and height) and the current time. International clock comparisons are now routinely performed for seismic stations via GPS with accuracy of the order of 50 nanoseconds. Generally microprocessor based REFTEK-111A GPS system is used in the digital seismic stations. It is self-contained in a self-sealing aluminum case. The TRIMBLE GPS antenna is mounted on the top of the case. It can provide the information regarding location and time serially for the host system i.e. the DAS for synchronization of the internal clock present in the DAS.

3.4 DIGITAL TELEMETRY SYSTEM

The digital telemetry is one of the most essential systems for near real time earthquake monitoring. It is useful for the stations situated at the remote places. The signal in the form of ground motion, from out stations is transmitted via very high frequency (VHF) radio links to a central receiving station. The output signal from the seismometers is coupled to the auto ranged single or three component digital modulators for appropriate signal conditioning which involves amplification,

multiplexing, digitization and conversion of the signal into Pulse Code Modulation (PCM) bit stream. This bit stream is transmitted through VHF radio transmitter. The equipments at remote stations operate on 12-volt batteries which are continuously charged using solar panel to maintain continuous data transmission. The signal is sampled at a rate of 100 SPS for single and three component stations. At the central receiving station, the remote station signals are received through VHF radio receivers which are coupled to multi-channel line interface unit (LIU). The LIU allows PCM data from all the remote stations to be multiplexed and the data is fed to digital to analogue (D/A) converters and then into a Helicorder drum recorder for the purpose of recording.

3.5 DETERMINATION OF AMPLITUDE FREQUENCY RESPONSE CURVE FOR AIZAWL SEISMIC STATION

In order to have the knowledge of source function, the prime requirement is to obtain true ground motion due to occurrence of an earthquake. The seismic signal recorded by a station on the surface of the earth is not the true ground motion produced by an earthquake source. Recorded signal is the combined effect of properties of source, propagating media and effect caused by recording process. Correction of effect of recording media to obtain true ground motion is one of the major tasks dealt with in this study. In order to observe the effect of recording media two parameters i.e. transfer function (Poles and Zeros) and the frequency response function are utilized (Mitra and Kaiser, 1993). The frequency response describes the characteristics of seismic recording system that deals with true ground motion. Basically the concept of the frequency response function is the Fourier transform of the output signal divided by the Fourier transform of the input signal. The modulus of frequency response function is exactly the amount of magnification.

In this study the magnification curves i.e. frequency response functions are quantitatively determined which are used to ascertain ground motion amplitudes from digital seismogram with necessary conversion. Ground motion amplitudes are commonly calculated from digital seismogram by dividing the signal amplitudes in counts by the value of the amplitude of the displacement /velocity frequency response function (magnification curve) at single frequency. While working out this, an important assumption has been made that the input signal is harmonic.

Table 3.2 shows the list of poles and zeros (transfer function) for different seismometers and recording system whose data are used for signal processing in subsequent chapters. These transfer functions, positions defined for a plane, are provided in a simple ASCII file ("pole-zero file"), which is created by using "text editor". In addition, an input signal free from any artificial noise, earthquake, etc. (i.e. zero vibration condition) is provided. From the list of poles and zeros correspondingly frequency response function is calculated. A complex multiplication of the frequency response function with the discrete Fourier spectrum of the input signal is performed. Finally inverse Fourier transform is calculated. The whole process is equivalent to convolving the input signal with the impulse response of the system. Evaluation of impulse response function is made based on potential change in onset following (Seidl and Stammler, 1984). Ultimately amplitude response function is obtained. Figure 3.2 show the amplitude frequency response for AZL (AIZAWL) station equipped with REFTEK 72A-07 digitizer cum CMG-40T.

Figure 3.2 shows approximately three regions with different slope in log-log plot. Outside of the central frequency band, roughly below 0.002 and 5Hz, the amplitude frequency response function decays rapidly, hence signals with frequencies outside this range are strongly attenuated while signal with frequencies between 0.002 to 5Hz could be well recorded. This frequency band is the passband for the recording system i.e. REFTEK 72A-07 and CMG-40T seismometer, in Aizawl seismic station, Mizoram. Within this passband, the amplitude frequency response is proportional to the angular frequency (□). For a velocity response function, the unit for amplitude would be counts/velocity i.e counts/nm/sec. It can be noted that the plateau value is 1.0 counts/nm/sec, which corresponds to the generator constant expressed in counts.

Determination of frequency response to the ground velocity first ascertains the true ground motion at a particular frequency. Secondly it ascertains the true knowledge of passband frequency that is required for waveform processing in subsequent chapters of the present study.

CHAPTER-IV

RECOMPUTATION OF EARTHQUAKE EPICENTERS AND PRESENT SEISMICITY TREND

4.1 INTRODUCTION

The region under investigation is the northeastern prolongation of the Indian Shield comprising Surma valley bounded by Post-Barail unconformity. Two prominent faults- the NE-SW trending Sylhet fault in the northern part of Surma valley (Nandy et el., 1983) and NW-SE trending Mat fault in the eastern part of Surma valley are conspicuously present in the study area. The seismotectonics of the region is the matter of interest for several researchers (Chandra, 1984; Mukhopadhyay and Dasgupta, 1988; Kayal et al., 2004, Kayal, 2008). Several studies on seismotectonics and tectonics of the region are carried out by Chaudhary and Srivastava (1976), Molnar (1984), Nandy and Dasgupta (1991) and Verma (1991). Present study comprises the re-look into the seismic activity of the region apart from the inferences made through seismicity parameters. Continuous monitoring of earthquakes during the last couple of years in Surma Basin with seismic stations of Agartala, Manipur, Shillong including a Broadband seismograph in Aizawl, the Capital city of Mizoram- has improved the knowledge about the present day seismic activity and seismotectonics of the region. The seismic activities are studied on the basis of data collected during 1969 to 2009. However most of the events are relocated during the period 1982 to 2009. These data are the hypocenter data file compiled jointly by RRL-Jorhat and NGRI-Hyderabad complemented by phase data from IMD-Shillong, IIG-Shillong, Manipur University, Gauhati University and Mizoram University. A close comparison with EHB location (www.isc.ac.uk/EHB) has been made for some moderate to large earthquakes. For these earthquakes the difference of hypocentral parameters is about 2-3 kms between these two datasets. Depths are poorly determined parameter if there is no nearby station surrounding the event. Since the studied region is monitored by station at Aizawl, Mizoram, and Shillong depths are constrained with the data made available from neighboring nearby stations. The magnitudes of the events are on the basis of signal duration calibration only.

4.2 RECENT LARGE AND DAMAGING EARTHQUAKES IN AND AROUND SURMA VALLEY

In the study of the past damaging earthquakes the limitation that is mainly observed is the inaccurate location of the event. Earlier catalogues does have many shortcomings, like inaccurate timing, location, magnitude, etc. Gupta et al. (1986) prepared a corrected list of earthquakes, which has a total of 504 entries for the period 1897 to 1964. It may be noted that 22 large earthquakes (magnitude $\geq$7.0), including two great earthquakes (M >8.0), occurred during the last 100+ years, since 1897 in Northeast India and its surroundings (Fig. 2.1a in Chapter-II).

The June 12, 1897 great earthquake (M 8.7) appears to be the first Indian earthquake for which instrumental records, recorded outside India, are available (Oldham, 1899). Gupta et al. (1986) have treated the earthquakes prior to 1897 as historical earthquakes. Based on a detailed literature survey, a descriptive list of the historical earthquakes was given by Oldham (1883). A brief description of a few significant historical earthquakes in Surma valley and adjoining region concerning Sylhet and Mat fault is given below.

4.2.1 Cachar Earthquake of 1869

The January 10, 1869 Cachar earthquake is one of the largest historical earthquakes in Northeast India region (Fig. 2.1a in Chapter-II). Some descriptions of this earthquake were given by Oldham et al. (1882). The felt area was about 6,65,600 sq. km. Several damages were reported in Guwahati, Cachar, Nagaland, Manipur and Sylhet (Bangladesh). Oldham et al. (1882) deduced the epicentral tract being 5-6 km wide and 32-48 km long, trending E15^{o}N-W15^{o}S, located around the intersection of latitude 26^{0}00′N and longitude 92^{0}40′E, at the northern border of the Jaintia Hills, Meghalaya. The suggested epicentral tract is located in the Kopili gap area (Nandy, 2001), the area between the Shillong Plateau and Mikir hills; and the focal depth was estimated at 50 km. From the description of damage pattern incorporated in the Memoir, G.S.I., Vol. 19, pt.1 (1882), the magnitude was estimated to be greater than 7.0, although the accurate magnitude was not given.

4.2.2 Srimangal Earthquake of 1918

It occurred on 7th July, 1918 at 10hr 22min 12 sec GMT in the Bengal Basin and is known as the Srimangal earthquake. It is one of the largest earthquakes that was recorded by a few local seismographs, viz. Bombay, Colaba and Calcutta. Its magnitude was 7.6. The epicenter was given at 24.5^0N and 91.0^0E, and depth of focus as 15 km. The meizoseismal zone covered an area of 332 sq km and was felt over 122,000 sq. km with few deaths. The maximum intensity X (Rossi-Forel scale) was reported around Srimangal ($24^0$15′, $91^0$42′) in Sylhet district, Bangladesh. Post earthquake investigation was carried out by Stuard (1926) and he reported that major axes of the isoseismal were aligned in the NW-SE direction. Nandy (2001) had, however, redrawn the major axes in the ENE-WSW direction, and suggested that the earthquake was originated by the high angle reverse Sylhet fault where it is intersected by NW trending Mat fault, the maximum damage and destruction being in the hanging wall side of the upthrow block. Stuard (1926) estimated the focal depth at about 14 km from the isoseismals, lying below the Balisera valley.

4.2.3 Cachar Earthquake of 1984

The Cachar earthquake, M_L 5.8, occurred on 30th December 1984 at 23h 33m 39.1s. The epicentre is at 24.598^0N latitude and 92.939^0E longitude having a depth of 33 km restricted (USGS report). Although not a large event magnitude-wise, it rocked the entire area and was responsible for a loss of about 20 human lives and considerable damage to property (GSI, 2000).

The maximum intensity of the earthquake reached VIII on the Modified Mercalli (MM) scale (GSI, 2000). The VIII intensity was assigned in view of the formation of fissures in flat ground through which sand and water were ejected. In the meizoseismal area of about 250 sq. km, a considerable damage was caused to a well designed concrete bridge and total collapse of the weak structures where they are intersected by NW trending Mat fault. Banks of Sonai and Barak Rivers were damaged very badly.

The earthquake was followed by seven felt aftershocks in the subsequent 11 days (Dube et al., 1986). It has a predominantly strike-slip focal mechanism solution with thrust component and tectonic setting of the area. From the location of epicenter,

it appears to have been related to a fault in the tectonic domains of the NE Sylhet fault.

4.2.4 Indo-Burma Earthquake of 1988

The Indo-Burma earthquake of August 6, 1988, M_L 7.5, originated at 00h 36m 29.6s (GMT) with latitude 25.116^0N, longitude 95.171^0E, and having 115 km depth (USGS report). It rocked the whole northeastern region of the country in the early morning of August 6 at 6.10 AM (local time). The tremor was felt all over Northeast India, Bangladesh, Nepal and parts of Burma. It lasted for about two minutes, and caused a loss of four human lives, considerable damage to buildings, railway tracts, roads, etc. Field survey showed that the maximum intensity reached VIII on the MM scale (GSI, 1988, unpublished report). Landslides, formation of fissures, ejection of sand, mud and water were observed at several places.

The focal mechanism study based on P-wave first-motions indicated thrust-faulting solution with a compressional stress parallel to the trend of tectonic feature of the Indo-Burman ranges (Banghar, 1990). The result of inversion, however, shows a mixture of strike-slip and reverse-fault mechanism (Chen and Molnar, 1990). They have well estimated the focal depth at 90 $\pm$ 10 km from the unambiguous P^p and S^p phases on both the long and short period seismograms. Considering the depth and the fault plane solution, there is little doubt that this large earthquake occurred within the subducted Indian plate. The deeper focal depth provided a plausible explanation for small number of casualties and less damage (Person, 1989). The centroid moment tensor solution is similar to that obtained by Chen and Molnar (1990).

These earthquakes indicate the characteristics of the fault. Sylhet fault is designated as high angle reverse fault. Moreover, from the location of epicenter, Cachar earthquake of 1984 shows that it has a predominantly strike-slip focal mechanism solution with thrust component.

4.3 RECENT SEISMICITY IN SURMA VALLEY AND ADJOINING REGION

Regional seismicity maps are prepared by several workers considering the data from various sources (e.g. Santo, 1969; Fitch, 1970; Chandra, 1975; Le Dian et al., 1984; Mukhopadhyay and Dasgupta, 1988). The earthquake listings published by the International Seismological Centre (ISC) and the United States Geological Survey (USGS) since 1964 were used by Kayal (1996 b, 1998) to prepare a seismicity map of the northeast region. It is observed that during this period, almost all the earthquakes of body-wave magnitude (m_b) $\geq$4.5 have been uniformly recorded and located. In addition to this, the great earthquakes (M>8.0) and large earthquakes (M>7.0), that occurred during the last 100+ years, since 1897 are also shown in this map. The seismic activities in two different tectonic zones in Surma valley and its vicinity are discussed below.

4.3.1 Indo-Burman Ranges

In the Indo-Burman ranges, the earthquake epicenters are highly concentrated. As many as 10 large earthquakes M>7.0 occurred during the last 100+ years since 1897. A depth section of the earthquakes in the NNE-SSW strike direction of the ranges, shows that the activity is intense and more or less uniform down to a depth of about 200 km, but beyond the latitude 26^0N there is a marked shallowing of the lower limit of activity where collision process has taken over the subduction process (Mitchell and McKerrow, 1975; Kayal, 1989 and 1996b). Two vertical cross sections of the earthquakes in perpendicular direction of the strike of the Indo-Burman ranges, which fall to the south of 26°N latitude, evidently show a (40-45°) dipping seismic zone or the *Benioff zone*. An envelope of the seismic zone beneath the Indo-Burman ranges is clearly indicated. The upper boundary of the envelope demarcates normal faulting in the subducting plate and thrust-faulting as well as strike-slip faulting in the overriding plate (Kayal, 1996b and 1998). The lower boundary completes the envelope of the seismic zone or the Benioff zone. The depth of the top boundary is about 25 km below the Shillong Plateau/Tripura fold belt, and the Benioff zone flexes beneath the Indo-Burman ranges. The thickness of the Benioff zone varies from 40 to 45 km. The Benioff zone structure is conformable with the observed Bouguer gravity

anomaly (Kayal, 1989 and 1996b). A similar observation was made by Mukhopadhyay and Dasgupta (1988).

The foci distribution in the inclined seismic zone suggests that depth penetration of the subducting lithosphere is about 200 km in the central part of the Indo-Burman ranges, and about 150 km to the south. The volcanic arc position corresponds to the deepest part of the Benioff zone. The shallower seismicity in the Burmese platelet to the east of the Benioff zone is related to the overriding plate seismicity and the shallower seismicity to the west of the Benioff zone is related to the plate-boundary/intraplate seismicity in the Indian plate (Kayal, 1996b). Bevis and Isacks (1984) studied in the ISC data, 1964-1986, and presented the hypocentral trend on a surface contour map. The eastern edge of the Indo-Burman ranges roughly coincides with the map projection of the 60 km depth contour of the Benioff zone. The map projection of 60 km depth contour approximately separates the accretionary complex from the southeast Asian continental crust. They further estimated that dip of the inclined Benioff zone varies from about 50^0 southeast in the north near the syntaxis to about 30^0 north northeast in the Bay of Bengal area.

The absence of intermediate depth earthquakes beyond about 26^0N marks the northern end of the Burmese arc. In the southern Burmese arc (south of 20^0N and north of 14^0N), it is reported that there are no well constrained hypocenters with depths greater than 50 km, and it is not possible to characterize the shape of the Benioff zone in this part of the arc (Ni et al., 1989; Kumar and Rao, 1995). This is possibly a transition zone between the Burmese arc and the Andaman-Sunda arc (Kayal et al., 2004).

4.3.2 Bengal Basin and Tripura Fold Belt

Bangladesh is surrounded by the regions of high seismicity which include the Himalayan Arc and Shillong plateau in the north, the Burmese Arc, Arakan-Yoma anticlinorium in the east and complex Naga-Disang thrust zones in the northeast. It is also the site of the Dauki Fault system along with numerous subsurface active faults and a flexure zone called Hinge Zone. These weak regions are believed to provide the necessary zones for movements within the basin area. In the seismic zonation map of Bangladesh, Surma valley is categorized into Zone-I, which is the highest earthquake

zone comprising the northern and eastern regions of Bangladesh with the presence of the Dauki Fault system of eastern Sylhet and the deep seated Sylhet Fault, and proximity to the highly disturbed southeastern Assam region with the Halflong thrust, Naga thrust and Disang thrust, is a zone of high seismic risk. The Chittagong-Tripura Folded Belt experiences frequent earthquakes, as just to its east is the Burmese Arc where a large number of shallow depth earthquakes originate.

Historical seismic catalogues (ISET, 1993) reveal that Bengal Basin has been affected by earthquake disasters since ancient times. Earthquakes occurring in 1664, 1828, 1852 and 1885 are shown to have Dhaka as epicentral area. Similarly other cities including cities in the Surma valley have been shown to be epicentral area of some of the major earthquakes in the past. Although the ancient records do not specify the earthquake epicenters by giving coordinates in terms of latitudes and longitudes, it is difficult to figure out whether these cities were directly hit by the earthquakes. However, occurrences of earthquakes both in the Basin and surroundings indicate that earthquake hazards exist in the Basin for a long time.

Information on earthquakes in and around Bengal Basin is available for the last 250 years. The earthquake record suggests that since 1900 more than 100 moderate to large earthquakes occurred in Bangladesh, out of which more than 65 events occurred after 1960. This brings to light an increased frequency of earthquakes in the last 40 years. This increase in earthquake activity is an indication of fresh tectonic activity or propagation of fractures from the adjacent seismic zones.

Recent seismic studies suggest that the Bengal Basin is characterized by low seismic activity, whereas a moderate activity is observed in the Tripura fold belt. The activity in the Bengal basin may be related to intraplate seismicity. One large earthquake m_b 7.6 occurred beneath the Bengal Basin on July 8, 1918. The epicentre of this event falls in the Srimangal area, Bangladesh, and is known as the Srimangal earthquake of 1918. The felt area was about 8,00,000 square miles. The activity in the Tripura fold belt, on the other hand, may be related to the plate-boundary activity. Recently a damaging earthquake, M_L 5.8, known as the Cachar earthquake of 1984, occurred in the Tripura fold belt.

In the present study, an attempt is made to observe the present seismicity pattern in the region with relocated events assuming any change in seismicity pattern what is described above.

4.4 DATABASE

The study utilizes the earthquake data file compiled jointly by RRL-Jorhat and NGRI-Hyderabad (1982-2009) complemented by phase data from IMD-Shillong, IIG-Shillong, Manipur University, Gauhati University and Mizoram University. Prior to the year 1982, ISC bulletins data during 1969 to1981 are incorporated in this study. The number of events obtained from ISC catalogue are only 231 while 4328 events are obtained from the bulletins as mentioned. Out of 4559 events, 2758 numbers of events could be relocated for better estimation of hypocentral parameters. Earthquakes since 1982, which are recorded in ISC are also incorporated in the data for re-estimation of Hypocentral parameters. A diagram representing the frequency distribution of network duration magnitudes, MD (A) for about 2758 earthquakes in Surma Valley is prepared (Fig. 4.1). Altogether 97% of events are ranged within the magnitude range of 2.0-5.9, highest numbers of events are observed within the magnitude range 4.0 - 4.9 which is around 55%. Twenty-five per cent of events are ranged between 3.0 - 3.9 while 11% of events are ranged between 2.0-2.9.

Frequency distribution in terms of depth (in km) concentration for about 2758 earthquakes in and around Surma Valley is constructed which highlights the number of earthquakes falling in each depth section (Fig. 4.2).

Simultaneously, data from different seismic stations in Surma valley such as Agartala, Manipur, Shillong including a Broadband seismograph station in Aizawl, are utilized which has improved the knowledge about the present seismic activity and seismotectonics of the region.

4.5 METHODOLOGY

This study deals with the present trend of seismicity activity in the region. The study covers an area between 90^{o}E and 95^{o}E longitudes and 22^{o}N and 26^{o}N latitudes in the Surma valley and its vicinity. Recomputation of hypocentral

parameters of all the earthquakes in the study region is done using HYPOCENTER (Lienert et al.,1986).

4.5.1 HYPOCENTER Program

In the present study HYPOCENTER program of Lienert et al. (1986) is used for the computer determination of hypocentral parameters of the earthquakes in Surma valley based on the crustal velocity model of Bhattacharyya et al. (2005) for a P-wave to S-wave velocity. This program combines the features of two well known algorithms HYPO71 and HYPOINVERSE with adaptive damping. Each column of the linearized condition matrix, which relates changes in arrival time to changes in hypocentral position, is centered and scaled to have zero mean and a norm of one. As per the program origin time is defined as the mean arrival time minus the mean travel time. The three least squares normal equations for hypocentral coordinates, with diagonal terms equal to one, are then solved iteratively by adding a variable damping factor, θ^2, to their diagonal terms before inversion. If the residual sum of squares increases, the program returns to the previous iteration, increase, θ^2, then try again. This procedure of adaptive damping, always results in residuals which are less than or equal to the HYPO71 and HYPOINVERSE residuals.

In addition to adaptive damping, the HYPOCENTER algorithm also incorporates the following four novel features:

1. Start with a θ^2 value of 0.005, which was found empirically to have little effect relative to the least squares solution. When $\sum \tau_I^2$ increases, θ^2 is increased by a factor of four. When $\sum \tau_I^2$ is decreasing, then θ^2 is decreased by a factor of 0.06, thereby increasing the speed of convergence. The factors used to increase and decrease θ^2 were determined empirically and were not critical to the performance of the algorithm.
2. The following convergence criteria were used: (a) coordinate corrections become < 0.05 km and (b) $\sum \tau_I^2$ does not decrease after θ^2 have been increased five times in succession.
3. Convergence is first achieved with the depth held fixed. Buland (1976) has pointed out that fixing depth significantly extends the domain of convergence for location problem. Depth is then freed, and convergence is searched for a second time.

4. Negative depths are treated similarly to increases in $\sum \tau_I^2$, i.e., the damping factor is increased. It was found that including station elevations in the calculation considerably improved the ability of arrays to locate shallow focus events. This is because the derivatives of arrival times with respect to depth at stations which are coplanar with an event are often all zero, resulting in a singularity in the condition equation matrix.

4.5.2 Magnitude

The most commonly used measurement for classifying the earthquakes by their relative size is magnitude. Further, magnitude, in first approximation, is proportional to the quantity of energy released during an earthquake. A number of different magnitude scales (Local Richter Magnitude, M_L, Body - wave magnitude, m_b, Surface wave magnitude, M_S, etc.,) have been developed, each based on the measurement of a specific type of seismic wave or phase that has propagated away from the earthquake source. As a result several different magnitude values are often assigned to the same earthquake. In practice, the various magnitude scales yield systematically different values of magnitude. Excellent reviews of magnitude scales and the quantification of earthquakes have been given by Richter, 1958, Bath, 1981, Kanamori, 1983 etc.

4.5.2.1 Local Richter Magnitude (M_L)

Richter (1935) developed the first magnitude scale (also known as Local Richter Magnitude Scale, (M_L), using maximum amplitude from Wood-Anderson seismograph (free period = 0.8s, magnification = 2,800). The procedure involves measuring the maximum amplitude of Wood - Anderson seismogram, measuring the distance from the epicenter based on the interval time between S and P phases and comparing the event to a standard or reference earthquake (Richter, 1935 and 1958). Richter defined magnitude 0 as an earthquake whose waves create a thousandth of millimeter amplitude on a seismogram, at a distance of 100 km. Magnitude increases logarithmically with the size of maximum amplitude; hence a measured amplitude of 1mm at 100 km corresponds to magnitude 3 earthquake. M_L magnitudes are determined according to the relation: M_L=Log A - Log A_0, where A is the maximum trace amplitude on the seismogram of Wood - Anderson

seismograph at a seismic station and A_0 compensates for the amplitude attenuation with epicentral distance. Digital data processing incorporates also running the digital spectrum following the frequency response of a Wood - Anderson instrument with the help of software for picking up the equivalent amplitude in connection with the estimation of M_L - magnitude (Kanamori and Jennings, 1978). Further, M_L "saturates" at about magnitude 7. Saturating means that even though the energy release of the earthquake continues to grow, the maximum of the magnitude scale becomes a constant or increases very slowly (Kanamori, 1983). The significance of M_L magnitude is that it uses the maximum amplitude corresponding to the free period of Wood - Anderson instrument which is, however, within the period range of common engineering structures.

4.5.2.2 Duration magnitude (M_D)

Magnitude (M_D) at a station is obtained on the basis of signal durations (S.D) and the signal duration calibration function. Signal duration at a station is defined as the duration between the first motion and the end of the signal where the signal becomes equal to the background noise level. Signal durations at a station are calibrated with known Local Richter Magnitudes (M_L), epicentral distance (Δ) and focal depth (h) by linear regression as per the relation of the form: $M_D=C_o+C_1\log_{10}$ (S.D.)$+C_2\Delta+C_3h$., whereas C_o, C_1, C_2, C_3 are the co-efficients. The (M_L) estimates are provided by the Central Seismological Observatory (C.S.O.), Shillong, operated by the Indian Meteorological Department (IMD), New Delhi. Arithmetic mean of duration magnitudes reported by different stations for an earthquake is termed as Network Duration Magnitude (M_D)A. And this Network Duration Magnitudes (M_D)A are used in the present study.

4.5.3 RELOCATING EARTHQUAKES

The accuracy of hypocenter determination depends not only on the distribution of the recording stations (e.g., Sato and Skoko, 1965) but also on what is known of the velocity structure between source and station, particularly in an area where lateral inhomogeneities are severe (e.g., Okada et al., 1970). Since the uncertainties involved in the earlier estimates of hypocentral parameters are of the order of 0–20 km, we have relocated these earthquakes utilizing the arrival time

data reported by relatively large number of seismic stations covering reasonable azimuth interval (GAP) distribution for each earthquake. GAP (Degrees) is the azimuth interval at the epicenter in which the number of seismic stations reporting the data are available. This is achieved by the integration of such data reported by the seismic stations operated by RRL-J/NGRI, India Meteorological Department, New Delhi, Wadia Institute of Himalayan Geology, Dehra Dun, Gauhati University, Guwahati, Assam and the stations operated by Manipur University, Manipur and Mizoram University, Mizoram in the Surma valley, Northeastern India especially during the period of Feb.15-May 15, 1993 and also similar data reported by Earthquake Data Reports published by United States Geological Survey for the earthquakes of magnitude ≥ 4.0 in the distance range of 0-5°. During the remaining period similar data reported by RRL-J/ NGRI, IMD networks of stations are considered for relocating the earthquakes. The crustal velocity model for a P-wave to S-wave velocity ratio of 1.75 reported by Bhattacharyya et al., 2005 is an average reference model used for locating the earthquakes in the study region. Hence, employing the arrival times of P- and S-waves reported by the above seismic stations in Northeast India region, about 2758 earthquakes of magnitude 2.0-5.5 from the period 1982 to 2009 were relocated following the HYPOCENTER location software package of Linert et al. (1986). The uncertainties involved in the estimates of epicenters and origin times are of the order 0-5 km and 0-0.5 sec. respectively (Fig. 4.3a, b and c). Since the uncertainties involved in the estimates of focal depths for 42, 28 and 26 per cents of total number of earthquakes located lie in the intervals 0-1km, 1-2km and 2-4 km respectively (Fig. 4.4), the depth control can be considered as reasonably good.

4.5.4 SEISMICITY MAP

After relocation of earthquakes, an analysis of the work is carried out by categorizing it into different sections as described below to obtain suitable results:

1. Seismicity map for the study area and the adjoining region has been prepared by plotting the earthquake data for the period from 1969 to 2009 over the generalized tectonic map of the Surma valley and its vicinity. The adjoining region of Surma valley i. e. Shillong Plateau and Indo-Myanmar region are

more active than the Surma valley. Sparse seismic activity is observed exactly in Surma valley as indicated by rectangle box even though the region is populated by two very active faults i.e. Mat fault and Sylhet fault (Fig. 4.5).

2. Using the same tectonic map as base, distribution of earthquake in terms of depth is prepared which indicate the distribution of depth of earthquakes within the study area. The earthquake events are categorized into different depth ranges depicted in different colors in order to obtain optimum result (Fig. 4.6).
3. Over the same epicentral region (Fig. 4.5), magnitude distribution of earthquake for events falling in the study area is prepared as illustrated in Figure 4.7. The legend in the figure shows the range of magnitudes for a particular event falling in each category.
4. To highlight the earthquake event which occurred along the Mat and Sylhet faults, a map is prepared where all earthquakes other than those along Mat and Sylhet faults are removed so as to showcase the number of shocks along both the faults (Fig. 4.8).

By applying the techniques mentioned above, detailed investigation of the study area by re-computation of earthquakes is done which throws light on the nature of seismicity of the region.

4.6 RESULTS

The area between 90^{o}E and 95^{o}E longitudes and 22^{o}N and 26^{o}N latitudes covering the region of this study experienced a large numbers of earthquake events during the period from 1969 to 2009.

Examination of the data shows that most of the events fall in the tectonic domains of the Assam shelf, Meghalaya Plateau and Mikir Hills, and Indo-Burmese Range. Surma and Bengal Basin have relatively low seismicity compared to the other regions. However the neighboring India-Burma subduction is very active. Figure 4.6 shows that the earthquake deepens to the SE direction of the Mat fault. It may be due to higher in-situ stress build up along SE direction of the fault. Tripura folded belt shows moderate activity. The seismic activity in the former may be related to an intra plate activity whereas in the later to plate-boundary activity. Seismic activities along

Mat and Sylhet faults are reasonably less than the other faults existed in the region. Most of the events associated to these two faults are shallower in depth in Surma valley. The magnitudes of the events are also found to be relatively low. Interestingly, intense seismic activity are observed within the area covered by Latitude 24^0 to 25^0 and Longitude 92^0 to 93^0 which is locked by Sylhet fault, Mat fault, Dauki fault and Main Boundary Thrust. It may be mentioned here that the Srimangal earthquake of 1918 (M=7.6) occurred beneath the Bengal basin along the Sylhet fault. Cachar earthquake of 1984 (M=5.6) occurred in the Tripura fold belt possibly due to movement along the Sylhet fault.

The region is dominated mostly by shallow focal depth earthquake i.e. < 70km events except for the Indo-Burmese Range where deeper focus earthquakes scattered along the range.

Most of the earthquake events falling in the Indo-Myanmar (Burmese) tectogenes have focal depths varying from 70-200 km where seismicity is more intense and defines the westerly convex broadly N-S subduction zone of the Indian plate.

The depth distribution plot (Fig. 4.6) indicates that the foci of maximum number of earthquake lie within 0 to 40 km depth. Beyond 40 km depth the foci distribution abruptly decreases. Among these sections highest number of foci lies within the depth range of 20-40 km which is around 1619 in numbers. Hence the seismogenic zone in Surma valley and adjoining region is constrained between 20-40 km.

Most of the events have magnitudes varied from 4.0-4.9, magnitudes of 3.0-3.9 constitute the next range followed by a range of 2-2.9 magnitudes. Majority of the events falls in the category of small earthquakes, moderate earthquakes of more than 5 magnitude made up the rest. So far the distribution of magnitudes are concerned maximum numbers of events are found to be within the range of 2.0-4.0. However , the region has also experienced events of magnitude more than 5.0. On the whole Surma valley and its vicinity experienced maximum number of events which occurred within the range of magnitude 3.0-5.0.

The main tectonic domains in this zone are E-W trending Dauki fault (which demarcates the boundary between the Meghalaya plateau and Bengal basin), NE trending Sylhet fault, NE-SW Hail-Hakula lineament, NS Jamuna fault, NW Padma lineament, NNW Tista fault, Mat and Tuipui faults. As such no remarkable seismic activity has been seen in Surma basin. A study of long term seismicity also does not show intense activity. Most active part of the basin is transgressed by Mat fault.

4.7 DISCUSSION

The seismological data of the ISC and USGS since 1969, the microearthquake analog data of the period 1982-98 and that of digital data from permanent network for the period 1999 to 2009, have been useful to a great extent to understand the earthquake source processes and the active faults in Surma valley and its vicinity. Simultaneously the study carried out by the relocation of the events not only improved the locations but also helped in better resolution to explain the seismotectonics of the study area.

Northeast India and adjoining region fall in the most intense seismic zone of the world. Out of the 5 great earthquakes (M>8) experienced by India, 2 occurred in this region. These are 1897 Great Assam and 1950 Assam earthquakes which had inflicted catastrophic damage to life and property. Besides, there were 15 incidences of large earthquakes (M>7) during the period from 1897 till date. Of these 7 events occurred in the Indo-Myanmar (Burmese) tectogene, 3 in the Meghalaya Plateau-Mikir Hills domain, two in the Eastern Himalaya, one in the syntaxis and two in the Bengal Basin. Concerning the database dealt in this study, it is clear that Surma valley and the adjacent areas are vulnerable to earthquake hazards.

Seismicity map for the study area and the adjoining regions, covering the area between 90^{o}E-95^{o}E longitudes and 22^{o}N-26^{o}N latitudes has been prepared by plotting the earthquake data for the period from 1969 to 2009 over the generalized tectonic maps of the region (Fig.4.5). Examination of the data shows that most of the events falling in the tectonic domains of the Indo-Burmese Range, Meghalaya Plateau and Mikir Hills, Eastern Himalaya and Assam shelf. Surma and Bengal basins have relatively low seismicity compared to the other regions (Fig.4.5). The region is dominated by shallow focal depth i.e., <70km events except for the Indo-Burmese Range where deeper focus earthquakes scattered along the range (Fig.4.6). The

earthquake events in these tectonic domains occur in diffused pattern having post-collisional intracratonic characteristics. On the other hand, most of the earthquake events falling in the Indo-Myanmar (Burmese) tectogenes have focal depths varying from 70-200 km where seismicity is more intense and defines the westerly convex broadly N-S subduction zone of the Indian plate. Filtering of other events to project the earthquakes that occur along Mat and Sylhet faults bears witness to the activeness of both the faults, although almost all the events are shallow focused and having magnitudes of less than 5.0 (Fig.4.8).

The Surma and the Bengal basin recorded quite a number of earthquake events, majority of which occurred within a depth of less than 60 km, followed by occurrence of certain events having depth upto 80km (Figs. 4.6 and 4.2). Most of the events have magnitudes ranges from 4-4.9 while magnitudes of 3-3.9 constitute the next range followed by a range of 2-2.9 magnitudes. All these events falls in the category of small earthquakes, moderate earthquakes of more than 5 magnitude made up the rest (Figs. 4.5 and 4.1), though a large earthquake (Srimangal earthquake of 1918) of 7.6Mb originate due to rupture along Sylhet fault where it is intersected by NW trending Mat fault, and the other occurring NW of Dhaka. Seismicity seems to be related with the conjugate fault system cutting across the basins and the N-S fold belt.

Relocation of events no doubt increased the precision of hypocentral parameters and understanding of the seismotectonics of the studied region which is well reflected in the frequency distribution pattern of RMS value, the error estimates of latitude, longitude and depth as well. The new hypocentral parameters deduced from relocations formed the basis of further analysis.

CHAPTER-V

ESTIMATION OF TRAVEL TIME OF P- AND S- WAVES

5.1 INTRODUCTION

5.1.1 Travel Time of P- and S-Waves

The fundamental data for seismological studies of the earth's interior are the travel times of seismic waves. The measurements available are the arrival times of seismic waves at receivers. To convert these to travel times, the origin time and location of the source must be known. These parameters, which are known for artificial sources, must be estimated from the observations of earthquake sources. Hence travel time data include information about both the source and the properties of the medium, and separating the two is a challenge in many seismological studies. The travel times are used to learn about the velocity structure within the source and the receiver. In general waves follow paths that depend on the velocity structure. Hence the structure through which waves travelled must be known. To illustrate these the travel time between two points are considered and the velocity could be found by dividing the distance by the travel time.

Travel Times of P- and S-waves has significant role in earthquake seismology. The precise estimates of P- and S-waves travel time of local earthquakes throws light on the regional crustal structure (Tandon 1954; Saha et al.,1981; Gupta et al., 1982; Joyner 1981). The travel time (T) versus epicentral distance (Δ) curve for P- and S-waves for different depth ranges always remain significant towards the estimation of velocity structure.

In 1930, Jeffreys, starting from the Zoppritz-Turner tables, inaugurated a series of successive approximations towards improved travel time table. In 1935 the first Jeffreys-Bullen tables were produced. Substantial refinements were incorporated in a new set of 'JB' tables first published in 1940. Compatible tables for near earthquake phases are also included. The tables are in a form which enables focal depth to be readily taken into account. The aim of the tables is to serve as a standard for the 'average' global earthquake.

Developments of modern seismology since the late 1980's have resulted in a large increase in seismological data and their accuracy. Recording of broadband

seismic signals has allowed several reassessments of the long-used classic travel time tables of Jeffreys and Bullen (1940). Discrepancies for these tables, although minor, were already pointed out by the author himself (Jeffreys, 1968). Moreover, the accuracy of source location today is incomparably greater than those that had been basis for the Jeffreys-Bullen tables.

Tandon (1954) was the first to develop a crustal model from travel times for Northeastern India regions. Subsequently, Saha et al. (1981) and Gupta et al. (1982) also proposed models. But it is a common experience that travel time for near earthquake phases vary from region to region because of regional variation in velocities. Moreover, crustal structure varies from region to region. Furthermore, the observed data will enable better and more accurate location of epicenters.

In this study an attempt is made to estimate both P-wave travel times and S-wave travel times, for earthquake events in the eastern part and northern part of Surma valley and its vicinity. A comparison of travel times with the findings of other studies are also made to revalidate the estimation.

5.2 DATABASE

Seismicity map for the study area and adjoining regions as given in Chapter-IV by plotting the earthquake epicenters during the period 1969 to 2009 over the generalized tectonic map of the region forms the database for this study. The area between 90^{o}E and 95^{o}E longitudes and 22^{o}N and 26^{o}N latitudes covering the region of this study experienced about 2758 earthquake events over a span of 40 years. Re-computation of hypocenters of all the earthquakes occurring in the eastern part and northern part of Surma valley is done using HYPOCENTER program of Lienert et al. (1986).

Using the arrival times of P- and S-waves of earthquakes and following the location algorithm package of Lienert et el., (1986) hypocentral parameters are computed based on the crustal velocity model of Bhattacharyya et. al., 2005 for determining P-wave to S-wave velocity ratios. The study also utilizes the hypocenter data file compiled jointly by RRL-Jorhat and NGRI-Hyderabad complemented by phase data from IMD-Shillong, IIG-Shillong, Manipur University, Gauhati University and Mizoram University. The accurate location of stations and epicenters are the most

important parameters towards this estimation of P- and S-wave travel times. The accrued and relocated database contains all these information.

5.3 METHODOLOGY

A combination of the methods of Wadati (1933), Riznichenko (1958) and Bune et al. (1960) is used for estimation of upper crustal velocity structure. Data required for velocity analysis using these methods are P- and S-wave travel times to various recording stations for a number of earthquakes and their epicentral locations.

In the first step Wadati method (Wadati, 1933) has been used for getting model-independent estimates of travel times of P- and S-waves to various stations. From these estimates of the origin times of earthquakes as well as P- and S-wave travel time ratios has been made. For this purpose, differences in arrival times of P- and S-phases were plotted against the P arrival time for each earthquake. Figure 5.2 to 5.8 gives examples of Wadati and Riznichenko diagrams obtained during the analyses. Such diagrams are classified depending upon whether the outliers among the plotted points were within 0.5 standard deviation (SD), between 0.5 and 1.0 SD, or more than 1.0 SD, respectively.

In the second step of the analysis, epicentral locations of more than 2750 earthquakes were estimated using the HYPOCENTER (Linert et al., 1986) hypocentral location program and an assumed velocity model (Khattri et al., 1983). This is because epicentral distances to recording stations are required for subsequent calculations. Also, estimates of epicentral coordinates are relatively insensitive to velocity models if an earthquake occurs within a recording array. This has been remarked by Nicholson and Simpson (1985) likewise.

In the next step of the analysis, the Riznichenko method (Riznichenko, 1958) was used to estimate the focal depths of earthquakes and the vertical travel times of P and S phases between the respective hypocenters and epicenters. Squares of the travel times (t^2) of either all the P or all the S phases from an earthquake are plotted against the squares of epicentral distances (x^2) of respective stations. Such graphs are called Riznichenko diagrams. The square root of intercept (t_{pz} or t_{sz}) on the t^2 axis of such a plot is the required time of vertical travel of the P- or S-waves between the hypocenter and the epicenter. The square root of inverse of the slope of a least squares line fitted

through the data points of a Riznichenko diagram when multiplied by a travel time, gives a focal depth estimate for that earthquake. Such focal depth estimates are denoted here as $h_{riz.}$ Those point or points on such plots which were two standard deviation away from a least squares line, were excluded and then fitted in a line in a least squares sense through the remaining data points. The slope of this line was used to calculate h_{riz} in such cases.

A detailed description of the methodology is given below

5.3.1 The Wadati's Method

The Method assumes that :

i) The Poisson's ratio along the ray paths for hypocenters to the recording station is constant, and

ii) The P- and S-waves start at the same time from the source.

The two assumptions are reasonably appropriate. The method computes origin time of the earthquake and the ratio of the travel time of P- and S-wave independent of the physical model for the earth. The arrival time difference between S- and P-waves (Ts-Tp) is plotted against the P arrival times. The plot contains data from all the network stations. For direct rays, a straight line fit occurs for the data. Due to reading inaccuracies and timing errors these are generally scattered and a least square fit is applied. The x-axis intercept is the origin time and is determined independent of the assumed velocity model. Slope of the line estimates the ts/tp (Fig. 5.1a). The method is well suited for shallow focus local earthquakes.

5.3.2 Riznichenko's Method

To draw the Riznichenko's diagram, the travel time of waves to stations and the corresponding epicentral distances are required. With an initial location of earthquake and origin time computed from Wadati's method, travel time P- and S-waves are computed (Fig. 5.1b)

Variation of t^2 with x^2 is plotted for a number of stations. A least square fit gives

$$t^2 = (x^2+h^2)/v_s^2$$

Where v_e is the effective velocity

h is the depth of focus, and

x is the epicentral distance

The v_e^2 so computed is neither the interval velocity nor simple average velocity.

In the final step of the analysis (the method of Bune et al., 1960), a cumulative plot of the vertical travel times of P- and S-waves with respect to estimated focal depths for all the earthquakes were obtained.

5.4 RESULTS

The Wadati and Riznichenko diagrams plots are made for the events around Sylhet fault region in the northern part and Mat fault region in the eastern part of Surma valley. Figures (Fig. 5.2 to 5.8) give such relations for the P-travel times at each of the depths under consideration. The Riznichenko diagrams clearly show the change in shape of the travel time versus distance curve with increasing focal depth, indicative of both a geometrical effect and an increasing P-wave velocity. The Wadati diagrams show systematic decreases in ts/tp, suggesting that the velocity for shear waves increases faster than that for the compressional waves in the upper levels of the crust. An interesting feature however, is the linearity of the Wadati diagrams. If ts/tp (and therefore Vp/Vs) indeed changes with depth, the linear relation assumed in the Wadati diagram is no longer valid (Kisslinger and Engdahl, 1973). Yet it is apparent that, at close distances and shallow focal depths, the expected curvature of the Wadati diagram is not sufficiently resolvable with the available data. Summary of average half-space velocities for P- and S-waves calculated using the Riznichenko technique and values for ts/tp from the Wadati diagram are shown. Values shown are those data that are plotted as a function of focal depth for each individual earthquake.

Figure 5.2 shows that Wadati diagrams for eastern part of Surma valley and its vicinity are well constrained so far as the values of *Ts-Tp vs. Tp* and *Ts-Tp vs. Ts* are concerned. The Ts-Tp values remains within 25-35 sec interval exclusively for two numbers of events (A B and C D) with less deviation from the linearity while Ts-Tp values lie within 10-40 sec interval for the same two numbers of events (E and F) with higher deviation from the linearity. Less variation is observed when compared with the travel time of P-wave while higher variation of Ts-Tp is reflected when plotted

with respect to travel time of S i.e. Ts. In this case, the Wadati plots have been carried out up to the depth range 7 to 20 km. Magnitudes for all these events are above 4.5.

Similarly, same trend is observed in case of the Wadati plot for eastern part of Surma valley and its vicinity as illustrated in the Figure 5.3 and Figure 5.4 where a different depth range up to 40 km and 56 km is considered respectively.

Simultaneously, the Riznichenko diagrams of earthquakes associated with events in the eastern part of Surma valley (Fig. 5. 5) are plotted against various depth intervals. All the plots indicate clear dependence of S-P travel time (Ts-Tp) with respect to epicentral distance (□). Interestingly, the S-P travel time does not vary much up to the depth range of 20 km with the increase in epicentral distances. However S-P travel time (Ts-Tp) is found to be larger with the increase of epicentral distance (□) exclusively for the depth range interval of 21 - 40 km.

For northern part of Surma valley, similar Wadati and Riznichenko diagrams are plotted in order to ascertain the travel times used to learn about the velocity of P-wave and S-wave of the structure within the source and the receiver. Since Wadati diagram depends only on the observed arrival times of P- and S-waves, Figure 5.6 allows to observe the dependence of arrival time on the epicentral distances. The plots indicate no other dependence on any other parameters out of hypocentral parameters. No significant change in dependence of depth is observed except some more linearity dependence in the depth range of 41- 60 km. The station wise plots however indicate the dependency of site characteristics of the particular station which is well reflected in the plots. There are some inconsistencies in the plots which might be due to the heterogeneous site pertaining to each station. Otherwise the trend, as observed and explained in Figure 5.5, remains the same.

The internal consistency of the data suggests that these values are useful as estimates of the first order variation in velocity structure and can be used to improve the velocity model used for location. For focal depths range from 7 to 40 km, the Riznichenko diagrams clearly show the change in shape of the travel time versus distance plot with increasing focal depth, indicative of both a geometrical effect and an increasing P-wave velocity. The Wadati diagrams show a systematic decrease in ts/tp, suggesting that the velocity for shear waves increases faster than that for the compressional waves in the upper part of the crust. Simultaneously, the nonlinearity

of the Wadati diagram indicate that ts/tp indeed changes with depth and it could be established that the diagram more or less resolve the plot.

5.5 DISCUSSION

The study deals with the estimation of travel times of P- and S-waves. It is interesting to note that lower crustal activity was very less in the study region prompting relocation of earthquake events. The relocation of events as made in Chapter-IV has considerably lowered the error pertaining to latitude, longitude and depth. The relocated events become an input to the study made in this chapter. In this study, it is observed that Ts-Tp is varying with depth and considerably possess some dependence of Tp and Ts on depth. Additionally, it is observed that ts/tp also decreases with depth, this implies that similar variation in velocity of P, velocity of S requires separate velocity structure for P and S if really accurate hypocentral parameters are required to be worked out. Several other studies (Archuleta, 1982; Cramer and Shakal, 1983) also find similar results. With the advent of digital data and the increasing use of three component stations, large number of good quality S-waves arrival are being recorded by micro earthquake networks. These S-wave arrivals require proper modeling if full advantage is to be taken of the increase resolution such as secondary arrivals can provide. In this study, accurate phase picking on P- and S-wave arrivals and subsequent locations no doubt contributed in a large way towards the travel time estimations. The simple geometries involved in the Riznichenko diagram were first discussed by Green (1938) although the semi-log form of presentation for using velocities determinations in earthquake focal depth was developed by Riznichenko. In this study, normal forms of presentations are made towards Ts-Tp versus epicentral distance.

CHAPTER-VI
VARIATION OF Vp/Vs VERSUS DEPTH

6.1 INTRODUCTION

It is well known that compressional and extensional seismic waves in the crust exhibit significant regional variations. P-wave and S-wave travel time propagating from focus with equal time independent of azimuth show different characteristics in various regions. The seismic signal which is recognized as the first arrival depends on the crust – upper mantle structure between source and receiver, instrumental magnification and the noise levels at the recording site. Simple technique involving the earthquake data, including Wadati-Riznichenko diagrams allows one to resolve the tradeoff in origin time and focal depth. Estimates of the average half space velocities for P- and S-waves, and of the travel time ratio (Ts/Tp) helps to understand the material property of the upper crust. A comprehensive variation of velocity of P- and S-wave arrivals with depth can be regarded as the path and site specific inhomogeneities between the source and receiver. Moreover, the technique i.e. the Wadati diagram depends only on the observe arrival times of P- and S-waves and is completely independent of any parameters used in the hypocentral location procedure. The ratio of a P-wave velocity over an S-wave velocity offers important information on the physical properties of the continental crust. The Vp/Vs ratio of crustal rocks are mainly controlled by the mineral contents of plagioclase with high Poisson ratio and silica with low Poisson ratio. The presence of crustal fluids of partial melting form a high Vp/Vs ratio because shear wave velocities diminish more at the presence of fluids within the upper crust than compressional wave velocities hence observation regarding Vp/Vs ratio could help to gain a better understanding about the characteristics of crust and researchers have used Vp/Vs ratio to infer the property of the crust.

In this chapter, an emphasis has been made to observe the variation of Vp/Vs ratio for shallow earthquakes recorded at close distances within the seismogenic zone in Surma valley along selected depths ranges to identify and to obtain reasonable physical properties of the crust underneath. Simultaneously how the valley is related to its adjoining region, so far as the physical properties among the regions are concerned, becomes useful in identifying gross lateral changes within the region.

6.1.1 Velocity Ratio (Vp/Vs)

The P-wave velocity is determined using the data of direct P arrivals. The $T_{p(obs)}$ i.e., observed P arrival for an earthquake can be written as:

$$T_{p(obs)} = T + \text{✚} T + ORG$$

where T = P wave travel time, ORG = origin time of the earthquake, and ✚T = the time correction which incorporates the error due to changes in elevation and/or geology of the seismograph stations.

P-wave velocity is then determined from the slope on a plot of $T_{p(obs)}$ versus hypocentral distance (distance between station and earthquake focus). Similarly S-wave velocity is also determined from S-wave arrival times.

Basically, as the first step, Wadati method is used for getting model independent estimates of travel times of P- and S-waves to various stations. From these estimates, the origin time of earthquakes as well as S-P travel time ratios are obtained. For this purpose, differences in arrival times of S and P phases are plotted against P arrival times for each earthquake.

The most direct method to estimate the Vp/Vs ratio with seismic data is to utilize travel times of P- and S-waves from crustal events. Both travel time of P- and S-waves are of great importance as these contribute to the knowledge of regional crustal structure immediately. The principal techniques involve the use of Wadati (1933) and Riznichenko (1958) diagrams as shown in Figure 5.1 (in Chapter-V). Both the methods have had a long history of use as primary tools in the earthquake location process. Wadati diagrams are used for determining origin times of regional earthquakes (Bune et al., 1960). The Wadati diagram is based on the linear relationship between the arrival time of P (Tp) and the time differences between P and S (Ts-Tp) for different recording stations for an earthquake as follows:

$$\mathbf{Ts–Tp=(Tp–To)(ts/tp–1)}$$

which brings forth an intercept that is an estimate of the origin time (To) and a slope that is a function of the average travel time ratio (ts/tp).

The linear relation produces a slope that is a function of the average half-space velocity (v). Following the Soviet practice (Bune et al, 1960), a plot is made on the log of the travel time against distance to lay emphasis on travel times to the nearer, more important stations.

These methods have the advantage because of their simplicity and robustness. The Wadati diagram depends only on the observed arrival times of P- and S-waves and is completely independent of any parameters used in the hypocentral location procedure. Normally, the Riznichenko diagram requires estimates of the origin time (To) and the epicentral distance (+). The origin time as determined from the Wadati diagram and distances as calculated from the trial computer location are used in practice. When stations are well distributed in azimuth around the epicenter, distances are generally well controlled. Velocities of P- and S-waves can then be easily determined. Estimates of focal depths can be used to identify cases where compensating errors in depth and origin time have constrained the focal depth to remain near the starting depth used in the computer location program.

The velocity information these methods provide is useful in a number of other ways. The techniques of Wadati and Riznichenko serve a number of uses in the routine processing of micro earthquakes locations; hypocenters can be checked for proper convergence; simple earth model can be developed; spatial variations in ts/tp can be mapped; focal mechanism solutions can be improved; and regional variations in velocity can be identified (Nicholson and Simpson, 1985). Of course their most common application has been to resolve the tradeoff in origin time and focal depth. Nicholson and Simpson (1985) find these methods have proved useful in a more fundamental sense of identifying significant earth structure and improving the general understanding of material properties of the upper crust.

The knowledge of physical properties of the crust, both upper and lower, can be made through proper estimation of Vp and Vs. In order to estimate the velocity of P- and S-wave, the travel time of P- and S-waves to stations and the corresponding epicentral distances are required. With an initial location of earthquake and origin time computed from Wadati's method, travel time P- and S-waves (t-tp; t-ts) are computed. Variation of t^2 with x^2 is plotted for a number of stations. A least square fit

is obtained which helps to determine the respective velocity of the wave with the following equation

$$t^2 = (x^2+h^2)/v^2 \qquad (1)$$

Where h is the depth of focus, *x* is the epicentral distance and *v* so computed is average velocity that is estimated.

The Vp/Vs ratio ranges between 1.69 to 1.75 in upper to lower crust. These differences in Vp/Vs ratio may be caused by lithological variations with depth. The variation of Vp/Vs ratio could be correlated with the geotectonics of the study area. A contour mapping of Vp/Vs could be made possible along different depth sections.

6.1.2 Previous Work on Estimation of P-Wave and S-Wave Velocities in NER

Several researchers worked towards the estimation of P-wave travel times in the studied region. One of such studies is that of Tandon (1954). From a study on the body waves of the great Assam earthquake of 15th August 1950 and its 54 aftershocks, he derived the crustal structure in the Assam region. He has obtained the following velocities for Pg, P* and Pn Waves: 5.58, 6.55 and 7.91 km/sec respectively. Assuming a mean depth of 13 km and using the intercept times, he obtained total crustal thickness of 46.3 km with 24.8 and 21.5 km thick upper and lower crust.

Sitaram et al., (1986) investigated the upper mantle velocity by teleseismic Pn arrival by using time-term method described by Scheidegger and Willmore (1957) and Willmore and Bancroft (1960) and found that the sub-Moho P-wave velocity exhibit a variation from 7.85 to 8.08 km/sec. Simultaneously, Kayal and De (1987) studied the seismic velocity of the uppermost mantle beneath the Shillong Plateau by applying the similar time-term method for the Pn arrivals of local earthquakes recorded by establishing temporary micro-earthquake networks and reported high mantle velocities (8.1-8.5 km/sec) beneath the Shillong plateau. In another study, De and Kayal (1990) estimated the upper crustal P-wave velocity by the time-distance plot method by using the P arrival data of the shallow (≤20 km) earthquakes in Shillong and Nowgong areas. They determined the upper and lower crustal P-wave velocity as 5.55 km/sec and 6.52 km/sec respectively using P arrival data of the shallow (≤ 35 km) earthquakes. Also, Baruah (1995) attempted to construct the crustal velocity model for NER India from the travel time analysis of body waves. Under a

Department of Science and Technology sponsored mulit-institutional project, Rai et al., (1999) used the time-term method (Kind, 1972; Hearn, 1984) to compute the Pn velocities and found that it varies from 8.3 to 8.5 km/sec beneath the Shillong-Mikir Hills and Assam valley area. In 1998, Kayal and Zhao first attempted to determine P- and S-wave tomography images of the crust and upper mantle beneath the Shillong plateau using temporary micro-earthquake network data obtained from seven to eight temporary seismograph stations and they reported lateral heterogeneities in the crustal velocity structure beneath the Plateau. Similarly, Sitaram et al., (2001) estimated the crustal velocity model below the Brahmaputra Valley region by travel time analysis of Pg, P^* and Pn waves. They also reported that the average Pn velocity is of the order of 8.0 to 8.5 km/sec and the depth of the Moho in the fore deep region is found to vary between 42 to 45 km. Bhattacharya et al., (2008) attempted to estimate 3D P-wave velocity structure of Northeast India region using the first arrival data of local earthquakes that were recorded by 77 temporary/permanent local seismic stations and they reported significant lateral as well as depth variation of velocity structures beneath the studied region. Presently, seismic activity in Northeast India is being monitored by state of the art digital seismograph network by various organizations. The data accrued from these stations allowed few researchers to adopt receiver function analysis technique (Kumar et al., 2004; Mitra et al., 2005 and Ramesh et al., 2005) to estimate the depth of Moho.

In regard to velocities of P-wave along propagation path involving major portion in Arakan-Yoma subduction region, Gupta et al. (1990) have analyzed travel times and estimated Pg and Pn velocities (km/sec) : (1) 5.64, 7.99; (2) 5.11, 7.83; and (3) 5.99 for the path to KOI, YYI and KHM stations. By analyzing the travel times for the earthquakes in various zones around Shillong Seismic Station, Khattri et al. (1988) have obtained apparent Pn-velocities (km/sec): 8.69 ± 0.8 and 7.8 to 8.25 in a NW direction towards Myanmar respectively. Using the time term method (Scheidegger and Willmore, 1957 and Willmore and Baucroft, 1960) Sitaram et al. (1988) have determined the inter-station velocities of Pn waves as 7.89-8.0 km/sec for Northeast India. Using the same method Sitaram et al. (1990) have analyzed the travel times for NER and derived Pg, P* and Pn wave velocities (km/sec): 5.64 ± 0.34, 6.53 ± 0.031 and 7.82 ± 0.07 respectively. In general, differences in velocity estimates

may be attributed to the method of treatment and propagation paths moving the different tectonic elements.

6.2 DATABASE

P- and S-wave arrival time data from shallow and intermediate depth earthquakes recorded by selected seismic stations network in the Northeast during 1982 to 2009 are used for this study. Origin time, epicentral coordinates (latitude and longitude) and depth of the earthquakes were determined using the HYPOCENTER computer program of Linert et al. (1986). For initial location of the microearthquakes the velocity of upper crust (0-20 km) was assumed to be 5.5 km/s and the lower crust (21-40 km) to be 6.5 km/s and the mantle (below 40 km) to be 8.1 km/s.

The reconstructed travel time of P- and S-waves versus epicentral distances obtained from the best linear fit of Wadati and Riznichenko diagrams derived in Chapter-V are used to determine the ratio of the velocity of Vp/Vs versus depth in Surma valley and its vicinity comprising the upper crust beneath Mat fault area in the eastern part and Sylhet fault area in the northern part.

The P- and S-wave velocities determined from the reconstructed arrival times are used for the estimation of crustal velocity model in Surma valley and its vicinity from the earthquake events as relocated in Chapter IV. Depth ranges are selected at 20 km intervals and the parameters are distributed accordingly.

In addition, a set of 20 earthquakes are used for determination of Vp and Vs associated to Mat fault region at different depth ranges and 19 earthquakes are used for determination of Vp and Vs in Sylhet fault region at different depth ranges respectively. Certain standards were used to select the earthquakes for this set ; firstly, the P and the S phases should be well recorded by at least five stations; secondly, the earthquake should occur within the study area and; finally, the reading of P and S phases should be accurate one which has been explained in detail in Chapter-IV.

6.3 Vp/Vs WITH DEPTH

The use of micro earthquakes to determine the orientation of active faults, focal mechanism solutions, and details of local crustal structure strongly depends on the velocity model used in the earthquake location process, and, as a consequence is

subjected to systematic errors introduced by inappropriate model parameters. With the advent of digital data and the increasing use of three-component stations, accompanied by additions of new stations in the Northeast, a large numbers of good quality P- and S-wave arrivals are being recorded. Separate velocity structure for P-wave is necessary if accurate and realistic earth model is to be determined. While employing the principal technique that involve the construction and analyses of Wadati and Riznichenko diagrams, we intend to obtain travel time ratio (ts/tp) at upper crustal depths and origin times that are independent of crustal velocity model and based on which the P-wave travel times as a function of epicentral distance are derived so as to obtain the velocity ratio (Vp/Vs) in the upper crust beneath study area inclusive of Mat fault and Sylhet fault region.

The data for the Wadati plot method are selected on the basis of the following criteria: (i) earthquakes are located within the seismic network (ii) the spatial distribution of earthquakes is as uniform as possible in the study area (iii) the events must have at least four S-P time intervals, (iv) the rms (root mean square) residual for events must be 0.5 sec or less, (v) P arrivals must have a residual of 0.5 sec or less and S arrivals 1.0 sec or less and (vi) the range of P arrival times must be greater than 4 sec.

The epicentral map of the earthquakes recorded during the above surveys is shown in Figure 4.1. The study area is divided into two regions: the northern part of Surma valley in the Bengal Basin and the eastern part of Surma valley in the Indo-Burmese arc. About 20 arrival times from earthquakes in region belonging to Mat fault area and 19 arrival times from earthquakes belonging to Sylhet fault region are used for the P-wave velocity study. The time-distance plots are as shown in Figures (5.2 – 5.8) in Chapter-V. Table 6.1 indicate the earthquake events to find out the velocity of P- and S-waves at selected depth ranges of 0-20 km, 21-40 km and 41-60 km respectively. Certainly variation in Vp/Vs ratio is observed at different depth sections. Although the variation is consistent among depth sections, it is inconsistent among two active faults in the region.

Apart from the estimations pertaining to the two faults, the lateral variation of Vp/Vs ratio at three distinct depth ranges are also observed for the Surma valley and the adjoining region.

6.4 RESULTS AND DISCUSSION

The Vp/Vs ratio down to a depth of 60 km from the obtained P- and S-wave travel times is computed. Vp/Vs ratio has been estimated by dividing Vp by Vs using the results obtained from Wadati and Riznichenko diagrams. It uses direct P- and S-waves with predominant frequencies of ~10 Hz, with the spatial scale of the heterogeneity in velocity structure. The Vp/Vs ratio so estimated are distributed among the depth ranges of 0-20 km, 21-40 km and 41-60 km respectively. Comparison of P-wave velocity estimates as reported by various investigators for Himalaya and Northeast India with the present study is shown in Table 6.2.

The Vp/Vs ratio for the Surma valley and its vicinity are distributed over the range 1.67 to 1.79 (Fig. 6.1). A highly inconsistent variation of Vp/Vs ratio is observed among three depths sections as well. In depth range of 0-20 km, Vp/Vs ratio is higher in the region bounded by latitude 22.5^{o} to 23.5^{o} and longitude 91.5^{o} to 92.5^{o} while rest of the region is characterized by dominance of lower Vp/Vs ratio. The scenario changes abruptly in case of the depth range 21-40 km. In this range, Vp/Vs ratio is least in the region bounded by latitude 25.5^{o} to 24.5^{o} and longitude 90.5^{o} to 92.5^{o} while the region near the latitude 24.5^{o} and 91.8^{o} indicate the highest dominance of values of Vp/Vs ratio. The distribution of Vp/Vs ratio is typical so far the depth range of 41-60 km is concerned. Lowest dominance of Vp/Vs ratio are observed in the eastern part of the Surma valley however the region with higher Vp/Vs ratio remains the same as observed in the depth range of 21-40 km. These variations obviously characterize the heterogeneity of the crust at different depth sections.

Simultaneously the distribution of Vp/Vs ratio are also observed in Figure 6.2 a,b,c for Mat fault region (eastern Surma valley) in different depth ranges. The velocity ratio (Vp/Vs) are found to be varying between 1.75 to 1.83 in 0-20 km depth range. However no remarkable variation is observed with the increase of depth up to 20 km (Fig. 6.2a). A notable variation in Vp/Vs ratio against increase in depth is observed in the depth range of 21-40 km. The Vp/Vs ratio is found to be consistently increasing with increase in depth up to 40 km. In the depth range of 40-60 km, a

sudden change in velocity Vp/Vs ratio is observed at a depth between 53 km and 54 km where it changes from 1.7 to 1.75.

Figure 6.3a and b depict the distribution of Vp/Vs in the northern part of Surma valley which is traversed by Sylhet fault. In Figure 6.3a, in the depth range of 20-40 km, a highly inconsistent nature of the velocity is observed at approximately 33 km depth where the velocity takes a sharp bends. The velocity ratio (Vp/Vs) suddenly decreases from ~1.77 to ~1.7 at this depth. This behavior of the sudden decrease in velocity maybe due to the in-heterogeneous nature of the crust. In the depth range of 40-60 km (Fig. 6.3b), however, a more or less uniform velocity is observed throughout the range where Vp/Vs ratio is at approximately 1.78.

In Mat fault region (eastern Surma valley) the variation is in the order of 1.74 (21-40 km) and 1.73 (41-60 km) whereas the average velocity-ratio (Vp/Vs) values for Sylhet fault region (northern Surma valley) in different depth ranges are 1.72 (21-40 km) and 1.75 (41-60 km) (Table 6.3). Similar spatial variation in velocity ratio (Vp/Vs) has been reported by Agarwal et al. (1975) and Kayal (1982) in other parts of the world. In this study no spatial variation of Vp/Vs is observed either for shallow (upper crust) or for deeper (lower crust) earthquakes. The differences in the Vp/Vs ratio are possibly caused mainly by lithological variations with depth.

Velocity of seismic waves varies depending on many physical conditions. Composition, saturation condition, temperature and ambient pressure play an important role in velocity variations. Composition may be more fundamental than the other factors because it is an intrinsic property of the local rocks. The differences in velocity among layers as shown in Table 6.1 may be caused by the differences in rocks composing each layer. It is well known that seismic velocity decreases as temperature increases (e.g. Fielitz, 1971; Sato et al., 1998). Fielitz (1971) measured as P- and S-wave velocity variations in different rocks at pressures of 400 MPa as a function of temperature. His result implied a different temperature dependence of Poisson's ratio for the rocks investigated. On the other hand, Kern and Richter (1981) measured Poisson's ratio for several rocks at a constant pressure of 600 MPa but with temperature varying from 20°C to 700°C and they concluded that Poisson's ratio did not change much with temperature; the average increase in Poisson's ratio for their rock samples was ~1%, within experimental error. It is difficult to precisely evaluate

the effect of temperature on the Vp/Vs ratio in the crust and the uppermost mantle because there have not been systematic laboratory measurements carried out under the temperature and pressure conditions at those depths (Nakajima et al., 2005).

On the basis of above findings a generalized model related to the distribution of Vp/Vs ratio of the area is suggested (Figures 6.2-6.6). In order to achieve the model the P- and S-wave velocity and Vp/Vs ratio of upper crust and lower crust for both the fault regions (Mat and Sylhet) are determined in this study.

It is proved unexpectedly difficult to obtain entirely consistent P and S models. It is apparent that some of the difficulty arose from uncertainty with regard to the depth of the focus. While trying to reduce the uncertainty, it was noted that the ratio of the travel time ts/tp for S- and P-wave follows a pattern and the pattern remains unchanged to some extent subject to the observation made at different depth sections. To be specific enough Vp/Vs ratios are observed in such a way that it could be established that some variations exist certainly when the depth increases. No remarkable variation in upper crustal region may be mainly due to the contribution of homogenous lithology specific to the region. However, variation in deeper depth could be due to the heterogeneous lithology existed in the region. Sometimes the locations of earthquakes are virtually independent of the origin time if a well set of earthquake events are distributed accordingly with respect to distance and azimuth. If however the observational data are confined to one or two quadrants the time of origin errors results in errors in the location as well as in the depth of focus (Lomnitz, 1977). The errors in times of origin, depth of foci and location contribute to the scatter in the travel times and obscure the determination of travel times and regional variations in travel times. Thus it is desirable that step should be taken to reduce the errors in times of origin. Until revised upper crustal travel time tables are prepared, times of origin determined from ts/tp will be useful as these depend only on the observed times since they are model dependent.

Vp/Vs ratio can, therefore, help to discriminate lithology. For instance the low velocity for the P-wave found for depth section 41-60 km in Mat fault region, could be produced by high velocity saturated material with high crack density. Sometimes, high velocity observed with low velocity ratio implies that the material is likely to have low crack densities, low intrinsic velocities and possibly higher effective stress

at that range. Similarly, lower Vp/Vs ratio at a depth of 21-40 km in Sylhet fault region maybe due to the reason that the region is guided by higher effective stress level for the properties of the rocks at depths involved in the brittle deformation associated with the earthquake faulting.

CHAPTER-VII
SOURCE CHARACTERISATION OF THE EVENTS ASSOCIATED WITH SYLHET AND MAT FAULTS AND ITS VICINITY

7.1 INTRODUCTION

Determination of focal mechanism solution permits characterization of the earthquake source most effectively with the estimation of fault geometry. Fault geometry is described in terms of the orientation of the fault plane and the direction of slip along the plane. However, the body wave, surface wave and the parameters such as equivalent forces at the source and seismic impulse response etc. are used to determine the orientation of fault plane and the direction of the movement associated with the earthquake. Since the majority of earthquake source processes are either complicated or cannot be observed directly, it has been necessary to find ways to determine source characteristics from seismic wave motion.

A seismogram is the main input to study the source process. A seismogram basically contains the information about the source, the path for wave propagation and influence of the recording instrument. Hence the study of source process is actually the isolation of source effect by correcting instrument response and path.

Bengal Basin and Tripura-Mizo fold belt in Surma valley experienced three recorded large earthquakes besides smaller magnitude earthquakes which release sizable energy daily. Understanding these earthquake occurrences and predicting ground motions during similar future great events needs detail seismic observations and their modeling. Modeling of earthquake source involves estimation of true characteristics of seismic source. The knowledge of seismic source process associated with each tectonic feature is not fully understood as yet in the study region.

The close vicinity of the Burmese subduction zone to the Himalayan collision zone across Northeast India produces complex tectonics giving rise to a high level of

seismicity. Using the hypocentral data of shallow earthquakes (h ≤70 km) for a period of 1969 to 2009, a large number of focal mechanism solutions and other geophysical data in correlation with major morphotectonic features in the Surma valley and the adjoining areas, a study is conducted to characterize the earthquakes in seismogenic sources within the region. Two different techniques are used for determination of focal mechanism solution. In case of events (M≥3.5) first motion polarity method has been used while waveform inversion technique is used for comparatively lower magnitude events (i.e. M≤3.5). In first motion or polarity method, pattern of radiated seismic wave are observed with a concept of first motion. Waveform inversion technique deals with the construction of synthetic seismogram for a realistic earth model and arbitrary fault geometry for comparing synthetics with observed data towards the determination of focal mechanism solution.

The present study aims to determine the focal mechanism of earthquakes occurred in Surma valley, with special reference to Sylhet fault in Bengal Basin and Mat fault in IBR, using the analogue and digital seismogram recorded by the regional seismic network and utilize the same to characterize the source zone as well.

7.2 DYNAMICS OF FAULTING

Rocks are very slowly but continuously moving and changing shape. Under high temperature and pressure condition within the earth, rocks can bend and flow. In cooler part of earth, rocks are colder and brittle and respond to large stresses by fracturing. Earthquakes are the agents of brittle rocks failure. A fault is a crack across which the rocks have been offset and ruptured. The style of faulting is an indicator of rock deformation and reflects the type of force pushing or pulling on the region. The style of faulting is a reflection of relative size of the different forces, in particular, the relative size of the vertical to the horizontal forces.

7.2.1 Types of Faults

Depending on the direction of crustal block movements due to vertical and horizontal force, there are three cases to consider. The vertical force can be the smallest, largest or the intermediate. If the vertical force is the largest, normal faulting is observed, if it is the smallest reverse/thrust faulting exists. The vertical force equivalent to intermediate force indicates strike-slip faulting. Normal faulting is

indicative of a region that is stretching. Reverse faulting reflects compressive forces squeezing a region while strike–slip faulting indicates neither extension nor compression but identifies a region where rocks are sliding past each other.

7.2.2 Fault Geometry

Fault geometry is described with the assumption that the fault is a planner surface across which relative motion of mass of rock occurred during an earthquake. This assumption is consistent with the seismic data although a real fault has a complicated geometry. The fault geometry indicates the fault plane and the direction of the slip along the plane. Fig. 7.1 shows that a fault plane with normal vector $\hat{n}$ separates footwall from the hanging wall (not shown). The slip vector, $\hat{d}$ describe the motion of the hanging wall block with respect to footwall block. The coordinate axes are chosen with X_3 vertical, X_1 oriented along the fault in the plane of the earth's surface and X_2 is the axis perpendicular to both X_1 and X_3.

In order to describe the orientation of the fault plane in geographic coordinates, two angular parameters are required. These are strike of the fault, ϕ i.e. the azimuth of the fault's projection onto the surface measured from north and the dip of the fault, δ i.e. the angle measured downward from the surface to the fault plane in the vertical plane perpendicular to the strike. The strike direction is defined such that the dip is $<90^o$. The actual motion of the two blocks on either side of the fault is defined by slip vector ($\hat{d}$) as shown in Fig. 7.1. The direction of the slip vector is given by angle of slip or rake (λ), measured in the plane of the fault from the strike direction to the slip vector showing the motion of hanging wall relative to footwall.

The strike ($0 \leq \phi < 360^o$), dip ($0 \leq \delta \leq 90^o$), rake ($0 \leq \lambda < 360^o$) and the slip vector $\hat{d}$ define the most basic seismic model of faulting or focal mechanism. In general, ϕ, δ and λ can vary over the finite fault surface with average value being used for simple models. The basic three types of faulting can be discussed in terms of ϕ, δ and λ of a fault. When the two sides of a fault slip horizontally relative to each other, the motion is called pure strike-slip ($\lambda = 0^o, 180^o$) and if dip (δ) is 90^o, the geometry is

called vertical strike-slip. For $\lambda = 0^o$, the hanging wall moves to the right, so that a point on the other side of the fault moves to the left; this type of fault movement is called left lateral strike-slip. If $\lambda = 180^o$, the fault movement is called right lateral. Dip slip type of faulting involves slip with a vertical component of the relative displacement of the two blocks. For $\lambda = 90^o$, the hanging wall moves upward causing thrust faulting and for $\lambda = 270^o$, it moves downward causing normal faulting. In general, λ have a value different than these special cases and the motion is then called oblique slip. If a fault is treated as rectangular, the dimension along the strike is called the fault length and the dimension in the dip direction is known as the fault width.

7.3 FOCAL MECHANISM SOLUTION USING P-WAVE FIRST MOTION DATA

Focal mechanism solution using P-wave first motion data is one of the simplest methods to determine fault geometry. The basic idea of this method is that, the polarity (direction) of the first P-wave arrival varies between seismic stations at different directions from an earthquake. The first motion is either compression, for the stations located such that material near the fault moves towards the station or dilatation, where the motion is away from the station. Thus, when a P-wave arrives at a seismometer from Earth's interior, a vertical component seismogram records an upward or downward first motion corresponding to either compression or dilatation. The P-wave first motion data and the azimuth of the recording stations are collected from different stations which forms the prime input to the determination of focal mechanism solution.

7.3.1 Data for P-Wave First Motion

Determination of focal mechanism solution using P-wave first motion data requires maximum number of seismograms recorded by different stations. As lower magnitude event is recorded by a very few stations, higher magnitude event ($M \geq 4.0$) is generally preferred for this method. The events having magnitude $M > 4.0$ are recorded by more than 45 numbers of seismic stations including the stations at teleseismic distances. The P and S phases are re-read from the available analogue seismograms obtained from the local seismic stations. These events are relocated based on crustal velocity model of Bhattacharya et al., (2005), using data for relatively larger number of seismic stations with reasonable degree of

azimuthally coverage. In this study, a few focal mechanism solutions are determined (as listed in Table 7.1) utilizing both P-wave 1st motion polarities and waveform modeling. These are made on the basis of high precision location determination, clear record of P-wave first motion polarity, high signal to noise ratio and recorded by maximum number of seismic stations.

Primarily, P-wave polarity, azimuth from the source, incident angle with respect to focal depth and epicentral distance in degrees etc. are the input for determination of focal mechanism solution. The P-wave first motion data are obtained from local stations as well as stations at teleseismic distances. ISC Bulletin provides P-wave first motion data from stations at teleseismic distances.

7.3.2 Methodology

The fault geometry is found from distribution of first motion data on a conceptual homogeneous sphere around the focus called focal sphere. In general Wolff's net (Fig. 7.2a) is used to project the geographical position of an observation station to a point where the tangent to the ray at the source intersects the focal sphere. The P-wave ray path leaving the source can be identified by two parameters: the azimuth from the source (ϕ_s) and the ray parameter or take off angle, i_h (Lay et al. 1995). The azimuth of the direction of the ray from the source and the takeoff angle prescribes a unique path through the earth to a point on the surface and the corresponding portion of the outgoing wave front is designed to reach that point, conveying the initial motion in the associated region of the outgoing wave. Depending on the distribution of P-wave first motions, the zone of compression and dilatations are identified. Focal mechanisms are determined using the steps as follows:

i. P-wave first motion data are obtained from the seismograms of each recording station.
ii. Azimuth (ϕs) and the epicentral distance (Δ) are calculated for known earthquake and recording stations.
iii. The take off angle, i_h is obtained from the table prepared by Hodgson, (1953) and, Pho and Behe (1972).
iv. Using ϕs and i_h the ray position is projected to each station on a lower hemisphere stereographic projection using Wulff's Net. Different symbols

are used to indicate the P-wave first motion. Open circles are used to indicate dilatation and filled circles for compression.

v. The first motion data are rotated on the stereo net to find a meridian line that separates compression from dilations. This plane is drawn along with the pole to the plane, which projects at 90^o from the plane.

vi. The data plot is rotated to find a second meridian that separates dilatations and compressions and passes through the pole of the first plane.

vii. Out of these two nodal planes the fault plane is ascertained based on the local geology inherited in the region.

viii. The strike and dip of the fault planes are determined as illustrated in Figure 7.2b. Rake is calculated from the poles.

ix. Pressure (P) and tension (T) axis is determined. The maximum compressive strain P is a pole lying on the plane containing the pole of the two fault planes. It lies in the dilatational quadrants 45^o from the two nodal planes. The minimum compressive stress axis, T lies in the compressional quadrant 45^o from the two planes.

x. The intermediate compressive stress axis, also called B axis or null axis, is determined along the line of intersection of the two nodal planes.

7.3.3 Fault Plane Solutions

The methodology described in section 7.3.2 are applied for the earthquakes occurred in the Surma valley. The focal mechanism solutions so obtained are listed in Table 7.1. A pictorial distribution of Fault plane solutions (obtained using first motion polarities and CMT solution) is shown in Fig. 7.3. As the first motion on the actual fault plane is the same as that on the auxiliary plane, which is perpendicular to the fault plane, so the first motion alone cannot resolve which plane is the actual fault plane. Additional geological information such as trend of known fault is used to infer the preferred fault plane.

7.4 FOCAL MECHANISM SOLUTION THROUGH WAVEFORM INVERSION

Waveform inversion is one of the most useful techniques to characterize an earthquake source with the estimation of source parameters like strike, dip, rake, seismic moment and moment magnitude, etc. The entire earthquake processes may be separated into three major elements: (a) the generation of seismic waves by the

source, (b) the passage of the waves through the earth and (c) detection and recording by the receiver which are well reflected in a seismogram. Now a days, the recent advancement of high dynamic range seismic instrumentation as well as development of new techniques (e.g. Kind 1979; Bouchon, 1981 and Bhattacharya 1992, etc.) made it possible to model each of the effects mathematically to develop a procedure to predict the character of a seismogram in a realistic model of Earth. Such a mathematical construction is known as a synthetic seismogram and the formalism of comparing synthetic and observed seismogram is known as waveform modeling (Lay et al., 1995). Waveform modeling is an iterative process in which difference between the observed and synthetic seismogram is minimized by adjusting the earth structure or source representation (Lay et al., 1995).

The present study aims to determine the focal mechanism solutions of smaller as well as moderate magnitude earthquakes through waveform inversion. Studies of small earthquake recorded digitally at short distances are extremely important because they provide information about the physics of the earthquake source process without too much contamination due to wave propagation (Saikia and Herrmann, 1985, 1986; Koch 1991a; Sileny et al., 1992; Schurr et al., 1999). The local earthquake records possess high frequency characteristics as influenced by crustal structure and source process. The major aim in modeling local broadband seismogram is to understand the complexity caused by wave propagation as well as the source mechanism with better accuracy.

7.4.1 Synthetic Seismogram

A seismogram is the combined effect of source, propagation path and seismograph response. Incorporating these effects theoretically a seismogram can be computed which is known as synthetic seismogram. In waveform inversion technique, while comparing the observed and synthetic seismogram some misfit error is observed which is minimized by testing with different crustal velocity model and source representation. A seismogram is a record of ground amplitudes as a function of time, [i.e. u(t)] which can be represented by a Fourier inverse transformation as given below

$$u(t) = \frac{1}{2\pi}\int_{-\infty}^{\infty} U(\omega)\exp(i\omega t)\, d\omega \qquad (7.1)$$

where U(□) is the Fourier transformation of ground motion and can be written as,

$$U(\omega) = \int_{-\infty}^{\infty} u(t)\exp(-i\omega t)\, dt \qquad (7.2)$$

The Fourier transformation of ground motion is given by

$$U(\omega) = M(\omega)\, E(\Delta, \omega) \qquad (7.3)$$

where $M(\omega)$ is the Fourier transformation of source time function $m(t)$; $E(\Delta, \omega)$ is the response while traveling through the medium and also depends on the type of source mechanism, source depth and epicentral distance (Δ). If equation 4.3 is multiplied by response $I(\omega)$ of the seismograph, Fourier transformation of the seismogram is obtained. Substituting $U(\omega)$ from equation (4.3) into (4.1) a time domain ground motion or synthetic seismogram can be generated. There are various methods for computation of synthetic seismogram. In this study, wave number or slowness integration method (Kind, 1978; Kind, 1979; Bhattacharya, 1992) is used. The essence of this algorithm is to propagate the stress-displacement vector through a heterogeneous crustal medium consisting of horizontally stratified isotropic layers; and its numerical scheme has been discussed in several papers (Haskell, 1964; Dunkin, 1965; Wang and Herrmann, 1980 and Herrmann and Wang, 1985)

For a shear dislocation in an earthquake it is seen that the vertical or radial components of synthetic seismogram is a linear combination of 3 basic fundamental focal mechanisms and the transverse component is linear combination of 2 fundamental mechanisms (Harkrider, 1976). The coefficients of the linear combination are functions of dip (□), slip (□) and strike (ϕ) of the fault. Following Kind (1979), Wang and Herrmann (1980), Herrmann and Wang (1985), Muller (1985) and Bhattacharya (1992) the vertical component seismogram at an epicentral distance Δ due to a point shear dislocation may be represented as,

$$\mathrm{Uz}(\Delta, t) = M_o\left[a.\,ZDD + b.\mathrm{ZDS} + \mathrm{c.\,ZSS}\right] \qquad (7.4)$$

Where M_o is the seismic moment; and the values of a, b and c is defined by

$$a = \sin\lambda + \sin 2\delta \qquad (7.4.a)$$

$$b = -\cos\lambda\cos\delta\cos\phi + \sin\lambda\cos 2\delta\sin\phi \qquad (7.4.b)$$

$$c = \tfrac{1}{2}\sin\lambda\sin 2\delta\cos 2\phi + \cos\lambda\sin\delta\sin 2\phi \qquad (7.4.c)$$

Also

$$ZDD = \tfrac{1}{2\pi}\int_{-\infty}^{\infty} S(\omega)I(\omega)d\omega\int_{0}^{\infty} F_1(\mathrm{k},\omega)\, J_0(\kappa,\Delta)\, dk$$

$$ZDS = \tfrac{1}{2\pi}\int_{-\infty}^{\infty} S(\omega)I(\omega)d\omega\int_{0}^{\infty} F_3(\mathrm{k},\omega)\, J_1(\kappa,\Delta)\, dk$$

$$ZDS = \tfrac{1}{2\pi}\int_{-\infty}^{\infty} S(\omega)I(\omega)d\omega\int_{0}^{\infty} F_5(\mathrm{k},\omega)\, J_2(\kappa,\Delta)\, dk$$

where $S(\omega)$ is Fourier transform of source time function $s(t)$ and $I(\omega)$ is seismograph response; F_1, F_3 and F_5 are Green's function required to describe the wave field due to an arbitrary point shear dislocation source in a plane layered elastic medium and are given in Wang and Herrmann (1980), Bouchon (1981) and Coutant (1989); J_o, J_1, J_2, … are Bessel functions (Bhattacharya, 1992). In the above equations, *ZDD* is the *Z*-component displacement of a 45^o dip-slip type source (i.e. $\lambda = 90^0$, $\delta = 45^0$, $\phi = 45^0$), *ZDS* is the *Z*-component displacement of a dip-slip type source ($\lambda = 90^0$, $\delta = 90^0$, $\phi = 90^0$) and *ZSS* is the *Z*-component displacement of a strike-slip type source ($\lambda = 0^0$, $\delta = 90^0$, $\phi = 45^0$).

Similarly, seismogram in the radial direction, $U_r(\Delta, t)$ can be obtained as

$$U_R(\Delta,t) = M_o[a.RDD + b.RDS + c.RSS] \qquad (7.5)$$

where, $RDD = \tfrac{1}{2\pi}\int_{-\infty}^{\infty} S(\omega)I(\omega)d\omega\int_{0}^{\infty} F_2(k,\omega)\, J_1(k,\Delta)\, k\, dk$

$$RDS = \tfrac{1}{2\pi}\int_{-\infty}^{\infty} S(\omega)I(\omega)d\omega\left[\int_{0}^{\infty} F_4(\mathrm{k},\omega)\, J_0(\mathrm{k},\Delta)\, k\, dk - \frac{1}{\Delta}\int_{0}^{\infty} F_4(k,\omega) + F_9(k,\omega)\, J_2(\mathrm{k},\Delta)\, k\, dk\right]$$

$$RSS = \tfrac{1}{2\pi}\int_{-\infty}^{\infty} S(\omega)I(\omega)d\omega\left[\int_{0}^{\infty} F_6(\mathrm{k},\omega)\, J_2(\mathrm{k},\Delta)\, k\, dk - \frac{2}{\Delta}\int_{0}^{\infty} F_6(k,\omega) + F_{10}(k,\omega)\, J_2(\mathrm{k},\Delta)\, k\, dk\right]$$

Here *RDD*, *RDS* and *RSS* are radial components for the basic mechanisms as mentioned. The value of a, b, and c are similar as given by equations 4.4.a, 4.4.b and 4.4.c respectively.

The corresponding transverse component seismogram is given by,

$$U_{\phi}(\Delta, t) = M_o[\dot{a}\, TDS + \dot{b}\, TSS] \qquad (7.6)$$

where $\dot{a} = \sin\lambda \cos 2\delta \cos\phi + \cos\lambda \cos\delta \sin\phi$ (7.6.a)

$$\dot{b} = \cos\lambda \sin\delta \cos 2\phi - \tfrac{1}{2}\sin\lambda \sin 2\delta \sin 2\phi \qquad (7.6.b)$$

and

$$TDS = \tfrac{1}{2\pi}. \int_{-\infty}^{\infty} S(\omega) I(\omega) d\omega \int_{0}^{\infty} F_9(k, \omega)\, J_0(k, \Delta)\, k\, dk$$

$$TDS = \tfrac{1}{2\pi}. \int_{-\infty}^{\infty} S(\omega) I(\omega) d\omega \int_{0}^{\infty} F_{10}(k, \omega)\, J_1(k, \Delta)\, k\, dk$$

Here F_9 and F_{10} are given by Wang and Herrmann (1980). It is considered that, *TDS* is a seismogram with $\lambda = -90^0$, $\delta = 90^0$, $\phi = 0^0$ and *TSS* is a seismogram with $\lambda = 0^0$, $\delta = 90^0$, $\phi = 0^0$. The expressions for vertical, radial and transverse components can be obtained by solving the equation of motion in an elastic medium and using boundary conditions including those at the source. The detail evaluations of the above equations are obtained from Kind (1979), Ingate et al. (1983), Kind and Odom (1983), Wang and Herrmann (1980), Herrmann and Wang (1985) and Bhattacharya (1992).

7.4.2 Green's Function

There are number of factors that influence the synthetic seismogram. One of the important factors is the Green's function. The source displacement can be characterized by a system of force couples (Aki and Richards, 1980). If a unit force vector $f(x_o, t_o)$ is applied at point x_o at time t_o, a complicated realistic source can be described as a sum of these force vectors. A seismogram represented by $u(x, t)$ measured by a receiver at position x, is a complicated function of velocity of the seismic waves and density structure of the Earth and includes multiple seismic phases. The $u(t)$ function varies for different source and receiver positions. For every $f(x_o, t_o)$

and *x*, there is a unique *u*(*t*) function that describes the Earth's response and can be computed if the Earth's structure is known to sufficient accuracy. For the purpose of evaluation of *u*(*t*), the source terms are separated from all the other details of the wave propagation by defining a function called Green's function, *G* (*x*, *t*), that gives the displacement at point *x* resulting from the unit force function applied at point x_o. *G* (*x*, *t*), is expressed as

$$u_i(x, t) = G_{ij}(x, t; x_o, t_o)\, f_j(x_o, t_o)$$

where *u* is the displacement, *f* is the force vector and *G* is known as the electrodynamic Green's function. The calculation of Green's function is complicated taking in to account all the elastic properties of the material and the appropriate boundary conditions. The Green's functions are calculated using only the far field asymptotic terms, since the high frequency seismograms of the local earthquakes is used for inversion.

7.4.3 Source Time Function

Earthquake signal at the source is the source time function produced by faulting. In simplest case of a short fault that slips instantaneously, the seismic moment function is a step function whose derivative is a simple source time function (Stein and Wysession, 2003). The displacement that occurs in the opposite sides of a fault during an earthquake is not instantaneous but occurs over some finite duration of rupture, because finite fault does not break totally at the same time, instead waves arrive first from the initial point of rupture and later from points further along the fault (Fig. 7.4). Figure 7.4 shows a fault of length L along which the rupture propagates at a rupture velocity V_R. It is considered that there is a receiver at a distance r_o and azimuth □□from initial point of rupture (Fig. 7.4a). If V is the velocity of a seismic wave, the first seismic wave arrival is at time r_o / V and the far end of the fault rupture at time L / V_R, giving a seismic arrival at time ($L / V_R + r / V$), where r is the distance from the far end to the receiver. Application of cosine law gives,

$$r^2 = r_o^2 + L^2 - 2 r_o L \cos\square$$

If source-receiver distance is greater than the finite fault length (i.e. r >L), then

$$r = r_o + L \cos\square$$

Therefore the time pulse due to the finite fault length is a boxcar of duration

$$T_R = L(1/V_R - \cos\theta) = L/V\,(V/V_R - \cos\theta)$$

known as rupture time. These expressions can be modified for different fault shapes and rupture propagation directions. The slip history for a source is a function of time which begins at time zero and ends at rise time (□□□ Source time function depends on derivative of slip history. The source time function can be obtained convolving the rupture time and the rise time. The duration of the source time function varies as a function of azimuth depending on the ratio of the rupture velocity (V_R) and the wave velocity (V).

7.4.4.1 Expression for Source Time Function

The source time function or the moment function, m(t) can be written as

$$m(t) = Mo\ S(t)$$

where Mo = seismic moment = μ_s.A.D

μ_s = Modulus of rigidity at the source

A = Area of the fault

D = Average slip (displacement) of the rock above the fault

and $S(t) = 0$ for $t \leq 0$

$= g(t)$ for $0 < t < \tau$

$= 1$ for $t > \tau$

In the range $0 < t < \tau$, g (t) has a maximum value of 1 which is attained at $t = \tau$□□□rise time. Here, m(t) is the equivalent point-source moment function of the actual extended source and Mo is moment estimate for the earthquake and τ agrees approximately with the rupture duration. The seismic moment function $m(t)$ describes the faulting process in terms of the rigidity of the material and history of the slip, D(t) and fault area A. The derivative of the moment function $m(t)$ i.e. $\dot{m}(t)$, reflects the pulse radiated from the fault, which propagates at the P-wave speed α and arrives at a distance r at time $t - r/\alpha$.

There are various choice of g(t): (a) Ramp function [$g(t) = t/\tau$□□, which begins at time zero and ends at the rise time, τ (Fig. 7.5a)□□ The derivative of the

ramp function is a boxcar□□(Fig. 7.5b)□□The area enclosed by ġ(t) is 1. It can be shown theoretically that far field P waveform is given by $\dot{m}(t)$ or $\dot{s}(t)$, where "˙" shows differentiation with respect to time. Sometimes ġ (t) as shown in Figure 7.5b is not in conformity with observed far field P-wave (which appears as pulse) and any other choice from the following source time functions can be considered. (b) Source time function proposed by Brustle and Muller (1983) suggests g(t) = 9/16 [1- cos □t/□ + 1/9(cos□□t/□ - 1)]. The graphical presentation of this function and its derivative are shown in Fig 7.5c,d. (c) Source time function suggested by Wang and Herrmann (1980) is given by

$$
\begin{aligned}
2T\dot{g}(t) &= 0 && t < 0 \\
&= 0.5\,(t/T)^2, && 0 < t \leq T \\
&= -0.5\,(t/T)^2 + 2(t/T) - 1, && T < t \leq 3T \\
&= 0.5\,(t/T)^2 - 4(t/T) + 8, && 3T < t \leq 4T \\
&= 0 && 4T < t
\end{aligned}
$$

Where T = □/4, □□is rise time. The derivative of source time function g (t) i.e. ġ(t) is shown in Fig.7.5e. The time function has a unit area and has spectral zero at certain frequencies. If T = *m*.□t, (m is some power of 2), then the spectral zero are at frequencies f_N, $f_{N/2}$, $f_{N/4}$….. $f_{N/2m}$ (f_N is the Nyquist frequency) defined by f_N= 1/2□*t* and N is also a power of 2. By choosing □ and □t such that one of the spectral zeros occur at the Nyquist frequency, the pulse can be synthesized and propagate through the model without the rippling introduced by an arbitrary sharp high frequency spectral cut off. (d) Triangular source time function ġ(t) is a less complicated far-field source time function. The graphical representation of a triangular source time function is as shown in Fig. 7.5f. (e) Trapezoidal source time function is trapezoidal in shape and characterized by rise time (□□□and□□rupture duration (T_R) as shown in Figure 7.5.g.

7.4.5 Digital Waveform Data

The data set consists of waveform from 63 number of selected local earthquake events (M < 3.5) recorded by local seismic network under operation in the region (Table 7.2 and 7.3). This study utilizes 2 numbers of events each that are

selected from the Sylhet fault region in Bengal Basin and Mat fault region in Tripura-Mizo fold belt. These selected events are recorded by seismic station at Aizawl (AZL), Mizoram. Selection is made on the basis of high signal to noise ratio, accurate epicentral location, clear and impulsive record of P and S phases and better azimuthal coverage. However, emphasis is given to the smaller earthquakes ($M \leq 3.5$) recorded at short distances for source mechanism study. Hypocentral parameters are determined following HYPOCENTER location program (Lienert et al., 1986). Estimation of hypocentral parameters indicate that the RMS time residuals are generally less than 0.25 sec resulting in epicentral and depth error of less than 1 km.

7.4.6 Preprocessing of Data for Inversion

The velocity seismograms selected for waveform inversion are prepared by removal of mean, tapering and band pass filtering. The lower and higher cut off values for the band pass filter depends on the background noise level that exists in the signal. All the three component seismograms are filtered using 8-pole Butterworth band pass filter (Scherbaum, 1994). The seismograms are filtered within the range 1-2, 2-4 Hz that give smooth noise free waveform to be used for inversion. The observed waveforms are corrected for instrument response so as to get the corresponding ground velocity. Using instrument response the amplitude counts are converted to cm/sec unit. The angle of incidence and the back azimuths for each event are calculated from the hypocentral parameters. The back-azimuth is the angle measured between the vector pointing from the station to the source and the vector pointing from the station to the north and the incidence angle is defined as the angle measured between the ray vector at the station (from the source to the station) and the vector pointing from the station straight up. Using the two parameters the observed waveforms are rotated to get vertical, radial and transverse components. After this, the vertical, radial and transverse components are windowed to a appropriate length to include the P and S onsets for each component excluding the later part of the S-wave i.e. coda wave, because coda waves are considered to be scattered waves with little relationship to the source process (Der et al., 1991).

7.4.6.1 Background Noise Evaluation

The broadband data at different stations have different site noise characteristics. In order to obtain an idea about the site characteristics, background noise evaluations are carried out. The power spectral estimates have been corrected for the system response and gain representing the sensor input. Stations instrumental in the Low Noise Model (Peterson, 1993), however decreased cultural noise (0.1-1s, 1-10 Hz) the highest power level (Red, Green and Blue) are not significantly higher (<26%) than the low noise model (LNM). After 1 sec the power level marginally (<10%) varies with LNM. The three lines approach the LNM indicating that the station minimum reflects actual ambient noise conditions across the whole spectrum.

Variable pass bands are used for the stations based on background noise evaluation. The low cut off is then set at the frequency where the signal to noise ratio (S/N) is above amplitude level of 1.0E-03 cm/sec. The higher cut-off, on the other hand, is set at 2.4-4.0 Hz to reduce the effect of scattering and to avoid the calculation of high frequency portion of the synthetic seismogram. The data is discarded if the bandwidth between two corners is too narrow.

7.4.6.2 Conversion of Amplitude from Counts to cm/sec

In a digital recording seismograph, the output from the seismometer (in the form of voltage) is fed to an amplifier and the amplified output is fed to digital recorder, which records the ground motion in terms of digital counts converting voltage into counts. In order to obtain the actual ground motion, the amplitude counts for the velocity seismograms are converted to centimeters/second using the instrument response.

An example for conversion of velocity seismogram recorded by the broadband station at Aizawl (AZL), Mizoram equipped with CMG-40T (Guralp make) sensor and REFTEK 72-A/07 data acquisition system with related parameters is as follows:

Data format = 24 bit

Sampling rate = 100 SPS

Velocity sensitivity = 1500 *V/m/s*

Analogue to digital (A/D) conversion factor = 1.907E-06 *Volts/counts*

Preamplifier gain = 1

The appropriate conversion is obtained as,

$$Ground\ Velocity = \frac{Amplitude\ (counts) * A/D\ \ Conversion\ \ factor\ (V/counts)}{pre\,amplifier\ \ gain * Sensitivity\ (V/m/s)}$$

$$= Amplitude\,(counts) * \frac{(1.907E-06\ V/coutns)}{1*1500\ V/m/s}$$

or, $$Ground\ Velocity = \left[\left(Amplitude\ counts\right) * \frac{(1.907E-06)}{1*1500} \right] \quad m/\sec$$

or , $$Ground\ Velocity = \left[\left(Amplitude\ counts\right) * 1.27E-7 \right] \quad cm/\sec$$

In case of REFTEK-72A/08 data acquisition system 1.907 □V corresponds to 1 digital count.

7.4.7 Crustal Velocity Model

A local crustal velocity model, which can generate the recorded characteristics of near earthquake phases, is very much essential for retrieval of source parameter of small events (M≤3.5). The high frequency characteristics of local and regional seismograms are influenced by complex velocity structure of the medium on small scale and source process (Sileny et al, 1992; Saikia, 1994; Sileny, et al., 1996). Generally the crustal structure is determined by matching the travel times of P and S waves without accounting for the amplitude. It is very difficult to use this type of average crustal velocity model in waveform modeling in case of high frequency seismograms. Besides defining gross crustal structure, it is very much necessary to define the shallow structure near the receiver so that the velocity model can predict the observed P-wave and S-wave amplitudes. Surma valley is a complex tectonic domain and the detailed crustal velocity structure is not properly known. Hence the logical approach is to start the focal mechanism inversion with the standard crustal model i.e. the model used for earthquake location in the region under study and to employ the focal depth from location procedure. In order to avoid ambiguity, two best strategies are made: (i) to perform location and calculation of take-off angle with these two models without first arriving interface wave and (ii) to calculate Green's

function and synthetic seismograms in realistic model while repeating the focal mechanism inversion with varying focal depths.

7.4.8 Methodology

It is assumed that the crustal velocity models used are realistic one and the hypocentral parameters of the studied events are accurate. The waveform inversion technique adopted in the present study is described as follows:

(i) The events recorded by the digital broadband stations are selected on the basis of high signal to noise ratio and clear record of P and S arrivals.

(ii) The 3-component digital records are converted to single column ASCII file and inspected for completeness and undesired instrumental influences. The multiple events in the same record are separated and the P-wave first motions are noted.

(iii) The observed waveforms are corrected for instrument response and rotated to get vertical, radial and transverse components after baseline correction and trend removal with the help of PITSA program (Scherbaum, 1994).

(iv) The seismograms are then low pass filtered below the corner frequency. The high frequency components are excluded because it is difficult to model high frequency components as it require a precise knowledge of detailed subsurface crustal velocity model which is not properly known for the study region.

(v) Green's functions are computed in the complex spectral domain for a given station source path with the help of PSV and SH computer programs modified after Bhattacharya (1992). These two programs are developed following Wang and Herrmann (1980) and Herrmann and Wang (1985). The program PSV calculates the Green's functions for the vertical and radial components and SH computes the Green's function for tangential components. Before computation the calculated time window is fixed to 20.48 seconds, so that frequency step is df = 1/20.48 Hz = 0.05 Hz. Such a special choice, together with the 2048 complex points, gives the time increment of synthetic seismograms of dt = 0.01 s. In calculating Green's function, the exact Earth flattening transformation is used following Intgate et al. (1983), thus preserving exactly the kinematics and dynamic properties of the wave field in the plane layered medium.

(vi) The source time function is generated for an assumed rise time using a computer program SW.

(vii) The Green's function are multiplied with the instrument response function and appropriate source time function generated in step (vi), so as to get the synthetic seismogram for the fundamental focal mechanisms as discussed (section 7.4.1). A computer program named GRAM is used for this purpose. Output of PSV, SH and SW along with the instrument response, I (t) are the inputs to GRAM. Output of this program results the synthetic seismograms for the fundamental mechanisms i.e. *ZDD, ZDS, ZSS, RDD, RDS, RSS, TDS* and *TSS*. While generating these reference seismograms a unit seismic moment Mo = 10^{20} dyne-cm is considered.

(viii) The synthetic seismograms for the fundamental focal mechanisms are combined linearly for vertical, radial and transverse components separately with different choices of λ, δ and θ as coefficients so as to get required synthetic seismograms for three components [U_Z(□□t), U_R(□□t) and U_T(□□t)] which matches with the observed seismogram. The absolute amplitude of the synthetic seismogram is matched with the observed seismogram with appropriate selection of M_o. This step uses a program GRAPH. Final validation of the best fitting solution is accomplished by comparing the observed and synthetic seismogram in time domain. For better reliability of the solution amplitude spectra of synthetic and observed are also matched in frequency domain. At the point of optimum domain fit, it is assumed that the parameters (λ, δ, θ□and Mo) used in computing the synthetic seismograms are best obtainable estimates for the event used.

7.5 RESULTS

7.5.1 Results of Fault Plane Solutions

The focal mechanism solutions of 67 numbers of events form the database for the present study (Fig. 7.3). Most of these solutions are obtained from GCMT database. Few solutions are determined for the present purpose by incorporating more than 45 stations data from ISC Bulletin, RRL-Jorhat and NGRI-Hyderabad seismological bulletin as well. Distribution of dataset for the events depicting the percentage of faulting type is shown in Table 7.4. It is observed that the region is

dominated by existence of higher percentage of strike-slip faulting. Table 7.1 indicates the events that comprises of focal mechanism solutions determined through first motion P-wave polarities, CMT solution and focal mechanism solutions obtained through waveform modeling. Four solutions (black and white) are obtained through waveform inversion (Fig. 7.3). Fault plane solutions for the events associated with Sylhet fault region in the northern part (Table 7.5) and Mat fault region (Table 7.6) in the eastern part are shown separately in Figures 7.6a and 7.7a respectively. A depth section of the beachball representing Fig. 7.6a is shown in Figure 7.6b. Figure 7.6 c, d, e, f indicate the associated nodal plane, P-axis orientation, T-axis orientation and both P- and T-axis orientation along the northern part of the Surma valley. Most of the nodal planes are oriented along North-South while P-axis orienetation is found to be along East-West. Similarly, a depth section of the beachball representing Figure 7.7a is shown in Figure 7.7b. Figure 7.7 c, d, e, f indicatating the associated nodal plane, P-axis orientation, T-axis orientation and both P- and T-axis orientation along the eastern part of the Surma valley. Most of the nodal planes are oriented along North-South while P-axis orientation is found to be along North of North-East.

The beachball presentation in Figures 7.6b and 7.7b for regions in the northern part and the eastern part respectively appears quite significant when a depth level of 41-60 km is considered. The events occurring within this depth range are characterized by the regime of dip-slip and thrust type of focal mechanisms. Figure 7.6c and 7.7c shows nodal planes of the respective focal mechanism solutions of the events associated with regions belonging to Mat fault and Sylhet fault. Most of the solutions are characterized by thrust and strike slip fault.

P and T-axis orientations (azimuth) have been plotted along the direction of Sylhet (Figs. 7.6d, e and f) and Mat faults respectively (Figs. 7.7d, e and f). It may be noted that in later figures as mentioned, the definition of the azimuth as would be seen in a map view is retained while the center of each line corresponds to the position in depth, of the solutions. An important observation is that P-axis (compressional axis) of all the events, including thrust, strike slip and normal type of solutions, are predominantly East-West directed along Sylhet fault while for Mat fault P-axis orientations are predominantly north north-easterly directed. The direction of the compressional axis long the respective fault indicate the prevailing stress condition of

the region. As thrust and strike-slip mechanisms dominate, these two state of mechanisms reflect N-S compression rather than E-W extension.

7.5.2 Results of Waveform Modeling

The focal mechanism solutions from Mat and Sylhet faults recorded by Aizawl station (AZL) obtained using waveform inversion technique are as described below:

(1) 26 February 2003 (Origin time: 17^h: 32^m: 17.00^s, Lat: 24.347^oN, Long: 91.543^oE, Depth: 20 km, Mag: 2.7 M_DA)

The event is associated with the Mat fault recorded by Aizawl seismic station (i.e. AZL) and other stations in the vicinity. The broadband seismogram recorded at AZL seismic station is used to apply the inversion technique for evaluation of source mechanism (Fig. 7.8a, b and c). The observed data is rotated to get vertical, radial and transverse component seismogram using incident angle 220^o and back azimuth 40^o. The inversion is carried out for a frequency band (1-2 Hz) which is below corner frequency (i.e. 10 Hz). The Green's functions are computed using velocity model Bhattacharya et al., 2005 for station source-path of 42 km at depth 33 km. The synthetic seismograms are calculated, assuming source time function suggested by Wang and Herrmann (1980) with source duration □□=0.3 sec. Possible focal mechanisms are evaluated for which the synthetic seismogram matches with the observed data. This is done by a grid search technique and the best mechanism thus obtained possesses the following parameters: Strike = 178^o, Dip = 76^o and Rake = 165^o. The seismic moment and the moment magnitude are found to be 5.978E+12 Nm and 2.6 Mw respectively. The agreement between the observed and the synthetic seismogram is shown in Figure 7.9a, b, c and d. A good matching is observed for P-wave in the vertical component and S-wave in horizontal component. The mechanism suggests that the event is caused by pure strike-slip faulting. The T- axis trends towards the southwest (azimuth = 134^o and plunge = 69^o) and the P-axis towards the northeast (azimuth = 224^o and plunge = 89^o) (Fig. 7.10a and b). The estimated source mechanism for this event is

	Strike	Dip	Rake
Np1	178	76	165
Np2	272	75	14

Seismic moment =5.98e+012

Mw =2.6

Faulting type: Strike-slip

(2) 27 July 2003 (Origin time: 27^h: 89^m: 12.07^s, Lat: 24.192^oN, Long: 92.262^oE, Depth: 20 km, M = 3.7 M_DA)

The event is associated with the Mat Fault located in Tripura-Mizo fold belt. It is well recorded by the local seismic station AGT, SHL, IMD and AZL. The waveform data from AZL station possesses comparatively higher signal to noise ratio than the other stations and therefore selected for inversion purpose (Fig. 7.11a, b and c). The inversion is carried out for a frequency band (0.2-1.0 Hz) below corner frequency (i.e. 4 Hz). The Green's functions are obtained for station source path of 9 km from the station AZL with source depth of 33 km assuming 1D velocity model of Mukhopadhyay et al., 1997. The grid search technique produces many solutions with higher correction coefficients for P- and S-wave amplitudes. The inferred solution is unable to predict the observed amplitudes of P- and S-wave at AZL station as excepted. So the attention is paid to smoothly modify the velocity model. The P-wave velocities are decreased from 6.3 km/sec to 5.9 km/sec at depth 5 km with Vp/Vs = 1.71 and the Green's functions are recomputed. Each mechanism obtained from grid search technique is tested by predicting the observed mechanism at AZL for P-wave group. Finally a solution with strike : 247^o, Dip: 22^o, and rake: 21^o is found for best double-couple solution from the waveform prediction. The T-axis of this mechanism give azimuth: 69^o and plunge: 41^o; and P-axis gives azimuth: 209^o and plunge: 55^o. A seismic moment of 3.34E+23 Nm dyne-cm is used. The moment magnitude is found to be Mw = 4.9 (Fig. 7.13a and b). The synthetics of AZL correlate very well with the observed seismogram (P-wave group) both in amplitude and phase for vertical and radial component while the transverse synthetic is not predicted well (Fig. 7.12a, b, c and d). Although the predicted amplitude range is found to be equivalent with the observed amplitude, the mismatch is due to contribution of noise exist in the observed transverse seismogram. The mechanism suggests that the event is caused by thrust with strike-slip component type of mechanism. The estimated source mechanism for this event is

	Strike	Dip	Rake		
Np1	247	22	21		
Np2	137			82	110

Seismic moment = 3.34E+23

Mw = 4.9

Faulting type: Thrust with strike-slip component mechanism

(3) 15 July 2003 (Origin time: 20^h: 90^m: 16.53^s, Lat: 24.361^oN, Long: 91.321^oE, Depth: 20 km, M= 3.3 M_DA)

The event is originated in the Bengal Basin. The event is recorded by a number of seismic stations in the Northeast. Velocity seismogram recorded by AZL seismic station is utilized to invert the waveform (Fig. 7.14a, b and c). A low pass filter 1-3 Hz is applied to eliminate the high frequency components and corrected for instrument response. The waveform is rotated to get vertical, radial and transverse components using incident angle (310^o) and back azimuth (130^o) calculated for AZL station. The Green's functions are computed for epicentral distance 50 km and at a depth of 37 km using velocity model of Bhattacharya et al., 2005 and convolved with different source time functions to obtain a synthetic seismogram which matches with the observed one. It is observed that the source time function suggested by Wang and Herrmann (1980) is a good choice for this event with assumed slip duration or rise time □□= 0.5 sec. Using fine grid search technique and applying amplitude constraints, the synthetic seismograms are generated for different choice of □□□□□and□□, so as to get a good matching between the synthetic and observed data. The best mechanism thus obtained has the following parameters: Strike= 159^o, Dip=87^o, Rake=174^o. Figure 7.15a and b shows the comparision of synthetic and observed seismogram. The mechanism suggests that the event is caused by pure strike-slip faulting. The P-axis trends toward the northeast (azimuth: 204^o and plunge: 87^o) and the T-axis toward the southwest (azimuth: 114^o and plunge: 83^o). An average seismic moment of 4.69E+12 Nm dyne-cm was used to predict the synthetic seismogram. The moment magnitude is found to be 2.5 Mw (Fig. 7.16a and b). The estimated source mechanism for this event is

	Strike	Dip	Rake
Np1	159	87	174
Np2	250	84	3

Seismic moment =4.696e+012

Mw =2.5

Faulting type : Strike-slip

(4) 30 June 2003 (Origin time: 13^h: 06^m: 00.07^s, Lat: 24.839^oN, Long: 91.838^oE, Depth: 20 km, Mag: 3.4 M_DA)

The event occurred near the intersection of Mat fault and Sylhet fault in the Surma valley. The event is modeled using the waveform from AZL station (Fig. 7.17a, b and c). The inversion is carried out for a frequency band (1-2 Hz) below corner frequency (i.e. 8 Hz). The seismogram from AZL station is rotated to get vertical, radial and transverse components using incident angle (349^o) and back azimuth (169^o) calculated for AZL station. The Green's functions are computed for epicentral distance 83 km from TZR station and focal depth of 33 km using velocity model of Bhattacharya et al., 2005. The synthetic seismogram with source duration □□□□0.3 sec, Mo = 5.889E+12 Nm and the mechanism maintaining Strike = 173^o, Dip= 89^o, Rake = 168^o fits the observed waveform data. The source time function suggested by Wang and Herrmann (1980) is assumed. The mechanism suggests a strike-slip component of motion. The P-axis trends toward the northeast (azimuth: 218^o and plunge: 86^o) and the T-axis toward the southwest (azimuth: 127^o and plunge: 85^o). The moment magnitude is found to be 2.6 Mw (Fig. 7.19a and b). A good agreement of synthetic and observed seismogram in case of P-wave is observed in the vertical component compared to the radial and transverse components whereas S-wave amplitude of the synthetics agrees up to some extent in all the three components as shown in Fig. 7.18a, b, c and d. The earthquake is triggered by Sylhet fault. The estimated source mechanism for this event is

	Strike	Dip	Rake
Np1	173	89	168
Np2	264	78	1

Seismic moment =5.889e+012

Mw =2.6

Faulting type : Strike-slip

7.6 DISCUSSION

This chapter deals with the determination of focal mechanism solution using P-wave first motion data and waveform inversion techniques. The events used for source mechanism study originate from Bengal Basin and Indo-Burman region.

The source mechanisms through P-wave first motion data are determined by acquiring data from local seismic network supplemented by phases from the stations at teleseismic distances. Focal mechanism solutions for the events M>4.0 are well constrained because of availability of required number of P-wave first motions. The uniform distribution of azimuth of a large number of stations is one of the important prerequisites for a reliable focal mechanism solution (Khattri, 1973). However this is not the case for the events (M<4.0) originated in NER. In case of these events estimated focal mechanism solutions are not well constrained due to sparse distribution of recording stations. This situation worsen in the case of events M<3.0. Determinations of focal mechanisms for these events tend to near impossible with first motion P-wave arrival because very less number of stations record these events. However, basic limitation in the study of focal mechanism through P-wave first motion method for shallow focus earthquake arises by virtue of the very limited coverage of focal sphere by the observation data. The coverage improves with the increase in depth of focus. These constraints are observed by various researchers (Khattri, 1973; Chandra, 1978 etc). The focal mechanism solution using P-wave first motion data use only a fraction of information contained in body waves. In the contrary the estimation of seismic moment and moment magnitudes are not possible.

Overcoming the constraint faced in P-wave polarity method, source mechanisms of few events (magnitude range 2.7-3.7) are carried out through waveform inversion. The studies of small magnitude earthquake at short epicentral distances are important as they are not influenced by too much contamination from source-path velocity structure. Estimation of source parameter of these earthquake events through waveform inversion gives better idea of path effect and amplitude information.

Simulations of synthetic seismograms are achieved to estimate the source parameters in order to define a source. The complex function of many variables i.e. Green's functions are deduced for each propagation path. The effect of propagation

path is simulated by convolving the source time function with Green's functions in the form of impulse trace for particular source duration. In the process, existing information regarding crustal velocity structure in the region is used for reliable focal mechanism solutions. The synthetic seismogram so predicted is compared with the observed seismogram by determining a suitable solution among number of admissible solutions. From the comparison of observed and synthetic seismogram it is seen that these seismograms do not match perfectly and that differences are mostly in the low amplitude high frequency details of the waveform. Der et al., (1991) also made similar observations. Therefore the seismograms are low pass filtered. This filtering process reduces the high frequency components which is not included in synthetic waveform. The error contained in the focal mechanism of these earthquakes through waveform inversion is difficult to quantify in an absolute sense because of the interdependence of the structure, source time functions and focal mechanisms on the final waveforms**.**

It is almost impossible to model local high frequency signal, unless the velocity structure is adequately known. It is observed that when a simple crustal model is used, the synthetic are too simple, much shorter than the real records. Then the inversion needs cutting and tapering of real records, which is avoided in this study. The study uses a bit upgraded crustal model, producing synthetics whose duration is comparable to real records. The use of velocity model by Bhattacharya et al., (2005) for the events produces reliable synthetic seismograms. This approach has made the solution most reliable.

The focal mechanism solutions obtained through waveform inversion and by P-wave polarity method indicate that the Surma valley is dominated by strike-slip and thrust faults. Strike-slip solutions that relate with Mat fault characterize the fault type and also solutions along the Sylhet fault indicate that the fault is dominated by strike-slip type of mechanism. Thrust fault with easterly/northeasterly dipping fault planes are observed in Indo-Burman ranges.

CHAPTER-VIII

SUMMARY AND CONCLUSIONS

8.1 SUMMARY AND CONCLUSIONS

Seismotectonic study is one of the most crucial and typical studies as far as seismically active regions are concerned. The most important components pertaining to the seismotectonic study are wide but these primarily and mainly relates to the better estimation of hypocentral parameters. Best estimated hypocentral parameters are the prime input to the seismotectonic study of any region. The study begins with the prediction of seismicity map which ascertains comparatively high and low seismically active region. A regional seismicity map for Surma valley and the adjoining region, covering the area bounded by longitudes 90^{o} to 95^{o}E and latitude 22^{o}N to 26^{o}N has been prepared by plotting the earthquake data for the period from 1969- 2010 (source: ISC) over the generalized tectonic maps of the region. From this study, it is concluded that most of the seismic events fall in the tectonic domains of the Surma basin, Meghalaya Plateau and Indo-Myanmar region. Surma and Bengal basins have shallow focal depth i.e.<70km except for a few events in the NW trending wedge shaped block lying between the Kopili and Bomdila faults. The earthquake events in these tectonic domains occur in diffused pattern having post-collisional intracratonic characteristics. On the other hand, most of the earthquake events falling in the Indo-Myanmar (Burmese) tectogenes have focal depths varying from 70-150 km where seismicity is more intense and defines the westerly convex broadly N-S subduction zone of the Indian plate. The region under investigation is the Northeastern prolongation of the Indian Shield comprising Surma valley bounded by Post-Barial unconformity, the NE-SW Sylhet fault and SE-NW Mat fault.

In this thesis, an attempt is made to re-look into the seismic activity of the region. In addition the study also tried to estimate the travel times of P and S waves apart from estimation of Vp/Vs ratio and the inferences made through focal mechanism solutions. The seismic activity are studied on the basis of data during the period 1969 to 2009 over a span of 40 years time incorporating more than 4500 events in the database (Fig. 4. 5). In order to infer the distribution of Vp/Vs ratio, correlation

with the crustal lithology and characterization of Mat and Sylhet fault are well addressed in this thesis.

The travel time of P- & S-wave and subsequent distribution of Vp/Vs along varying depths plays an important role to understand the seismotectonic of the region. On a local scale the main objective is to determine the precise variation of travel time ratios along depth sections. No study is, however, made to estimate this aspect using travel times of P- and S-waves of the local earthquake events recorded from local broadband seismic stations in the studied region. Picking up of precise reading of seismic phases of the local earthquakes in the analog records of earlier seismic networks was difficult. With the advent of digital seismic network permitting precise detection of seismic phases, however, it is possible to estimate the travel times of P- and S-waves. Besides this, an attempt is made to incorporate the variation of Vp/Vs ratio in depth sections. Additionally, source characterizations are made by studying the source mechanism inferred from first motion P-wave polarity and waveform inversions.

Chapter-II gives the general introduction to the tectonic settings of Surma valley and the adjoining regions. The seismicity plot of the studied region demonstrates well defined trends of seismicity that correspond to local and regional tectonic settings. A new modified tectonic map has been developed for the study area in GIS environment using satellite imageries. This map incorporates all the major faults and lineaments that are common and uncommon in GSI map of 2001. Geotectonic settings of Surma valley have been described on the basis of this map in this chapter. This map for the Surma valley is thought to be accurate one because it is digitally prepared, geo coded and GIS based.

Estimation of true ground motion is the prime pre-requisite for digital signal processing e.g. spectral analysis, waveform inversion, path modeling etc. This study tries to formulate an amplitude frequency response function by correcting the effect of recording media for the respective station equipped with digital seismograph. A methodology for this is described briefly in Chapter III. The estimated central frequency band is 0.002-5.0 Hz for the digitizer equipped with CMG-40T sensor. The pass band so estimated indicates the plateau value nearly 1 count/nm/sec towards amplitude. The plateau value ascertains the true ground motion. In this chapter,

amplitude frequency response to the ground velocity with known pole zero distribution for AZL station in Surma Valley has been established.

Determination of precise location of epicenters and depth are the prime input for better understanding of the true seismicity pattern of a region. Chapter-IV incorporates the methodology for determination of relocated values of precise hypocentral parameters. A total of 2578 numbers of events recorded during 1982 to 2009 by local seismic network (RRL-J, NGRI-Hyderabad are relocated) have been used for determination of hypocentral parameters. Hypocentral parameters so determined form the basic database to the present study where uncertainties involved in the estimates of origin time are of the order of 0.0-0.02 sec for about 80% of the total number of events. Similarly, the uncertainties involved in the estimates of focal depths are 0-2 km for a total of 85% numbers of earthquakes relocated. The seismogenic zone in Surma valley and its adjoining region is constrained between 20-40 km. On the whole Surma valley and its vicinity experienced maximum number of events which occurred within the range of magnitude 3.0-5.0.

In Chapter-V an attempt is made to estimate the travel times of P- and S-waves from the relocated hypocentral parameters made in Chapter-IV. The detailed methodology and data analysis following Wadati and Riznichenko diagram are described in this chapter. The Wadati and Riznichenko plots are made for the events around Sylhet fault region in the northern part and Mat fault region in the eastern part of Surma valley. The Wadati diagrams show systematic decrease in ts/tp, suggesting that the velocity for shear waves increases faster than that for the compressional waves in the upper levels of the crust. Wadati diagrams for eastern part of Surma valley and its vicinity shows that the plots are well constrained so far the values of *Ts-Tp vs. Tp* and *Ts-Tp vs. Ts* are concerned. Riznichenko diagrams clearly show the change in shape of the travel time versus distance curve with increasing focal depth, and is indicative of both a geometrical effect and an increasing P-wave velocity. Riznichenko diagrams are plotted against various depth intervals. All the plots indicate clear dependence of S-P travel time (Ts-Tp) with respect to epicentral distance ($+$). The travel times so estimated forms the basis for the estimation of Vp/Vs ratio in Chapter V.

In Chapter VI, the distribution of crustal velocity ratio (Vp/Vs,) has been made in Surma valley comprising Mat fault region in the eastern part and Sylhet fault region in the northern part. The Vp/Vs ratio for the Surma valley and its vicinity are distributed over the range 1.67 to 1.79. Low values of Vp/Vs ratio are observed in the eastern part of the Surma valley. These variations obviously characterize the heterogeneity of the crust at different depth sections. The distribution of Vp/Vs velocity ratio in Mat fault region (eastern Surma valley) in different depth ranges are found to be varying between 1.75 to 1.83 in 0-20 km depth range. The distribution of Vp/Vs velocity ratio in the northern part of Surma valley which is traversed by Sylhet fault establishes a different picture. In the depth range of 20-40 km, a highly inconsistent nature of the velocity is observed at approximately 33 km depth where the velocity takes a sharp bends. The velocity ratio (Vp/Vs) suddenly decreases from ~1.77 to ~1.7 at this 33 km depth. This behavior of the sudden decreases in velocity may be due to the in-heterogeneous nature of the crust. In the depth range of 40-60 km, however, a more or less uniform velocity is observed throughout the range where Vp/Vs ratio is at approximately 1.78. Vp/Vs ratio could be utilized to discriminate lithology of the study area. For instance the low velocity for the P-wave found for depth section 41-60 km in Mat fault region could be produced by high velocity saturated material with high crack density. Sometimes, high velocity observed with low velocity ratio implies that the material is likely to have low crack densities, low intrinsic velocities and possibly higher effective stress at that range. Similarly, lower Vp/Vs ratio at a depth of 21-40 km in Sylhet fault region may be due to the reason that the region is guided by higher effective stress level for the properties of the rocks at depths involved in the brittle deformation associated with the earthquake faulting.

Chapter VII interprets the focal mechanism solutions that are obtained by using P-wave polarity method and waveform inversion technique. To decipher the style of current deformation in the valley, 67 focal mechanism solutions have been examined. The earthquakes occurring in the Surma Basin, giving mostly thrust solutions with strike-slip component, are related to the tectonics of Indo-Myanmar tectonogens as this domain belongs to Neogene outer arc regime for the eastward subducting Indian plate. Variable amount of thrusting and strike slip faulting affect the N-S trending structures in Surma basin which is not well depicted revealing the

present day displacement pattern (Jade et. al., 2007). P and T-axis orientations (azimuth) have been plotted along the directions of Mat fault in eastern part and Sylhet fault in northern part of the Surma valley respectively. An important observation is that P-axis (compressional axis) of all the events, including thrust, strike slip and normal type of solutions, are predominantly north-north westerly along Sylhet fault while for Mat fault P-axis orientations are predominantly north north-easterly directed. The direction of the compressional axis long the respective fault indicate the prevailing stress condition of the region. As thrust and strike-slip mechanisms dominate, these two state of mechanisms reflect N-S compression rather than E-W extension. Present observation on seismicity are in agreement with studies made by Molnar(1984), Nandy and Dasgupta (1991) and Verma(1991).

Waveform inversions of four local earthquake events recorded by Aizawl (AZL) station are able to produce the source parameters, seismic moment and moment magnitude. Significant phases like P- and S-wave and P- wave groups in a seismogram are inverted with an aim to generate synthetics and compared with observed seismogram. Focal mechanism solutions determined through waveform inversion for comparatively lower magnitude earthquake show that most of the source are characterized by strike-slip type of faulting. A good agreement between the observed and synthetic seismogram observed for best mechanism indicate that solutions are mostly reliable with reference to the velocity structure used. Moreover the study finds that a low pass filtered seismogram is best suited for inversion rather than high frequency component. This study shows that seismograms recorded from a short epicentral distance can be modeled, provided the velocity structure is reasonably well known. Hence the study depicts that both the Sylhet and Mat faults are characterized by Stike-slip faulting.

The conclusion made in the present study could be used as a primary input to the earthquake hazard assessment in Surma valley and its vicinity.

8.2 SCOPE OF FUTURE STUDY

Present study covers the seismicity of Surma valley particularly with respect to two prominent faults, Mat and Sylhet. Although considerable work is accomplished applying different techniques and approach in the region, extensive research was

needed to be conducted in order to have an in-depth knowledge of this tectonic domain.

In order to understand earthquake prediction/precursor substantially, in addition to monitoring seismicity, both the faults under consideration (Sylhet and Mat faults) along with other faults/lineaments in the Surma valley, require a permanent multi-parameter geophysical observatory for precursor studies and close monitoring of crustal deformation across the fault zone by GPS measurements. Large and damaging earthquakes that occurred in the study region are a clear reminder of the devastation that is due to happen anytime in the future. In this respect, investigations relating to paleoseismology, precursor study and microzonation may be useful in mitigating seismic hazards.

So far any assessment for predicting future earthquakes from statistical analysis or analysis of past earthquake events is concerned, it is unlikely to yield any tangible and useful result, until in-depth knowledge of tectonic evolution, characteristics of individual and distinct tectonic domain is obtained through rigorous field geological and geophysical investigations. Attempt has to be made to synthesize all available updated information on geology, tectonic, gravity, seismicity including those derived from the remote sensing technique of Surma valley and the adjoining region to bring out the active tectonics of the region and to identify the seismogenic structures or earthquake source zone so that future research in these fields can be rightly oriented with identified thrust areas having the objective for mitigation of earthquake hazards in this highly vulnerable region of our country.

BIBLIOGRAPHY

Anand, A. and Jain, A. K., 1987. Earthquakes and deformational structures (seismites) Holocene sediments from the Himalayan-Andaman Arc, India, *Tectonophysics,* **133**, 105-120.

Aki, K. and Richards, P.G., 1980. Quantitative Seismology, Theory and Methods. *Vol. I and II, WH Freeman, San Francisco.*

Archuleta, R.J., 1982. Analysis of near source static and dynamic measurements from the 1979 Imperial Valley earthquake. *Bull Seism. Soc, Am.* **72,** 1927-1956.

Banghar, A. R., 1990. Mechanism solutions of two recent Indian earthquakes. *Symposium on recent advances in seismology and their applications, Bangalore, India,* July 16-19, Abs. vol. 555-3.

Baranowski, J., Ambruster, J. and Seeber, L., 1984. Focal depths and fault plane solutions of earthquakes and active tectonic of the Himalaya. *J. Geophys. Res.,* **89 (B8),** 6918-6928.

Baruah, M., 1995. Body waves investigations in Northeast India. *Ph.D. thesis, Dibrugarh University, Assam, India (Unpublished).*

Bender, F., 1983. Geology of Burma. *Borntrager, Berlin, 293, Gebruder Bomtraeger, Verlin.*

Bevis, M. and Isacks, B.I., 1984. Hypocentral trend surface analysis: Probing the geometry of Benioff zones. *J. Geophys. Res.,* **89,** 6153-6170.

Bhattacharya, S.N., 1992. Crustal and upper mantle velocity structure of India from surface wave dispersion. In : Guest Editor. Gupta, H.K., Seismology in India – An Overview. *Current Science., Special Issue.* **62 (1&2),** 94-100.

Bhattacharya, S. N. and Dattatrayam, R. S., 2000. Recent advances in seismic instrumentation and data interpretation in India. *Curr. Sci,* **79,** 1347-1358.

Bhattacharya, P.M., Pujol, J., Majumdar, R.K. and Kayal, J.R., 2005. Relocation of earthquakes in the northern region using joint hypocentre determination method. *Curr. Sci*., **89**, 1404-1413.

Bouchon, M., 1981. A simple method to calculate Green's functions for elastic layered media, *Bull. Seism. Soc. Am.*, **71**, 959-971.

Brunnschweiler, R.O., 1966. On the geology of the Indoburman ranges. *Geol, Soc. Australia Jour.,* **13**,127-194.

Brustle, W. and Muller, G., 1983. Moment and duration of shallow earthquakes from Love-wave modelling for regional distances. *Phys. Earth Planet. Int.,* **32**, 312-324.

Bune, V.I., M. V. Gzovskiy, et al., 1960. Methods for a detailed study of seismicity. *Izv. Acad. Sci. USSR, Trudy*, **9**, no. 176, 327 (in Russian).

Chakravorthy, K.C. and Ghosh D.P., 1960. Seismological study of the crustal layers in Indian region from the data of near earthquakes. *Proc. Second World Conf. Earthq. Engg. Tokyo and Kyoto, Japan, July 11-18, 1960, Science council of Japan,* Vol. III, 1633-1642.

Chandra, U., 1978. Seismicity, earthquake mechanisms and tectonics along the Himalayan mountain range and vicinity. *Phys. Earth Planet. Inter.,***16**, 109-131.

Chandra, U., 1984. Seismicity earthquake mechanisms and tectonics of Burma, 200N-280 N. *Geophys. J. Roy Astro. Soc.,* **40**, 367-381.

Chaudhury, S.K., 1975. Gravity and crustal thickness in the Indo – Gangetic plains and Himalayan region, India. *Geophys. J. R. Astron. Soc.,* **40**, 441-452.

Chaudhary, H.M. and Srivastava, H.N., 1976. Seismicity and focal mechanism of some recent earthquakes in northeast India. *Annal di Geophys* **29**, 41-56.

Chauhan, R.K.S. and Singh, R.N., 1965. Crustal studies in Himalayan region. *J. Indian Geophys*. **2**, 51-57.

Chen W. P. and Molnar, P., 1990. Source parameters of earthquakes and intraplate deformation beneath the Shillong Plateau and the Northern Indoburman ranges. *J. Geophys. Res.*, **95**, 12527-12552.

Coutant, O., 1989. Program of Numerical Simulation AXITRA. *Research report, LGIT, Grenoble.*

Curray, J.R. and Moore, D.G., 1971. Growth of the Bengal deep sea fan and denudation in the Himalayas. *Bull. Geol. Soc. Am.* **82**, 563-572.

Curray, J.R. and Moore, D.G., 1974. Sedimentary and tectonic process in the Bengal deep-sea fan and geosyncline, in The Geology of Continental Margins. *Edited by C.A. Burke and C.L. Drake*, 617-628, Springer-Verlag, New York.

Curray, J.R., Moore, D.G., Lawver, L.A., Emmel, F.J., Raitt, R.W., Henry, M. and Kieckhefer R., 1979. Tectonics of the Andaman Sea and Burma. *Am. Assoc. Pet. Geol. Mem. 29, In : Geological and Geophysical Investigation of Continental Margins,* Ed : J.S. Watkins, L. Montadert and P. Dickenson, 189-198.

Curray, J.R., Emmel, F.J., Moore, D.G. and Raitt, R.W., 1982. Structure tectonics and geological history of the northeastern Indian Ocean, In : *The Ocean Baisns and Margins,* **vol. VI,** The India Ocean, ed. AEM. Nairn and F.G. Stehli, 399-450, Plenum, New York.

Das, S. and Filson, J.R., 1975. On the tectonics of Asia. Earth Planet. *Sci. Lett.,* **28**, 241-253.

Das Gupta, S.K. 1999. Seismic hazard assessment: local geological effects of strong ground motion. *Proc. Sem. on Earthquakes and Landslides: Natural disaster mitigation, Calcutta*, 44-51.

Das Gupta, S., Bhattacharya, A. and Jana, T.K., 1998. Quantitative assessment of seismic hazard in Eastern-Northeastern India through Poisson probability density function analysis. *Jour. Geol. Soc. India, Vol. 52, pp. 181-194.*

Datta, A. N., 1961. An estimates of the roots of the Himalayas from seismological evidence. *Bull. Nat. Inst. Sci. India,* **22**, 32 – 41.

Der, Z.A., Shumway, R. H. and Hirano, M.R., 1991. Time domain waveform inversion – A frequency domain view; How well we need to match waveform? *Bull. Seism. Soc. Am.*, **81**, 2351-2370.

Dewey, J. F. and Bird, J. M., 1970. 'Mountain Belts and Global tectonics.' *J. Geophys. Res.* **75**, 2625-2647.

Dube, R.K., Dattatrayam, R.S., Singh, M., Srivastava, H.N., 1986. Seismicity of northeast India with reference to the Cachar earthquake of December 1984. *Proceedings Int. Sump. Neotectonics in South Asia, Dehradun, India Feb. 18-21*, 378-395.

Dunkin, J. W., 1965. Computation of modal solutions in layered, elastic media at high frequencies. *Bull. Seism. Soc. Am.*, **55**, 335-358.

Evans, P. and Crompton, W., 1946. Geological factors in the gravity interpretation by evidence from India and Burma. *Quart. J. Geol. Soc., London,* **102**, 211 – 249.

Evison, F.F., 1977. Fluctuation of seismicity before major earthquakes. *Nature*, **226**, 710-712.

Fielitz, K., 1971. Elastic wave velocities in different rocks at high pressure and temperature up to 750°C. *J. Geophys.*, **37**, 943-956.

Fitch, T.J., 1970. Earthquake mechanism in the Himalayan, Burmese and Andaman regions and continental tectonics in central Asia. *J. Geophys. Res.* **75**, 2699-2709.

Fitch, T.J., 1972. Plate convergence, transcurrent faults and internal deformation adjacent to southeast Asia and the western Pacific. *J. Geophys. Res.*, **77,** 4432-4460.

Gaur, V.K. and Bhattacharji, J.C., 1983. Gravimetric determination of the shape of Mohorovicic Discontinuity in Peninsular and north-eastern India. *Paper presented at I.U.G.G. General Assembly at Hamburg, Germany, Aug. 15-27, 1983.*

Ghose, A.K. and Bhattacharya, S.N., 2004. Crustal structure in southern and central West Bengal using deep seismic sounding explosion data. *Mausam* **55**, no. 1, 177-182

G.S.I., 2000. Seismotectonic Atlas of India and its environs. *Geol. Surv. India, sp. Pub., Ed. P.L. Narula, S.K. Acharya and J. Banerjee*, 86.

Guha, S.K. and Bhattacharya, U., 1984. Studies on prediction of seismicity in northeast India. *Proc. World Conf. On earthquake Engineering San Francisco USA, July, 21-27.*

Gulatee, B.L., 1958. Isostasy in India. *Bull. Nat. Inst. Sci. India,* No.11.

Gupta, H.K., 1985. Cachar earthquake of December 31, 1984- Is it a signal for the beginning of seismic activity? *Jour. Geol. Soc. India.* **26**, 145-147.

Gupta, H. K. and Narain, H., 1967. Crustal structure in Himalayan and Tibet plateau region from surface wave dispersion. *Bull. Seism. Soc. Am.,* **57**, 235 – 248.

Gupta, H. K., Singh, S. C., Dutta, T. K., and Saikia, M. M., 1982. Seismicity studies in Northeast India. *Proc. Symp. Seismicity and Microzonation, Seattle, Washington.*

Gupta, H. K. and H. N. Singh, 1986. Seismicity of the North-East India Region. *J. Geol. Soc. India,* **28**, 367-406.

Gupta, H.K., Singh, S.C., Dutta T.K. and Saikia M.M., 1984. Recent investigations of North East India seismicity. *Proc. Internatl. Symp. Continental Seismicity and Earthquake Prediction. Go Gongxu and Ma Xing – Yuan (Editors), Seismological Press, Beijing,* 63 – 71.

Gupta, H.K., Rajendran, K. and Singh, H.N., 1996. Seismicity of northeast India region, Part I: The data base. *J. Geol. Soc. India* **28** (28), 335-365.

Gupta, H.K. and Singh, H.N., 1989. Precursory to moderate magnitude to great earthquakes in northeast India region. *Tectonophysics,* **167**, 255-298.

Gupta, H.K., Fleitout, L. and Froidevaux, C., 1990. Lithospheric subduction beneath the Arakan-Yoma fold belt : Quantitative estimates using gravimetric and seismic data. *J. Geol.Soc.India,* **35**, 235-250.

Haines, A.J. and Holt, W.E., 1993. A procedure for obtaining the complete horizontal motions within zone of distributed deformation from the inversion of strain rate data. *J. Geophys. Res.,* **98**, 12057-12082.

Haskell, N.A., 1964. Radiation pattern of surface waves from point source in a multi layered medium. *Bull. Seism. Soc. Am.,* **54,** 377-393.

Havskov, J. and Ottemoeller, L., 2001. Seisan: The earthquake analysis software user manual. *Institute of Solid Earth Physics, University of Bergen, Norway,* 277.

Hayden, H.M., 1918. Relationship of the Himalaya to the Indo-Gangetic plain and the Indian Peninsula. *Rec. Geol. Surv. India,* **43**, 138-157.

Harkrider, D.G., 1976. Potentials and displacements for two theoretical seismic source. *Geophys. J.,* **47**, 97-133.

Herrmann, R.B. and Wang, C.Y., 1985. A comparison of synthetic seismogram. *Bull. Seism. Soc. Am.,* **75**, 41-56.

Hodgson, J.H. and Storey, R.S., 1953. Tables extending Byerly's fault plane technique to earthquakes of any focal depth. *Bull. Seism. Soc. Am.,* **43**, 49-61.

Holt, W.E. and Wallace, T.C., 1990. Crustal thickness and upper mantle velocities in the Tibetan Plateau region from the inversion of regional Pn waveforms: Evidence for a thick lid beneath southern Tibet. *J. Geophys. Res.,* **12**, 499-12,525.

Holt, W.E., James, F., Ni., Wallace, T.C. and Haines, A. J., 1991. The Active Tectonics of the Eastern Himalayan Syntaxis and Regions. *J. Geophys. Res*., **96**, No. B9, 14,595-14632.

Ingate, S.F., Bock, G. and Kind, R., 1983. Synthesis of complete *SH* seismograms. *Geophys. J. R. astr. Soc.,* **75**, 261-274.

Jeffreys, H. and Bullen, K. E., 1940. Seismological Tables. *British Assn. for the advancement of science, Gray Milne trust, London.*

Joyner, W. B. and Boore, D. M., 1981. Peak horizontal acceleration and velocity from strong-motion records including records from the 1979 Imperial Valley, California, earthquake. *Bull. Seism. Soc. Am.,* **71**, 2011–2038.

Kaila, K. L., Reddy, P.R. and Narain, N., 1968a. Crustal structure in the Himalayan foothills of North India from P-wave data of shallow earthquakes. *Bull. Seism. Soc. Am.*, **58(2**), 597-612.

Kaila, K. L., Reddy, P. R. and Narain, N., 1968b. P-wave travel times from shallow earthquakes recorded in India and inferred upper mantle structure. **Bull. Seism. Soc. Am., 58**, 1879-1897.

Kaila, K.L., Reddy, P.R. and Tripathi, K.M., 1977. Deep seismic sounding studies in India. *J. Indian. Geophys. Un.,* **XIV**, 1-17.

Kaila, K.L., Reddy, P.R., Mau, D.M., Venkateswar, N., Krishna, V.G. and Prasad, A.S.S.S.R.S., 1992. Crustal structure of the West Bengal basin, India from deep seismic sounding investigations. *Geophys. J. Int.,* **III,** 45-66.

Kaila, K.L. and Sain, K., 1997. Variation of crustal velocity structure in India as determined from DSS studies and their implications on regional tectonics. *J. Geol. Soc. Ind.,* **49**, 395-407.

Kanamori, H. and Cipar, J., 1974. Focal processes of the Great Chilean earthquake of May 22, 1960. *Phys. Earth Planet. Int.,* **9**, 128-136.

Kayal, J.R., 1982. Seismic velocity-ratio in the crust and uppermost mantle in southeast Wellington province, New Zealand. *Pure and Appl. Geophys.,* **120**, 809-819.

Kayal, J.R. 1986. Analysis of strong phases other than P and S from a microearthquake survey in the Wellington region, New Zealand. *Bull. Seism. Soc. Am.* **76**, 1347-1354.

Kayal, J.R., 1987. Microseismicity and source mechanism study: Shillong Plateau, Northeast India. *Bull. Seism. Soc. Am.,* **77**, 184-194.

Kayal, J.R., 1989. Subduction structure at the India/ Burma plate boundary : Seismic and gravity evidences. 28th *Int. Geol. Cong., USA,* **2**, 164-165.

Kayal, J.R. and Zhao, D., 1998. Three-dimensional seismic structure beneath Shillong Plateau and Assam Valley, Northeast India. *Bull. Seism. Soc. Am*., **88**, 667-676.

Kayal, J.R.,1996. Earthquake source processes in northeast India: a Review, *J. Himalayan Geol.,* **17**, 53-69.

Kayal, J.R., 1991. Earthquake prediction in Northeast India – A review. *Pure Appl. Geophys.*, **136**, 297-313.

Kayal, J. R., 2008. Large and great earthquakes in stable continental region of India. *A review, J. Geol. Soc. Mem*. **68**, 31-46 (invited paper).

Kayal, J. R. and Reena de, 1987. Pn-velocity study using a temporary seismographic network in the Shillong Plateau: North-East India. *Bull. Seism. Soc. Am.,* **77**, No. 5, 1718-1727.

Kayal, J. R., De, R. and Chakraborty, P., 1993. Microearthquakes at the Main Boundary Thrust in Eastern Himalaya and the present-day tectonic model. *Tectonophysics,* **218**, 375-381.

Kayal, J.R., Gaonkar, S.G., Chakraborty, G.K. and Singh, O.P., 2004. Aftershocks and seismotectonic implications of the 13th September 2002 earthquake (MW 6.5) in the Andaman Sea basin. *Bull. Seism. Soc. Am.,* **94(1),** 326-333.

Kern, H. and Richter, A., 1981. Temperature derivatives of compressional and shear wave velocities in the crustal and mantle rocks at 6 kbar confining pressure. *J. Geophys*., **49**, 47-56.

Khattri, K., 1973. Earthquake focal mechanism studies – A review. *Earth Science Review,* **9**, 19-63.

Khattri, K.N., 1987. Great earthquakes, seismicity gaps and potential for earthquake disaster along the Himalayan plate boundary. *Tectonophysics,* **138**, 79-92.

Khattri, K.N., Wyss, M., Gaur, V.K., Saha, S.N. and Bansal, V.K., 1983. Local seismic activity in the region of Assam gap, NE India. *Bull. Seism. Soc. Am.,* **73**, 459-469.

Kind, R., 1978. The reflectivity method for a buried source. *J. Geophys.,* **44**, 603-612.

Kind, R., 1979. Extensions of the reflectivity method. *J. Geophys.,* **45**, 373-380.

Kind, R. and Odom, R. I., 1983. Improvement to layer matrix methods. *J. Geophys.,* **53**, 127-130.

Kisslinger, C. and Engdahl, E. R., 1973. The interpretation of the Wadati diagram with relaxed assumptions. *Bull. Seism. Soc. Am.,* **63**, 2176-2176.

Koch, K., 1991. Moment tensor inversion of local earthquake data-I. Investigation of the method and its numerical stability with model calculation, *Geophys. J. Int.,* **106**, 305-319.

Kono, M., 1974. Gravity anomalies in the east Nepal and their implications to the crustal structure of the Himalayas. *Geophys. J. R. Astron. Soc.,* **39**, 283-299.

Kumar, M.R., Solomon Raju, P., Uma Devi, E., Saul, J. and Ramesh, D.S., 2004. Crustal structure variations in northeast India from converted phases. *Geophys. Res. Lett.,* **31**, L17605-doi 10.10.29 2004 GL020576.

Lay, Thorne and Wallace, Terry, C., 1995. Modern Global Seismology. *Academic Press, New York, USA*, 521.

Le dain, A. Y., Tapponnier P. and Molnar P., 1984. Active Faulting and Tectonics of Burma and surrounding regions. *J. Geophys. Res.,* **89**, 459-472.

Lienert, B.R., Berg, E., and Frazer, L.M., 1986. HYPOCENTER : An earthquake location method using centered, scaled and adaptively damped least squares. *Bull. Seism. Soc. Am.,*. **76**, 771-783.

Mathur, L. P. and Evans, P., 1964. Oil in India. *Proc. 22nd Int. Geol. Congr., New Delhi.,* 86.

Mitchell, A. H. G., 1981. Phanerozoic plate boundaries in mainland SW Asia, The Himalayas and Tibet. *J. Geol. Soc. London*, **138**, 109-122.

Mitchell, A.H.G and Mckerrow, W.S., 1975. Analogous evolution of Burma Orogen and the Scottish Caledonides. *Geol. Soc. Am. Bull.*, **86**, 305-315.

Mitra, S.K. and Kaiser, J.F., 1993. Handbook for Digital Signal Processing. *John Wiley and Sons, 1243.*

Mitra, S., Pristley, K., Bhattacharya, A. and Gaur, V.K., 2005. Crustal structure and earthquake focal depths beneath northeastern India and southern Tibet. Geophys. *J. Int*., **160**, 227-248, doi: 10.1111/j.1356-246X.2004.02470.x.

Mitra, S., Priestley, K., Gaur, V.K., Rai, S.S. and Haines, J., 2006. Variation of Rayleigh wave group velocity ispersion and seismic heterogeneity of the Indian crust and uppermost mantle. *Geophys. J. Int.*, **164**, 88-98.

Mitra, S., Bhattacharya, S.N. and Nath, S.K., 2008. Crustal structure of the western Bengal Basin from joint analysis of teleseismic receiver functions and Rayleigh-wave dispersion. *Bull. Seism. Soc. Am.*, **98**, 6, 2715-2723.

Molnar, P., 1984. Structure and tectonics of the Himalaya constraints and implication of geophysical data. *Ann. Rev.Earth Planet Sci.*, **12,** 489-518.

Molnar, P. and Tapponnier, P., 1975. Cenozoic tectonics of Asia: Effects of a continental collision. *Science,* **189**, 419-426.

Molnar, P., Chen, W. P., Fitch, T. J., Tapponnier, P., Warsi, W. E. K. and Wu, F. T., 1977. Structure and Tectonics of the Himalayas: A brief history of relevant Geophysical observations. *Editions de C.N.R.S.,* **268**, 269-293.

Molnar, P. and Tapponnier, P., 1977. Relation of tectonics of eastern China to the Indian-Eurasia collision: application of slipline field theory to large scale continental tectonics. *Geology,* **5**, 212-216.

Mukhopadhyay, M. and Das Gupta, S., 1988. Deep structures and tectonics of Burmese arc: Constraints from earthquake and gravity data. *Tectonophysics,* **149**, 299-322.

Mukhopadhyay, M., 1984. Seismotectonics of transverse lineament in the eastern Himalaya and its foredeep. *Tectonophysics,* **109**, 227-240.

Mukhopadhyay, S., Chander, R. and Khattri, K.N., 1997. Crustal properties in the epicentral tract of the Great 1897 Assam Earthquake, northeastern India. *Tectonophysics,* **283**, 311-330.

Muller, G., 1985. The reflectivity method: a tutorial. *J. Geophys.*, **58**, 153-174.

Nakajima J., Takei Y. and Hasegawa A., 2005. Quantitative analysis of the inclined lowvelocity zone in themantle wedge ofNortheastern Japan: a systematic change of melt-filled pore shapes with depth and its implications for melt migration. *Earth Planet. Sci. Lett.,* **234**, 59-70.

Nandy, D. R., 1983. The Eastern Himalaya and the Indo-Burman orogen in relation to the Indian Plate movements. *Geol. Surv. Ind. Misc. Pub.,* **43**, 153-159.

Nandy, D.R. and Das Gupta, S., 1991. Seismotectonic domains of northeastern India and adjacent areas: Geology and Geodynamics of Himalayan collision zone. *pt.2 : Physics and Chemistry of earth,* **18**, No. I-II, Pergamon Press PLC., Oxford, 271-384.

Nandy, D.R., 1986. Geology and tectonics of Arakan-Yoma—A reappraisal. *GEOSEA V. Proc.II, Bull.Geol. Soc. Malaysia,* **20**, 137-148.

Nandy, D.R., 2001. Geodynamics of Northeastern India and the adjoining region. *ACB publications, 207.*

Narain, H., 1973. Crustal structure of Indian subcontinent. *Tectonophysics,* **20**, 249-260.

Nicholson, C. and David. W. Simpson, 1985. *Bull. Seism. Soc. Am.,* **75**, No. 4, 1105-1123.

Ni, J. and Barazangi, M., 1983. High frequency seismic wave propagation beneath the Indian Shield, Himalaya arc, Tibetan plateau and surrounding regions : High uppermost mantle velocities and efficient Sn propagation beneath Tibet. *Geophys. J. R. Astron. Soc.,* **72**, 665-689.

Ni, J. and Barazangi, M., 1984. Seismotectonics of Himalayan collision zone : Geometry of the underthrusting Indian Plate beneath the Himalaya. *J. Geophys. Res.,* **89**, 1147-1163.

Ni, J.F., Guzman-speziale, M., Bevis, M., Holt, W.E., Wallace, T.C. and Seager, W., 1989. Accretionary tectonics of Burma and the three dimensional geometry of the Burma subduction zone. *Geology,* **17**, 68-71.

Oldham, T. and Oldham, R.D., 1882. The Cachar earthquake of 10th January 1869, ed. By R.D. Oldham. *Geol. Surv. India Mem.,* **19**, 1-98.

Oldham, T.,1883. A Catalogue of Indian earthquakes from the earliest to the end of A.D. 1869. *Memo. Geol. Surv. Ind.,* **19** (3), 1-53.

Oldham, R.D., 1899. Report of the great earthquake of 12th June, 1897. *Mem. Geol. Surv. Ind.,* **29**, 1-379.

Person, W.J., 1989. Seismological notes – July – August 1988. *Bull. Seismol. Soc. Am.,* **79**, 925-932.

Pho, T.P. and Behe, L., 1972. Extended distances and angle of incidence of P waves. *Bull. Seism. Soc. Am.,* **62**, 885-902.

Qureshy, M. N., 1969. `Thickening of Basaltic Layer as Possible Cause for the Uplift of Himalaya - A Suggestion Based on Gravity Data.' *Tectonophysics,* **2,** 137-157.

Qureshy, M.N., 1971. Relation of gravity to elevation and rejuvenation of blocks in India. *Jour. Geophys. Res.,* **76** (12), 545-557.

Rai, S.S., Srinagesh, D. and Sarma. P.V.S.S.R., 1996. Morphology of the subducted Indian plate in the Indo-Burmese convergence zone. *Proc. Indian.Acad.Sci. (Earth Plan.Sci.),* **105**, 441-450.

Rai, S.S., Priestley, Keith, Suryaprakasham, K., Srinagesh, D., Gaur, V.K. and Du, Z., 2003. Crustal shear velocity structure of the south Indian shield. *J. Geophys. Res.,* **108**, B2, 2088, doi : 10.1029/2002JB001776.

Ramesh, D.S., Kumar, M.R., Devi, E.U., Raju, P.S. and Yuan, X., 2005. Moho geometry and upper mantle images of northeast India. *Geophys.Res. Lett.,* **32**, 14301-14304, doi: 10.1029/2005GL022789.

Rao, N. P. and Kalpna, 2005. Deformation of the subducted Indian lithospheric slab in the Burmese arc. *Geophys. Res. Lett.,* **32**.

Rastogi, B. K., Singh, J. and Verma, R. K., 1973. `Earthquake Mechanisms and Tectonics of Assam - Burma Region.' *Tectonophysics,* **18**, 355-366.

Ravi Kumar, M. and Purnachandra Rao, N., 1994. Significant trends related to the slab seismicity and tectonics in the Burmese arc region from Harvard CMT solutions. *Phys. Earth Planet. Inter .,* **90.**

Ravikumar, M., Purnachandra Rao, N. and Chalam, S. V., 1996. A seismotectonic study of the Burma and Andaman arc regions using centroid moment tensor data. *Tectonophysics*, **253**, 155-165.

Reddy, P. R., Prasad, A. S. S. S. R. S. and Dipankar Sarkar, 1998. Velocity modelling of Bengal Basin refraction data—refinement using multiples. *J. Appl. Geophys.*, **39**, 109-120.

Refraction Technology, 1996. Technical Introduction to the 72A series data acquisition system. *Technical Reference Documents,* 1-19.

Richter, C.F., 1958. Elementary Seismology. *W.H.Freeman & Co., San Francisco*, 768.

Riznichenko, Y. V., 1958. Methods for large - scale determination of focus coordinates of nearby earthquakes and velocities of seismic waves in the focal region. *Tr. Inst. Fiz. Zemli. Akad. Nauk SSR.* **4.**

Riznichenko, Yu.V., 1958. The study of seismic conditions. *Bull. Acad. Sci. USSR. Geophys. Soc.,* **9**, 615-622.

Saha, B.P., 1965. M2 or first shear mode continental Rayleigh waves from Russian nuclear explosion of 30th Oct. 1961. *Indian J. Met. Geophys.*, **16**, 270-280.

Saha, S. N., Gaur, V. K., Bansal, V., Wyss, M. and Khattri, K., 1981. Microearthquakes in North East India. Symp. *Earthq. Disaster Mitigation, March 4-6, 1981, Univ. Roorkee, Roorkee (India),* **2,** 65-76.

Saikia, C.K., 1994. Modified frequency-wave number algorithm for regional seismograms using Filon's quadrature: modeling of Lg waves in eastern North America. *Geophys. J. Int.*, **118**, 142-158.

Saikia, C.K. and Herrmann, R.B., 1985. Application of waveform modeling to determine focal mechanisms of four 1982 Miramichi aftershocks. *Bull. Seism. Soc. Am.*, **75**, 1021-1040.

Saikia, C.K. and Herrmann, R.B., 1986. Moment tensor solution of three 1982 Arkansas swarm earthquakes by waveform modeling. *Bull. Seism. Soc. Am.,* **76,** 709-723.

Santo, T., 1969. Regional Studies on the Characteristic Seismicity of the world, Part II. From Burma down to Java. *Bull. Earthq. Res. Inst., Tokyo,* **47**, 1049-1061.

Santo, T., 1969. On the characteristics seismicity in south Asia from Hindukush to Burma. *Bull. Int. Inst. Seism. Earthquake Engg.,* **6**, 65-67.

Sato, H., Muro, K. and Hasegawa, A., 1998. Three-dimensional mapping of magma source and transport regions from seismic data: The mantle wedge beneath northeastern Japan. *Pure Appl. Geophys*., **153**, 377-398.

Satyabala, S.P., 1998. Subduction in the Indo-Burman region. Is it still active? *Geophys Res. Lett.*, **25**, 3189-3192.

Seidl, D. and Stammler, W., 1984. Restoration of broad band seismogram (part-I). *J. Geophys.*, **54**, 114-122.

Scheidegger, A. E. and Willmore, P. L., 1957. The use of least square method for the interpretation of data from seismic surveys. *Geophysics,* **17,** 4-22.

Scherbaum, F., 1994. *Basic Concepts in Digital Signal Processing for Seismologists. Lecture Notes in Earth Sciences,* **53**, *Springer, Heidelberg,* 158.

Schurr B. and Nabelek J., 1999. New techniques for the analysis of earthquake sources from local array data with an application to the 1993 Scotts Mills, Oregon, aftershocks sequence. *Geophys. J. Int.,* **137**, 585-600.

Seeber , L., Armbruster, J. G. and Quittmeyer, R. C., 1981. Seismicity and Continental Subduction in the Himalaya area. In: Zagros, Hindukush, Himalaya: Geodynamic Evolution. *(H. K. Gupta and Delany Eds.) Amer. Geophys. Union. Geodynamic Sr*., **3**, 215-242.

Sengupta, Supriya, 1966. Geological and geophysical studies in western part of Bengal basin. India, Am. Assoc. Petrol. Geol. Bull., **50** (5), 1001-1017.

Sileny, J., Panza, G.F. and Campus, P., 1992. Waveform inversion for point source moment tensor retrieval with variable hypocentral depth and structural model. *Geophys. J. Int.*, **109**, 259-274.

Sarmah, S.K., 1999. The probability of occurrence of a high magnitude earthquake in Northeast India. *Jour. Of Geophysics,* **20**(3), 129-135.

Sileny, J., Campus, P. and Panza, G.F., 1996. Seismic moment tensor resolution by waveform inversion of a few local noisy records - I. Synthetic tests. *Geophys. J. Int*., **126,** 605-619.

Sitaram, M.V.D., George, J., Rao, P.G. and Saikia, M.M., 1988. Pn – wave velocities in the uppermost mantle beneath North East India. *Symp. Earthq. Prediction : Present Status*, July, 1986, 267-275.

Sitaram, M.V.D., George, J., Rao, P.G. and Saikia, M.M., 1990. Travel times of P – waves in North East India. *Studia Geoph. et geod.,* **34**, 96-137.

Stein, S. and Wysession, M., 2003. An introduction to seismology, earthquakes, and earth structure. *Blackwell Publishing,* 512.

Stuard, M., 1926. The Srimangal earthquake of 8th July, 1918. *Mem. Geol. Surv. India*, **46**(1), 1-70.

Tandon, A.N., 1954. A study of Assam earthquake of August 1950 and its aftershocks. *Indian J. Met. Geophys*., **5,** 95-137.

Tandon, A.N. and Chaudhury, H.M., 1964. Thickness of earth's crust between Delhi and Shillong from surface wave dispersion. *Ind. J. Met. Geophys*., **15**, 467-479.

Tandon, A. N. and Srivastava, H. N., 1975. ` Focal mechanism of Some Recent Himalayan Earthquakes and Regional Plate Tectonics.' *Bull. Seism. Soc. Am.* **65**, 963-969.

Tiwari, R. P., 2000. Earthquake hazards and mitigation in India with special reference to north-eastern region. *Envis Bull. Him. Eco. & Dev*., **8** (2): 15-22

Tiwari, R. P., 2002. Status of Seismicity in the Northeast India and Earthquake Disaster Mitigation. *Envis Bulletin. Him. Eco. & Dev*., **10**(1), 10-21.

Verma, R. K., 1991. Seismicity of the Himalaya and the northeast India, and nature of continent-continent collision. In: Sharma KK (ed) *Geology and Geodynamic evolution of the Himalayan collision zone.* Part II: 345-370.

Verma, R.K., Mukhopadhyay, M. and Ahluwalia, M.S., 1976a. Earthquake mechanisms and tectonic features of northern Burma. *Tectonophysics*, **32**, 387-399.

Verma, R. K., Mukhopadhyay, M. and Ahluwalia, M. S., 1976b. Seismicity, Gravity and Tectonics of Northeast India and Northern Burma, Bull. Seism. Soc. Am., **66** (5), 1683-1694.

Verma, R.K. and Mukhopadhyay, M., 1977. An analysis of gravity field in Northeastern India. *Tectonophysics*, **42,** *283-317.*

Verma, R.K. and Subrahmanyam, C., 1984. Gravity anomalies and the Indian lithosphere: Review and analysis of existing gravity data. *Tectonophysics*, **105**, 141-161.

Wang, C.Y., and Herrmann, R.B., 1980. A numerical study of P-, SV-, and SH- wave generation in a plane layered medium. *Bull. Seism. Soc. Am.*, **70**, 1015-1036.

Wadati, K., 1933. On the travel time of earthquake waves. *II, Geophys. Mag*. & 101-111.

Willmore, P.L. and Bancroft, A.M., 1960. The time – term approach to refraction seismology. *Geophys. J. R. Astron. Soc*., **3,** 419-432.

Table 3.1 List of 33 seismic stations with its parameters used for the present study operated by NEIST-J, NGRI-H, Gauhati University, Manipur University, Mizoram University and Indian Meteorological Department, Shillong.

Sl. No.	Station Name	Station code	Location		Elevation	Data Format
			Latitude (^oN)	Longitude (^oE)	(m)	
1	Aizawl	AZL	23.724	92.732	820	Digital
2	Along	ALN	28.154	94.786	261	Digital / Analogue
3	Bansiaphal	BSL	25.858	90.734	250	Analogue
4	Bazengdaba	BGD	25.900	90.517	210	Analogue
5	Bhairabkunda	BKD	26.890	92.120	210	Digital
6	Boko	BOKO	26.005	91.227	50	Analogue
7	Bokoliaghat	BOK	26.093	93.139	50	Digital / Analogue
8	Dauki	DKI	25.191	92.030	100	Analogue
9	Dokmok	DMK	26.216	93.062	200	Digital / Analogue
10	Goalpara	GOP	26.117	90.417	75	Analogue
11	Guahati Univ.	GAU	26.152	91.667	69	Digital / Analogue
12	Guwahati	GWH	26.150	91.710	69	Digital / Analogue
13	Imphal	IMP	24.745	93.929	784	Digital
14	Jogighopa	JPA	26.239	90.575	42	Digital
15	Kaziranga	KZI	26.578	93.406	135	Digital / Analogue
16	Krishnai	KSN	26.050	90.634	60	Analogue
17	Manikganj	MND	25.924	90.676	40	Digital
18	Manipur Univ.	MAN	25.036	93.702	800	Digital
19	Nangalbibra	NGL	25.472	90.702	330	Digital
20	Nanoi	NNI	26.402	93.100	50	Digital
21	Nongstoin	NGN	25.533	91.272	700	Analogue

22	Numaligarh	NLG	26.583	93.731	80	Digital
23	Numba	NBA	24.678	93.446	900	Digital
24	Rupa	RUP	27.203	92.401	1470	Digital / Analogue
25	Seijusa	SJA	26.938	92.999	150	Digital
26	Shillong	SHL	25.566	91.859	1590	Digital / Analogue
27	Silghat	SIL	26.601	92.997	66	Digital
28	Songsak	SNK	25.717	90.534	1100	Analogue
29	Tezpur	TZR	26.617	92.783	140	Digital
30	Tura	TUR	25.550	90.333	305	Analogue
31	Ukhrul	UKH	25.075	94.353	1798	Digital
32	Willium Nagar	WMN	25.500	90.633	260	Digital/ Analogue
33	Ziro	ZIR	27.460	93.767	1066	Digital / Analogue

Table 3.2 Poles and Zeros for the seismometers.

Digitizer Type	Sensor Type	Vertical		Horizontal		Normal-izing factor
		Poles (Hz)	Zeros (Hz)	Poles (Hz)	Zeros (Hz)	
Reftek 72A-07/08	**CMG-3ESP** (Natural period = 60)	$-23.56\times10^{3} \pm j23.56\times10^{-3}$ -50 ± j32.2	0 0 138 ± j144	$-23.56\times10^{3} \pm j23.56\times10^{-3}$ -50 ± j32.2	0 0 138 ± j144	2304000
Reftek 72A-07/08	CMG-40T (Natural period = 30)	-0.02356 ± j 0.02356 -180.0 -160 -80	0 0 159	-0.02356 ± j 0.02356 -180.0 -160 -80	0 0 159	2304000
Reftek 72A-08	CMG- 3T (Natural period = 120)	$-5.89\times10^{3} \pm j5.89\times10^{-3}$ -180.0 -160 -80	0 0	$-5.89\times10^{3} \pm j5.89\times10^{-3}$ -180.0 -160 -80	0 0	2304000

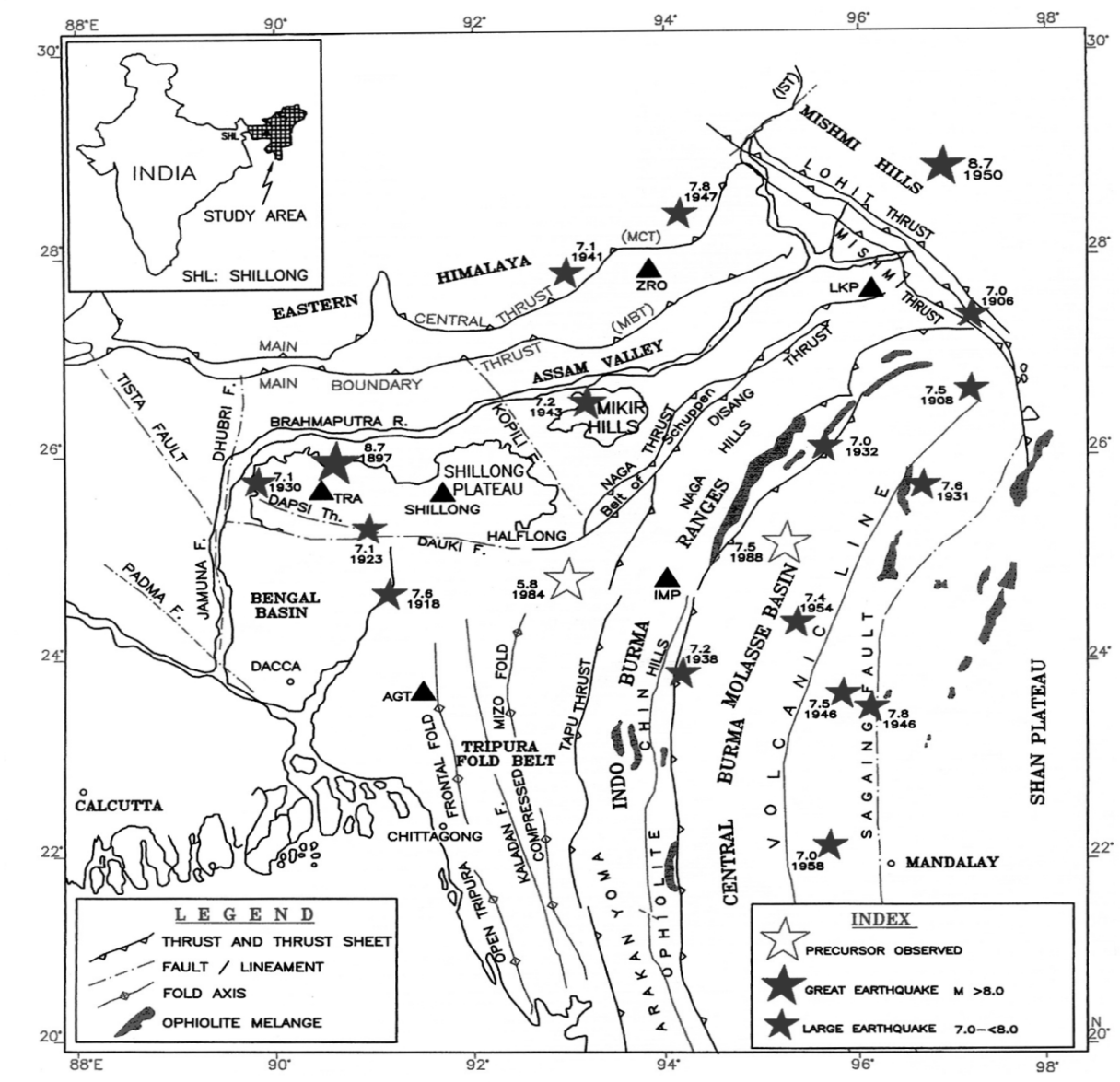

Fig.1.1 Tectonic map of NE India region showing large earthquakes (M> 7.0) including two great (M ~ 8.7) earthquakes (solid stars), two recent damaging earthquakes are shown by open stars (Kayal, 1998).

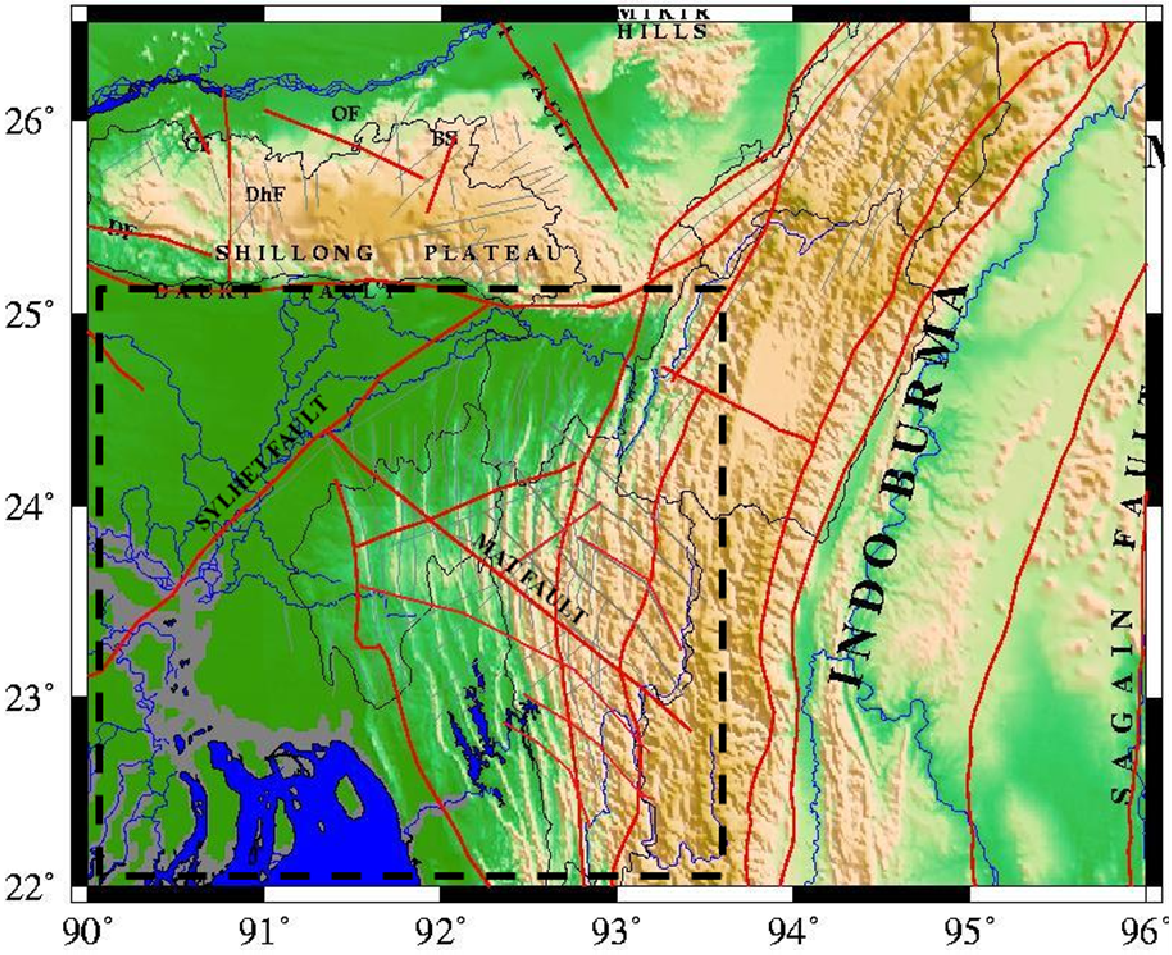

Fig.1.2 Study area showing major tectonic domains.

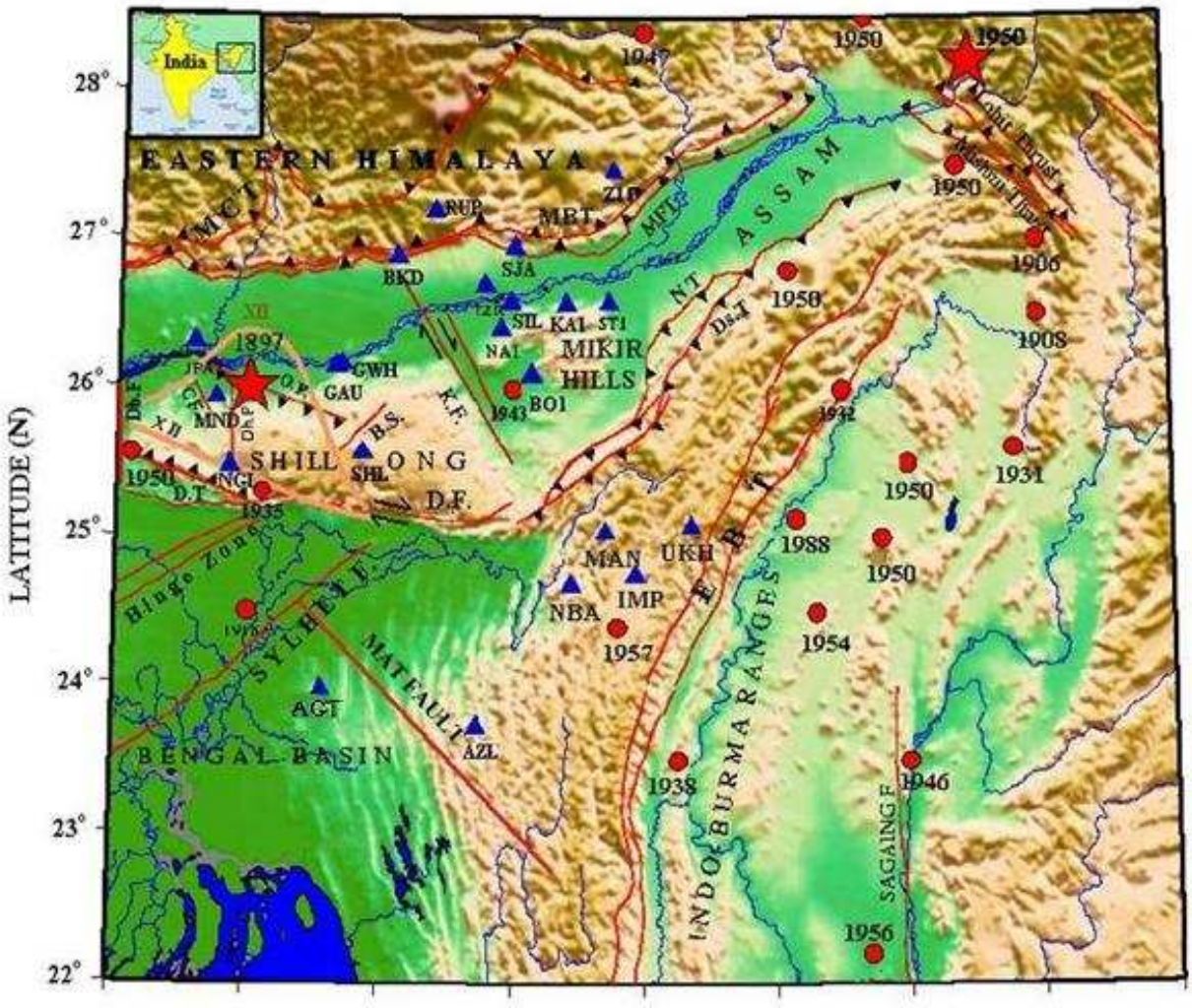

(a)

Fig.2.1(a) Tectonic settings of NER India and surrounding regions including Surma Valley. MCT: Main Central Thrust, MBT: Main Boundary Thrust, DF : Dauki Fault, : DhF: Dudhnoi Fault, KF: Kopili Fault, NT : Naga Thrust, DsT : Disang Thrust, EBT : Eastern Boundary Thrust, IBR : Indo Burma Ranges, MF: Mat Fault, SF: Sylhet Fault. Large and damaging earthquakes that occurred in the region are shown with red stars (Kayal et. al. 2006).

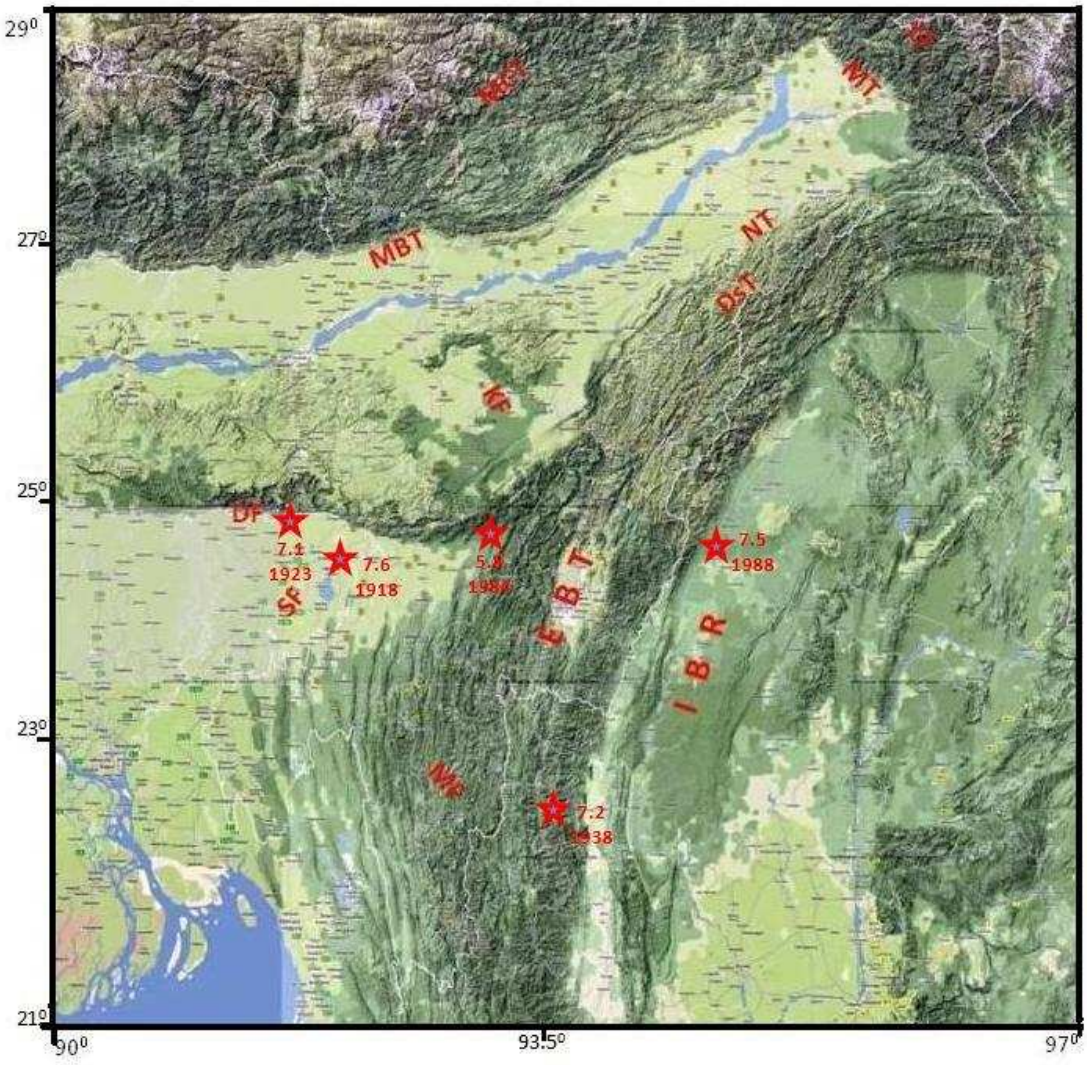

(b)

Fig.2.1(b) The GIS map obtained from Google map API for delineation of faults and lineaments.

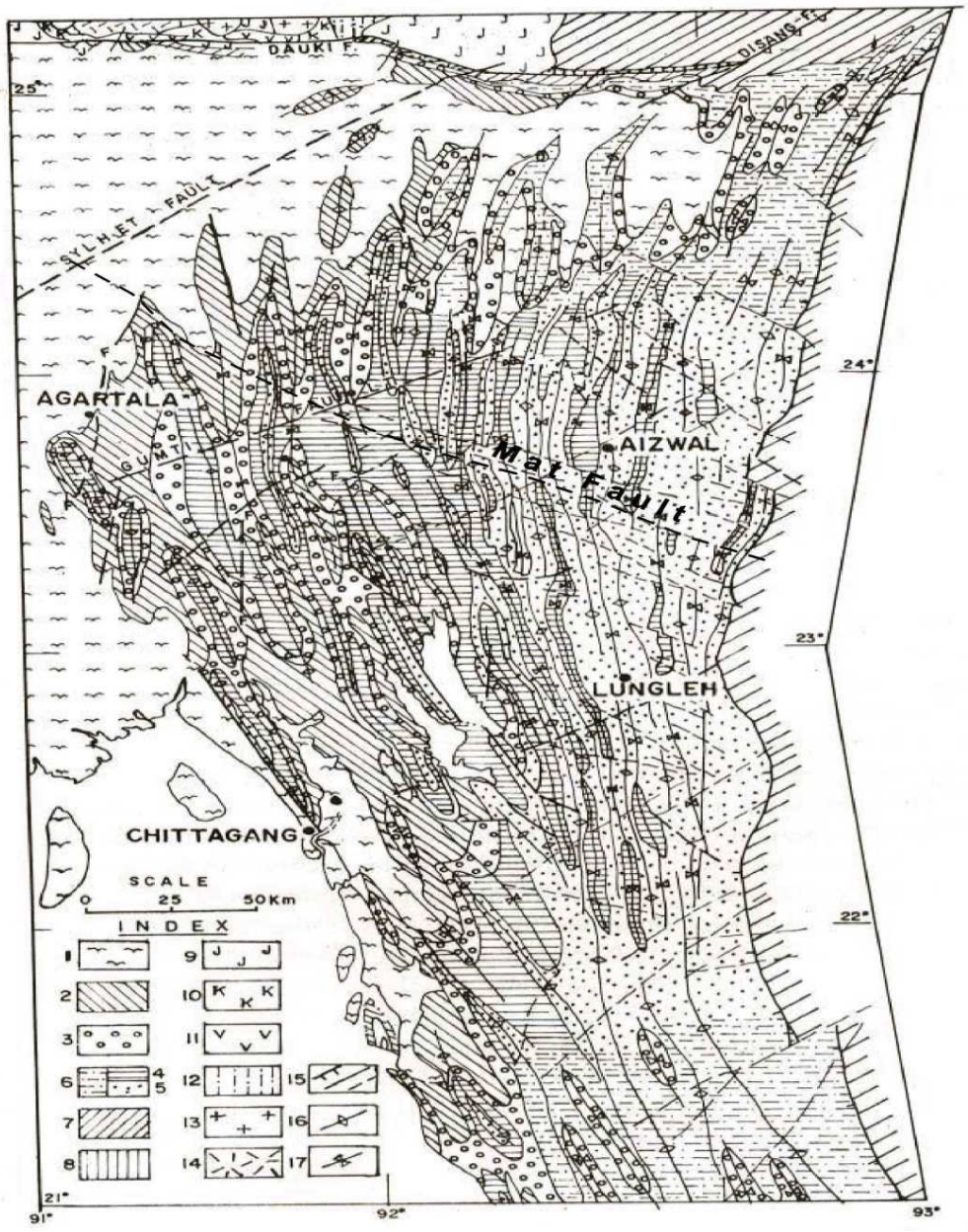

Fig.2.2 Geology of Tripura-Mizoram accretionary belt (Nandy, et al., 1983).

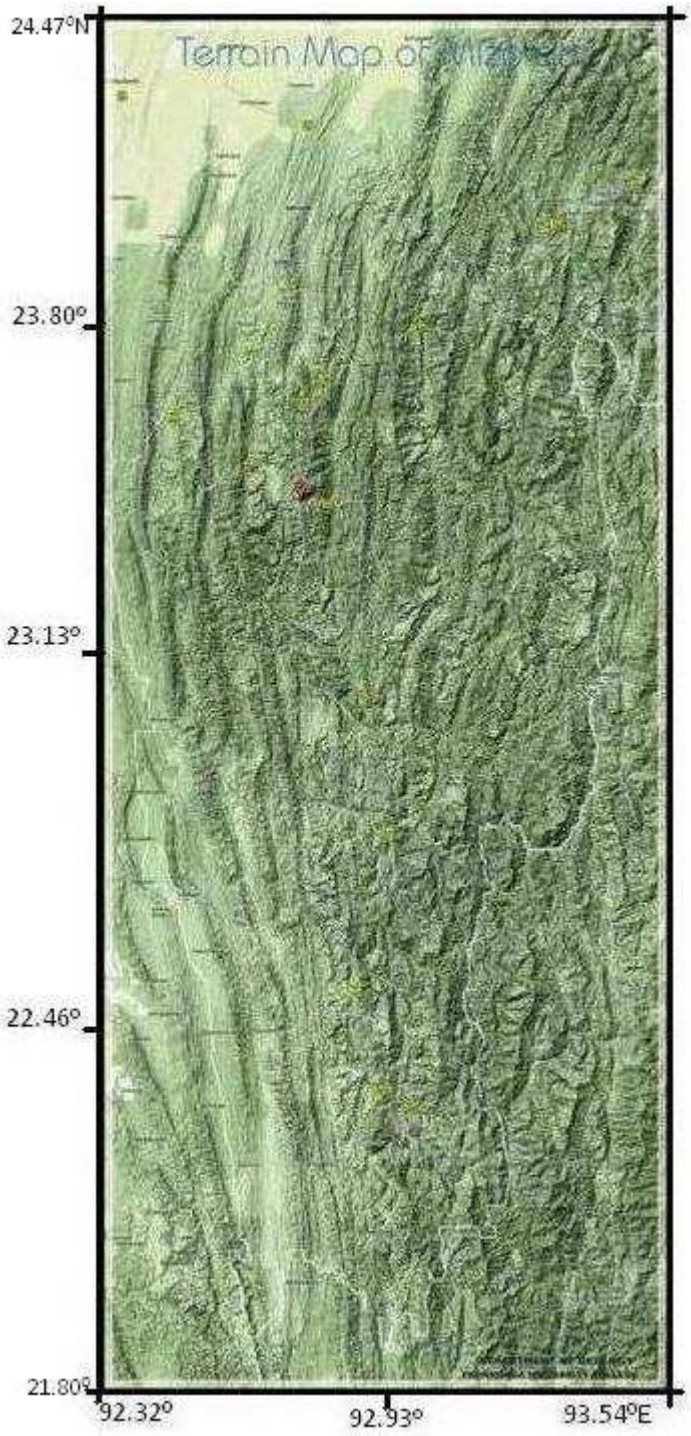

(a)

Fig.2.3(a) Tectonic Map of Mizoram showing Mat fault and other prominent lineaments.

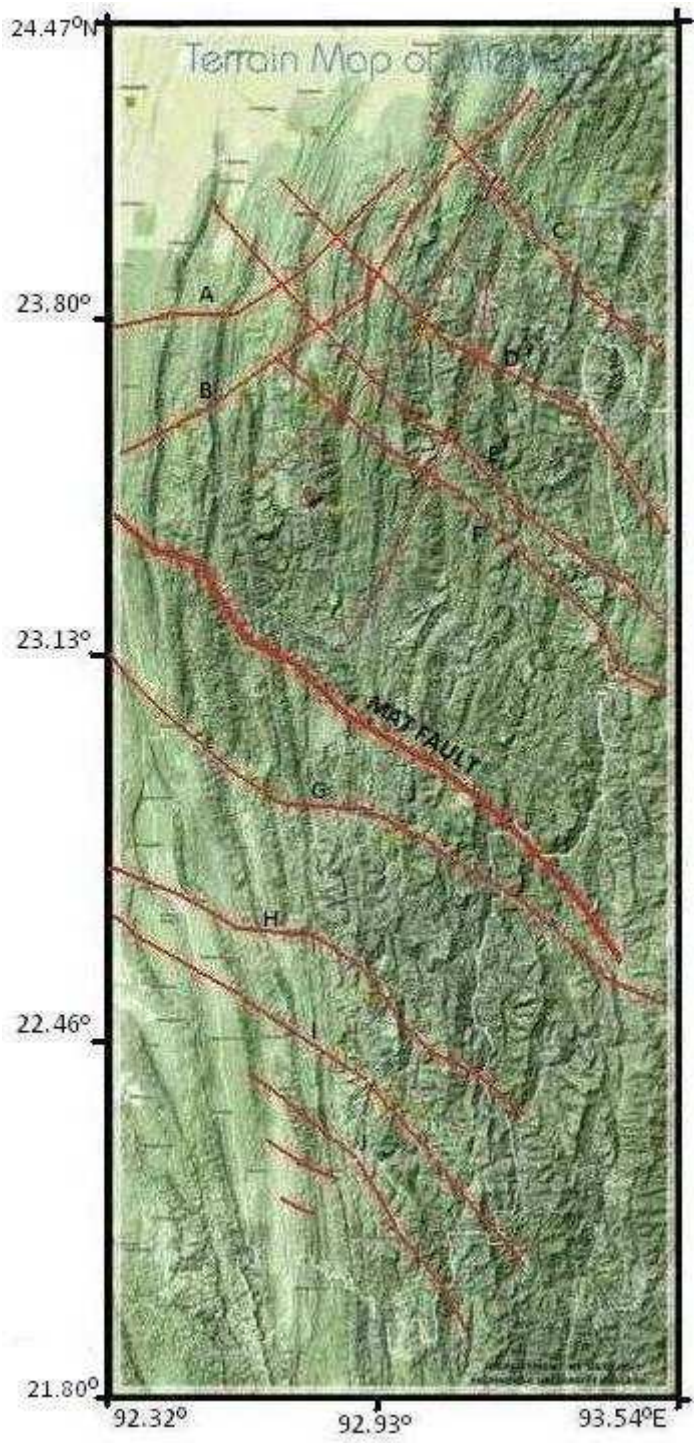

(b)

Fig.2.3(b) Delineation of Mat fault and other lineaments and faults (A-J) over the tectonic map (Fig. 2.3(a)). These faults and lineaments excepting Mat fault have not yet been described.

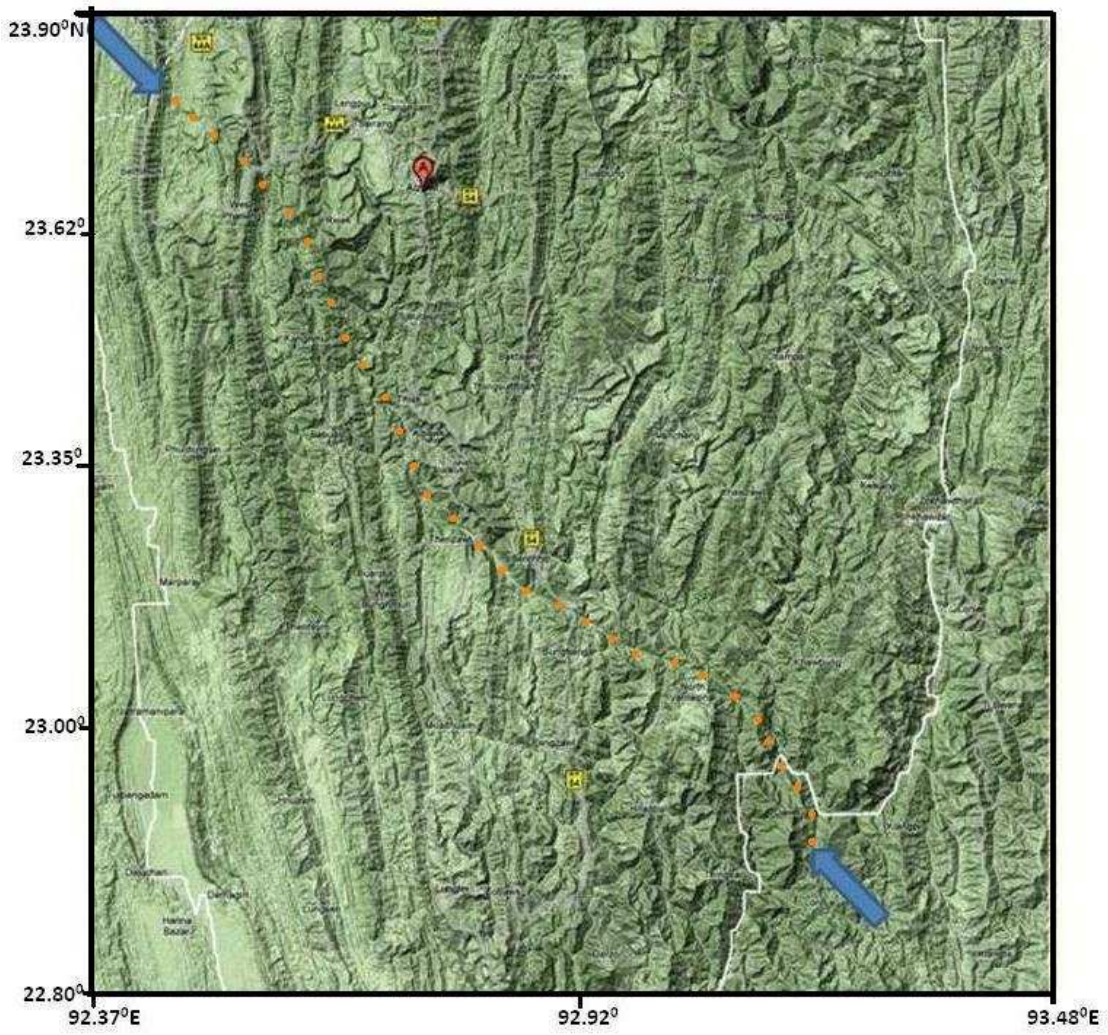

Fig.2.4 Enlarge view of Mat fault showing its trend direction marked by dotted line.

Fig.2.5 Satellite imagery of Bengal Basin including Tripura-Mizo fold belt showing Mat fault and Sylhet fault (Source: World Wind).

Fig.2.6 View of the valley created by Mat fault between Serchhip and Thenzawl Towns in Mizoram.

Fig.2.7 A part of Mat fault as seen from East Lungdar village in Mizoram.

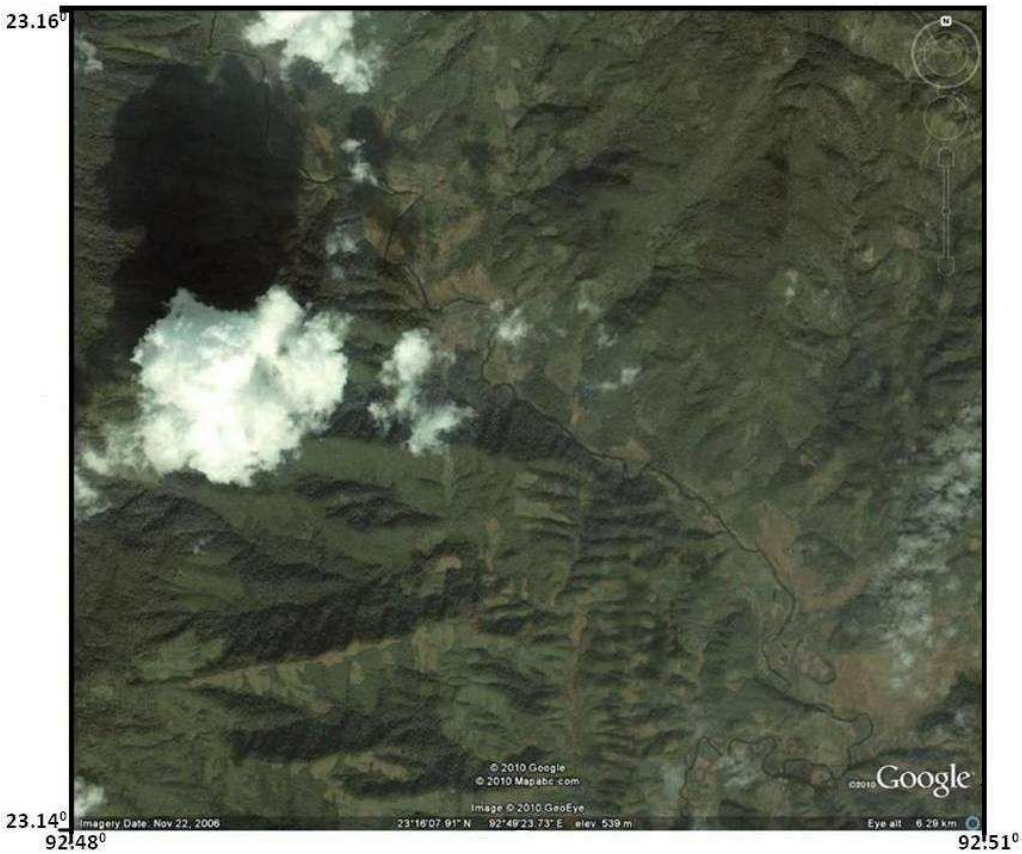

Fig.2.8 View of Mat fault from Google map. Mat river (from which the name Mat fault is derived) flows along the curve of the fault against the normal N-S trend of the hills between Serchhip and Thenzawl towns of Mizoram.

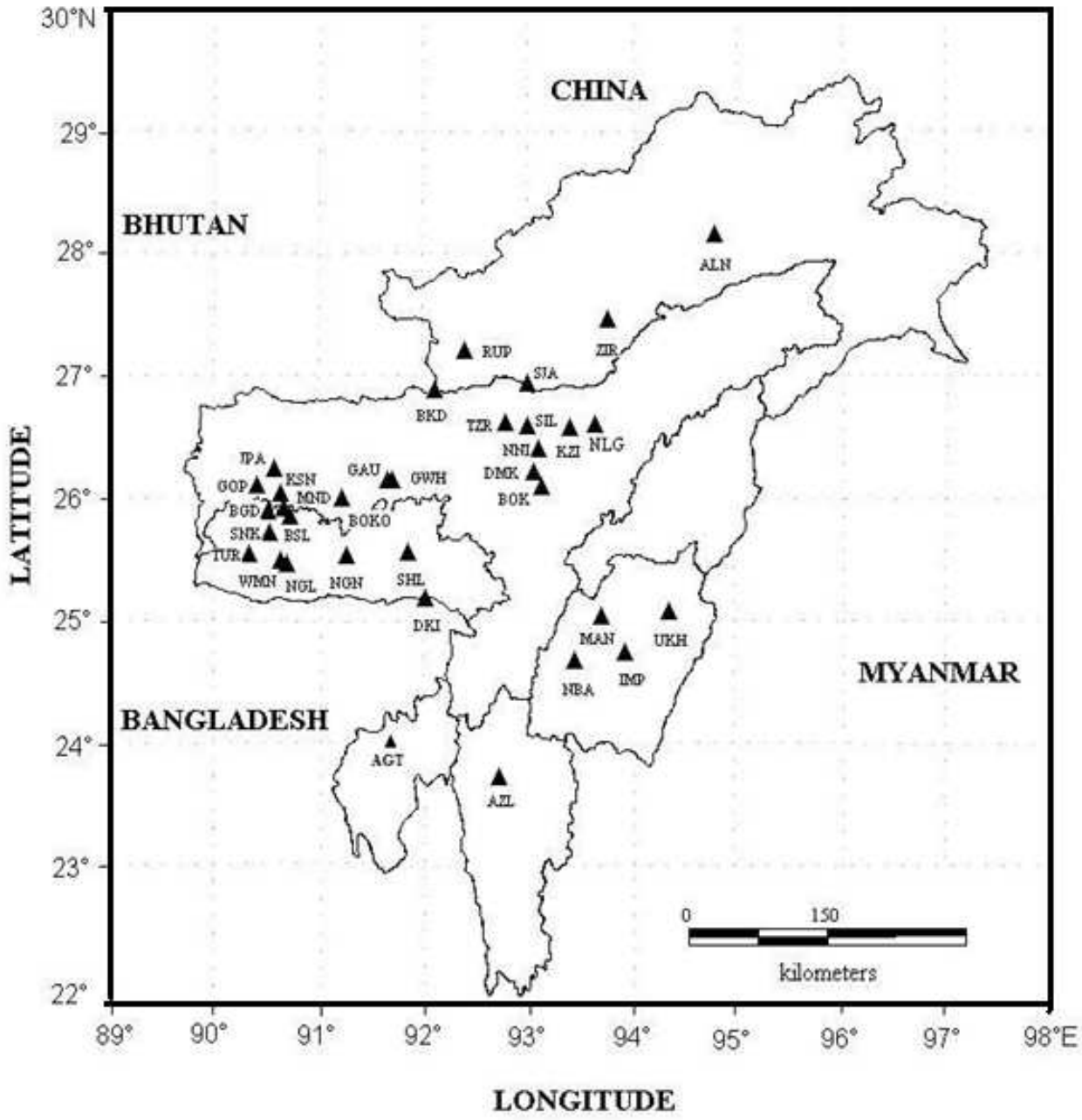

Fig.3.1 Location of 33 seismic stations used for the present study operated by RRL-Jorhat, NGRI-Hyderabad, Gauhati University, Manipur University, Mizorzm University and India Meteorological Department (IMD).

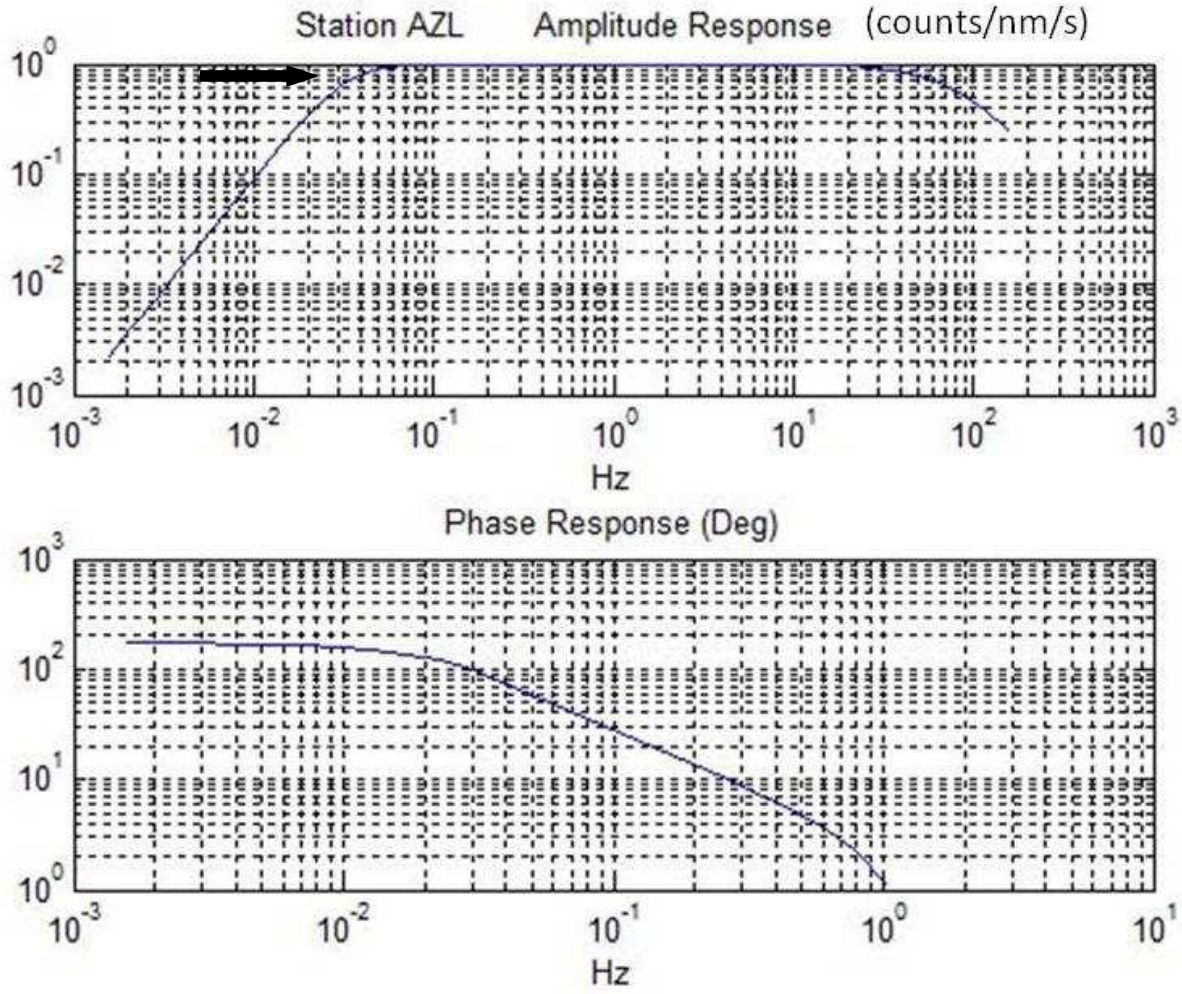

Fig.3.2 Figures showing example of amplitude and phase response to the ground velocity with known pole-zero distribution for AZL (Aizawl) seismic station. The arrows in the figure (top) indicate plateau as value 1.0 counts/nm/s.

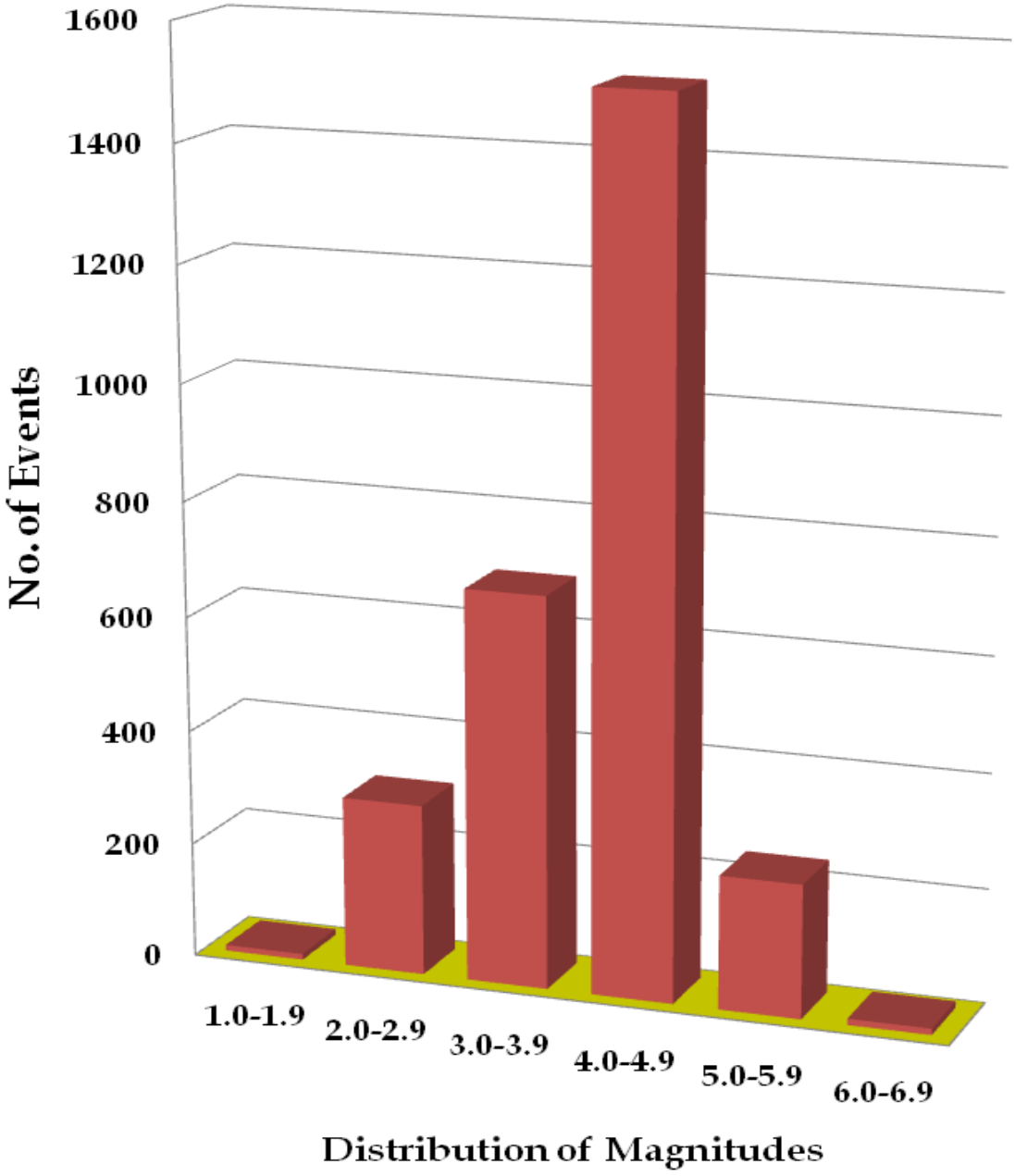

Fig.4.1 Frequency Distribution of Network Duration Magnitudes, MD(A) for about 2758 earthquakes in Surma Valley and its vicinity.

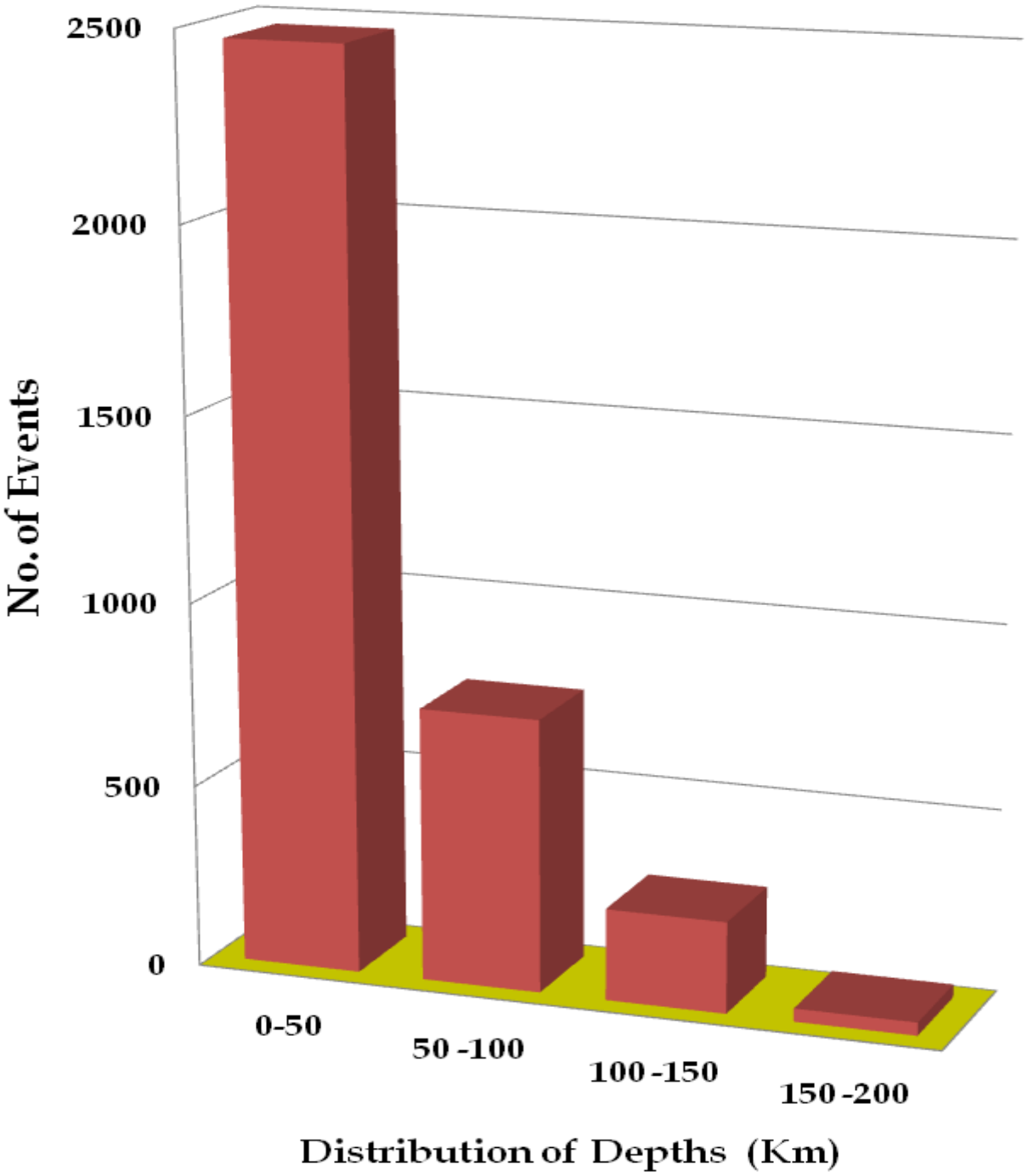

Fig.4.2 Frequency Distribution in terms of Depth (in km) for about 2758 earthquakes in Surma Valley and its vicinity.

(a)

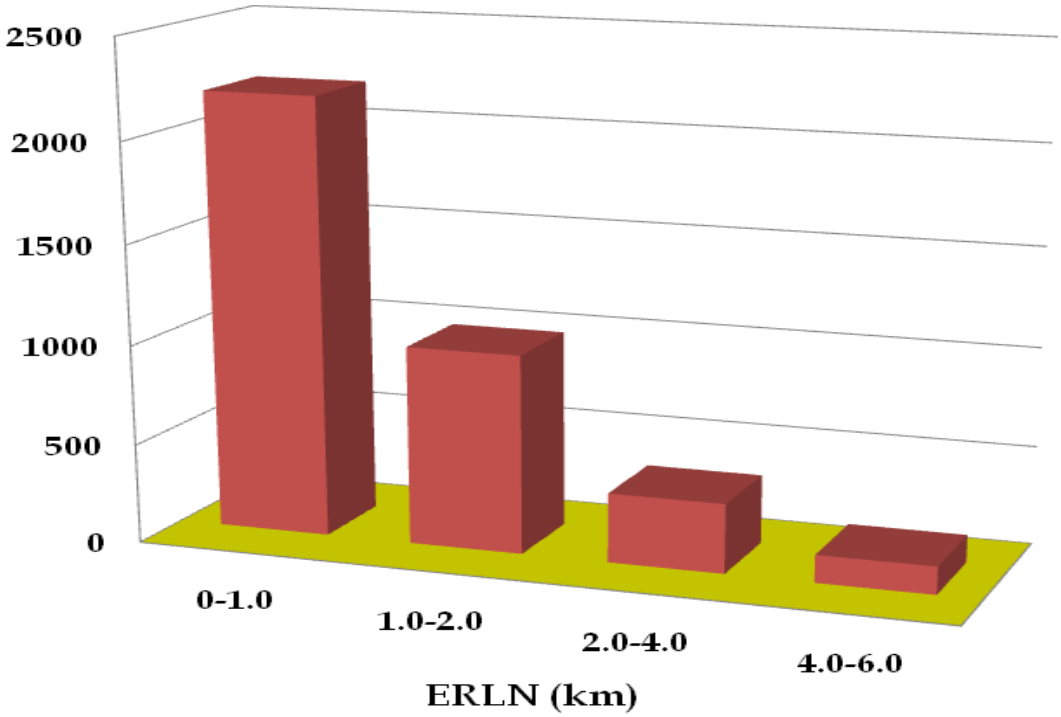
2500
2000
1500
1000
500
0
0-1.0
1.0-2.0
2.0-4.0
4.0-6.0
ERLN (km)

(b)

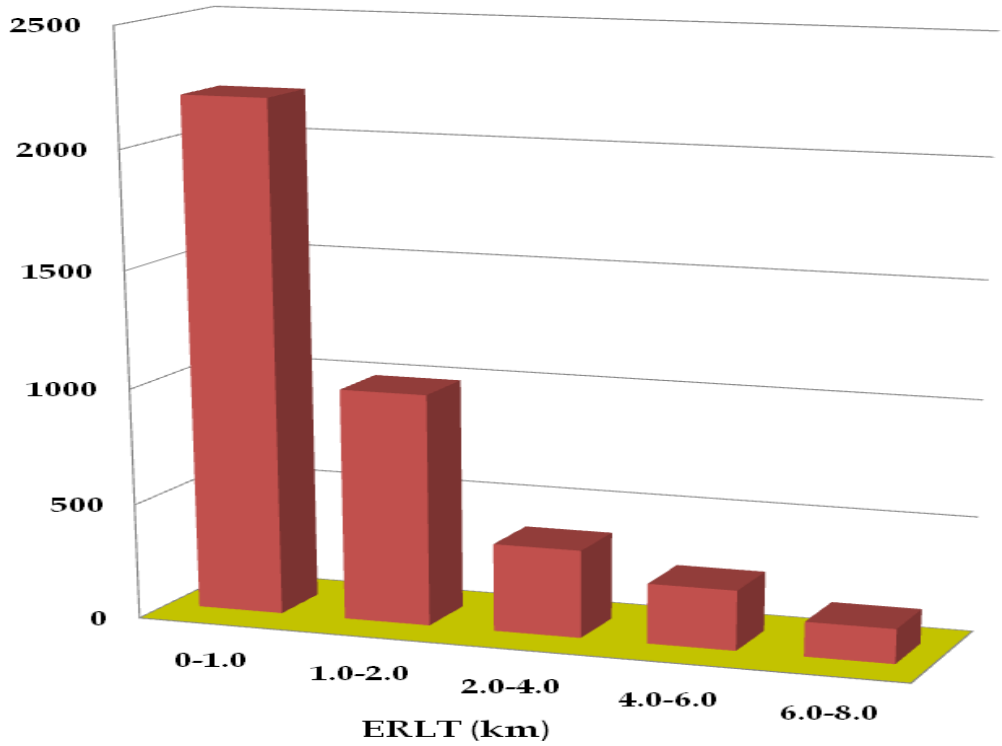
2500
2000
1500
1000
500
0
0-1.0
1.0-2.0
2.0-4.0
4.0-6.0
6.0-8.0
ERLT (km)

Cont

d.

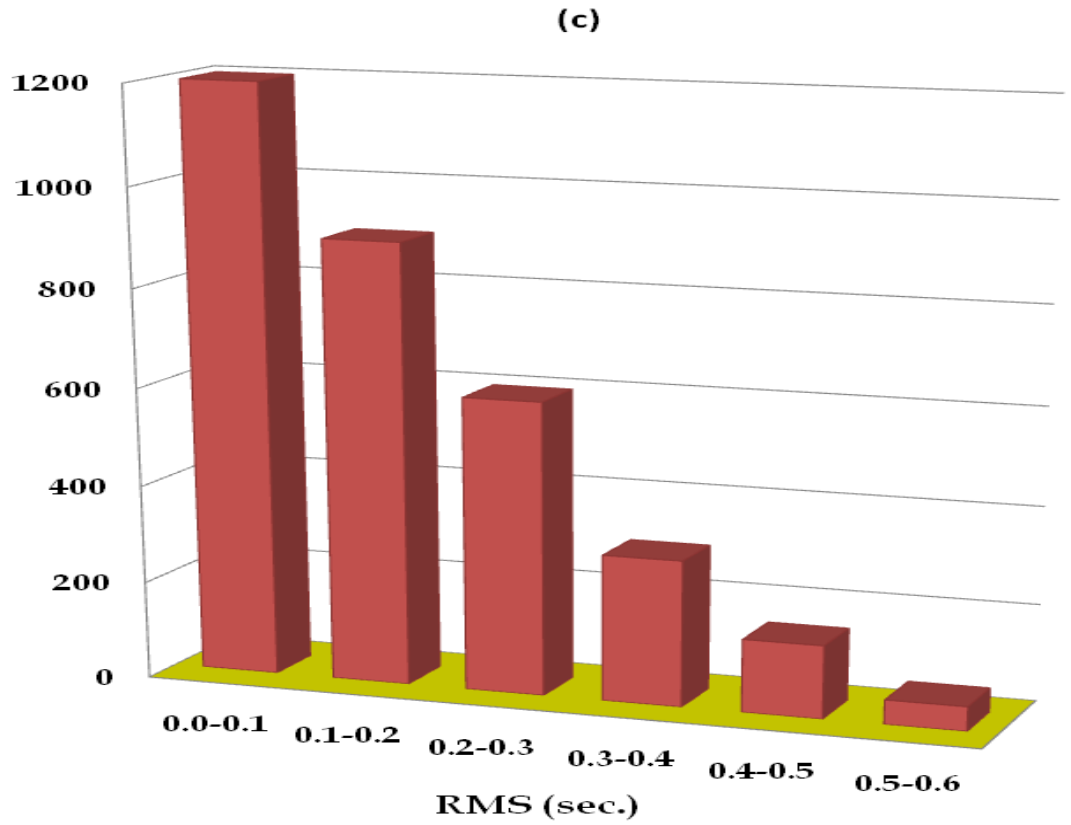

Fig.4.3 Frequency distribution of the estimates of (a) Longitudes (ERLN) of the epicenters (b) Latitudes (ERLT) of the epicenters and (c) Root Mean Square (RMS) for the origin times and uncertainties involved in the estimates of for the earthquakes in Surma valley and its vicinity during the period 1969-2009 considered in the present study.

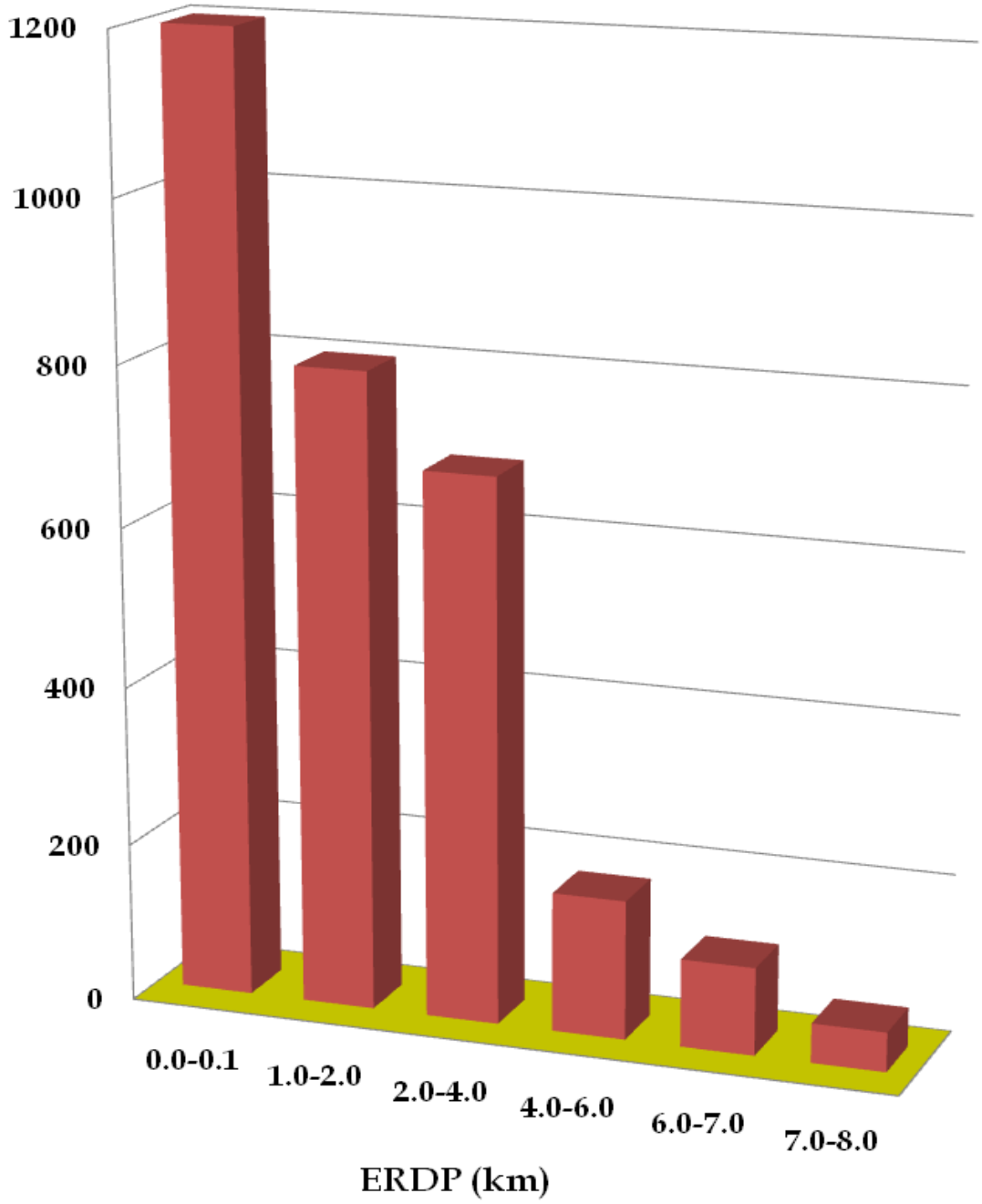

Fig.4.4 Frequency distribution of uncertainties involved in the estimates of focal depth (ERDP) for the earthquakes in Surma valley and its vicinity during the period 1969-2009 considered in the present study.

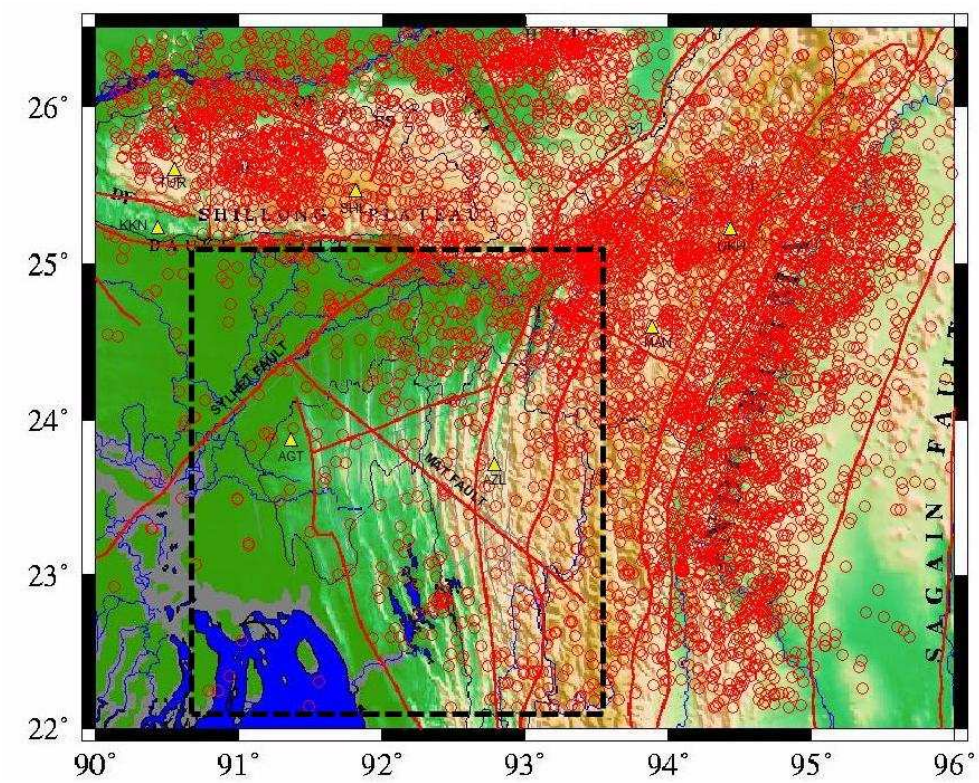

Fig.4.5 Seismicity plot of Surma valley and its vicinity. The rectangular box indicates the events within Surma valley.

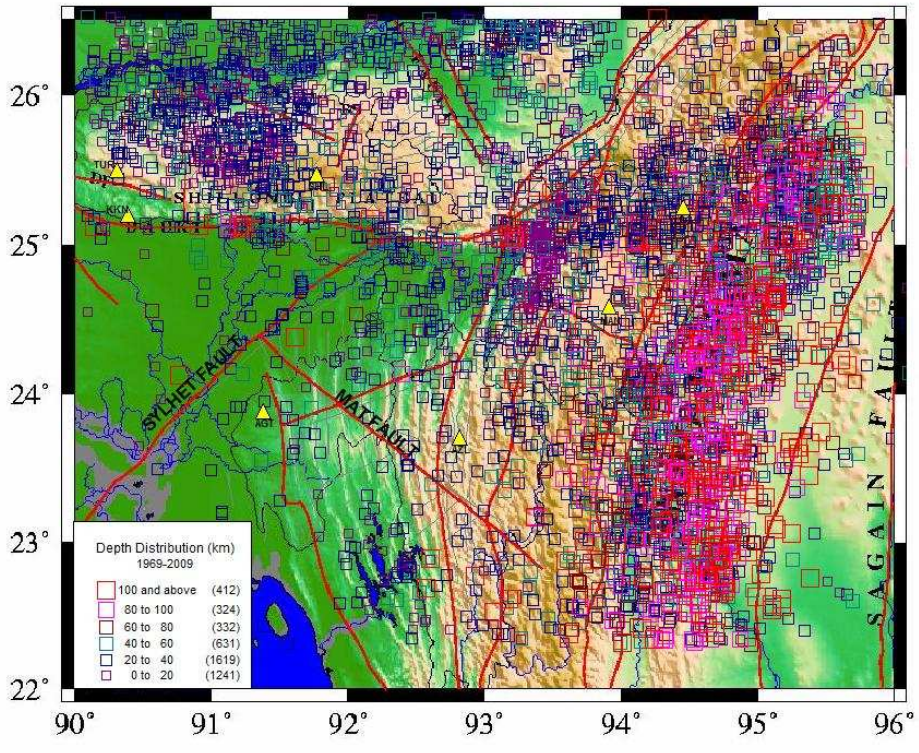

Fig.4.6 Depth Distribution of earthquakes in Surma valley and its vicinity.

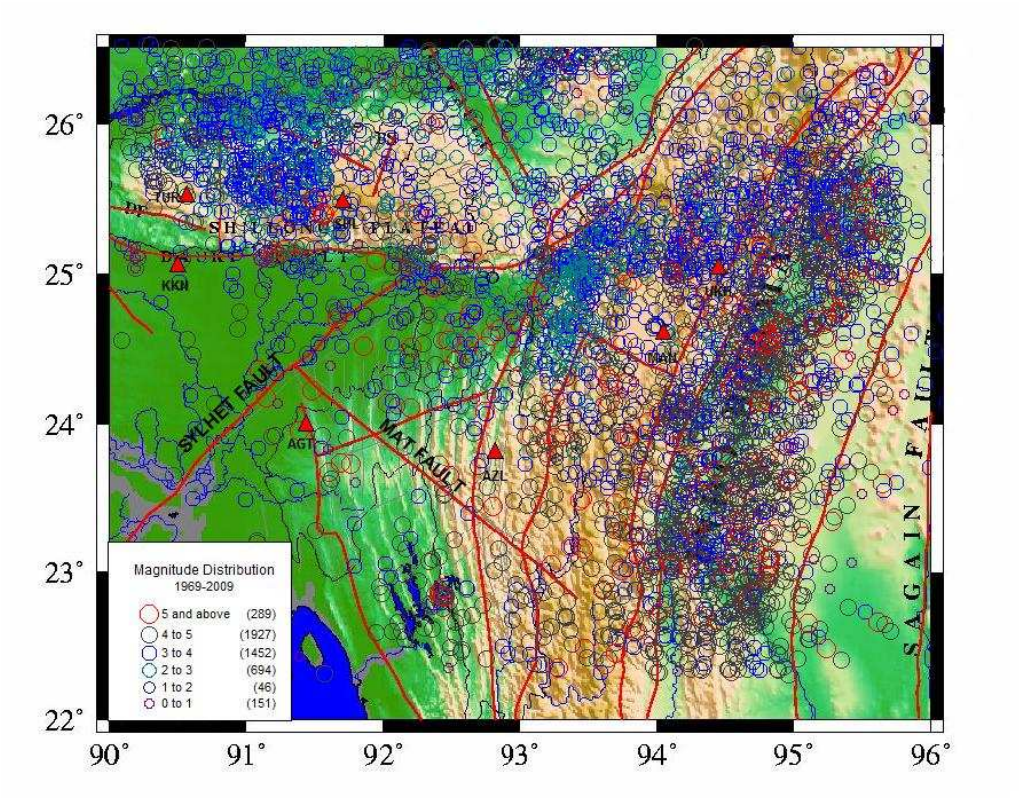

Fig.4.7 Magnitude Distribution of earthquakes in Surma valley and its vicinity.

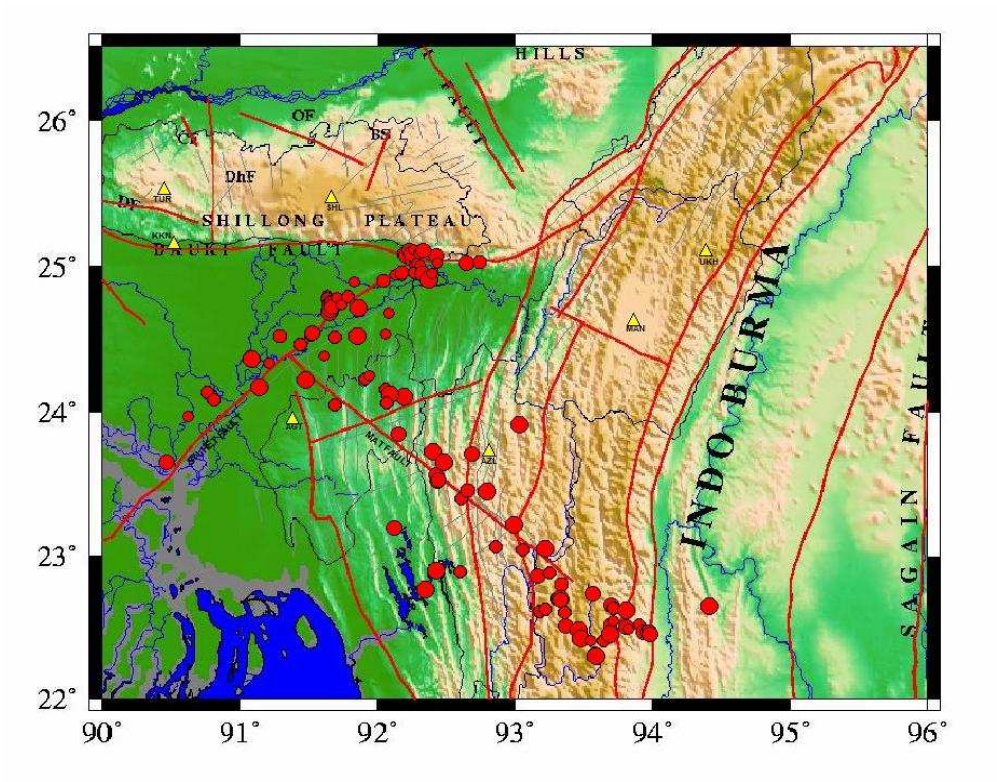

Fig.4.8 Seismicity along Sylhet fault and Mat Fault. Other earthquakes are removed to show activeness of both faults.

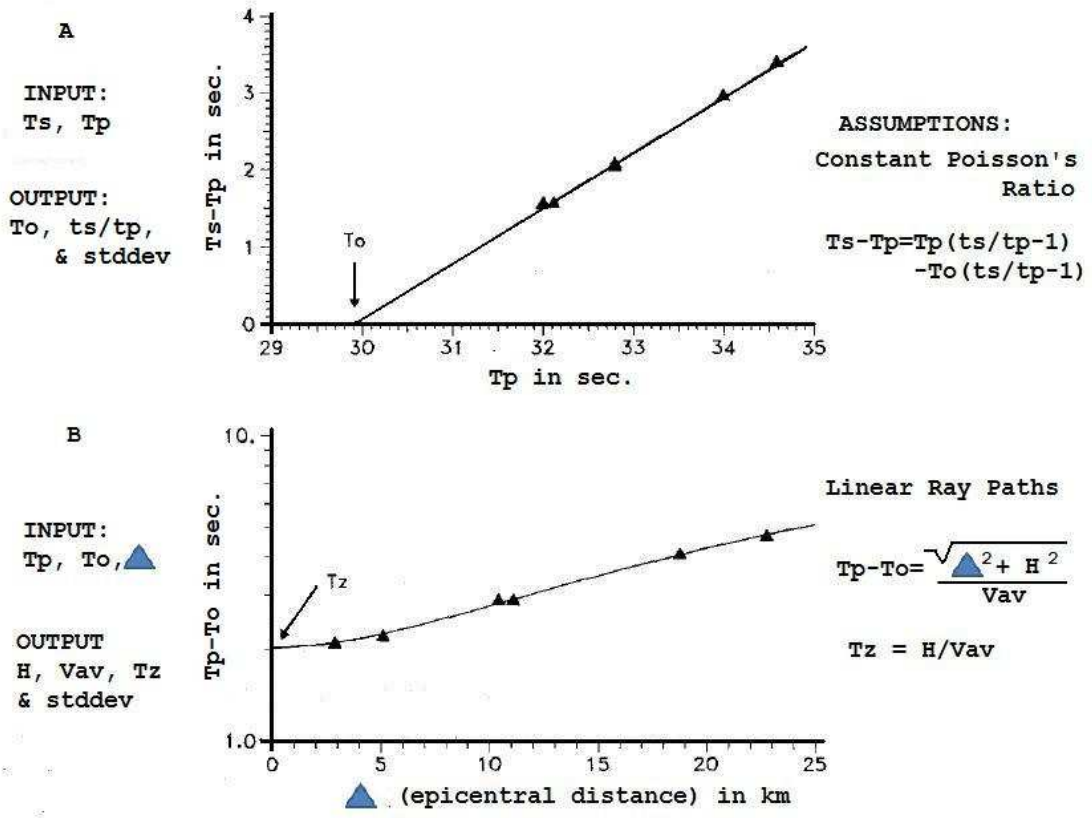

Fig.5.1 Equations and figures for (A) Wadati diagrams and (B) Riznichenko diagrams. To the left are input and output parameters, in the middle are the graphical forms, and to the right are the equations.

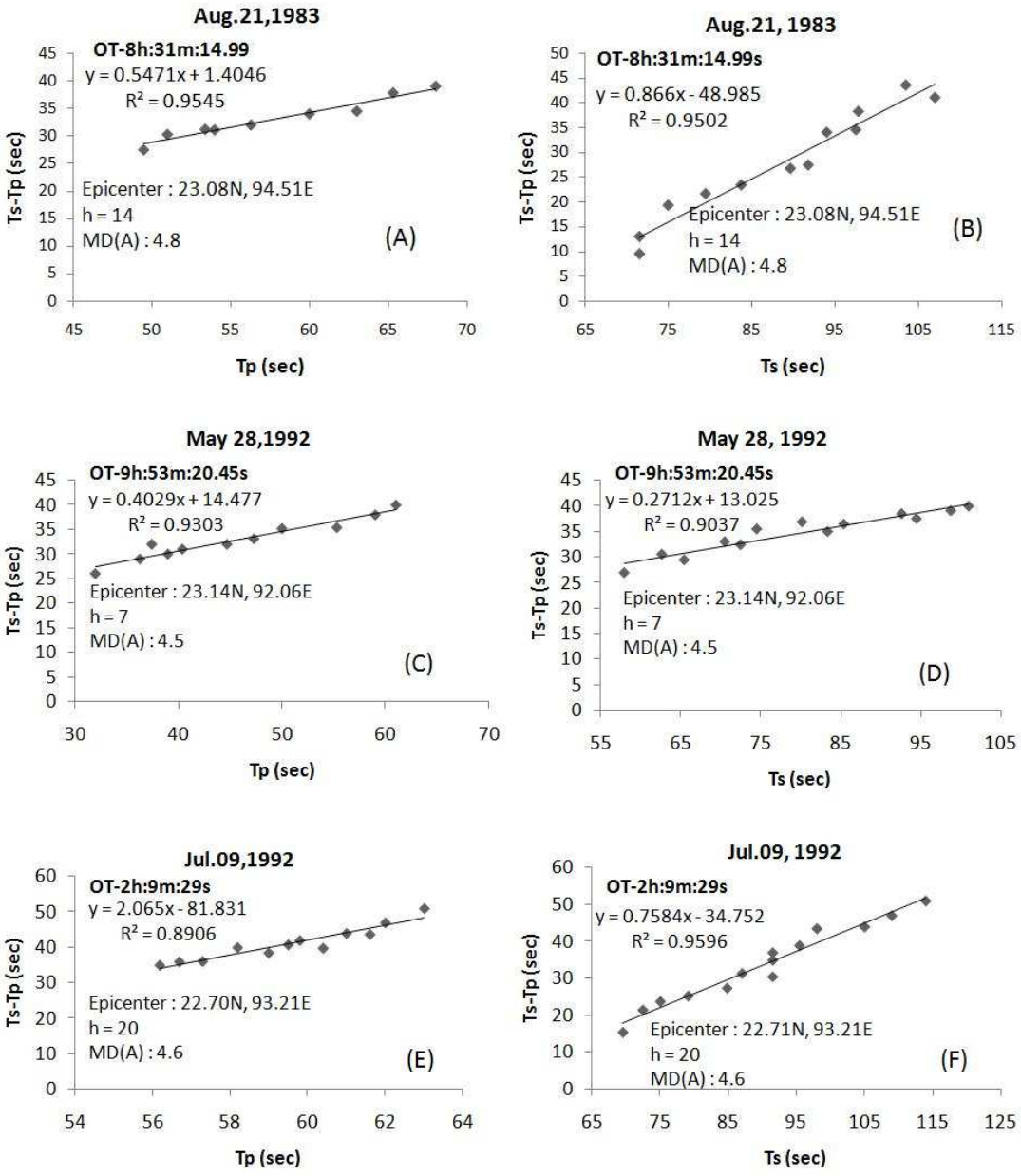

Fig.5.2 Wadati diagrams (A, B, C, D, E and F) for the earthquakes associated with events in the eastern part of Surma valley at depths (h) ranging between 0-20 km. Ts-Tp versus Tp and Ts-Tp versus Ts denote interval between the arrival time of P- and S-waves and arrival time of P- and S-waves at a seismic station respectively. Linear relations for the determination of P- and S-wave at a specific depth, involving Ts-Tp/Tp, Ts-Tp/Ts and origin time (O.T) are also shown.

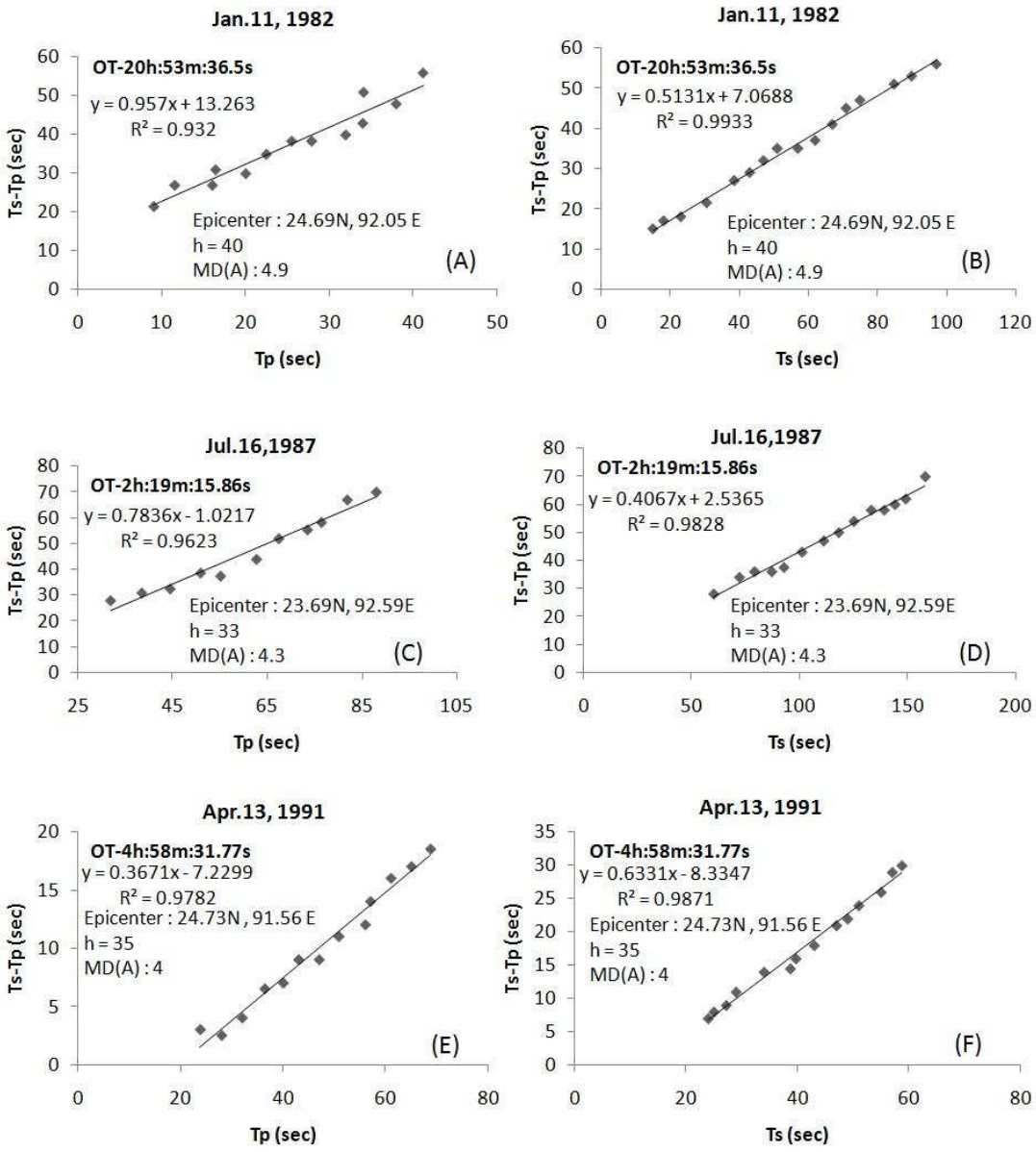

Fig.5.3 Wadati diagrams (A, B, C, D, E and F) for the earthquakes associated with events in the eastern part of Surma valley at depths (h) ranging between 21-40 km. Ts-Tp versus Tp and Ts-Tp versus Ts denote interval between the arrival time of P- and S-waves and arrival time of P- and S-waves at a seismic station respectively. Linear relations for the determination of P and S wave at a specific depth, involving Ts-Tp/Tp, Ts-Tp/Ts and origin time (O.T) are also shown.

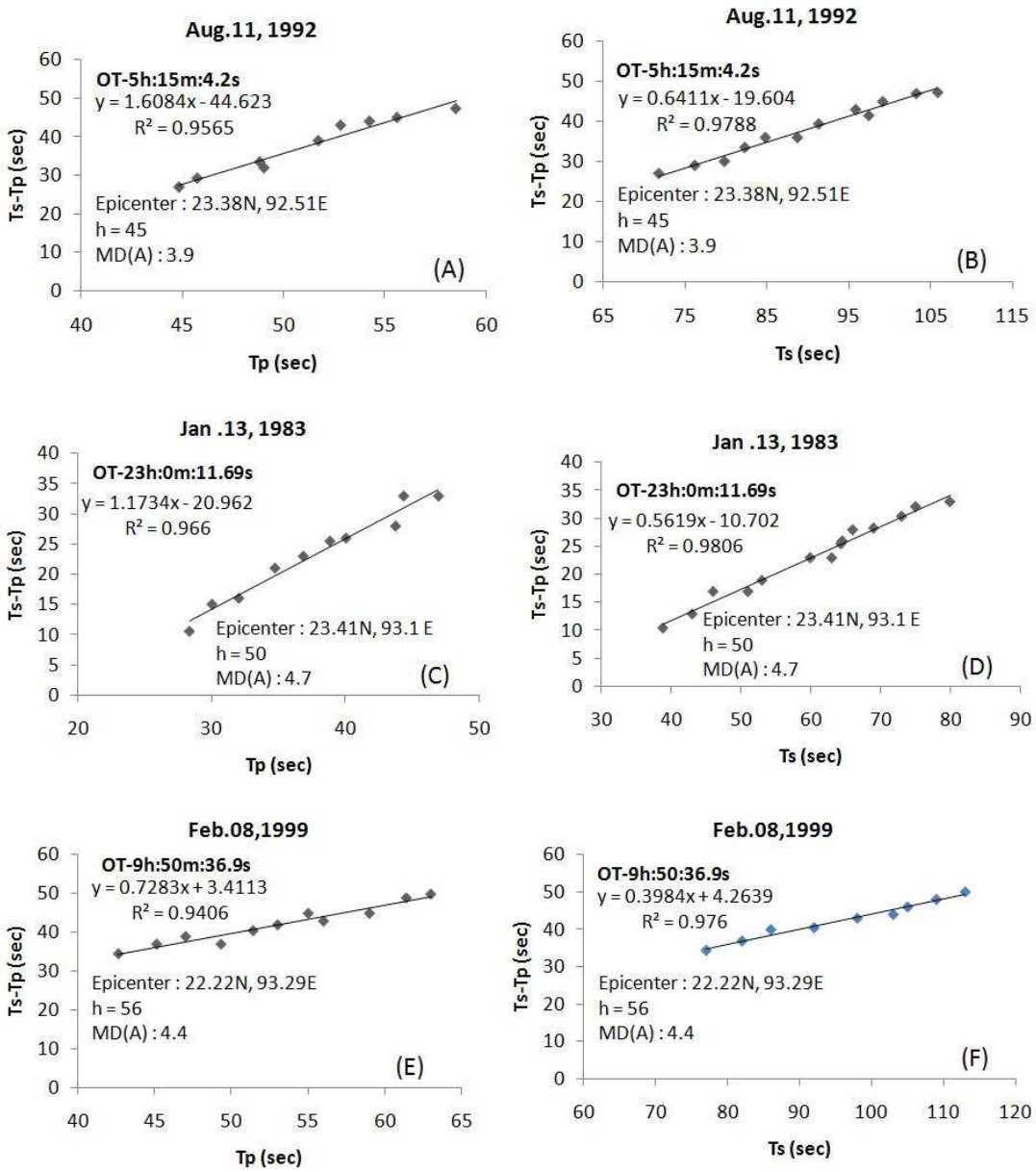

Fig.5.4 Wadati diagrams (A, B, C, D, E and F) for the earthquakes associated with events in the eastern part of Surma valley at depths (h) between ranging between 41-60 km. Ts-Tp versus Tp and Ts-Tp versus Ts denote interval times of P- and S-waves and arrival time of P- and S-waves at a seismic station respectively. Linear relations for the determination of P- and S-wave at a specific depth, involving Ts-Tp/Tp, Ts-Tp/Ts and origin time (O.T) are also shown.

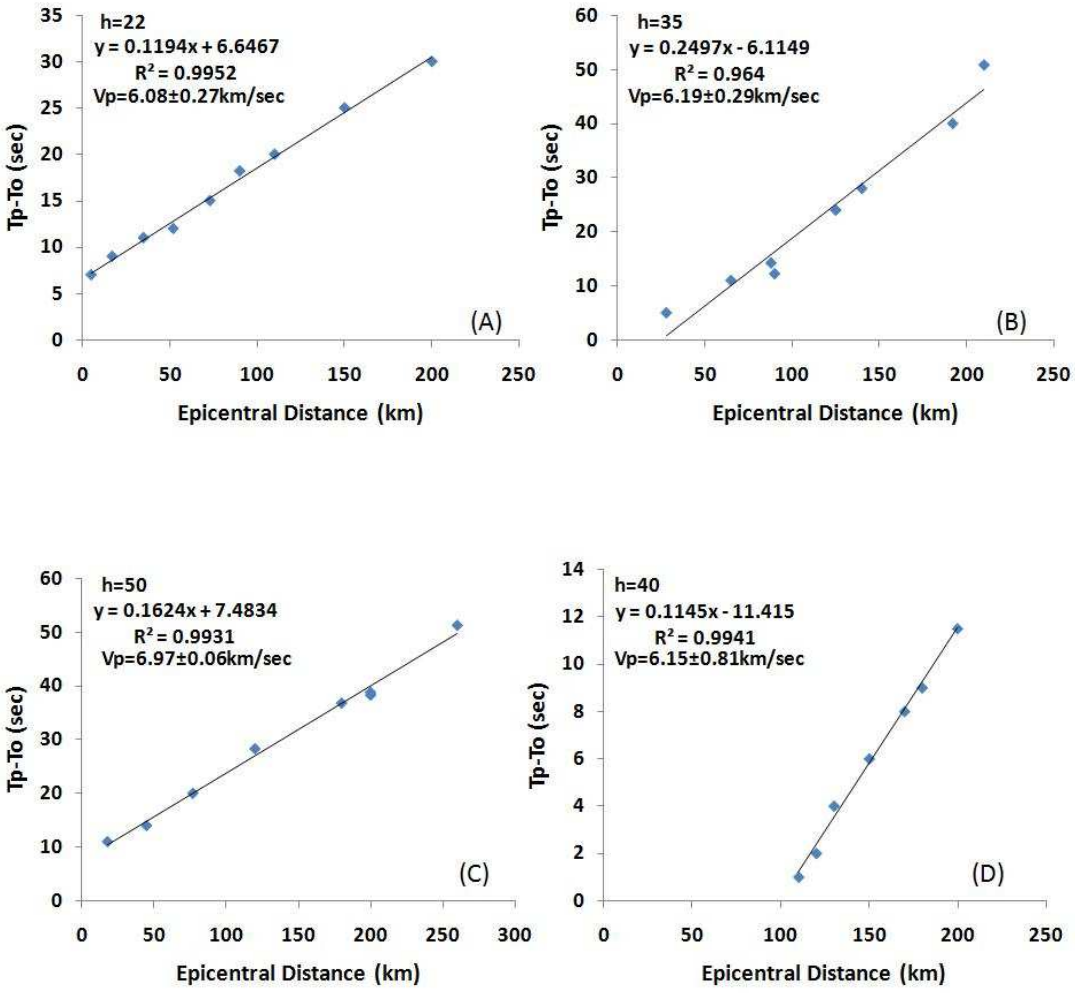

Fig.5.5 Riznichenko diagrams (A, B, C and D) of earthquakes associated with events in the eastern part of Surma valley as recorded in different selected seismic stations in the northeast. Linear relation between Tp-To and epicentral distance (+) are also shown for the events at different depth ranges.

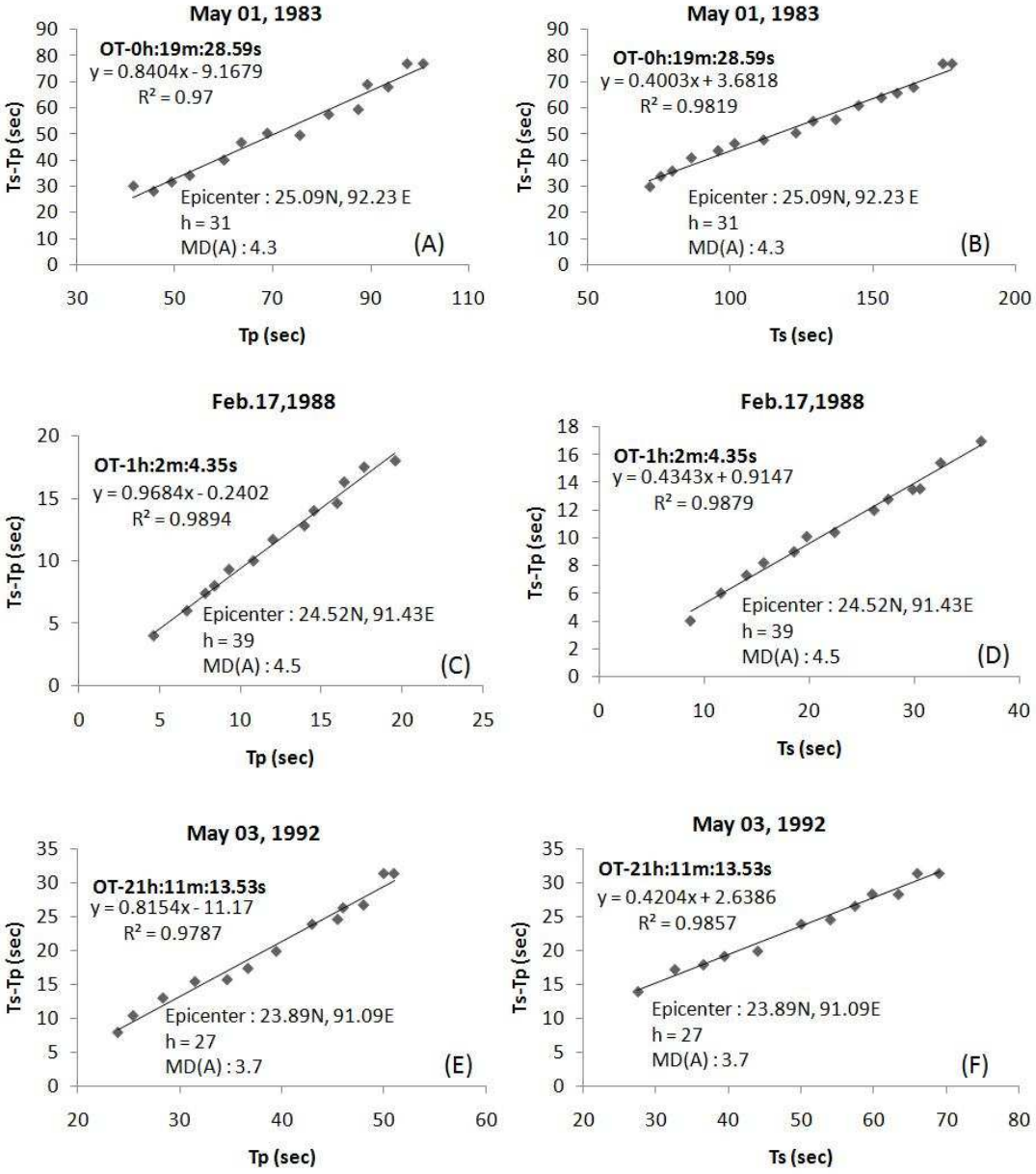

Fig.5.6 Wadati diagrams (A, B, C, D, E and F) for the earthquakes associated with events in the northern part of Surma valley at depths (h) ranging between 21-40 km. Ts-Tp versus Tp and Ts-Tp versus Ts denote interval between the arrival time of P- and S-waves and arrival time of P- and S-waves at a seismic station respectively. Linear relations for the determination of P- and S-wave at a specific depth, involving Ts-Tp/Tp, Ts-Tp/Ts and origin time (O.T) are also shown.

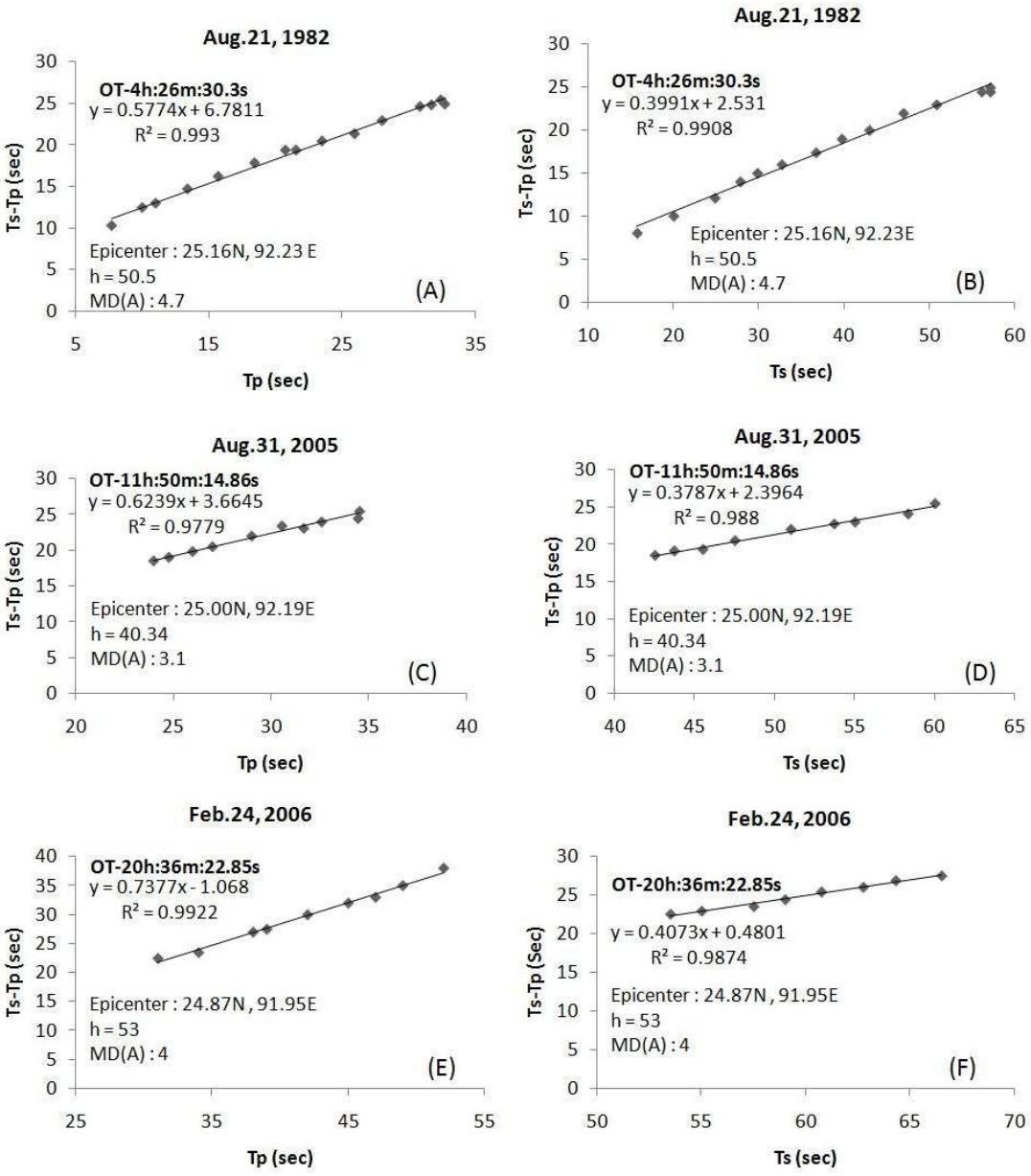

Fig.5.7 Wadati diagrams (A, B, C, D, E and F) for the earthquakes associated with events in the northern part of Surma valley at depths (h) ranging between 41-60 km. Ts-Tp versus Tp and Ts-Tp versus Ts denote interval between the arrival time of P- and S-waves and arrival time of P- and S-waves at a seismic station respectively. Linear relations for the determination of P- and S-wave at a specific depth, involving Ts-Tp/Tp, Ts-Tp/Ts and origin time (O.T) are also shown.

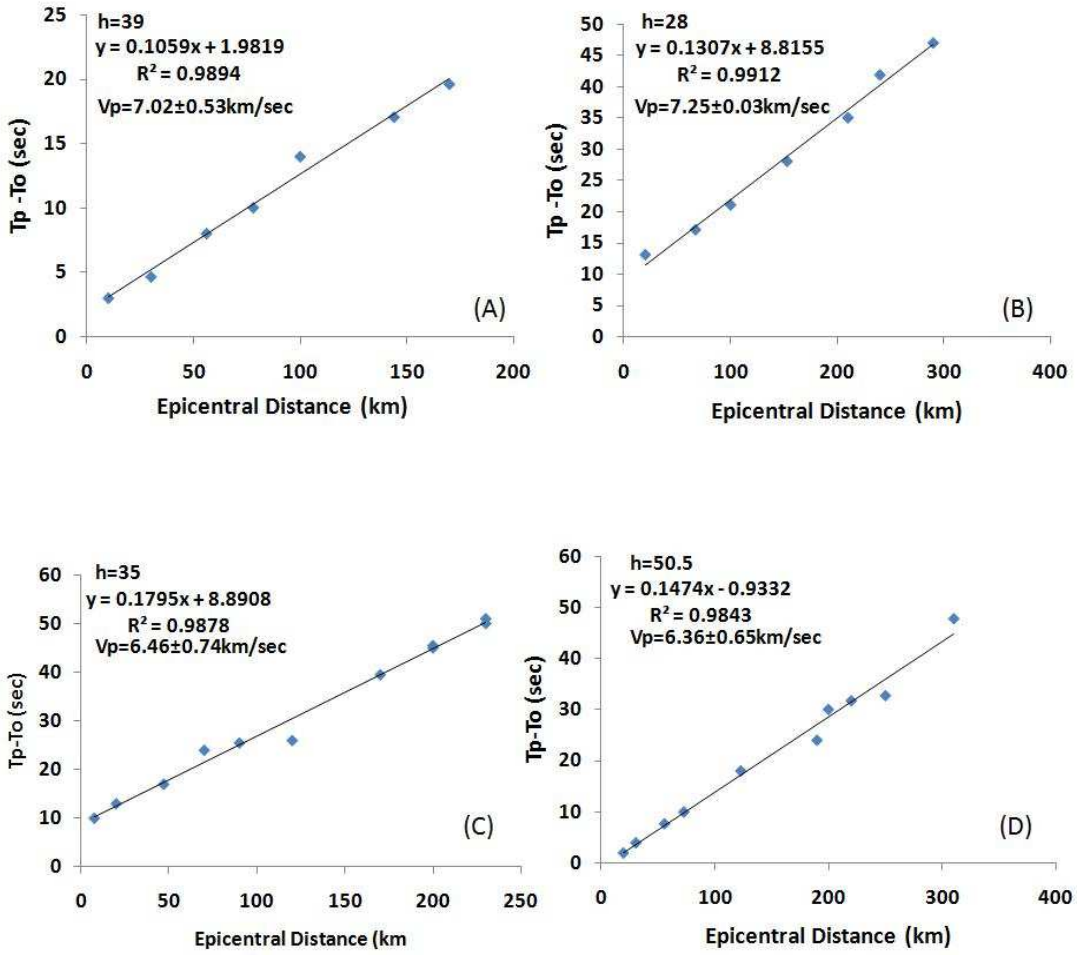

Fig.5.8 Riznichenko diagrams (A, B, C and D) of earthquakes associated with events in the northern part of Surma valley as recorded in different selected seismic stations in the northeast. Linear relation between Tp-To and epicentral distance (+) are also shown for the events at different depth ranges.

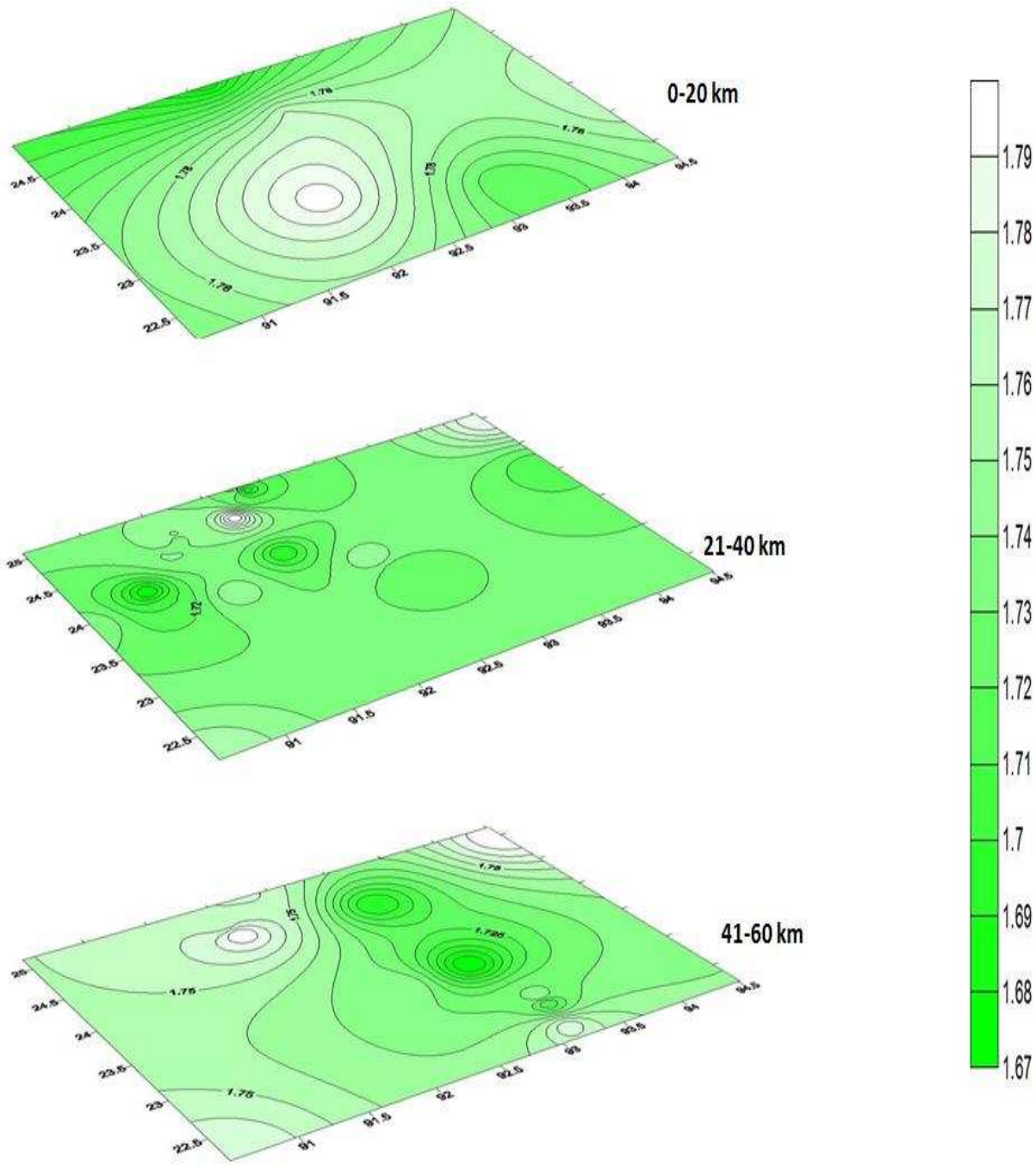

Fig.6.1 Vp/Vs variation at different depth ranges in Surma valley. The color scale indicate the Vp/Vs ratio. The area covers 22-25^{0}N and 90^0-94.5^{0}E.

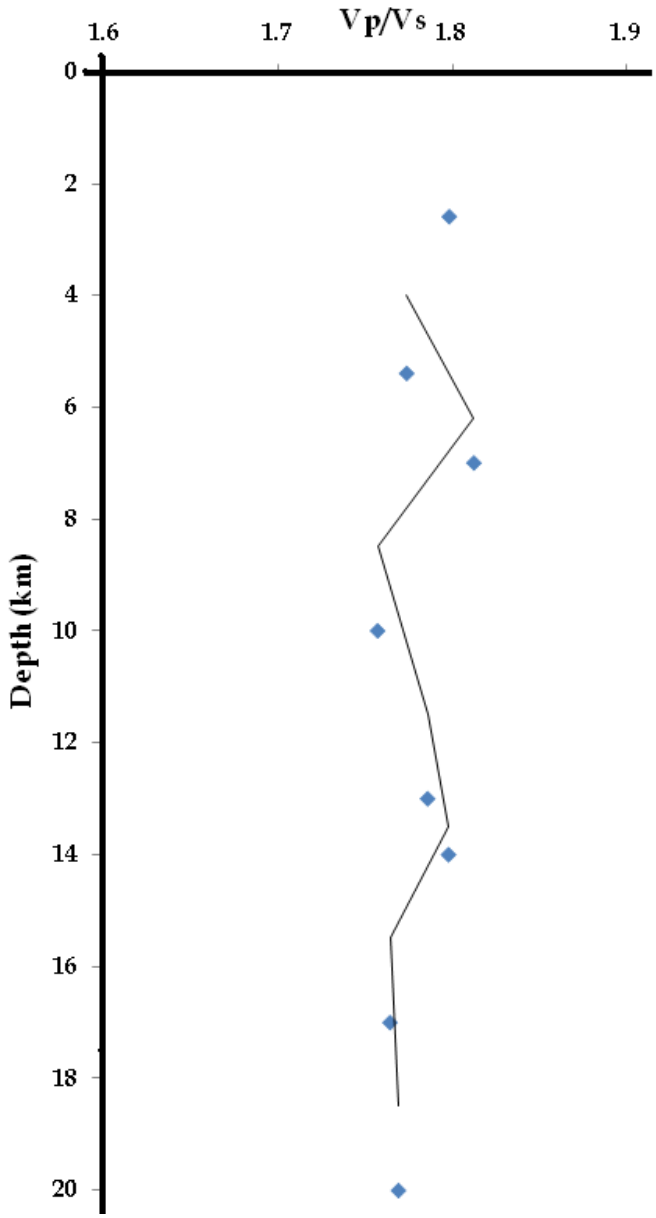

Fig.6.2(a) Depth Variation at 0-20 km range in Mat fault region (eastern Surma valley). The velocity Vp/Vs ratios varies between 1.75 to 1.83.

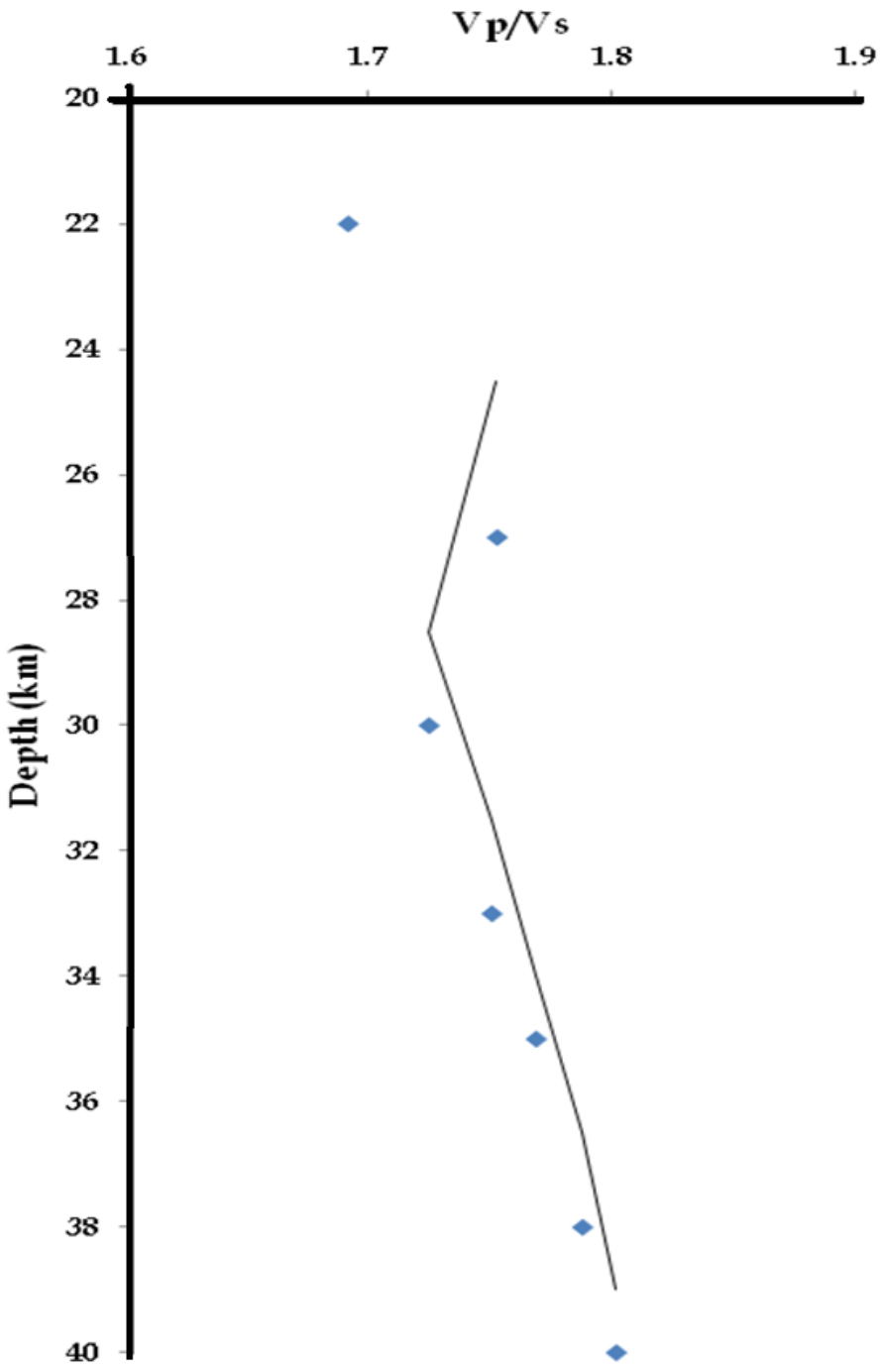

Fig.6.2(b) Depth Variation at 21-40 km range in Mat fault region (eastern Surma valley). The velocity Vp/Vs ratios increases from 1.69 to a maximum of 1.79.

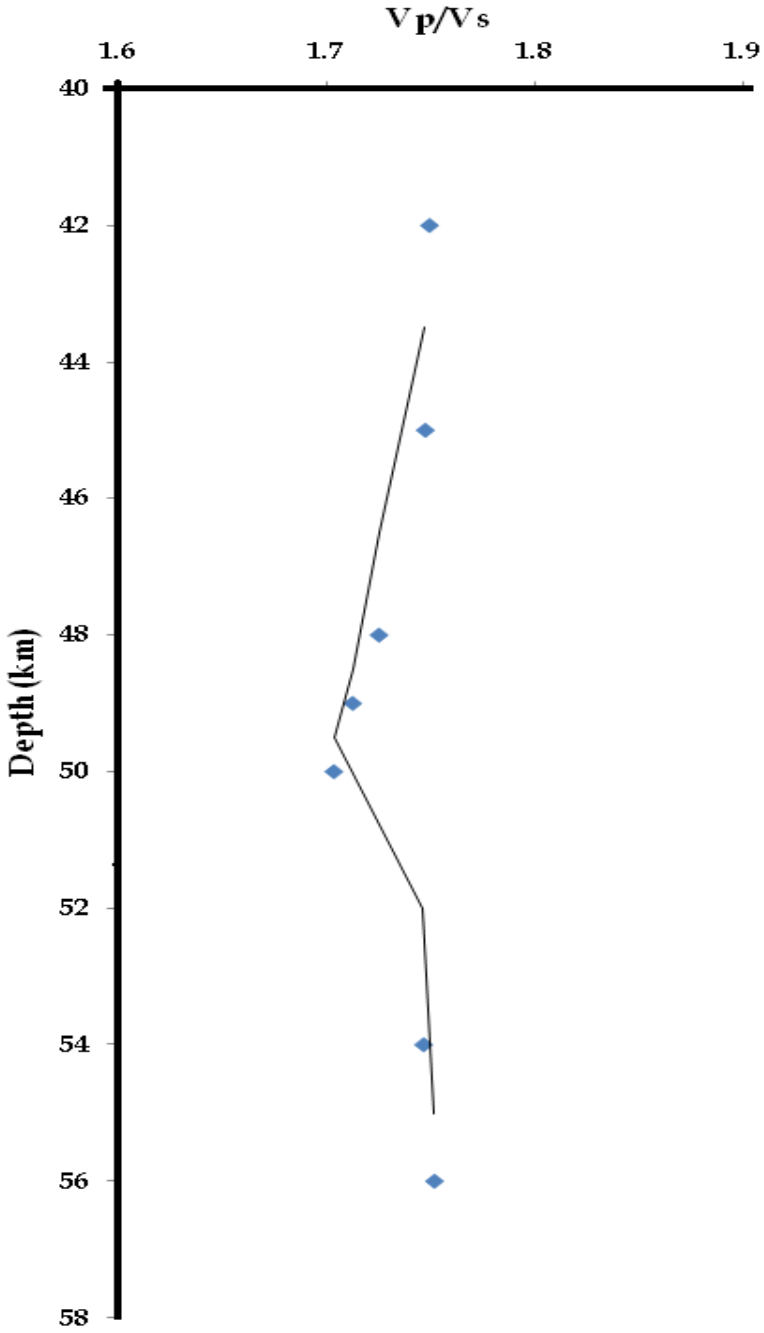

Fig.6.2(c) Depth Variation at 41-60 km range in Mat fault region (eastern Surma valley). Vp/Vs ratios vary from 1.7 to 1.75.

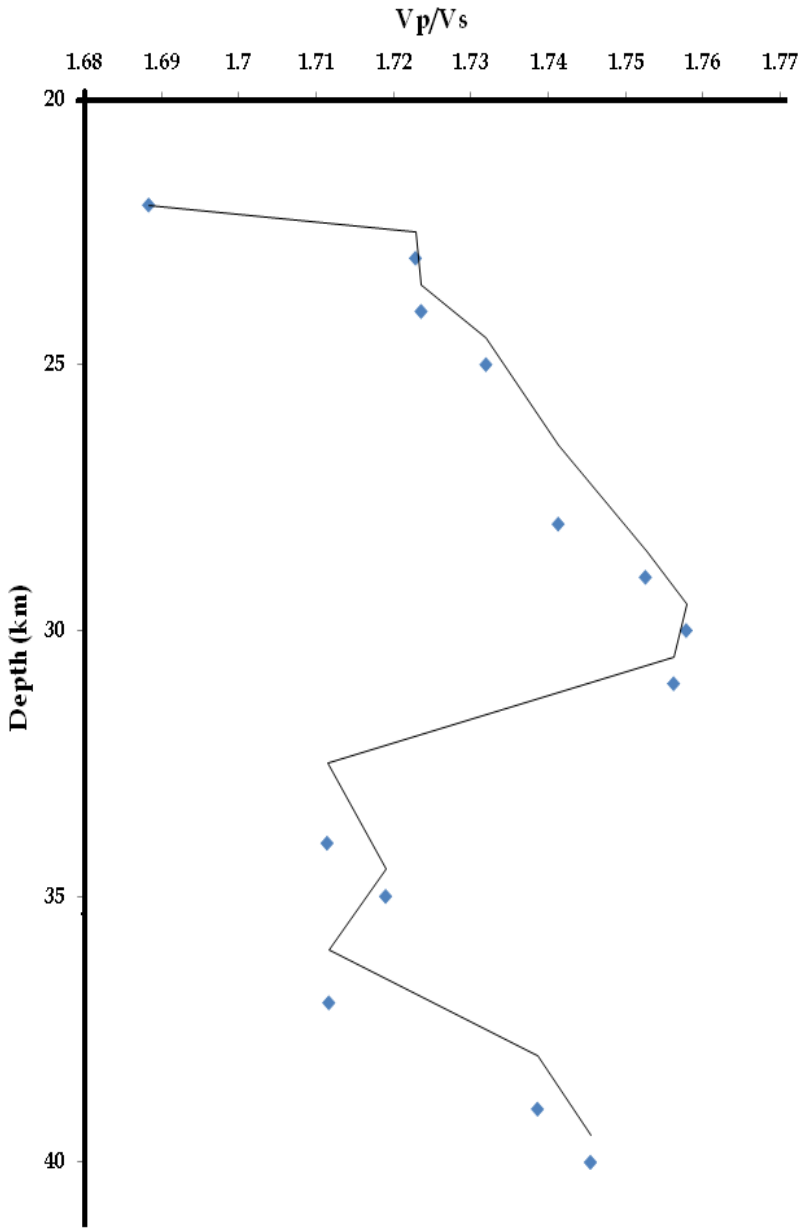

Fig.6.3(a) Depth Variation at 21-40 km range in Sylhet fault region (northern Surma valley). Sudden changes in velocities Vp/Vs ratios are observed at depths of 23 and 33 km.

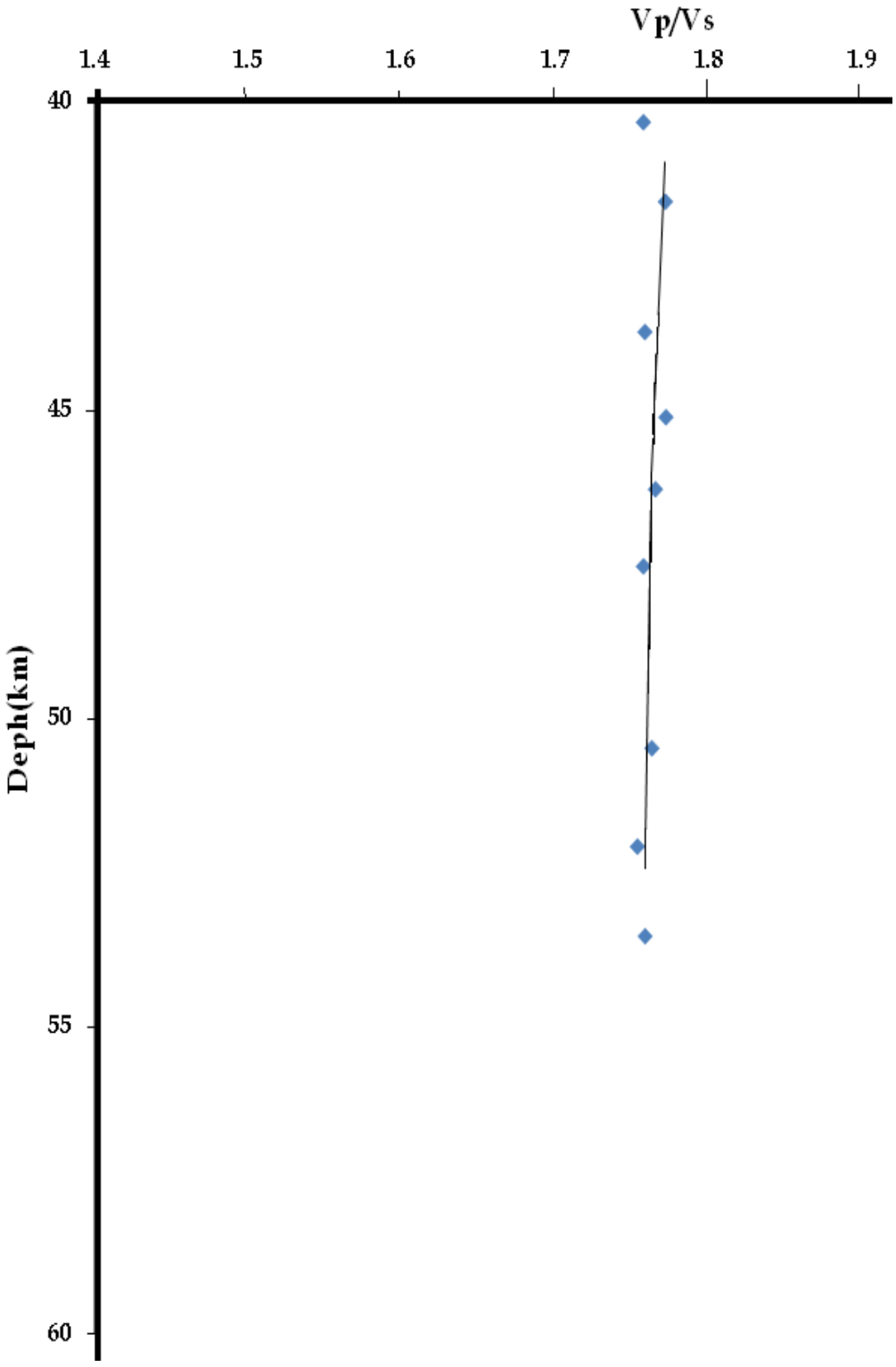

Fig.6.3(b) Depth Variation at 41-60 km range in Sylhet fault region (northern Surma valley). Velocity (Vp/Vs) ratio is more or less uniform through the range.

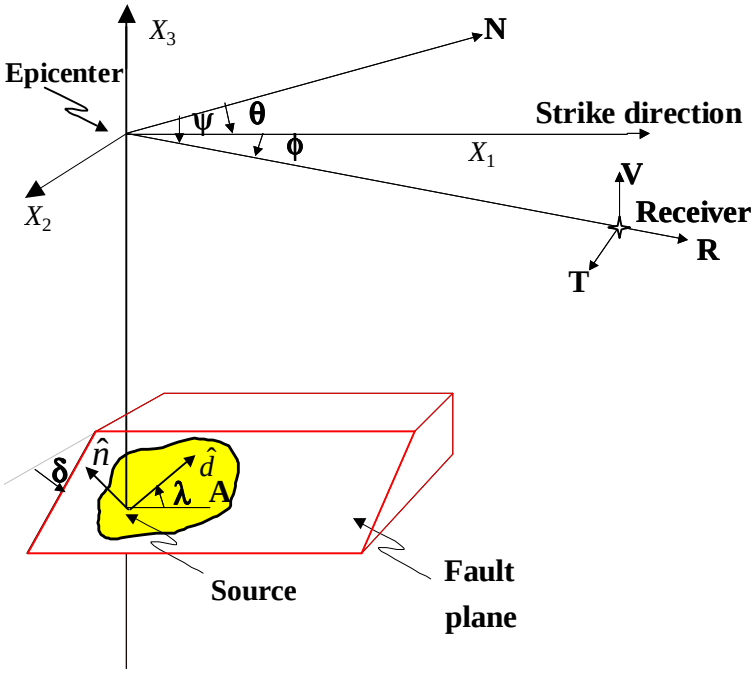

Fig.7.1 Fault Geometry used in earthquake studies. A: area affected on the fault plane (After Kanamori and Cipar, 1974).

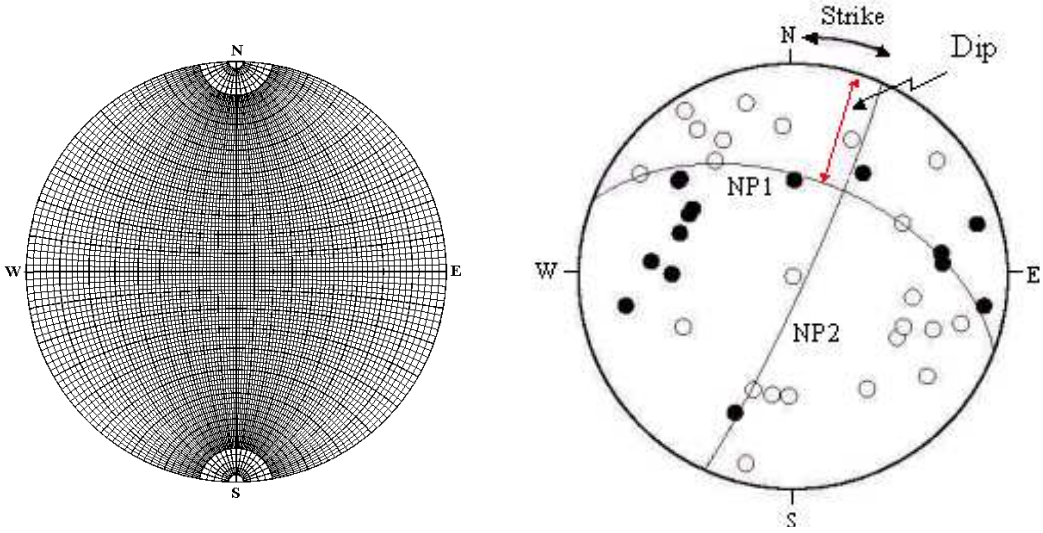

Fig.7.2 (a) Wulff's net (b) an example showing the nodal planes, strike and dip.

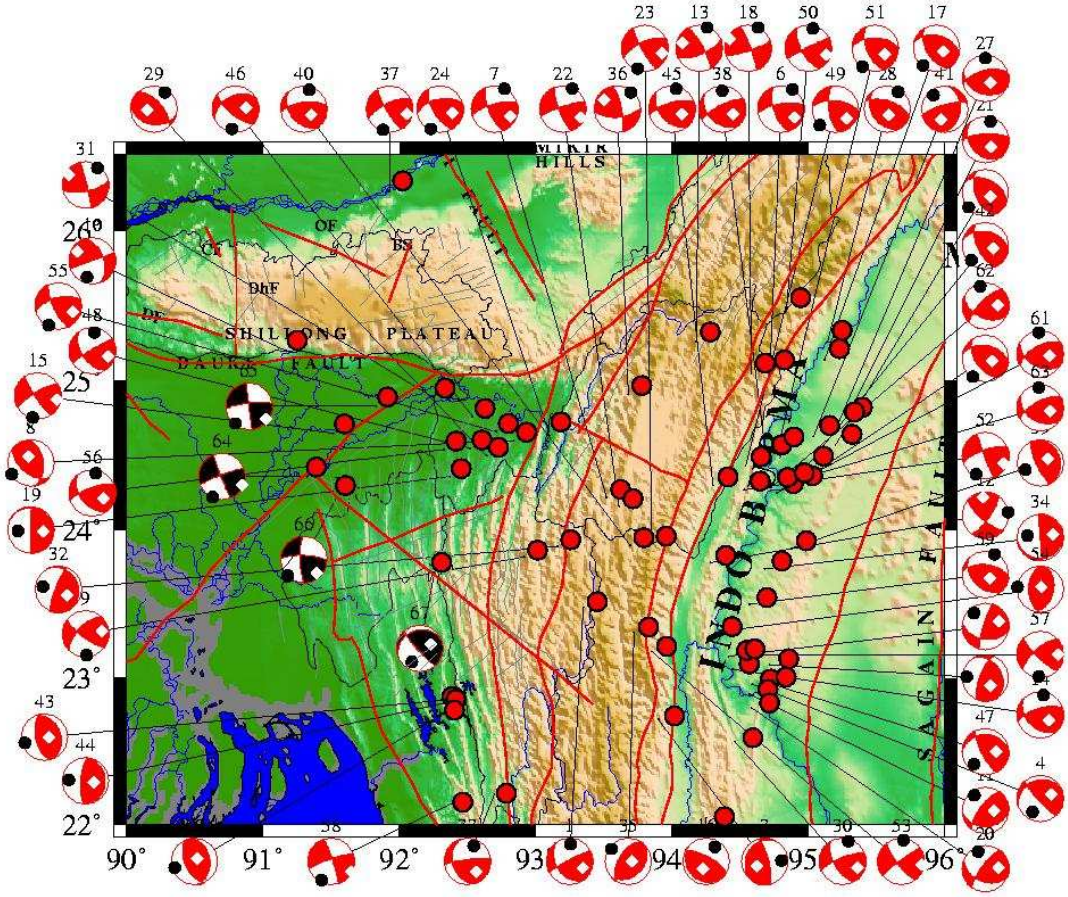

Fig.7.3 Beachball representation of the focal mechanism solutions in the Surma valley and its vicinity. The black colored beachball represent the focal mechanism solutions through waveform inversion whereas red coloured beachball represent the focal mechanism solution obtained from P-wave first motion.

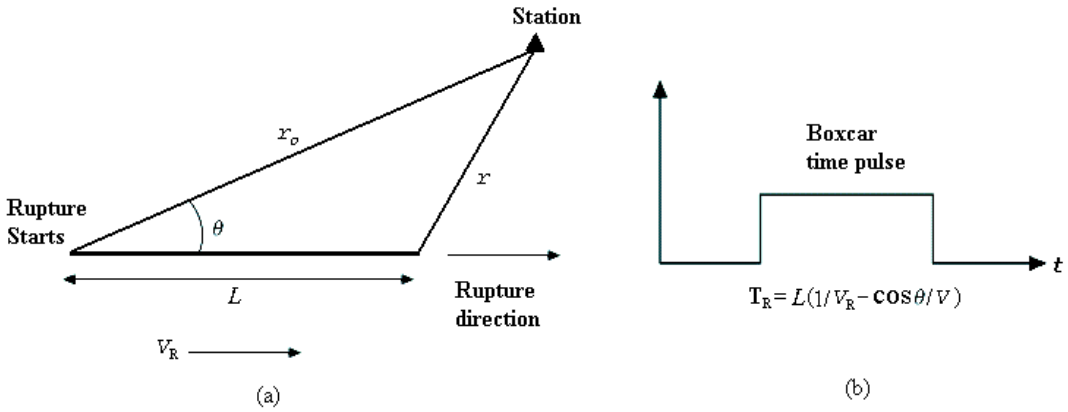

Fig.7.4 (a) For a fault of length L, the duration of the source time function varies as a function of azimuth, depending on the variation of the rupture velocity V_R and wave velocity V and (b) the time pulse due to the finite fault length "L" which is a "boxcar" of duration (Stein and Wysession, 2003).

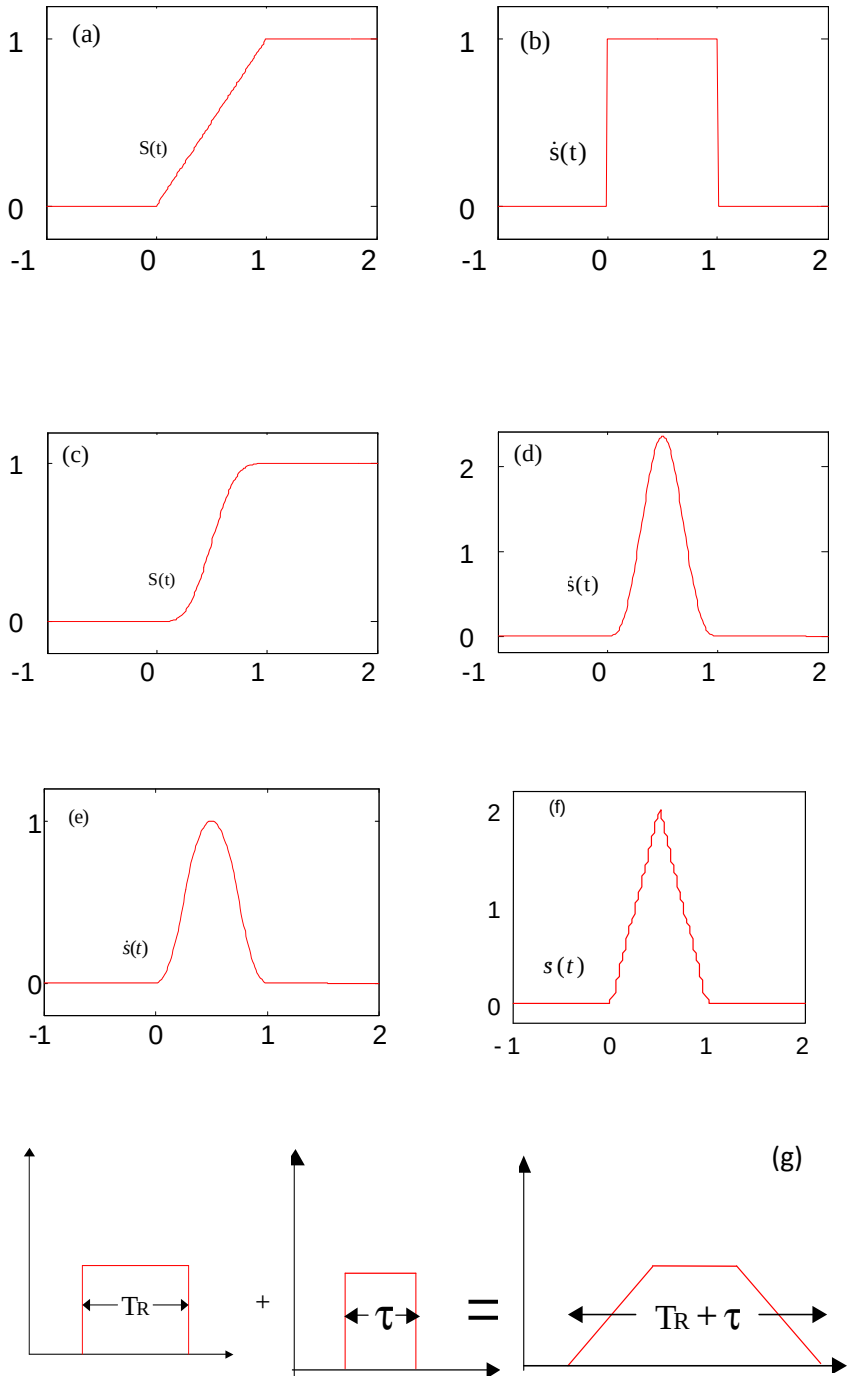

Fig.7.5 Different source time functions: (a) ramp function (b) derivative of ramp function (c) by Brustle and Muller (1983) (d) derivative of Brustle and Muller source (e) by Wang and Herrman (1980) (f) Triangular and (g) Trapezoidal source time function.

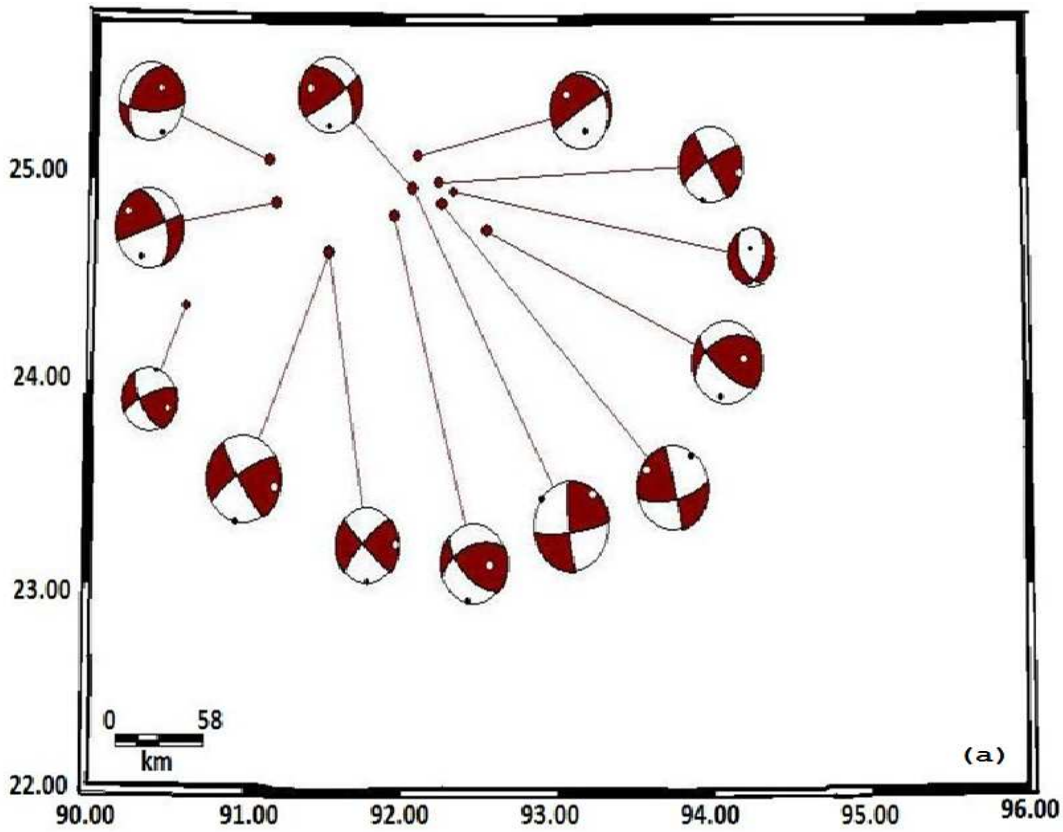
25.00
24.00
23.00
22.00
90.00
91.00
92.00
93.00
94.00
95.00
96.00
0
58
km
(a)

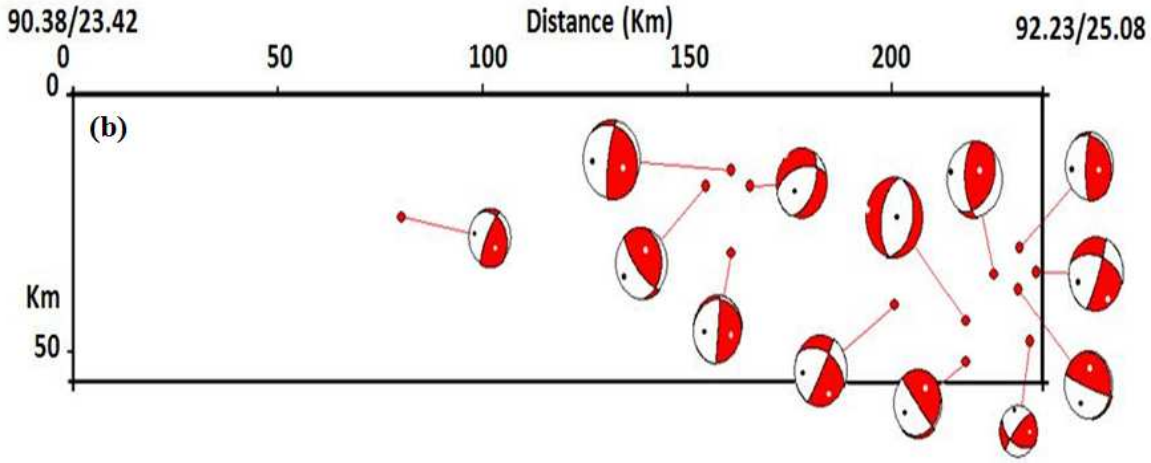
90.38/23.42
Distance (Km)
92.23/25.08
0
50
100
150
200
0
(b)
Km
50

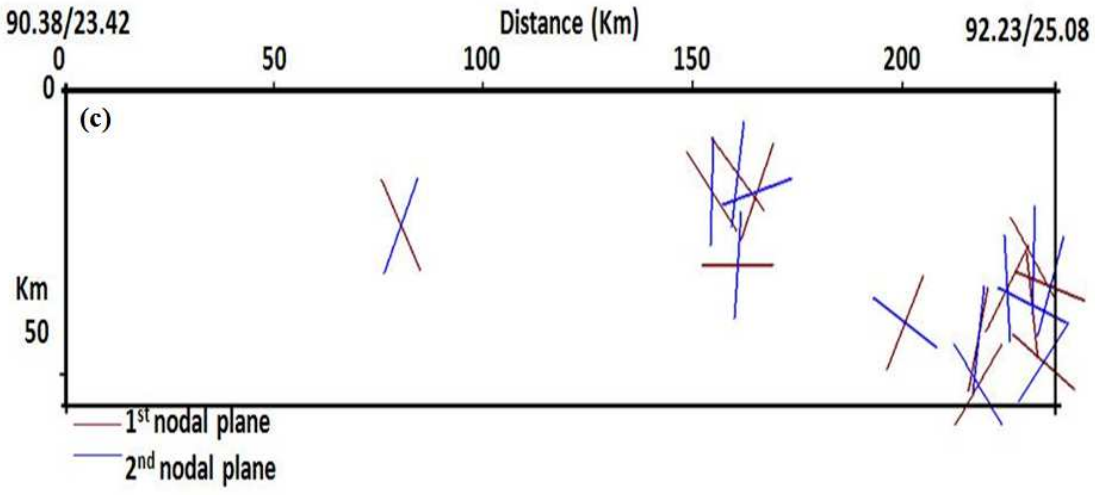
90.38/23.42
Distance (Km)
92.23/25.08
0
50
100
150
200
0
(c)
Km
50
1st nodal plane
2nd nodal plane

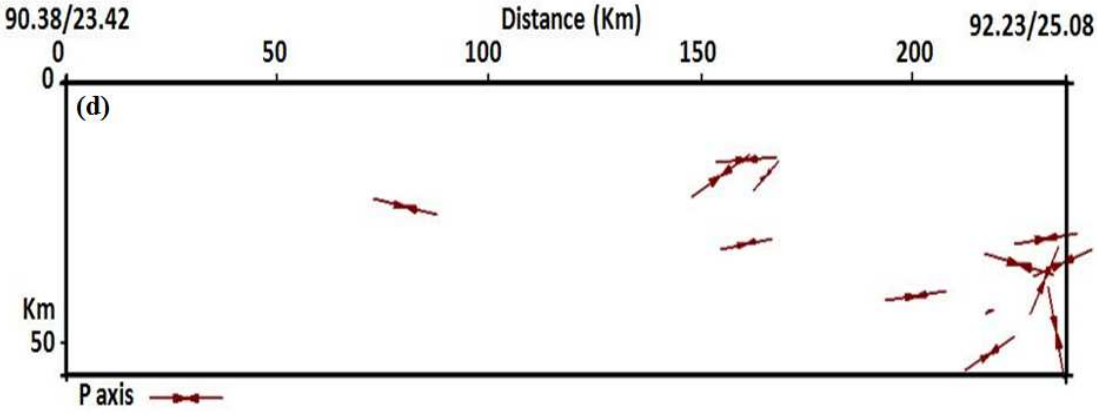
90.38/23.42
Distance (Km)
92.23/25.08
0
50
100
150
200
0
(d)
Km
50
P axis

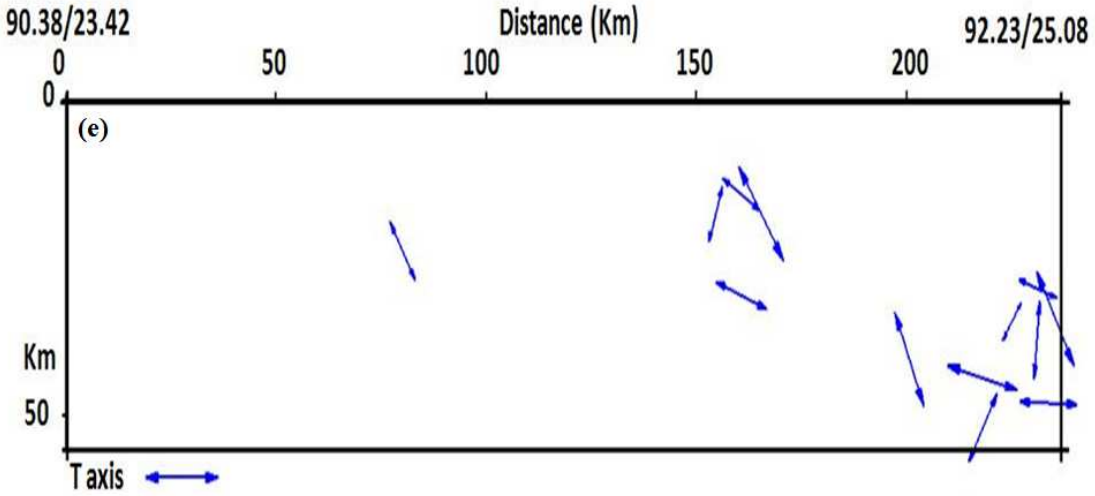
90.38/23.42
Distance (Km)
92.23/25.08
0
50
100
150
200
0
(e)
Km
50
T axis

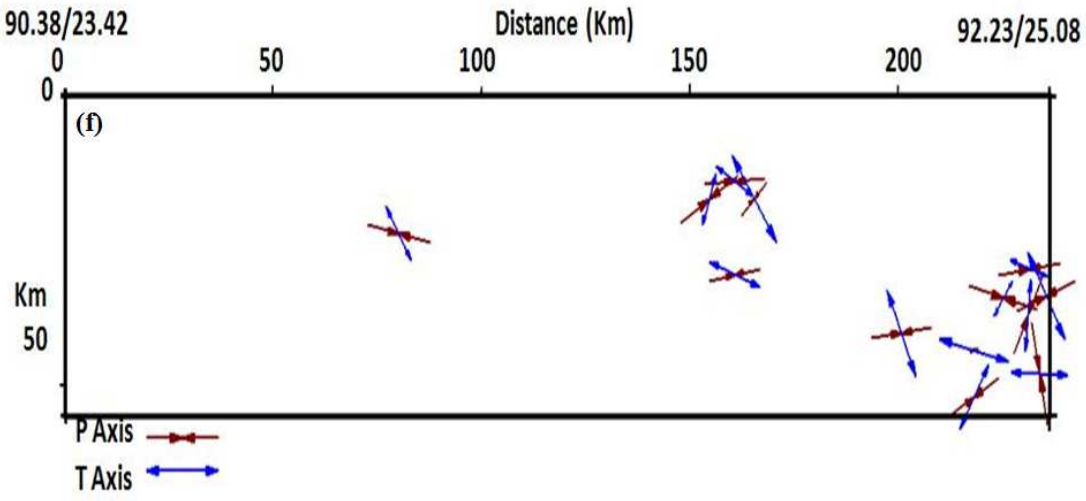

Fig.7.6 Fault plane solutions associated with the earthquake events in the northern part of Surma valley :- (a) Location of epicenters with their respective fault orientations (b) Depth Section plot. (c) Orientatios of the Nodal Planes. (d) Plot of P - axis orientations. (e) Plot of T- axis orientations. (f) Plot of P and T-axis orientations.

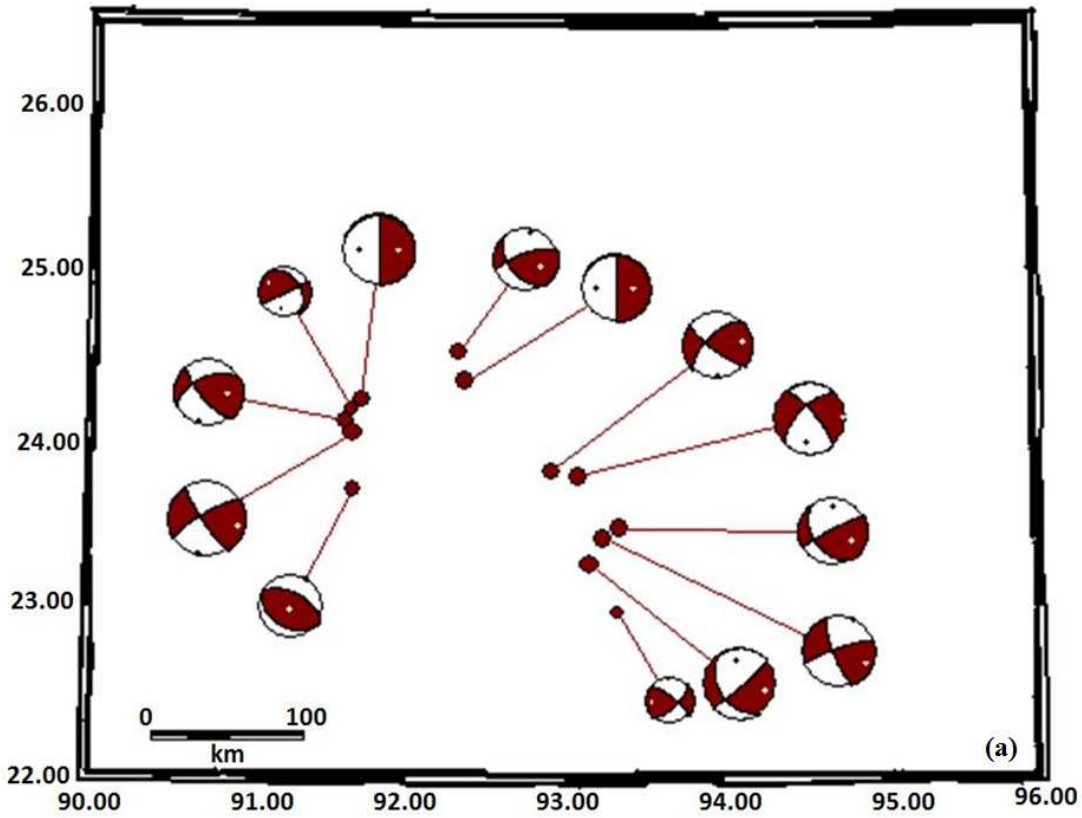

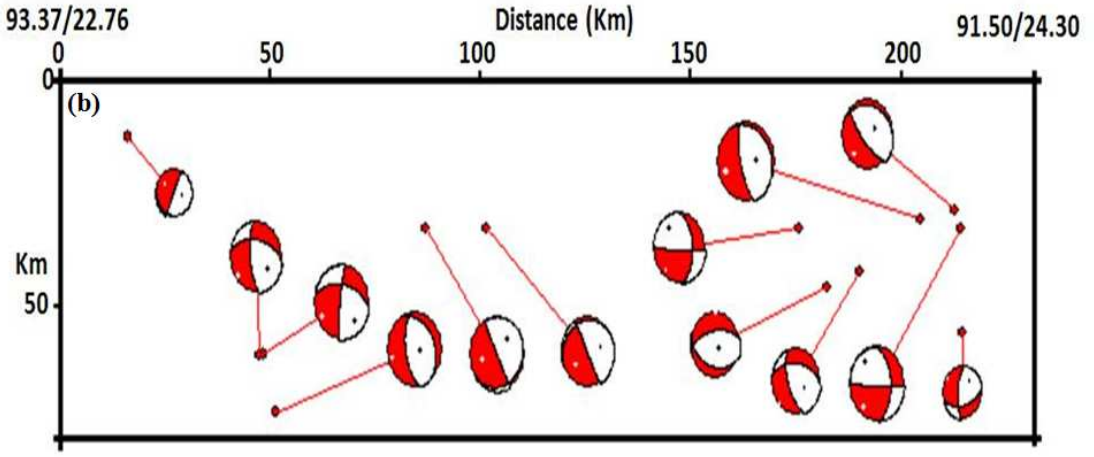
93.37/22.76
Distance (Km)
91.50/24.30
0
50
100
150
200
(b)
Km
50

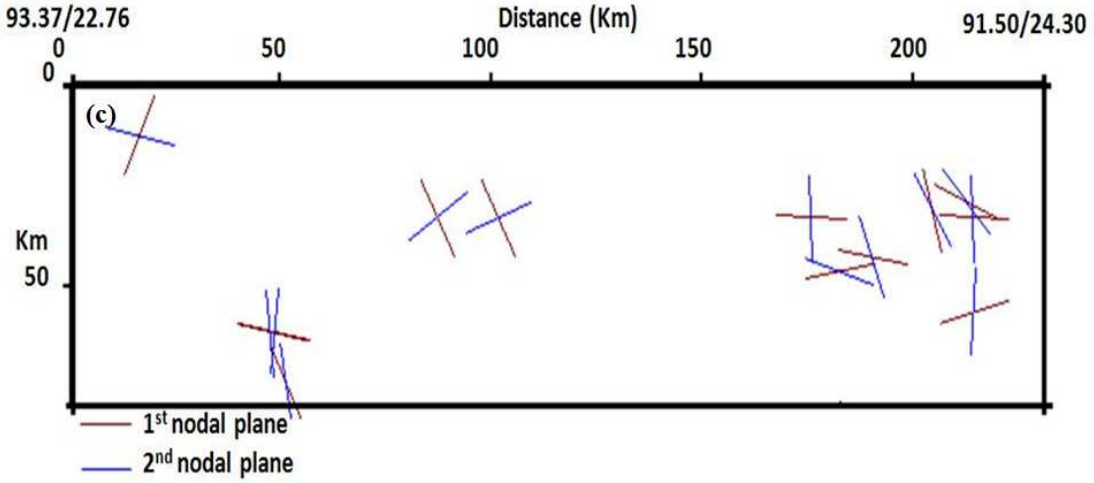
93.37/22.76
Distance (Km)
91.50/24.30
0
50
100
150
200
(c)
Km
50
1st nodal plane
2nd nodal plane

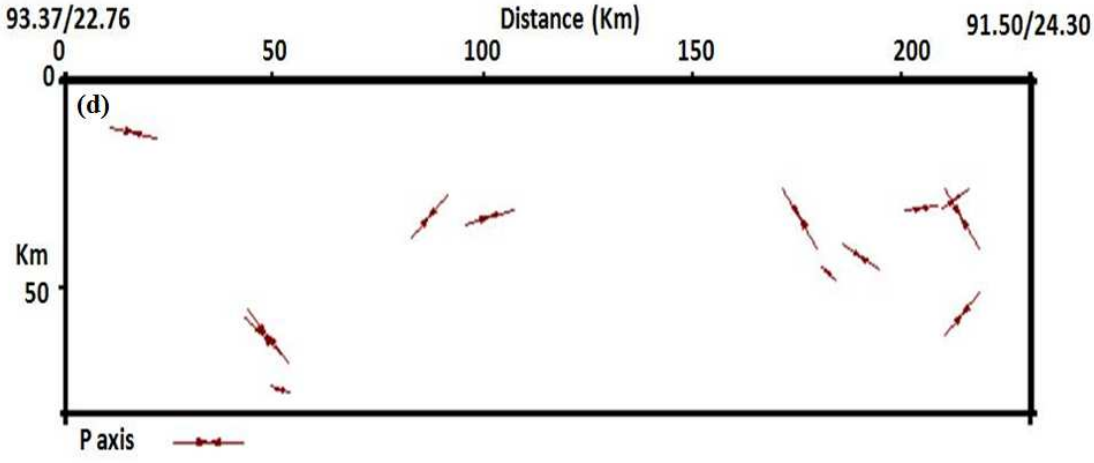
93.37/22.76
Distance (Km)
91.50/24.30
0
50
100
150
200
(d)
Km
50
P axis

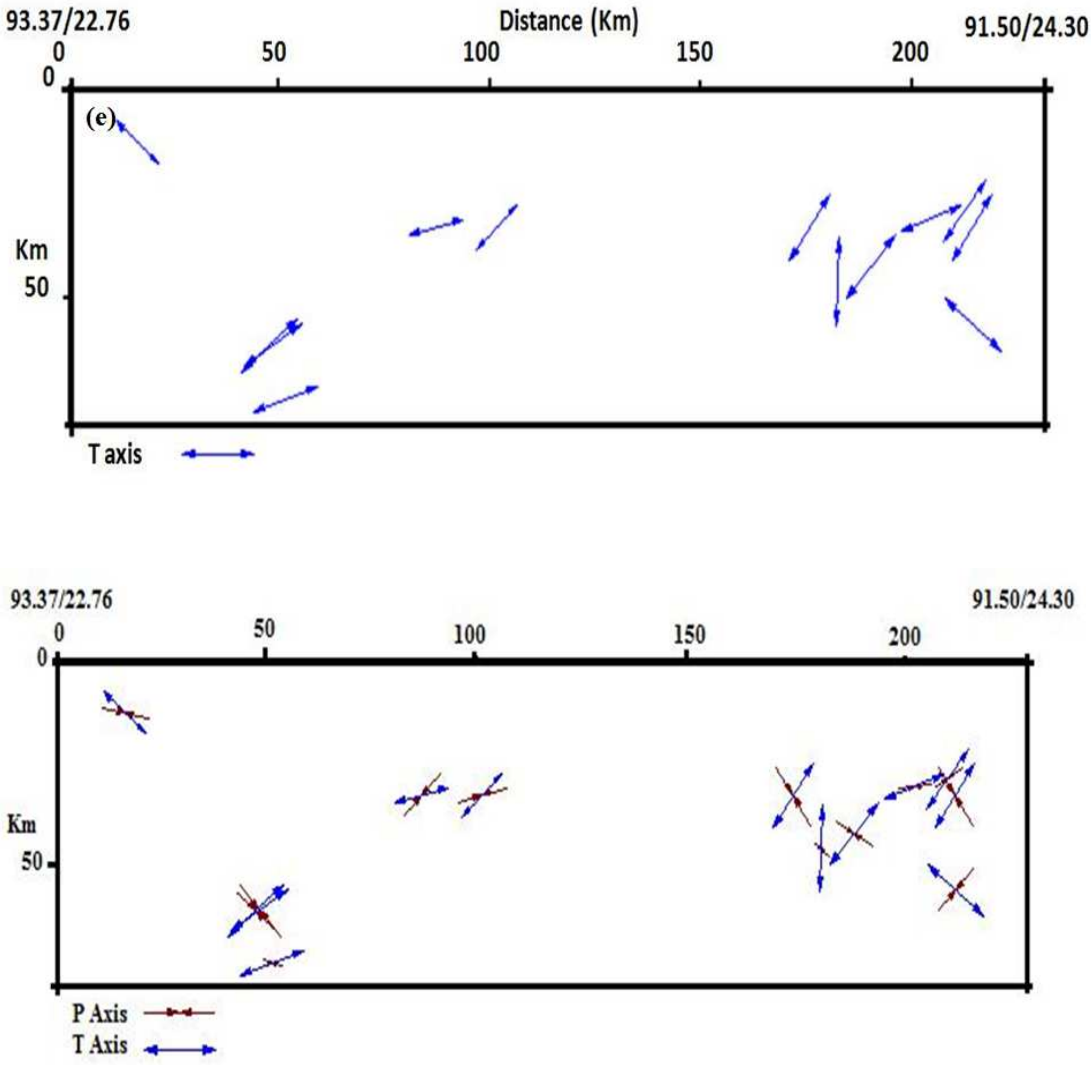

Fig.7.7 Fault plane solutions associated with the earthquake events in the eastern part of Surma valley :- (a) Location of epicenters with their respective fault orientations (b) Depth Section plot. (c) Orientatios of the Nodal Planes. (d) Plot of P - axis orientations. (e) Plot of T- axis orientations. (f) Plot of P and T- axis orientations.

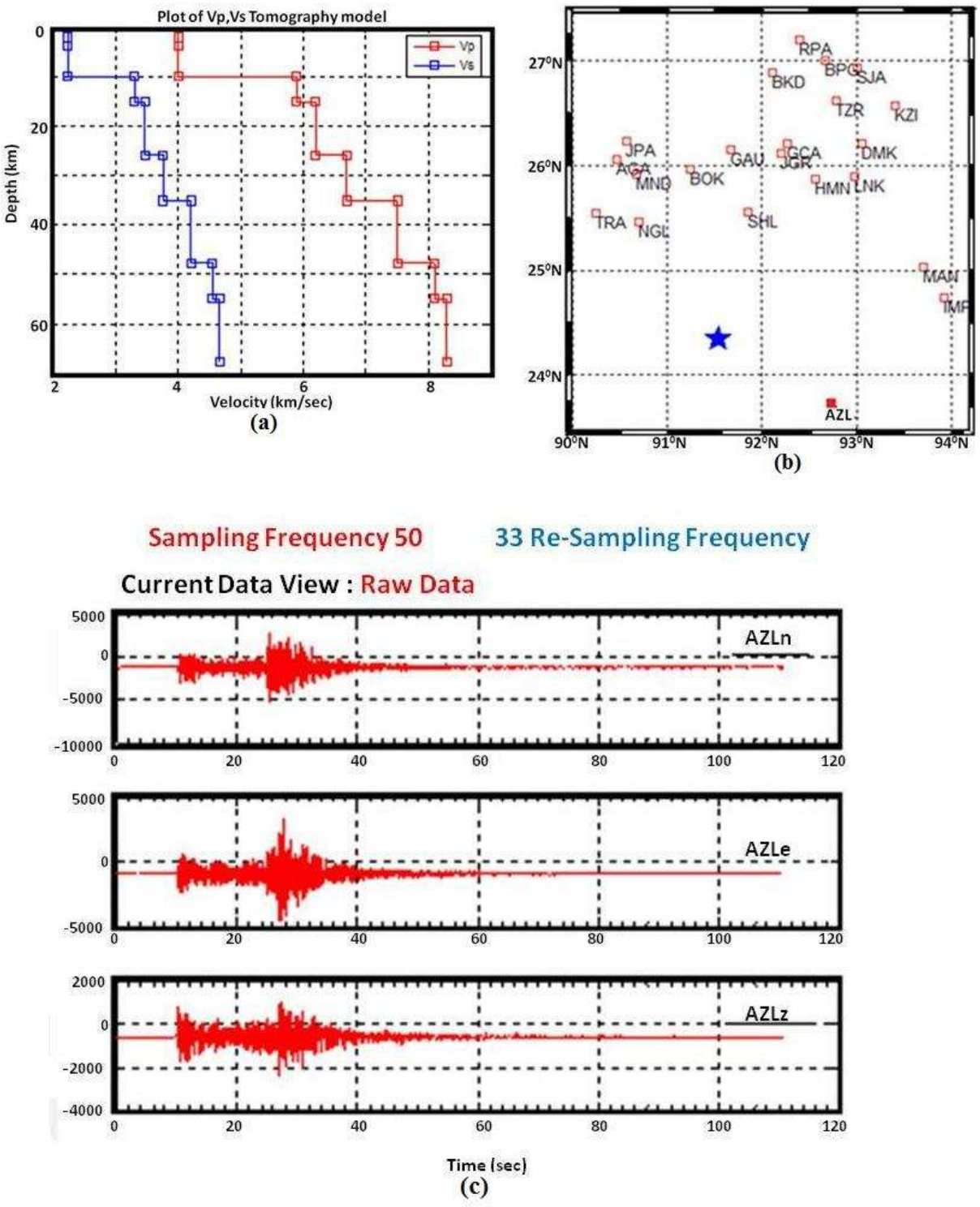

Fig.7.8 (a) One dimensional initial velocity model (Bhattacharya et al., 2005) used for waveform inversion, (b) Epicenter (marked as star) of the event used in waveform inversion and (c) Raw waveform of AZL station of the event as shown in (b) used for the waveform inversion of event associated with Mat fault.

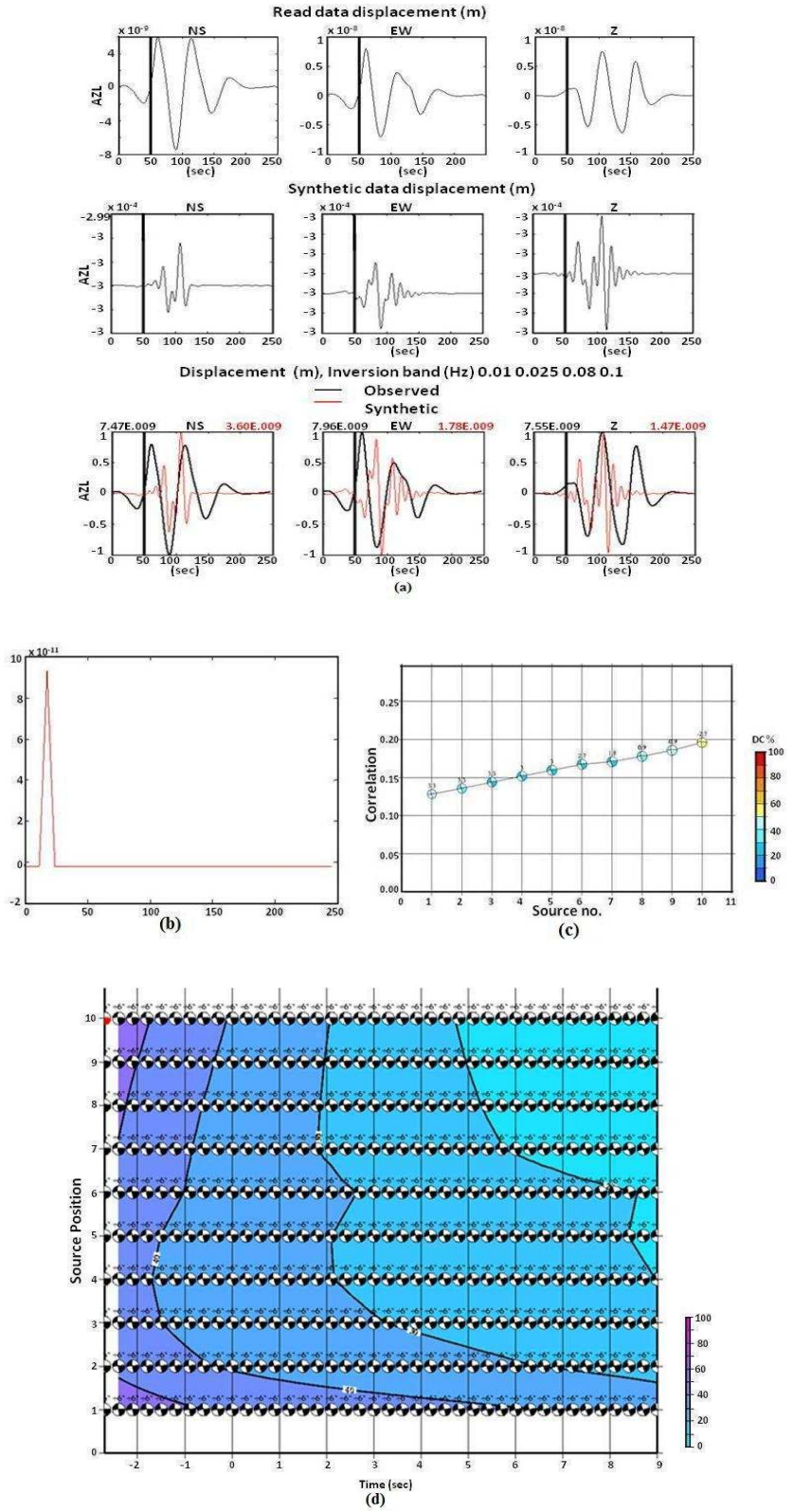

Fig.7.9 (a) An example of comparison (below) between observed (top) and synthetic seismogram (middle) of event as in Fig.7.19(b) source-time function plot (c) Correlation curve represented by percentage variation of double couple with reference to depth and (d) correlation between source position and time for DC% and for best solution.

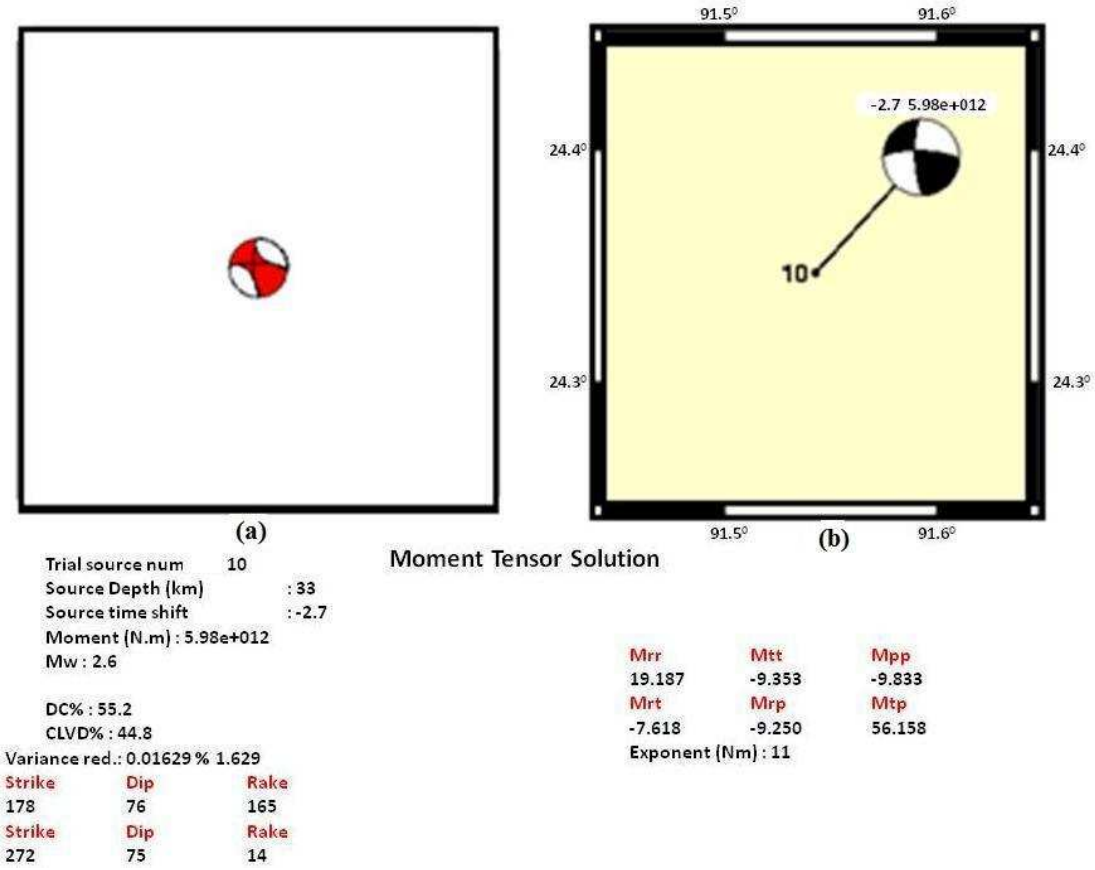

Fig.7.10 Best possible Moment tensor solution as inferred for the earthquake epicenter as shown in the Fig.7.8(b).

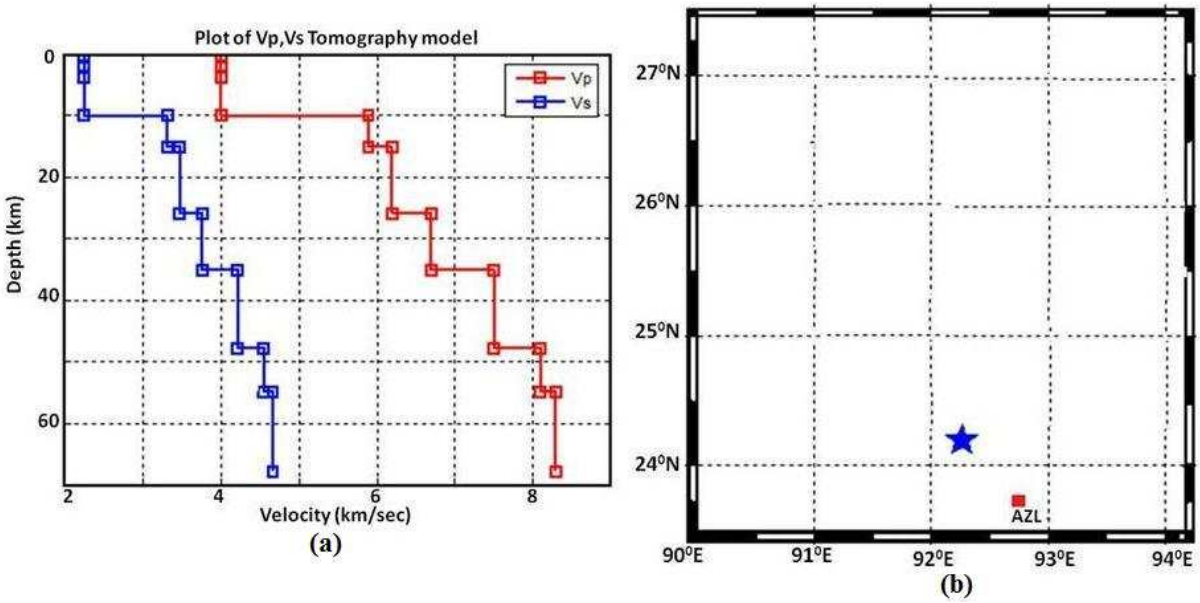
Plot of Vp,Vs Tomography model
Vp
Vs
Depth (km)
Velocity (km/sec)
(a)
27°N
26°N
25°N
24°N
AZL
90°E
91°E
92°E
93°E
94°E
(b)

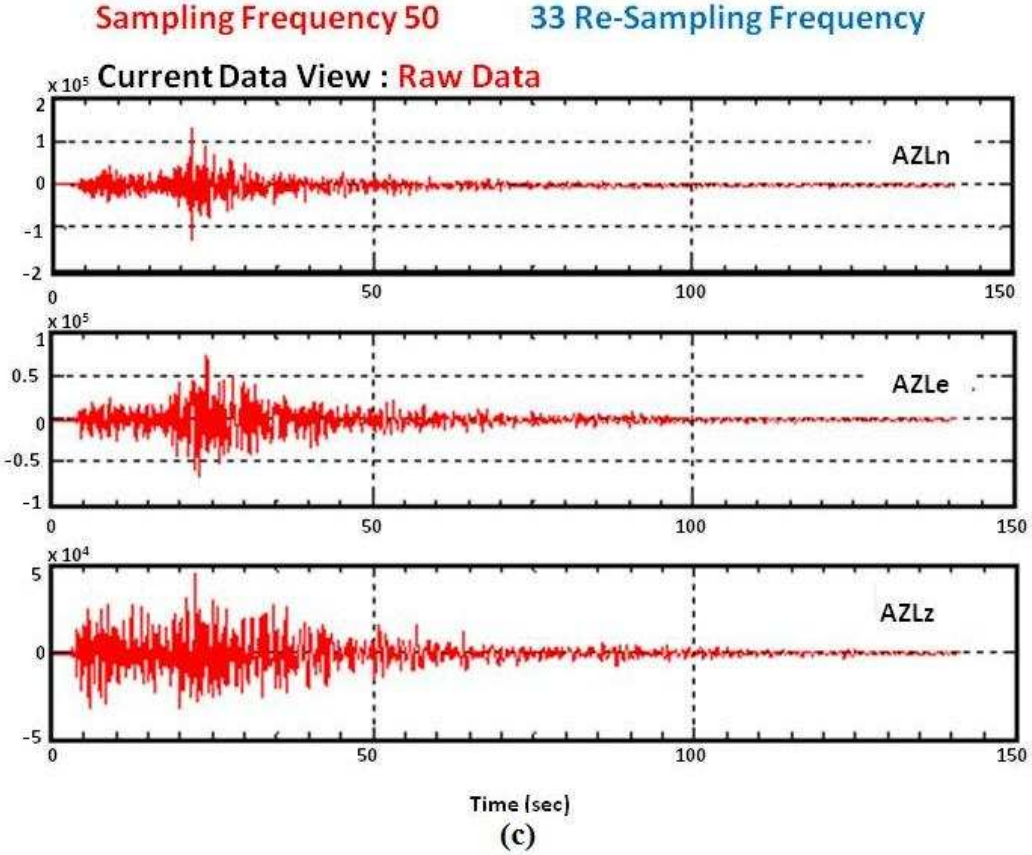
Sampling Frequency 50
33 Re-Sampling Frequency
Current Data View : Raw Data
AZLn
AZLe
AZLz
Time (sec)
(c)

Fig.7.11 (a) One dimensional initial velocity model (Bhattacharya et al., 2005) used for waveform inversion, (b) Epicenter (marked as star) of the event used in waveform inversion and (c) Raw waveform of AZL station of the event as shown in (b) used for the waveform inversion of event associated with Mat fault.

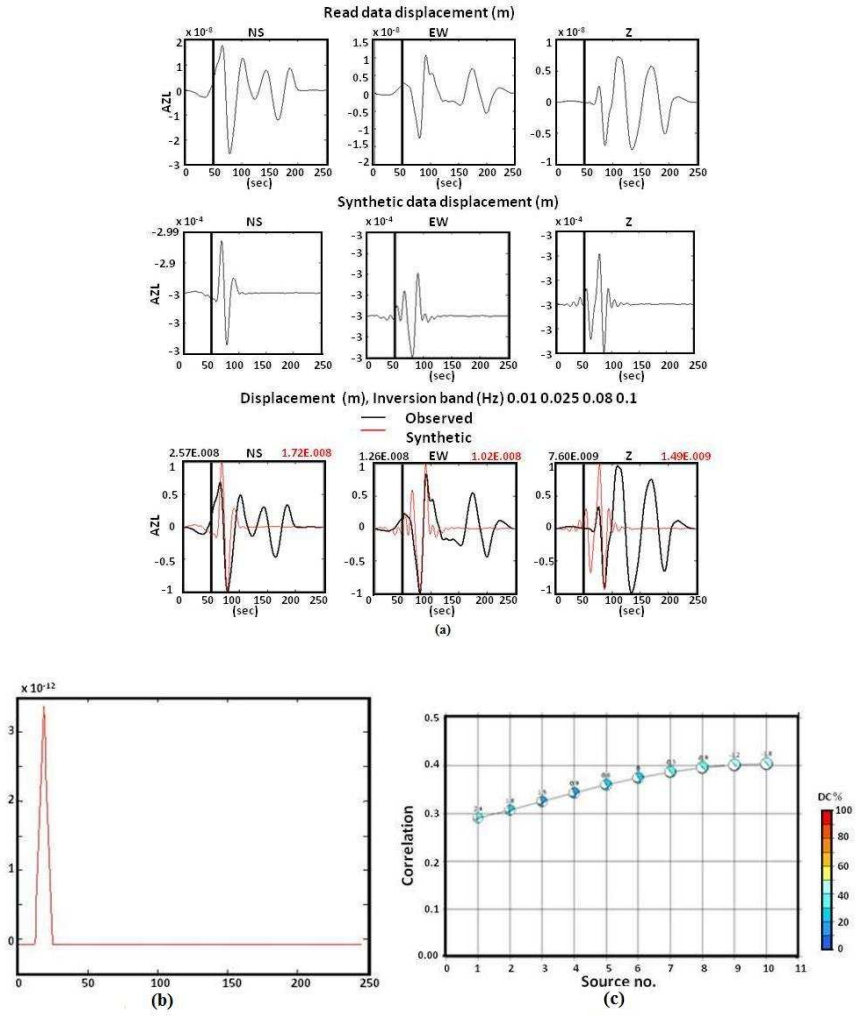

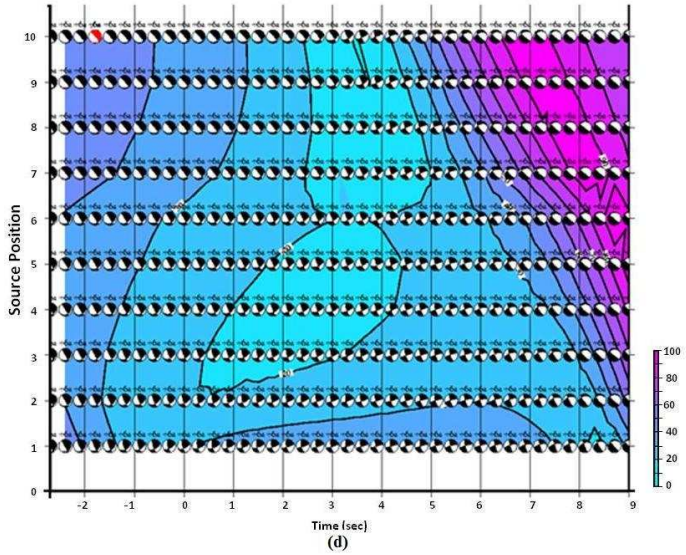

Fig.7.12 (a) An example of comparison (below) between observed (top) and synthetic seismogram (middle) of event as in Fig.7.22(b) source-time function plot (c) Correlation curve represented by percentage variation of double couple with reference to depth and (d) correlation between source position and time for DC% and for best solution.

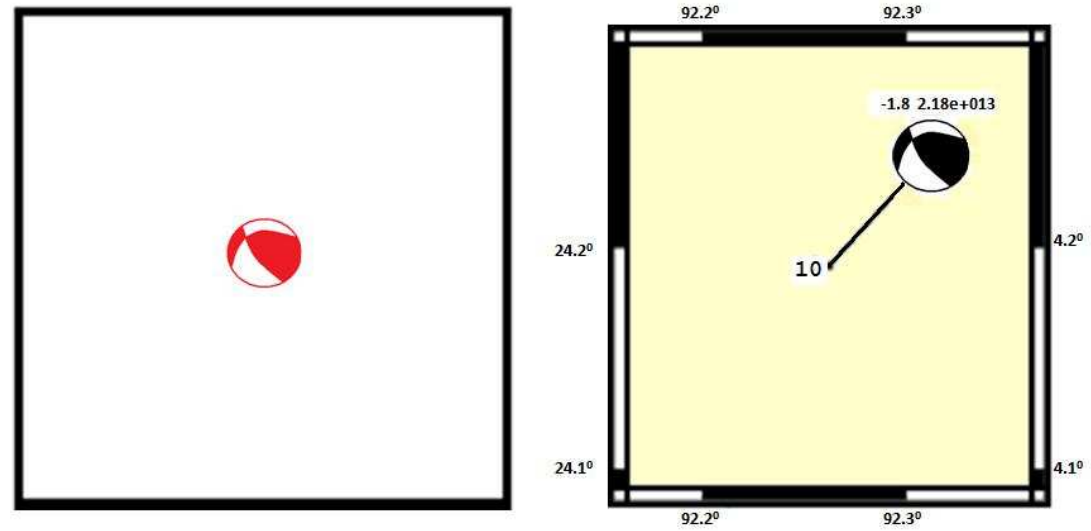

Moment Tensor Solution

Trial source number : 10
Source Depth (km) : 33
Source time shift : -1.8
Moment (N.m) : 3.34E+23
Mw : 4.9

DC% : 43.8
CLVD% : 56.2
Variance red.: 0.2744 % 27.44

Strike	Dip	Rake
247	22	21
Strike	Dip	Rake
137	82	110

Mrr	Mtt	Mpp
1.006	1.956	-2.962
Mrt	Mrp	Mtp
14.570	-14.566	6.488

Exponent (Nm) : 12

Fig.7.13 Best possible Moment tensor solution as inferred for the earthquake epicenter as shown in the Fig.7.11(b).

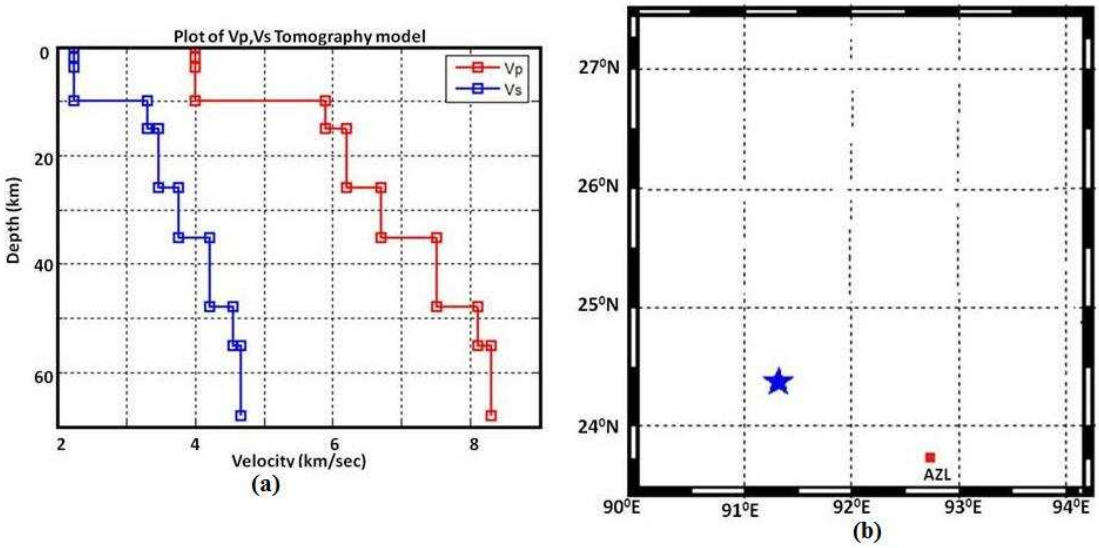
Plot of Vp,Vs Tomography model
Vp
Vs
Depth (km)
0
20
40
60
2
4
6
8
Velocity (km/sec)
(a)
27°N
26°N
25°N
24°N
AZL
90°E
91°E
92°E
93°E
94°E
(b)

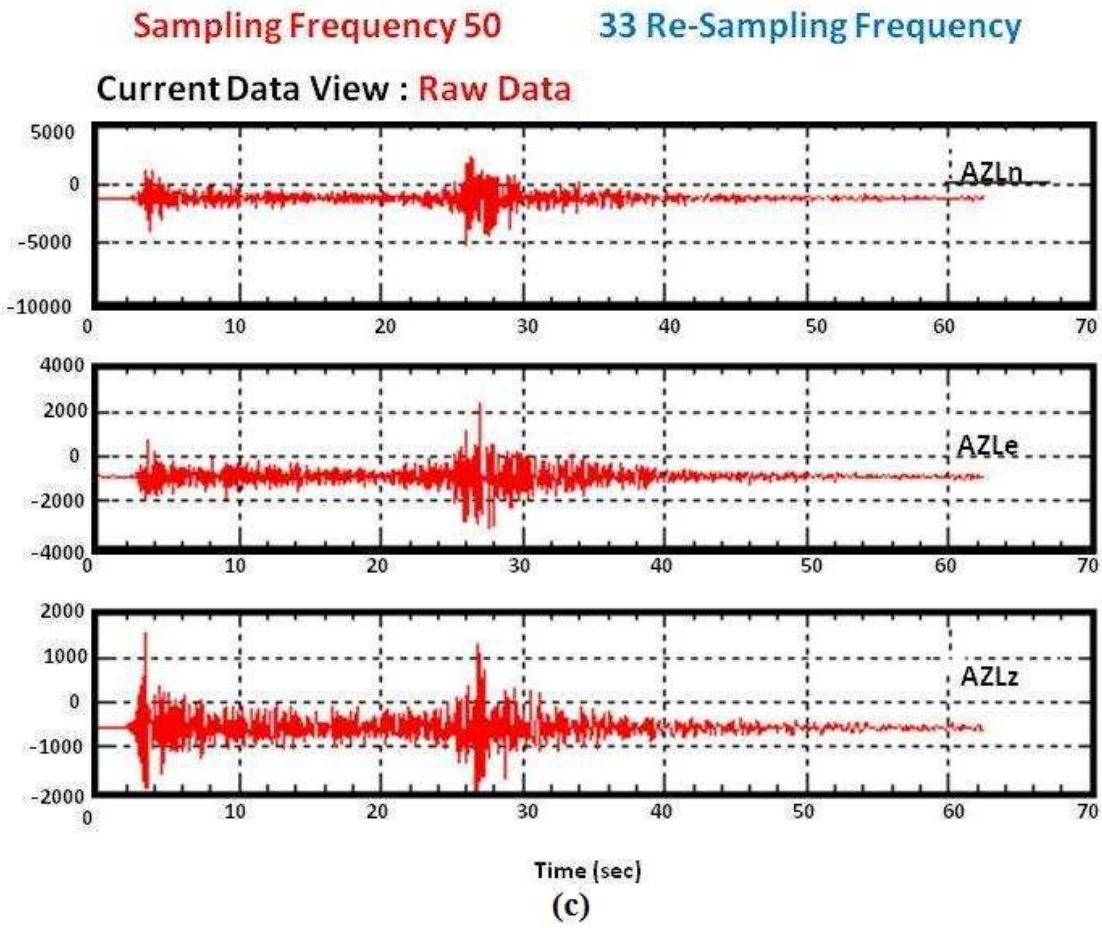

Fig.7.14 (a) One dimensional initial velocity model (Bhattacharya et al., 2005) used for waveform inversion, (b) Epicenter (marked as star) of the event used in waveform inversion and (c) Raw waveform of AZL station of the event as shown in (b) used for the waveform inversion of event associated with Sylhet fault.

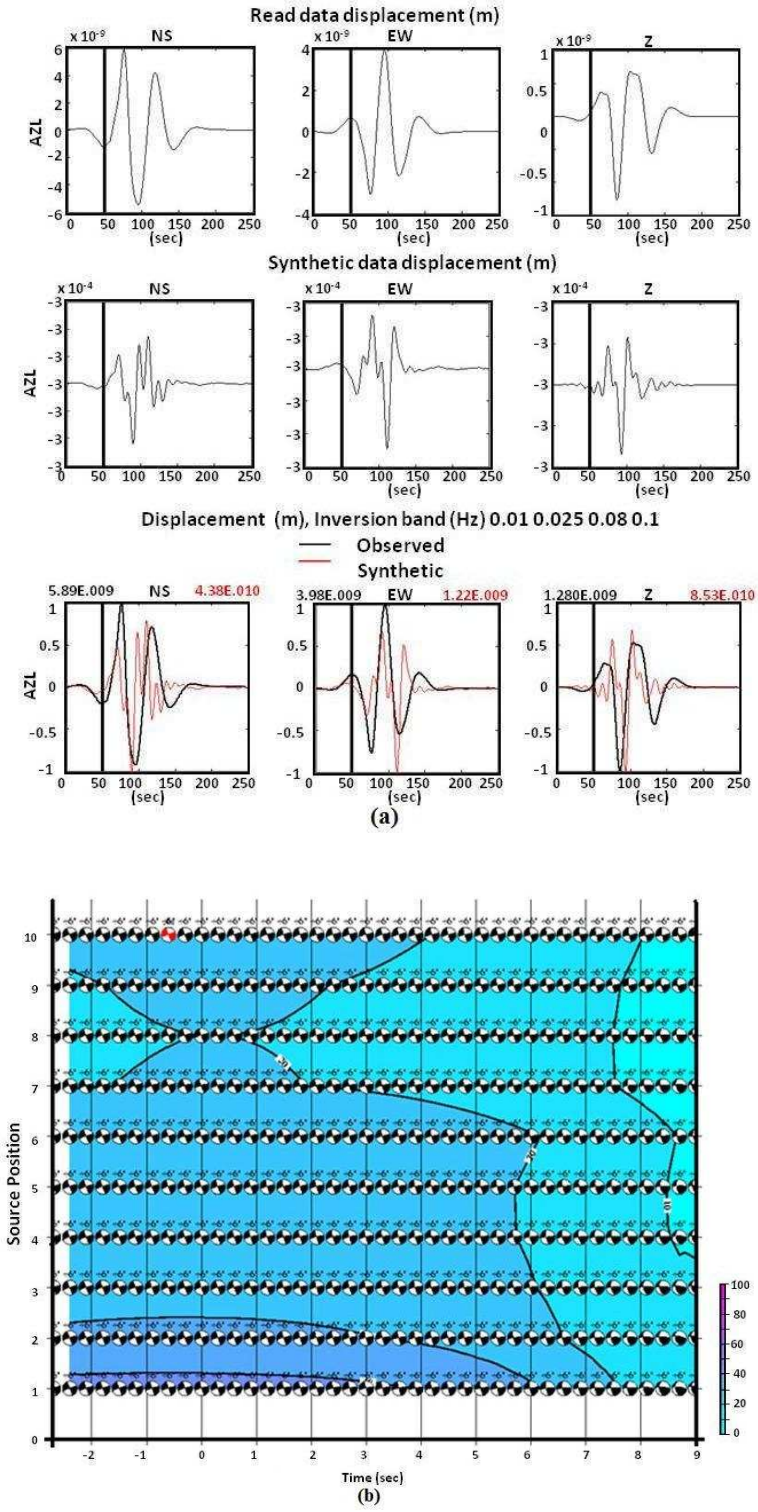

Fig.7.15 (a) An example of comparison (below) between observed (top) and synthetic seismogram (middle) of event as in Fig.7.25(b) correlation between source position and time for DC% and for best solution.

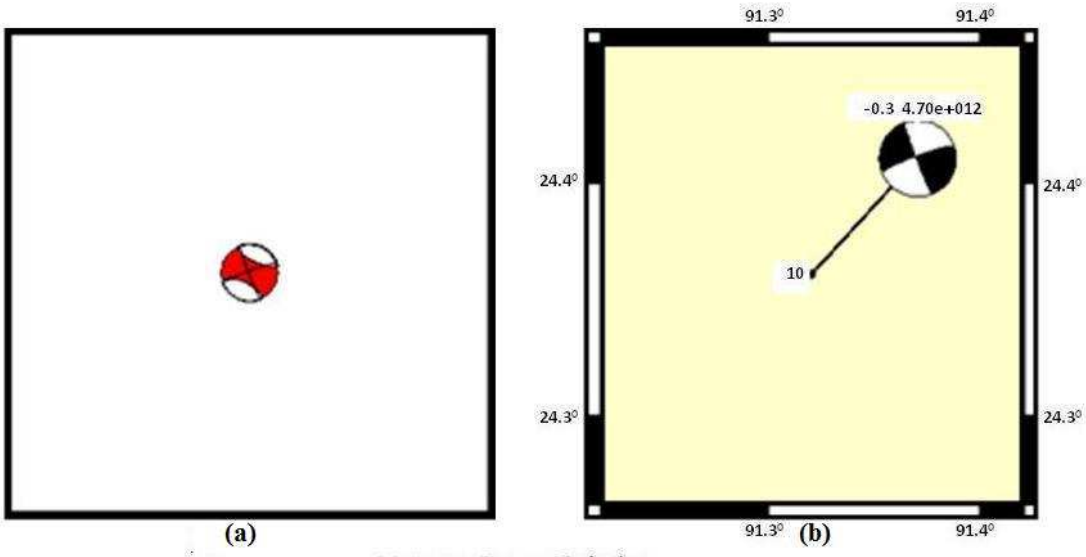

Moment Tensor Solution

Trial source numbe
Source Depth (km) : 33
Source time shift : -0.3
Moment (N.m) : 4.696e+012
Mw : 2.5

DC% : 22
CLVD% : 78
Variance red.: 0.04052 % 4.052

Strike	Dip	Rake
159	87	174
Strike	Dip	Rake
250	84	3

Mrr	Mtt	Mpp
21.037	-38.807	17.770
Mrt	Mrp	Mtp
1.955	-2.357	32.613

Exponent (Nm) : 11

Fig.7.16 Best possible Moment tensor solution as inferred for the earthquake epicenter as shown in the Fig.7.14(b).

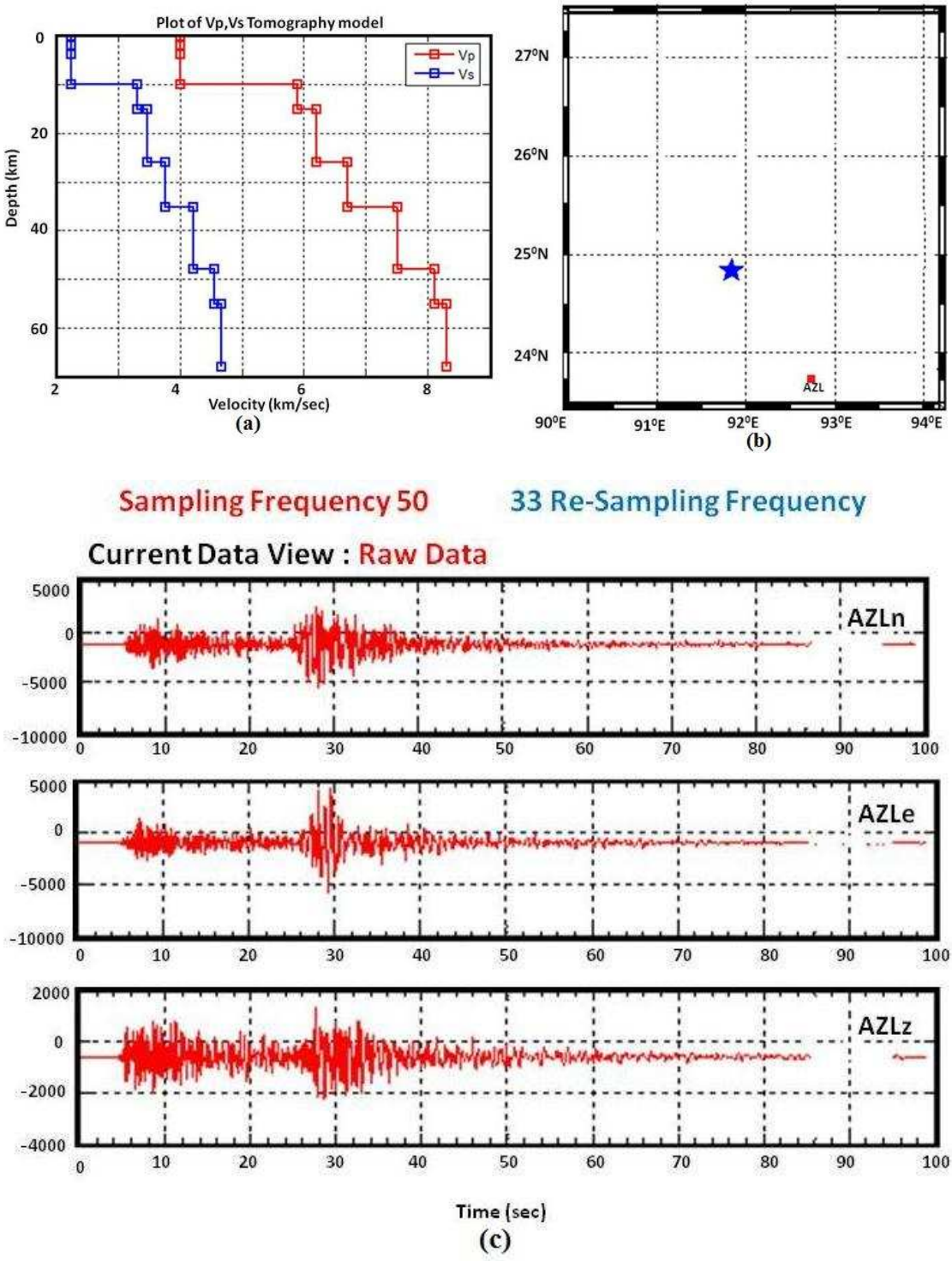

Fig.7.17 (a) One dimensional initial velocity model (Bhattacharya et al., 2005) used for waveform inversion, (b) Epicenter (marked as star) of the event used in waveform inversion and (c) Raw waveform of AZL station of the event as shown in (b) used for the waveform inversion of event associated with Sylhet fault.

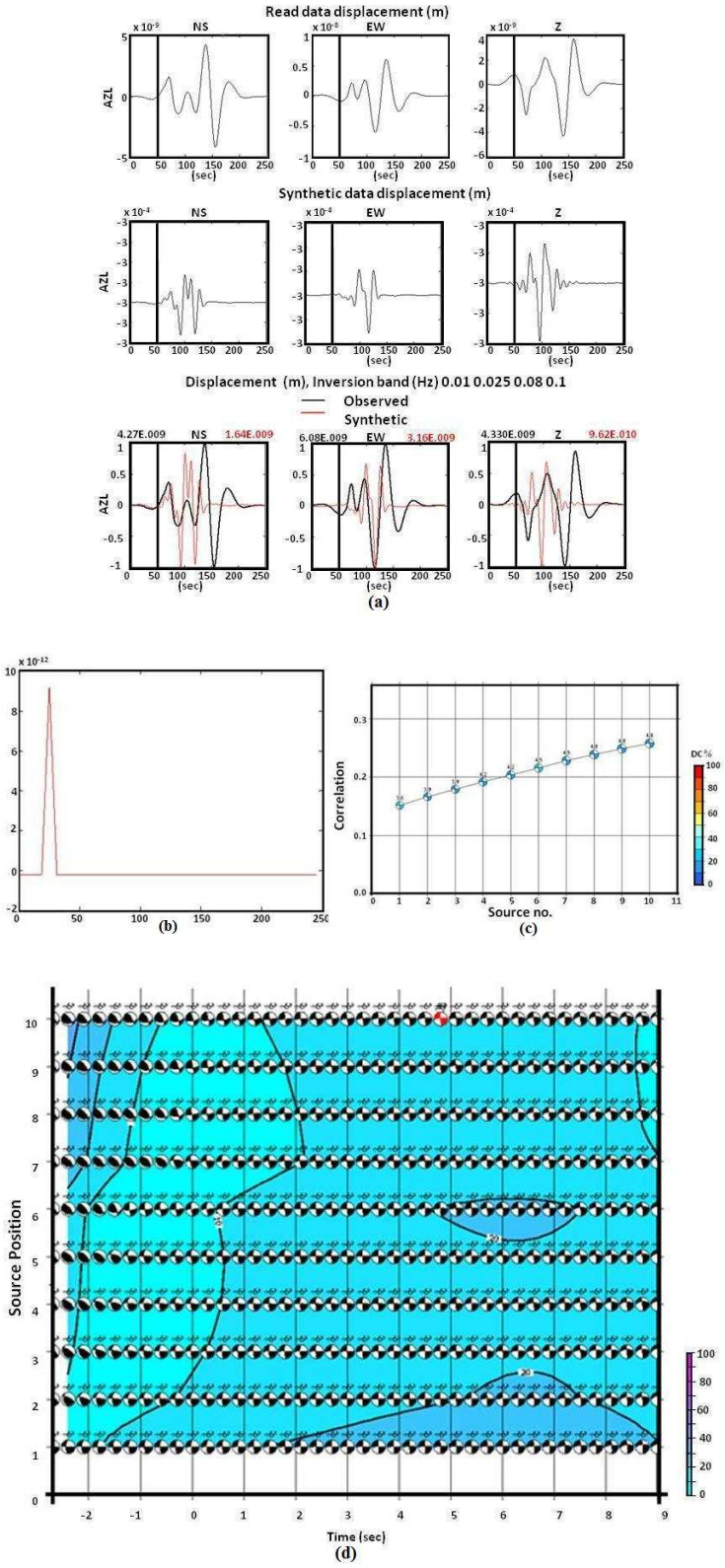

Fig.7.18 (a) An example of comparison (below) between observed (top) and synthetic seismogram (middle) of event as in Fig.7.28(b) source-time function plot (c) Correlation curve represented by percentage variation of double couple

with reference to depth and (d) correlation between source position and time for DC% and for best solution.

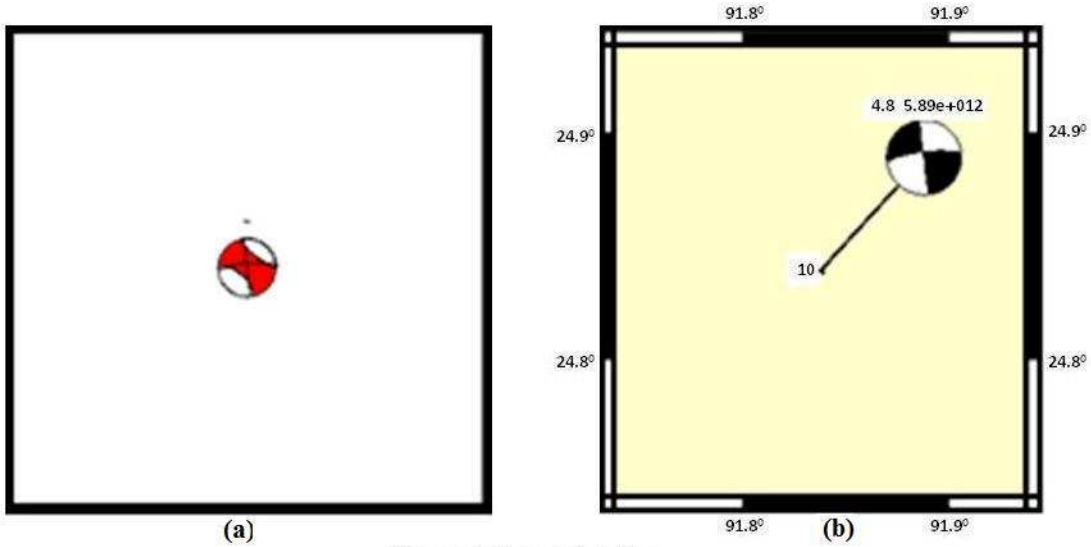

Moment Tensor Solution

Trial source number : 10
Source Depth (km) : 33
Source time shift : 4.8
Moment (N.m) : 5.889e+012
Mw : 2.6

DC% : 18.7
CLVD% : 81.3
Variance red.: 0.04052 % 4.052

Strike	Dip	Rake
173	89	168
Strike	Dip	Rake
264	78	1

Mrr	Mtt	Mpp
26.002	-23.957	-2.045
Mrt	Mrp	Mtp
8.849	-9.778	51.645

Exponent (Nm) : 11

Fig.7.19 Best possible Moment tensor solution as inferred for the earthquake epicenter as shown in the Fig.7.17(b).